DIELS-ALDER HYDROGELS AND MICELLES FOR OCULAR DRUG DELIVERY
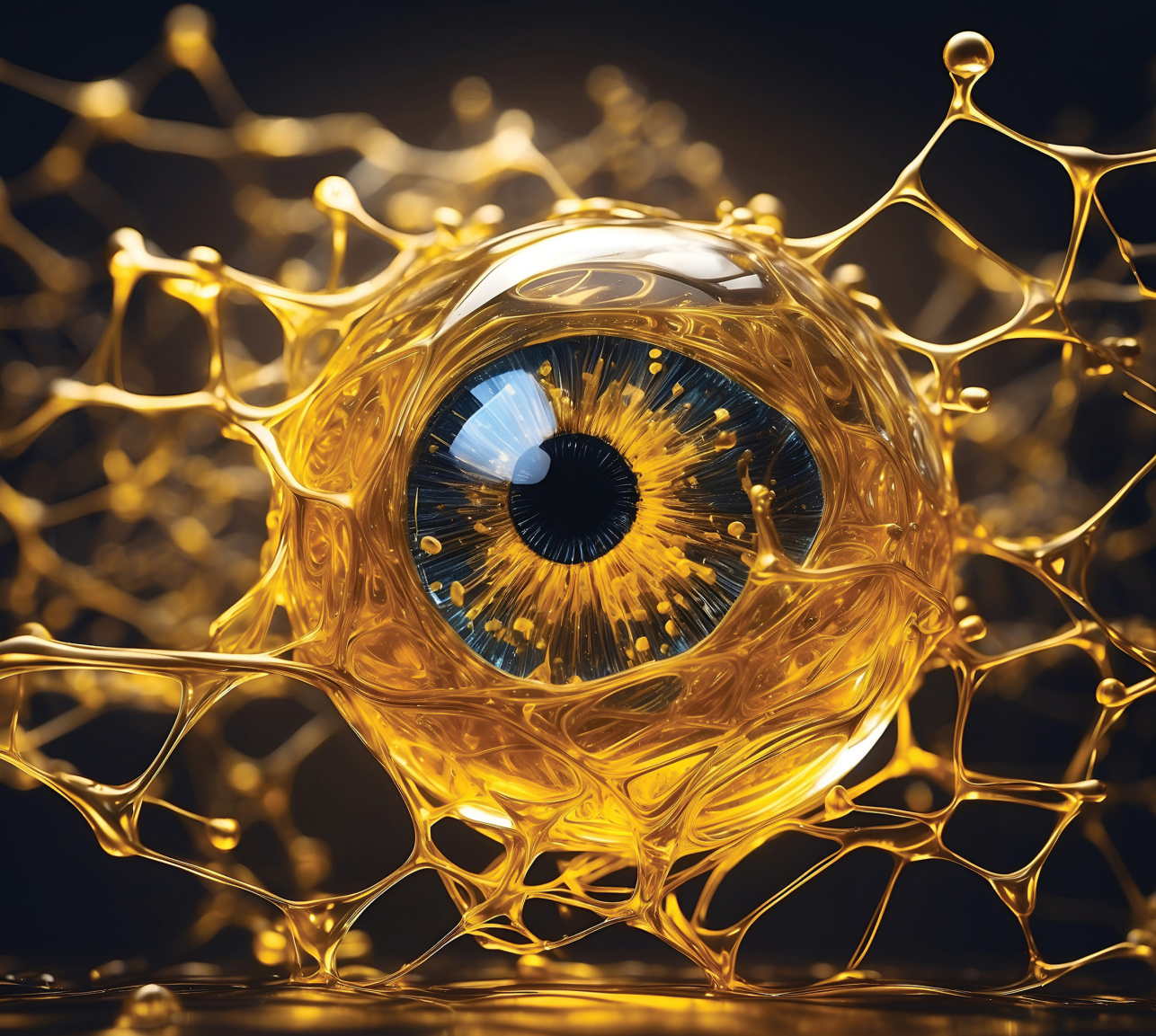
FROM DESIGN TO PRECLINICAL EVALUATION

Blessing C. Ilochonwu

DIELS-ALDER HYDROGELS AND MICELLES FOR OCULAR DRUG DELIVERY: FROM DESIGN TO PRECLINICAL EVALUATION

Blessing C. Ilochonwu

2024

Diels-Alder Hydrogels and Micelles for Ocular Drug Delivery: From Design to Preclinical Evaluation

Diels-Alder Hydrogels and Micelles for Ocular Drug Delivery:
From Design to Preclinical Evaluation

Diels-Alder Hydrogelen en Micellen voor Oculaire Geneesmiddelafgifte: Van Ontwerp tot Preklinische Evaluatie

(met een samenvatting in het Nederlands)

Proefschrift

ter verkrijging van de graad van doctor aan de
Universiteit Utrecht
op gezag van de
rector magnificus, prof. dr. H.R.B.M. Kummeling,
ingevolge het besluit van het college voor promoties
in het openbaar te verdedigen op

maandag 29 januari 2024 des middags te 12.15 uur

door

Blessing Chidimma Ilochonwu
geboren op 27 juni 1992
te Nnewi, Nigeria

Promotoren:

Prof. dr. ir. T. Vermonden
Prof. dr. ir. W.E. Hennink

Beoordelingscommissie:

Prof. dr. R. Censi
Dr. R. Eelkema
Prof. dr. ir. J.C.M. van Hest
Prof. dr. J.P.G. Sluijter
Prof. dr. G. Storm

"But those who hope in the Lord will renew their strength. They will soar on wings like eagles, they will run and not grow weary, they will walk and not faint."

Isaiah 40:31

To my Father and Mother

whose boundless dreams and sacrifices have inspired mine

Table of contents

Chapter 1

General Introduction

Blessing C. Ilochonwu

INTRODUCTION

1   Biomaterials in Ocular Therapy

A biomaterial is defined as "a substance that has been engineered to take a form which, alone or as part of a complex system, is used to direct, by control of interactions with components of living systems, the course of any therapeutic or diagnostic procedure, in human or veterinary medicine"[1]. Biomaterials have gained significant attention for pharmaceutical applications especially in the field of long acting injectables and targeted drug delivery systems. Moreover and importantly, in recent years, many biomaterials have been investigated for the development of ocular drug delivery systems.[2] The development of ocular drug delivery systems is a rapidly growing field, driven by the increasing prevalence of ocular diseases such as glaucoma, age-related macular degeneration, and diabetic retinopathy.[3-5] Novel therapeutic agents, including new biological entities (NBEs) and new chemical entities (NCEs), have shown great promise for the treatment of ocular diseases.[6-8] However, ocular barriers, including the corneal and conjunctival epithelium, the blood-retinal barrier, and intraocular fluid dynamics, pose significant challenges for efficient drug delivery to the target sites (for example the retina).[9, 10] polymeric drug delivery systems offer unique opportunities to realize sustained drug release, improved bioavailability, and targeted delivery to the site of action, making them highly promising materials for pharmaceutical applications. Various types of biomaterials, such as hydrogels, polymer and lipid-based nanoparticles, and polymeric microspheres have been extensively studied in preclinical evaluations for ocular drug delivery, showing both advantages and challenges (see Table 1). Some biomaterials-based formulations have reached clinical evaluation or are currently used in clinical practice as discussed in more detail in **Chapter 2** of this thesis. One notable example is Ocusert, a pilocarpine-releasing formulation that ensures sustained release of the loaded drug for ocular conditions and boost patient compliance.[11, 12] Ozurdex, a dexamethasone PLGA implant, advances long-lasting drug delivery, particularly for macular edema.[13, 14]

Many drug delivery biomaterials for ocular applications are polymer-based, allowing for precise control over their physicochemical properties, including e.g. injectability, biodegradability, and controlled release kinetics.[15] These characteristics enable them to release the loaded therapeutics in the eye and thereby enhance ocular drug availability and duration at the aimed site of action which makes them promising candidates for improving ocular drug therapies. Ocular availability refers here to the extent at which a drug is absorbed and becomes available for therapeutic action in the various components of the eye, taking into account both static barriers (such as the cornea, dermis, retinal tissues, and retinal vessels) and dynamic barriers (including conjunctival tissues, tear drainage, and lymphatic drainage).[16-18] These barriers collectively impact the ability of a drug to effectively reach its target within the eye and to exert its intended therapeutic effects.[19]

The utilization of biomaterials in preclinical research and development has the potential to revolutionize ocular drug therapy, leading to improved clinical treatment outcomes for various

ocular conditions.[20] This thesis focuses on exploring innovative biomaterial-based formulations for ocular drug delivery.

Table 1 Frequently investigated ocular biomaterials in preclinical studies.

Drug Delivery System	Composition	Advantages	Disadvantages	Ref.
Hydrogels	Natural or synthetic polymers	Localized and sustained delivery, suitable for protein delivery, prolonged drug release, enhanced drug stability	Potential for inflammation	[21-24]
Nanoparticles (NP$_S$)	Natural or synthetic polymers, lipids, inorganic and carbon based materials	Improved ocular bioavailability, enhanced drug stability, improved drug solubility, prolonged drug release, targeted delivery, Intracellular delivery	Potential toxicity	[25-30]
Microspheres	Natural or synthetic polymers, lipids	Prolonged drug release, localized delivery, enhanced drug stability,	Potential for inflammation	[31, 32]
Polymer based implants	Synthetic polymers	Approved for ocular therapy, Prolonged drug release, localized delivery, high loading,	Invasive administration, some are not degradable, potential for discomfort	[33-36]
Contact lenses	Hydrogels or silicone polymers	Corrective eyewear, prolonged drug release, easy administration	Potential for discomfort	[37, 38]

2   Polymer-Based Biomaterials

Polymeric biomaterials have an essential role in the development of drug delivery systems for various pharmaceutical applications including ophthalmic drug delivery.[15] Polymers are made up of repeating units of so-called monomers and can be classified based on their origin, ionic charge, chemical and physical characteristics, and sensitivity to the surrounding environment.

The **origin-based classification** divides polymers into natural, synthetic, and semisynthetic polymers.[39] Some examples of natural polymers include hyaluronic acid,[40] collagen, [41]and cellulose.[42] Synthetic polymers often used for biomedical and pharmaceutical applications are PEG (poly(ethylene glycol), PLLA (poly-L-lactic acid), PLGA (poly(lactic-co-glycolic acid)), PCL (polycaprolactone), poly(oxozalines) and PNIPAM (poly(N-isopropylacrylamide)).[43-47] Semisynthetic polymers used for drug deliver include chitosan[48] and carboxymethylcellulose.[49]

The **ionic charge-based classification** divides water soluble polymers into cationic, anionic, neutral, and zwitterionic polymers. This classification provides insight into the polymer's interactions with other molecules in the surrounding environment, such as proteins, biopolymers

(collagen, hyaluronic acid), and even cells. For example, cationic polymers can bind to negatively charged cell membranes, while anionic polymers can bind to positively charged proteins. Commonly used cationic polymers include polyethylenimine[50, 51] and chitosan.[48, 52] Anionic polymers include for example alginate[53, 54], hyaluronic acid[55-57] and dextran sulphate.[58, 59] Neutral polymers include poly(ethylene glycol) and zwitterionic polymers among which poly(sulfobetaine methacrylate) (pSBMA)[60], poly(2-methacryloyloxyethyl phosphorylcholine) (pMPC)[61] and polysarcosines.[62]

The **degradation-based classification** divides polymers into biodegradable and non-biodegradable. Biodegradable polymers can break down in the body over time, which can be useful for drug delivery applications where a sustained release of the drug is desired particularly when the release is governed by the degradation kinetics of the polymer.[63] Non-biodegradable polymers can provide longer-lasting drug delivery, but may need to be surgically removed once they released their content. Examples of biodegradable polymers include poly(lactic-co-glycolic acid)[64] and poly(e-caprolactone) (PCL)[65, 66], while non-biodegradable polymers include poly(ethylene glycol)[67] and poly(N-isopropylacrylamide)[68]. Biodegradation primarily occurs through the hydrolysis of ester bonds, but it can also involve the breakdown of urethanes, ortho esters, anhydrides, carbonates, and more.[69, 70] Additionally, alternative biodegradation mechanisms, including enzymatic cleavage of esters and peptide bonds, as well as the reduction of thiol bridges, have been explored.[71]

The **sensitivity to the surrounding environment-based classification** divides polymers into temperature-sensitive, pH-sensitive, electro-responsive, and photo-responsive polymers.[72] This classification is useful for designing drug delivery systems that can be triggered to release their payload in response to specific conditions. Temperature-sensitive polymers like poly(N-isopropylacrylamide) and poloxamers can be used to prepare biomaterials that encapsulate drugs or release their drug payload when exposed to a certain temperature.[68, 73, 74] PH-sensitive polymer based materials like poly(acrylic acid) release their drug payload in response to changes in pH.[75] Materials based on electro-responsive polymers like poly(pyrrole) and poly(3,4-ethylenedioxythiophene) release their drug payload in response to electric fields[76-78], while photo-responsive materials containing azobenzene-based polymers or spiropyran-based polymers release their drug payload in response to a light trigger.[79-81] Overall, understanding the various classifications of polymers can provide important information about their properties and potential applications in drug delivery systems[82].

2.1 Polymer architectures and polymerization techniques

Different polymer architectures like block copolymers, branched polymers, and multi-arm polymers (Figure 1) can be used to create biomaterials with unique properties. Homopolymers are synthesized by polymerization of one type of monomer and copolymers are synthesized from two or more monomers. Dendrimers, known for their tree-like structure, are typically considered homopolymers, as they consist of repeating monomeric units that are chemically identical.[83] Copolymers combine the properties of different types of monomers. Various types of copolymers include block copolymers (homopolymer units arranged in blocks), random copolymers (monomer

units arranged randomly), alternating copolymers (monomer units alternate) and gradient copolymers (exhibit a smoothly transitioning composition along their chains).[84] In Figure 1, various other common polymer structures are depicted, such as multi-arm polymers, graft polymers, branched polymers, and dendrimers, all widely employed in diverse biomedical applications.
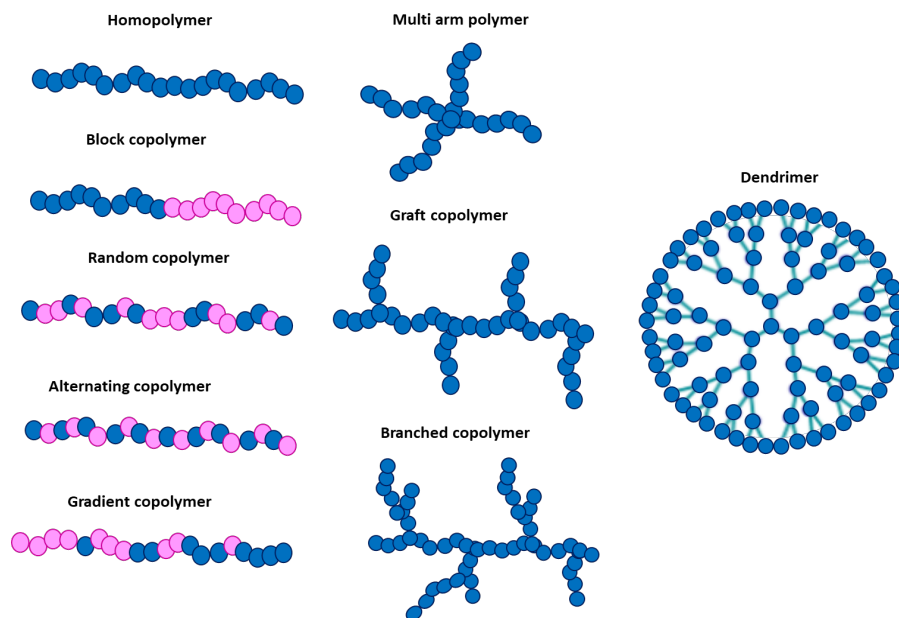
Figure 1 General polymer architectures

Various polymerization techniques are available to synthesize different types of polymers. Free radical polymerization (FRP), reversible addition-fragmentation chain transfer (RAFT) and atom transfer radical polymerization (ATRP) are known examples of radical polymerization techniques that enable the synthesis of diverse copolymer structures. Although there are many more well-known polymerization techniques [85-88], this section focusses on FRP and ATRP as these polymerization techniques were used in this thesis to synthesize the polymers used for the design of ocular drug delivery systems. FRP is historically the most commonly used radical polymerization technique. Controlled radical polymerizations have emerged more recently including ATRP, which is the main polymerization technique used in this thesis.

Free radical polymerization

FRP is a basic synthesis route to obtain a variety of different polymers. In fact many of the commercially available synthetic polymers are prepared by using this type of reaction and provides a broad range of materials for various applications.[89] This polymerization method forms polymers by the consecutive addition of free radical building blocks and was defined by IUPAC in 1996 as "a chain polymerization in which the kinetic chain carriers are radicals"[84]. Thus FRP is a chain growth polymerization, [90] however, the major limitation of this technique

is the limited control over molecular weight, polydispersity, and structures like block copolymers cannot be obtained.

Atom transfer radical polymerization

Atom transfer radical polymerization (ATRP) is a well-studied controlled/living radical polymerization (CRP) method that allows for the synthesis of well-defined polymer architectures with tailored functionalities.[91] Professor Matyjaszewski is credited with discovering copper-mediated ATRP, one of the most robust CRP methods.[92] ATRP is a controlled radical polymerization process that involves reversible reactions between a "dormant species" and a transition metal complex, typically copper, resulting in the formation of propagating radicals and higher oxidation state metal complexes. The propagating radicals continue to grow the polymer chain through the addition of monomers. The catalytic cycle is terminated when the halogen atom originally associated with the transition metal complex transfers to the growing polymer chain, leading to the formation of a new halogenated end group. This new halogenated end group represents the final product of the ATRP process. ATRP offers certain advantages over free radical polymerization, including better control over molecular weight and lower polydispersity.[93] Importantly, in contrast to classical free radical polymerization, ATRP also offers the possibility to synthesize block copolymers.[91, 94]

3   Hydrogels

Hydrogels are three-dimensional networks of hydrophilic synthetic or natural polymer chains that are crosslinked by physical and/or chemical bonds.[95] These hydrophilic networks can absorb large amounts of water or physiological fluids, up to 99% of their weight, while maintaining their structure.[96] The hydrophilic character of the polymeric backbone and/or functional groups attached to the main chain are responsible for the water absorption, while the presence of crosslinks between the polymers keeps the structure stable.[97] Despite primarily consisting of liquid (water), hydrogels maintain their shape and do not exhibit flow behavior, except in some examples situations where shear is applied. This uniqueness arises from their intermediate viscoelastic state, neither entirely liquid nor entirely solid.[97, 98] These properties make hydrogels very suitable for numerous biomedical and pharmaceutical applications[99, 100, 114], as shown in Figure 2. hydrogels generally offer a high degree of biocompatibility as well as desirable physical characteristics.[101, 102] Hydrogels can serve as scaffolds to provide structural integrity to tissue constructs[103, 104], control drug[105] and protein delivery[106-108] to tissues and cultures, and act as adhesives or barriers between tissue and material surfaces.[43, 109, 110] The first successful use of hydrogels in biomedicine dates back to the early 1950s when Wichtlerle and Lim[111] designed crosslinked poly(hydroxyethyl methacrylate) (pHEMA) for ophthalmology applications, producing the first synthetic hydrogel used for soft contact lenses.[112, 113]
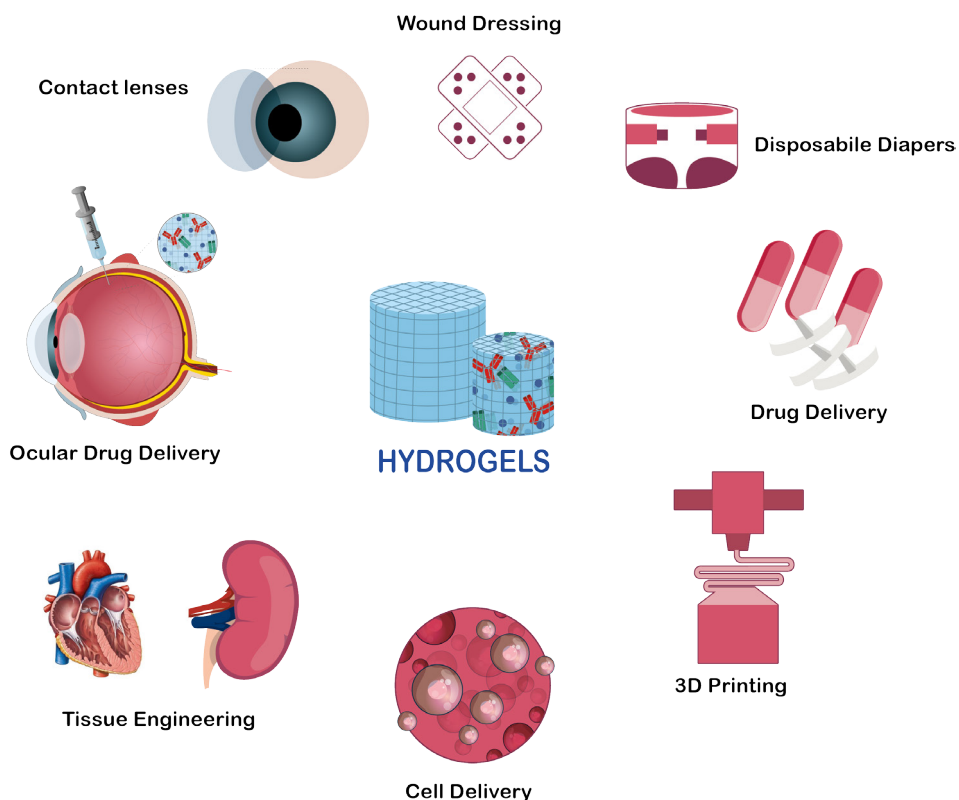
Figure 2 The use of hydrogels in different applications.

Hydrogels possess unique properties (Figure 3) that make them attractive biomaterials for ophthalmic applications due to their soft and elastic texture, as well as their high water content.[115, 116] Hydrogel's highly porous structure allows for the diffusion of oxygen, metabolites, and nutrients, facilitating contact and interaction with biological tissues.[117, 118] Their porosity can be easily adjusted by controlling the crosslink density and affinity to water. Hydrogels can also be designed to be injectable, and thereby minimally invasive and to degrade over tunable time frames.[119-121] Hydrogels are suitable matrices for encapsulating drugs, especially large biotherapeutics, within their porous structure, offering controlled and prolonged drug release, which can result in a high local concentrations of a pharmaceutical active substance for an extended period.[122-124] Drug release from hydrogels can proceed through different mechanisms, such as diffusion, swelling and degaration (and combinations thereof) depending on the formulation.[117] The controlled drug kinetics can be tuned to enhance the efficacy of a specific treatment while reducing potential side effects.

IDEAL PROPERTIES
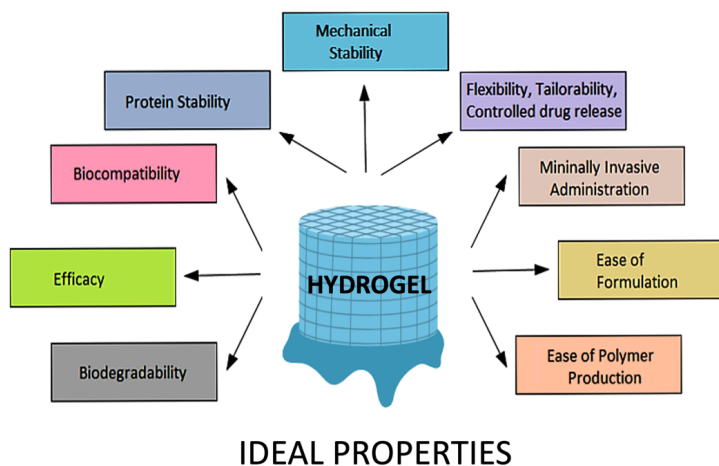
Figure 3 The attractive properties of hydrogels for ophthalmic drug delivery applications.

4   Crosslinking Strategies for Hydrogels

As mentioned above, the hydrophilic polymer chains in hydrogels are held together by crosslinks, which can be either of physical or chemical nature[125, 126]. Physical crosslinking involves the use of physical interactions, such as hydrogen bonding, hydrophobic interactions, inclusion complexes, stereo-complexes, chain entanglements and ionic interactions, to create a three-dimensional network.[126] On the other hand, chemical crosslinking involves the formation of covalent bonds between polymer chains to create the network. Chemical crosslinking can be achieved through various methods such as free radical polymerization[127], Michael-type addition[128], or click chemistry[129] to mention a few. Crosslinking restricts the movement of the hydrophilic polymer chains, transforming a viscous polymer solution into an elastic gel. The physical characteristics of the hydrogel are influenced by the degree of crosslinking, whereby a low degree of crosslinking leads to softer hydrogels, while a higher degree of crosslinking results in stiffer hydrogels. The timing of a crosslinking procedure can be important as well. For implantable hydrogels, the polymers are crosslinked prior to a surgical procedure. However, crosslinking can also occur *in vivo* (*in situ*) after administration of viscous aqueous polymer solution at a specific location in the body. The advantage of the last strategy is that a minimally invasive manner by e.g. injection can be used for *in situ* gel formation.

Hydrogels that are formed by both physical and chemical crosslinks are particularly fascinating. Physical crosslinks lead to rapid stabilization of the network after injection, while subsequent chemical crosslinking ensures the formation of a mechanically stable polymeric network.[130-132]

Stimuli responsive hydrogels

Stimuli responsive hydrogels are defined as materials that undergo changes in response to stimuli. These stimuli may be of physical or chemical nature: temperature, pH, solvent, pressure, ionic strength, light, concentration of specific biomolecules. In response to these stimuli

hydrogels can swell, shrink, degrade or polymer solutions can undergo a sol to gel transition. Stimuli sensitive polymers are widely applied for the design of injectable *in situ* forming hydrogels.[133-135] These innovative biomaterials can be designed to be injectable and therefore offer several benefits including patient comfort, less invasive administration and cost reduction compared to hydrogels that require a surgical intervention prior to their application.[136] Furthermore, the use of *in situ* forming hydrogels allow encapsulation of small drugs as well as biotherapeutics and even living cells, overcoming complexities and limitations associated with post-loading techniques[135, 137, 138]. Among the different types of stimuli sensitive hydrogels, thermosensitive polymers are of great interest as aqueous solutions of these polymers can be converted into hydrogels when the temperature changes.[68] When thermosensitive polymers dissolved in water pass their lower critical solution temperature (LCST), the polymer chains collapse and aggregate (Figure 4). Poly-(N-isopropyl acrylamide, PNIPAM)-based polymers are one of the most studied thermosensitive systems due to their ability to self-assemble above 32 °C.[74] In this way, aqueous solutions of these polymers form *in situ* hydrogels after administration, due to a sol-gel transition from room temperature to body temperature.
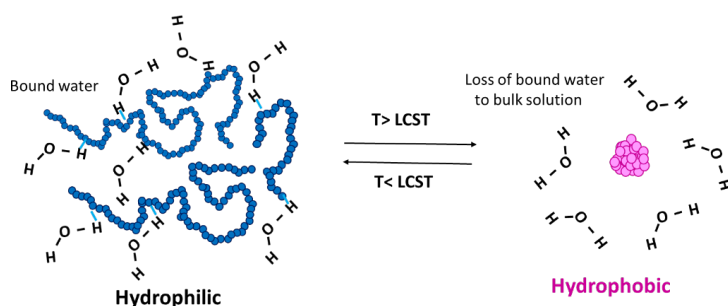
Figure 4 Thermosensitive polymer in aqueous solution: below the LCST, the polymer chains form hydrogen bonds with water molecules. Above the LCST, hydrogen bonds between polymer and water are broken, resulting in dehydration and self-assembly of the polymer chains.

Diels Alder Chemical Crosslinking

In this thesis, the focus is on the Diels-Alder (DA) reaction as a chemical crosslinking method. As previously mentioned, there are several ways to achieve chemical crosslinking, such as free radical polymerization, Michael-type addition, and click chemistry, among others. Click chemistry, in particular, has revolutionized macromolecular synthesis and biomaterials science due to its wide scope, high efficiency, selectivity, and ease of product purification.[139] Importantly, many click reactions can be conducted in aqueous media under mild conditions, making them highly advantageous.[140, 141] The Diels-Alder reaction is a type of click reaction that has gained attention as a crosslinking method for the design of a variety of biomaterials.[142-145] The reaction involves the addition of a dienophile to a diene, resulting in the formation of a cyclohexene ring. This reaction can occur between various dienophiles and

dienes, and the reaction conditions such as temperature, solvent, and the presence of a catalyst can be varied to tailor and control the reaction rate. The DA reaction's reversibility by retro-DA (rDA) allows for dynamic covalent crosslinking, where crosslinks can be broken and reformed, and the rate of these reactions can be tuned by parameters such as pH or temperature.[146, 147] The furan-maleimide couple, a prevalent DA crosslink (Figure 5), can undergo a progressive degradation process under physiological conditions. It begins with a rDA reaction and proceeds to the ring-opening hydrolysis of the maleimide group, forming inert maleamic acid. This removes maleimide groups from the DA/rDA equilibrium, resulting in irreversible crosslink cleavage. This chemistry holds potential for applications in ocular drug delivery to enhance ocular therapy, a subject of recent research interest.[148, 149]
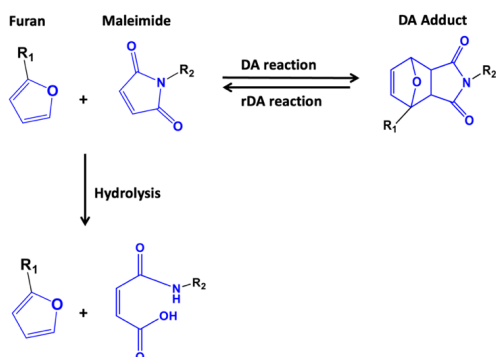
Figure 5 Schematic representation of maleimide furan DA reaction

5   Nanoparticles for Ocular Therapy: Introduction to Polymeric Micelles

Nanoparticles are small particles, typically ranging in size from 1 to 200 nm, that can be made from a variety of materials such as lipids, polymers, and metals. Nanoparticles offer distinct advantages[27], including targeted delivery, controlled release, and convenient administration, rendering them valuable in diverse medical applications, including ocular therapy[150, 151]. Drug loaded nanoparticles have shown great potential in ocular drug delivery by improving the bioavailability and stability of biological entities and chemical entities for improved ocular pharmacokinetics.[150, 152] Their small size allows them to overcome biological barriers, such as the retina, and reach the target site with enhanced drug efficacy.[18] Nanoparticles can also provide controlled release of drugs, protect drugs from (enzymatic) degradation, improve drug solubility and permeability within the retinal structure.[153, 154] In current research, various nanoparticle types are under investigation for ocular applications, among which polymeric nanoparticles including micelles, nanogels and polymersomes and lipid nanoparticles (Figure 6). This section will specifically emphasize polymeric micelles due to their utilization in this thesis.

Polymeric micelles: presenting flower like micelles

Polymeric micellar nanoparticles have emerged as a promising platform for drug delivery due to their attractive physicochemical properties and the ability to encapsulate and conjugate

different types of drugs.[155-157] They are formed by the self-assembly of amphiphilic block copolymers in an aqueous solution, resulting in a core-shell structure.[158, 159] The hydrophobic core can solubilize and retain hydrophobic drugs, while the hydrophilic shell ensures their colloidal stability in aqueous environment. Micelles' morphology and dimensions can be precisely tailored through the manipulation of polymer composition and molecular weight as well as by the processing conditions.[160] Amphiphilic AB diblock copolymers assemble into star-shaped micelles above their critical micelle concentration (CMC), while ABA triblock copolymers, characterized by a hydrophilic midblock (B) and outer hydrophobic blocks (A), exhibit self-assembly into structures resembling flowers, which are commonly referred to as flower-like micelles (FLM)[161, 162] (Figure 6). Remarkably, it has been demonstrated that FLM typically boast a lower CMC and enhanced stability compared to their star-like counterparts.[161-163] These characteristics hold significant promise for the solubilization and delivery of hydrophobic drugs.[26] For the development of a truly impactful nanomedicine platform for ocular drug delivery, the formulation must prioritize robust stability to prevent premature disintegration and drug release. Although FLM generally have good stability, a commonly employed approach to further enhance their in vivo stability involves core-crosslinking.

Core-crosslinked micelles

Core-crosslinked polymeric micelles (CCPMs) have gained attention as a promising drug delivery platform in recent years.[161, 164, 165] These micelles are formed by covalent crosslinking of the hydrophobic core, providing enhanced stability. Factors such as particle size, surface charge, and composition can influence the behavior of these colloidal particles in the ocular environment, including biodistribution and cellular uptake[27, 154] CCPMs are highly tunable, and can easily be modified with functional groups for conjugation of drugs, targeting moieties, and imaging agents.[150, 155] In general, CCPMs show great potential in ocular drug delivery[155, 166] and their ability to encapsulate and release drugs will also be presented in this thesis.
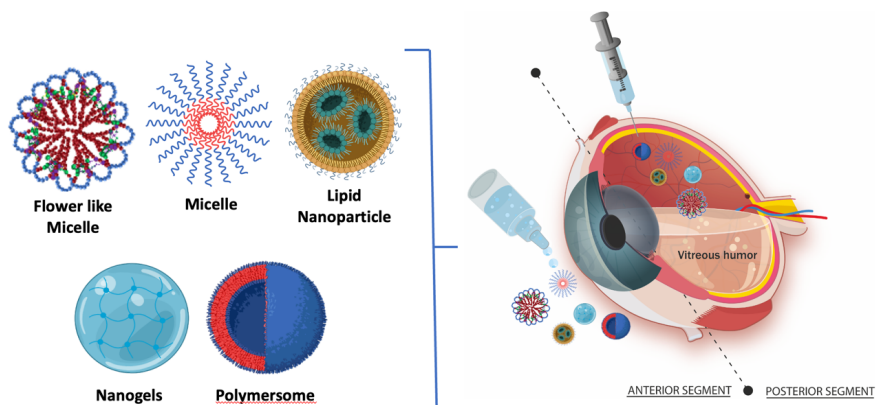
Figure 6 Nanoparticles in ocular therapy, some images of particles were created with BioRender.com.

6   Aim and Outline of this Thesis

This thesis is a product of research conducted within the OcuTher Innovative Training Network (ITN), which aimed to train a new generation of early-stage researchers (ESRs) to tackle the complexities of ocular drug delivery. The focus of OcuTher was the evaluation of various compounds, including both existing drugs and potential drug candidates, in conjunction with innovative drug delivery systems, all with the goal of treating retinal diseases like macular degeneration, diabetic retinopathies, and ocular inflammation. The OcuTher consortium united academic and industry experts, channeling their expertise to advance ocular therapeutics. The research detailed in this thesis primarily contributed to development and assessment of novel biomaterials for sustained intraocular drug delivery, and contributed to studies focused on the biodistribution, efficacy, and safety of candidate drugs in innovative ocular formulations. This thesis specifically aimed to address the challenges of intravitreal drug delivery by developing sustained/controlled-release formulations based on Diels-Alder (DA) crosslinked biomaterials, such as hydrogels and core- crosslinked polymeric micelles. The primary objectives were to create novel injectable formulations for easy administration through small needles, providing prolonged drug release and enhancing drug penetration into the retina.

Chapter 2 highlights hydrogel formulations for intravitreal protein delivery to the posterior segment of the eye to improve therapeutic outcome and patient compliance. The rational design of intravitreally administered drug delivery systems, both preclinical and clinically investigated, is extensively discussed. The currently used polymers, crosslinking mechanisms and methods, *in vitro/in vivo* models, preclinical and clinical advancements are discussed together with the limitations and perspectives of these biomaterials.

Chapter 3, the DA reaction was exploited to crosslink hyaluronic acid-bearing furan groups (HAFU) with 4-arm PEG10K-maleimide (4APM) to yield hydrogels that enable sustained release of bevacizumab, a clinically used therapeutic protein for ocular therapy to treat patients suffering from macular degeneration. The effects of polymer composition and the ratio between functional groups on the physicochemical properties of hydrogels were systematically investigated, together with intravitreal gel stability and protein release kinetics.

Chapter 4 describes the *in vivo* pharmacokinetic profile and ocular safety of hyaluronic acid-PEG-based DA *in situ* forming hydrogels for sustained intraocular delivery of bevacizumab to investigate the suitability of this formulation for ocular therapies.

Chapter 5 introduces a novel in situ forming thermosensitive hydrogel system based on two thermosensitive ABA triblock copolymers bearing either furan or maleimide moieties. The formulation was designed to rapidly form a polymer network at body temperature by physical self-assembly of the thermosensitive blocks. The rapidly formed physical network is subsequently stabilized by the DA chemical crosslinking in the hydrophobic domains of the polymer network. The sustained release of an anti-VEGF antibody fragment with or without the corticosteroid dexamethasone was investigated to get insight into the potential of the system as an intraocular drug delivery system.

Additionally, i**n Chapter 6,** an injectable DA core-crosslinked flower-like micelle formulation was designed using previously developed thermosensitive ABA block copolymers (where A represents a thermosensitive block and B represents a permanently hydrophilic block). This design aims to enhance retinal tissue penetration and intracellular drug delivery, potentially making it useful in ocular therapy**.** Preliminary ocular safety and particle kinetics were evaluated in a rat eye model.

Finally, **Chapter 7** provides a summarizing discussion of the findings of the research chapters of this thesis, together with recommendations for further improvements. Furthermore, in **Chapter 7** industrial development of the potential pharmaceutical product described in **Chapter 3** was discussed to gain more insights into potential upscaling of such kinds of biomaterials.

REFERENCES

[1] D.F. Williams, On the nature of biomaterials, Biomaterials, 30 (2009) 5897-5909.

[2] A. Patel, K. Cholkar, V. Agrahari, A.K. Mitra, Ocular drug delivery systems: An overview, World J Pharmacol, 2 (2013) 47-64.

[3] U.N. Das, Diabetic macular edema, retinopathy and age-related macular degeneration as inflammatory conditions, Arch Med Sci, 12 (2016) 1142-1157.

[4] T.Y. Wong, U. Chakravarthy, R. Klein, P. Mitchell, G. Zlateva, R. Buggage, K. Fahrbach, C. Probst, I. Sledge, The natural history and prognosis of neovascular age-related macular degeneration: a systematic review of the literature and meta-analysis, Ophthalmology, 115 (2008) 116-126.

[5] R. Cheloni, S.A. Gandolfi, C. Signorelli, A. Odone, Global prevalence of diabetic retinopathy: protocol for a systematic review and meta-analysis, BMJ Open, 9 (2019) e022188.

[6] A. Mandal, D. Pal, V. Agrahari, H.M. Trinh, M. Joseph, A.K. Mitra, Ocular delivery of proteins and peptides: Challenges and novel formulation approaches, Adv Drug Deliv Rev, 126 (2018) 67-95.

[7] J. Jacob, H. Brie, A. Leys, L. Levecq, F. Mergaerts, K. Denhaerynck, S. Vancayzeele, E. Van Craeyveld, I. Abraham, K. MacDonald, Six-year outcomes in neovascular age-related macular degeneration with ranibizumab, Int J Ophthalmol, 10 (2017) 81-90.

[8] S.A. Gaballa, U.B. Kompella, O. Elgarhy, A.M. Alqahtani, B. Pierscionek, R.G. Alany, H. Abdelkader, Corticosteroids in ophthalmology: drug delivery innovations, pharmacology, clinical applications, and future perspectives, Drug Deliv Transl Res, 11 (2021) 866-893.

[9] J. Barar, A.R. Javadzadeh, Y. Omidi, Ocular novel drug delivery: impacts of membranes and barriers, Expert Opin Drug Deliv, 5 (2008) 567-581.

[10] V. Agrahari, V. Agrahari, A. Mandal, D. Pal, A.K. Mitra, How are we improving the delivery to back of the eye? Advances and challenges of novel therapeutic approaches, Expert Opin Drug Deliv, 14 (2017) 1145-1162.

[11] H.A. Quigley, I.P. Pollack, T.S. Harbin, Pilocarpine Ocuserts: long-term clinical trials and selected pharmacodynamics, Archives of ophthalmology, 93 (1975) 771-775.

[12] N. Navneet, S. Sukhmanpreet, M. Prince Ahad, C. Mandeep Singh, A. Manisha, K. Deepinder Jeet, K. Rahul, S. Abhay, Priyanka, K. Nishant, Ocuserts: A novel ocular-drug delivery method: An update, World Journal of Biology Pharmacy and Health Sciences, 13 (2023) 470-477.

[13] A. Chan, L.S. Leung, M.S. Blumenkranz, Critical appraisal of the clinical utility of the dexamethasone intravitreal implant (Ozurdex) for the treatment of macular edema related to branch retinal vein occlusion or central retinal vein occlusion, Clin Ophthalmol, 5 (2011) 1043-1049.

[14] T. Sherman, V. Raman, Incomplete scleral penetration of dexamethasone (Ozurdex) intravitreal implant, BMJ Case Rep, 11 (2018) e227055.

[15] J.C. Imperiale, G.B. Acosta, A. Sosnik, Polymer-based carriers for ophthalmic drug delivery, J Controlled Release, 285 (2018) 106-141.

1

[16] V.P. Ranta, E. Mannermaa, K. Lummepuro, A. Subrizi, A. Laukkanen, M. Antopolsky, L. Murtomaki, M. Hornof, A. Urtti, Barrier analysis of periocular drug delivery to the posterior segment, J Control Release, 148 (2010) 42-48.

[17] V. Agrahari, A. Mandal, V. Agrahari, H.M. Trinh, M. Joseph, A. Ray, H. Hadji, R. Mitra, D. Pal, A.K. Mitra, A comprehensive insight on ocular pharmacokinetics, Drug delivery and translational research, 6 (2016) 735-754.

[18] E.M. Del Amo, A.K. Rimpela, E. Heikkinen, O.K. Kari, E. Ramsay, T. Lajunen, M. Schmitt, L. Pelkonen, M. Bhattacharya, D. Richardson, A. Subrizi, T. Turunen, M. Reinisalo, J. Itkonen, E. Toropainen, M. Casteleijn, H. Kidron, M. Antopolsky, K.S. Vellonen, M. Ruponen, A. Urtti, Pharmacokinetic aspects of retinal drug delivery, Prog Retin Eye Res, 57 (2017) 134-185.

[19] S. Mandal, K. Shiva, K.P. Kumar, S. Goel, R.K. Patel, S. Sharma, R. Chaudhary, A. Bhati, N. Pal, A.K. Dixit, Ocular drug delivery system (ODDS): Exploration the challenges and approaches to improve ODDS, Journal of Pharmaceutical and Biological Sciences, 9 (2021) 88-94.

[20] W. Shatz, J. Aaronson, S. Yohe, R.F. Kelley, Y.N. Kalia, Strategies for modifying drug residence time and ocular bioavailability to decrease treatment frequency for back of the eye diseases, Expert Opin Drug Deliv, 16 (2018) 43–57.

[21] R.C. Cooper, H. Yang, Hydrogel-based ocular drug delivery systems: Emerging fabrication strategies, applications, and bench-to-bedside manufacturing considerations, J Control Release, 306 (2019) 29-39.

[22] J.J.K. Derwent, W.F. Mieler, Thermoresponsive hydrogels as a new ocular drug delivery platform to the posterior segment of the eye., Trans Am Ophthalmol Soc, 106 (2008) 206-214.

[23] S.K. Kushwaha, P. Saxena, A. Rai, Stimuli sensitive hydrogels for ophthalmic drug delivery: A review, Int J Pharm Investig, 2 (2012) 54-60.

[24] B.C. Ilochonwu, A. Urtti, W.E. Hennink, T. Vermonden, Intravitreal hydrogels for sustained release of therapeutic proteins, J. Controlled Release, 326 (2020) 419-441.

[25] R.C. Nagarwal, R. Kumar, J.K. Pandit, Chitosan coated sodium alginate-chitosan nanoparticles loaded with 5-FU for ocular delivery: in vitro characterization and in vivo study in rabbit eye, Eur J Pharm Sci, 47 (2012) 678-685.

[26] S. Jiang, Y.L. Franco, Y. Zhou, J. Chen, Nanotechnology in retinal drug delivery, Int J Ophthalmol, 11 (2018) 1038-1044.

[27] R. Bisht, A. Mandal, J.K. Jaiswal, I.D. Rupenthal, Nanocarrier mediated retinal drug delivery: overcoming ocular barriers to treat posterior eye diseases, Wiley Interdiscip Rev Nanomed Nanobiotechnol, 10 (2018).

[28] S. Tavakoli, K. Peynshaert, T. Lajunen, J. Devoldere, E.M. Del Amo, M. Ruponen, S.C. De Smedt, K. Remaut, A. Urtti, Ocular barriers to retinal delivery of intravitreal liposomes: Impact of vitreoretinal interface, J Control Release, 328 (2020) 952-961.

[29] V. Junnuthula, A. Sadeghi Boroujeni, S. Cao, S. Tavakoli, R. Ridolfo, E. Toropainen, M. Ruponen, J.C.M. van Hest, A. Urtti, Intravitreal Polymeric Nanocarriers with Long Ocular Retention and Targeted Delivery to the Retina and Optic Nerve Head Region, Pharmaceutics, 13 (4) (2021) 445.

[30] A. Pandhare, P. Bhatt, Y. Pathak, Nanomaterials for ocular tissue engineering and regeneration, in: Advanced 3D-Printed Systems and Nanosystems for Drug Delivery and Tissue Engineering, 2020, pp. 255-275.

[31] X. Kong, W. Xu, C. Zhang, W. Kong, Chitosan temperature-sensitive gel loaded with drug microspheres has excellent effectiveness, biocompatibility and safety as an ophthalmic drug delivery system, Exp Ther Med, 15 (2018) 1442-1448.

[32] I. Bravo-Osuna, V. Andres-Guerrero, A. Arranz-Romera, S. Esteban-Perez, I.T. Molina-Martinez, R. Herrero-Vanrell, Microspheres as intraocular therapeutic tools in chronic diseases of the optic nerve and retina, Adv Drug Deliv Rev, 126 (2018) 127-144.

[33] ClinicalTrials.gov, Effect of Intravitreal Long Acting Dexamethasone Implant, Ozurdex in Patients With Diabetic Macular Edema, in, https://clinicaltrials.gov/ct2/show/NCT01698749, 2012.

[34] J.E. Chang-Lin, M. Attar, A.A. Acheampong, M.R. Robinson, S.M. Whitcup, B.D. Kuppermann, D. Welty, Pharmacokinetics and pharmacodynamics of a sustained-release dexamethasone intravitreal implant, Invest Ophthalmol Vis Sci, 52 (2011) 80-86.

[35] J. Wang, A. Jiang, M. Joshi, J. Christoforidis, Drug delivery implants in the treatment of vitreous inflammation, Mediators Inflamm, 2013 (2013) 780634.

[36] J.L. Bourges, C. Bloquel, A. Thomas, F. Froussart, A. Bochot, F. Azan, R. Gurny, D. BenEzra, F. Behar-Cohen, Intraocular implants for extended drug delivery: therapeutic applications, Adv Drug Deliv Rev, 58 (2006) 1182-1202.

[37] G. Chwalik-Pilszyk, A. Wisniewska, Influence of Selected Ophthalmic Fluids on the Wettability and Hydration of Hydrogel and Silicone Hydrogel Contact Lenses-In Vitro Study, Materials, 15 (2022) 930.

[38] L.C. Bengani, K.H. Hsu, S. Gause, A. Chauhan, Contact lenses as a platform for ocular drug delivery, Expert Opin Drug Deliv, 10 (2013) 1483-1496.

[39] D.-W. Cho, J.-S. Lee, J. Jang, J.W. Jung, J.H. Park, F. Pati, Natural, synthetic and semi-synthetic polymers, in: Organ Printing, Morgan & Claypool Publishers, 2015, pp. 7-1-7-10.

[40] C. Buckley, E.J. Murphy, T.R. Montgomery, I. Major, Hyaluronic Acid: A Review of the Drug Delivery Capabilities of This Naturally Occurring Polysaccharide, Polymers, 14 (2022) 3442.

[41] A.B. Shekhter, A.L. Fayzullin, M.N. Vukolova, T.G. Rudenko, V.D. Osipycheva, P.F. Litvitsky, Medical applications of collagen and collagen-based materials, Current Medicinal Chemistry, 26 (2019) 506-516.

[42] N. Chen, H. Wang, C. Ling, W. Vermerris, B. Wang, Z. Tong, Cellulose-based injectable hydrogel composite for pH-responsive and controllable drug delivery, Carbohydr Polym, 225 (2019) 115207.

[43] Z. Zhang, J. Ni, L. Chen, L. Yu, J. Xu, J. Ding, Biodegradable and thermoreversible PCLA-PEG-PCLA hydrogel as a barrier for prevention of post-operative adhesion, Biomaterials, 32 (2011) 4725-4736.

1

[44] A.M. Alhalafi, Applications of polymers in intraocular drug delivery systems, Oman J Ophthalmol, 10 (2017) 3-8.

[45] W.C. Lee, Y.C. Li, I.M. Chu, Amphiphilic poly(D,L-lactic acid)/poly(ethylene glycol)/poly(D,L-lactic acid) nanogels for controlled release of hydrophobic drugs, Macromol Biosci, 6 (2006) 846-854.

[46] M.A. Haq, Y. Su, D. Wang, Mechanical properties of PNIPAM based hydrogels: A review, Mater Sci Eng C Mater Biol Appl, 70 (2017) 842-855.

[47] R. Hoogenboom, Poly(2-oxazoline)s: a polymer class with numerous potential applications, Angew Chem Int Ed Engl, 48 (2009) 7978-7994.

[48] M.J. Alonso, A. Sanchez, The potential of chitosan in ocular drug delivery, J Pharm Pharmacol, 55 (2003) 1451-1463.

[49] R.R. Barbucci, Novel carboxymethylcellulose-based microporous hydrogels suitable for drug delivery, Journal of Biomaterials Science, Polymer Edition, 15 (2004) 607-619.

[50] Z. Chen, Z. Lv, Y. Sun, Z. Chi, G. Qing, Recent advancements in polyethyleneimine-based materials and their biomedical, biotechnology, and biomaterial applications, J Mater Chem B, 8 (2020) 2951-2973.

[51] M.M. Andersson, R. Hatti-Kaul, Protein stabilising effect of polyethyleneimine, J Biotechnology, 72 (1999) 21-31.

[52] H. Hamedi, S. Moradi, S.M. Hudson, A.E. Tonelli, M.W. King, Chitosan based bioadhesives for biomedical applications: A review, Carbohydr Polym, 282 (2022) 119100.

[53] R. Ahmad Raus, W.M.F. Wan Nawawi, R.R. Nasaruddin, Alginate and alginate composites for biomedical applications, Asian J Pharm Sci, 16 (2021) 280-306.

[54] K.Y. Lee, D.J. Mooney, Alginate: properties and biomedical applications, Prog Polym Sci, 37 (2012) 106-126.

[55] T. Ito, I.P. Fraser, Y. Yeo, C.B. Highley, E. Bellas, D.S. Kohane, Anti-inflammatory function of an in situ cross-linkable conjugate hydrogel of hyaluronic acid and dexamethasone, Biomaterials, 28 (2007) 1778-1786.

[56] A. Famili, K. Rajagopal, Bio-Orthogonal Cross-Linking Chemistry Enables In Situ Protein Encapsulation and Provides Sustained Release from Hyaluronic Acid Based Hydrogels, Mol Pharm, 14 (2017) 1961-1968.

[57] J.H. Sze, J.C. Brownlie, C.A. Love, Biotechnological production of hyaluronic acid: a mini review, 3 Biotech, 6 (2016) 67.

[58] W. Chaiyasan, S.P. Srinivas, W. Tiyaboonchai, Mucoadhesive chitosan-dextran sulfate nanoparticles for sustained drug delivery to the ocular surface, J Ocul Pharmacol Ther, 29 (2013) 200-207.

[59] S. Ramasundaram, G. Saravanakumar, S. Sobha, T.H. Oh, Dextran Sulfate Nanocarriers: Design, Strategies and Biomedical Applications, Int J Mol Sci, 24 (2022).

[60] R. Lalani, L. Liu, Synthesis, characterization, and electrospinning of zwitterionic poly(sulfobetaine methacrylate), Polymer, 52 (2011) 5344-5354.

[61] R. Xie, Y. Tian, S. Peng, L. Zhang, Y. Men, W. Yang, Poly(2-methacryloyloxyethyl phosphorylcholine)-based biodegradable nanogels for controlled drug release, Polymer Chemistry, 9 (2018) 4556-4565.

[62] A. Birke, J. Ling, M. Barz, Polysarcosine-containing copolymers: Synthesis, characterization, self-assembly, and applications, Progress in Polymer Science, 81 (2018) 163-208.

[63] B. Osi, M. Khoder, A.A. Al-Kinani, R.G. Alany, Pharmaceutical, biomedical and ophthalmic applications of biodegradable polymers (BDPs): literature and patent review, Pharm Development Technology, 27 (2022) 341-356.

[64] E.M. Elmowafy, M. Tiboni, M.E. Soliman, Biocompatibility, biodegradation and biomedical applications of poly(lactic acid)/poly(lactic-co-glycolic acid) micro and nanoparticles, Journal of Pharmaceutical Investigation, 49 (2019) 347-380.

[65] R. Boia, P.A.N. Dias, J.M. Martins, C. Galindo-Romero, I.D. Aires, M. Vidal-Sanz, M. Agudo-Barriuso, H.C. de Sousa, A.F. Ambrosio, M.E.M. Braga, A.R. Santiago, Porous poly(epsilon-caprolactone) implants: A novel strategy for efficient intraocular drug delivery, J Control Release, 316 (2019) 331-348.

[66] E. Archer, M. Torretti, S. Madbouly, Biodegradable polycaprolactone (PCL) based polymer and composites, Physical Sciences Reviews, (2021) 0074.

[67] A. D'Souza A, R. Shegokar, Polyethylene glycol (PEG): a versatile polymer for pharmaceutical applications, Expert Opin Drug Deliv, 13 (2016) 1257-1275.

[68] E.H. Marzieh Najafi, Wim E. Hennink,Tina Vermonden, Poly(Nisopropylacrylamide): Physicochemical Properties and Biomedical Applications, John Wiley Sons, Ltd, 2018.

[69] J. Heller, Ocular delivery using poly(ortho esters), Adv Drug Deliv Rev, 57 (2005) 2053-2062.

[70] N. Kumar, R.S. Langer, A.J. Domb, Polyanhydrides: an overview, Advanced Drug Delivery Reviews, 54 (2002) 889-910.

[71] C.-C. Chu, Biodegradable polymeric biomaterials: an updated overview, Biomaterials, (2007) 6-1-6-22.

[72] P. Bawa, V. Pillay, Y.E. Choonara, L.C. du Toit, Stimuli-responsive polymers and their applications in drug delivery, Biomedical Materials, 4 (2009) 022001.

[73] P. Zarrintaj, J.D. Ramsey, A. Samadi, Z. Atoufi, M.K. Yazdi, M.R. Ganjali, L.M. Amirabad, E. Zangene, M. Farokhi, K. Formela, M.R. Saeb, M. Mozafari, S. Thomas, Poloxamer: A versatile tri-block copolymer for biomedical applications, Acta Biomater, 110 (2020) 37-67.

[74] M.J. Ansari, R.R. Rajendran, S. Mohanto, U. Agarwal, K. Panda, K. Dhotre, R. Manne, A. Deepak, A. Zafar, M. Yasir, S. Pramanik, Poly(N-isopropylacrylamide)-Based Hydrogels for Biomedical Applications: A Review of the State-of-the-Art, Gels, 8 (2022) 454.

[75] K.M. Huh, H.C. Kang, Y.J. Lee, Y.H. Bae, pH-sensitive polymers for drug delivery, Macromol Res, 20 (2012) 224-233.

[76] E. Cheah, M. Bansal, L. Nguyen, A. Chalard, J. Malmstrom, S.J. O'Carroll, B. Connor, Z. Wu, D. Svirskis, Electrically responsive release of proteins from conducting polymer hydrogels, Acta Biomater, 158 (2023) 87-100.

[77] J.R. Smith, Conducting Polymers as Drug Release Systems, in: D. Lamprou (Ed.) Nano- and Microfabrication Techniques in Drug Delivery : Recent Developments and Future Prospects, Springer International Publishing, Cham, 2023, 1-19.

[78] M. Bansal, A. Dravid, Z. Aqrawe, J. Montgomery, Z. Wu, D. Svirskis, Conducting polymer hydrogels for electrically responsive drug delivery, J Control Release, 328 (2020) 192-209.

[79] J. Cui, A. Del Campo, Photo-responsive polymers: properties, synthesis and applications, in: M.R. Aguilar, J. San Román (Eds.) Smart Polymers and their Applications, Woodhead Publishing, 2014, pp. 93-133.

[80] P. Xiao, J. Zhang, J. Zhao, M.H. Stenzel, Light-induced release of molecules from polymers, Progress in Polymer Science, 74 (2017) 1-33.

[81] E.R. Ruskowitz, C.A. DeForest, Photoresponsive biomaterials for targeted drug delivery and 4D cell culture, Nature Reviews Materials, 3 (2018) 17087.

[82] M. Chelu, A.M. Musuc, Polymer Gels: Classification and Recent Developments in Biomedical Applications, Gels, 9 (2023) 161.

[83] A.S. Chauhan, Dendrimers for Drug Delivery, Molecules, 23 (2018).

[84] A.D. Jenkins, P. Kratochvíl, R.F.T. Stepto, U.W. Suter, Glossary of basic terms in polymer science (IUPAC Recommendations 1996), Pure Applied Chemistry, 68 (1996) 2287-2311.

[85] G. Odian, Principles of polymerization, John Wiley & Sons, 2004.

[86] C. Liu, C.-Y. Hong, C.-Y. Pan, Polymerization techniques in polymerization-induced self-assembly (PISA), Polymer Chemistry, 11 (2020) 3673-3689.

[87] G. Yilmaz, Y. Yagci, Light-induced step-growth polymerization, Progress in Polymer Science, 100 (2020).

[88] K. Parkatzidis, H.S. Wang, N.P. Truong, A. Anastasaki, Recent Developments and Future Challenges in Controlled Radical Polymerization: A 2020 Update, Chem, 6 (2020) 1575-1588.

[89] D. Braun, Origins and Development of Initiation of Free Radical Polymerization Processes, Int J Polymer Science, 2009 (2009) 1-10.

[90] C. Barner-Kowollik, P. Vana, T.P. Davis, The Kinetics of Free-Radical Polymerization, in: Handbook of Radical Polymerization, 2002, pp. 187-261.

[91] D.J. Siegwart, J.K. Oh, K. Matyjaszewski, ATRP in the design of functional materials for biomedical applications, Prog Polym Sci, 37 (2012) 18-37.

[92] T.E. Patten, K. Matyjaszewski, Atom Transfer Radical Polymerization and the Synthesis of Polymeric Materials, Adv Mater, 10 (1998) 901-915.

[93] C. Boyer, N.A. Corrigan, K. Jung, D. Nguyen, T.K. Nguyen, N.N. Adnan, S. Oliver, S. Shanmugam, J. Yeow, Copper-Mediated Living Radical Polymerization (Atom Transfer Radical Polymerization

1

and Copper(0) Mediated Polymerization): From Fundamentals to Bioapplications, Chem Rev, 116 (2016) 1803-1949.

[94] A. Mühlebach, S.G. Gaynor, K. Matyjaszewski, Synthesis of Amphiphilic Block Copolymers by Atom Transfer Radical Polymerization (ATRP), Macromolecules, 31 (1998) 6046-6052.

[95] N.A. Peppas, A.S. Hoffman, 1.3.2E - Hydrogels, in: W.R. Wagner, S.E. Sakiyama-Elbert, G. Zhang, M.J. Yaszemski (Eds.) Biomaterials Science (Fourth Edition), Academic Press, 2020, pp. 153-166.

[96] N.A. Peppas, A.G. Mikos, Preparation methods and structure of hydrogels, in: Hydrogels in medicine and pharmacy, CRC press, 2019, pp. 1-26.

[97] N.A. Peppas, B.D. Barr-Howell, Characterization of the cross-linked structure of hydrogels, in: Hydrogels in medicine and pharmacy, CRC press, 2019, pp. 27-56.

[98] X. Zhao, X. Chen, H. Yuk, S. Lin, X. Liu, G. Parada, Soft Materials by Design: Unconventional Polymer Networks Give Extreme Properties, Chem Rev, 121 (2021) 4309-4372.

[99] A.S. Hoffman, Hydrogels for biomedical applications, Adv Drug Delivery Rev, 64 (2002) 18-23.

[100] Q. Chai, Y. Jiao, X. Yu, Hydrogels for Biomedical Applications: Their Characteristics and the Mechanisms behind Them, Gels, 3 (2017) 6.

[101] S. Naahidi, M. Jafari, M. Logan, Y. Wang, Y. Yuan, H. Bae, B. Dixon, P. Chen, Biocompatibility of hydrogel-based scaffolds for tissue engineering applications, Biotechnol Adv, 35 (2017) 530-544.

[102] X. Xue, Y. Hu, Y. Deng, J. Su, Recent Advances in Design of Functional Biocompatible Hydrogels for Bone Tissue Engineering, Adv Funct Mater, 31 (2021) 2009432.

[103] B.V. Slaughter, S.S. Khurshid, O.Z. Fisher, A. Khademhosseini, N.A. Peppas, Hydrogels in regenerative medicine, Adv Mater, 21 (2009) 3307-3329.

[104] N. Contessi Negrini, M. Bonnetier, G. Giatsidis, D.P. Orgill, S. Fare, B. Marelli, Tissue-mimicking gelatin scaffolds by alginate sacrificial templates for adipose tissue engineering, Acta biomaterialia, 87 (2019) 61-75.

[105] C.A. Dreiss, Hydrogel design strategies for drug delivery, Current Opinion in Colloid & Interface Science, 48 (2020) 1-17.

[106] R. Censi, P. Di Martino, T. Vermonden, W.E. Hennink, Hydrogels for protein delivery in tissue engineering, J Controlled Release, 161 (2012) 680-692.

[107] S.R. Van Tomme, W.E. Hennink, Biodegradable dextran hydrogels for protein delivery applications, Expert Rev Med Devices, 4 (2007) 147-164.

[108] T. Vermonden, R. Censi, W.E. Hennink, Hydrogels for protein delivery, Chem Rev, 112 (2012) 2853-2888.

[109] C. Ghobril, M.W. Grinstaff, The chemistry and engineering of polymeric hydrogel adhesives for wound closure: a tutorial, Chem Soc Rev, 44 (2015) 1820-1835.

[110] M.W. Grinstaff, Designing hydrogel adhesives for corneal wound repair, Biomaterials, 28 (2007) 5205-5214.

[111] O. Wichterle, D. LÍM, Hydrophilic Gels for Biological Use, Nature, 185 (1960) 117-118.

[112] J. Lamb, T. Bowden, The history of contact lenses, Contact lenses, (2019) 2-17.

[113] R.A. Kyle, D.P. Steensma, M.A. Shampo, Otto Wichterle--Inventor of the First Soft Contact Lenses, Mayo Clin Proc, 91 (2016) e45-46.

[114] F. Ali, I. Khan, J. Chen, K. Akhtar, E.M. Bakhsh, S.B. Khan, Emerging Fabrication Strategies of Hydrogels and Its Applications, Gels, 8 (2022) 205.

[115] S. Bashir, M. Hina, J. Iqbal, A.H. Rajpar, M.A. Mujtaba, N.A. Alghamdi, S. Wageh, K. Ramesh, S. Ramesh, Fundamental Concepts of Hydrogels: Synthesis, Properties, and Their Applications, Polymers, 12 (2020) 2702.

[116] T.C. Ho, C.C. Chang, H.P. Chan, T.W. Chung, C.W. Shu, K.P. Chuang, T.H. Duh, M.H. Yang, Y.C. Tyan, Hydrogels: Properties and Applications in Biomedicine, Molecules, 27 (2022) 2902.

[117] N.A. Peppas, S.R. Lustig, Solute diffusion in hydrophilic network structures, in: Hydrogels in medicine and pharmacy, CRC press (2019) 57-84.

[118] O. Lieleg, K. Ribbeck, Biological hydrogels as selective diffusion barriers, Trends Cell Biol, 21 (2011) 543-551.

[119] C.H. Wang, Y.S. Hwang, P.R. Chiang, C.R. Shen, W.H. Hong, G.H. Hsiue, Extended release of bevacizumab by thermosensitive biodegradable and biocompatible hydrogel, Biomacromolecules, 13 (2012) 40-48.

[120] B.C. Ilochonwu, M. Mihajlovic, R.F. Maas-Bakker, C. Rousou, M. Tang, M. Chen, W.E. Hennink, T. Vermonden, Hyaluronic Acid-PEG-Based Diels-Alder In Situ Forming Hydrogels for Sustained Intraocular Delivery of Bevacizumab, Biomacromolecules, 23 (2022) 2914-2929.

[121] F. Raza, H. Zafar, Y. Zhu, Y. Ren, A. Ullah, A.U. Khan, X. He, H. Han, M. Aquib, K.O. Boakye-Yiadom, L. Ge, A Review on Recent Advances in Stabilizing Peptides/Proteins upon Fabrication in Hydrogels from Biodegradable Polymers, Pharmaceutics, 10 (2018) 16.

[122] J. Li, DJ. Mooney, Designing hydrogels for controlled drug delivery, Nat Rev Mater, 1 (2016) 1-17.

[123] T. Vermonden, S.S. Jena, D. Barriet, R. Censi, J. van der Gucht, W.E. Hennink, R.A. Siegel, Macromolecular Diffusion in Self-Assembling Biodegradable Thermosensitive Hydrogels, Macromolecules, 43 (2010) 782-789.

[124] X. Xu, Y. Weng, L. Xu, H. Chen, Sustained release of Avastin(R) from polysaccharides cross-linked hydrogels for ocular drug delivery, Int J Biol Macromol, 60 (2013) 272-276.

[125] W.E. Hennink, C.F. van Nostrum, Novel crosslinking methods to design hydrogels, Adv Drug Delivery Rev, 54 (2002) 13-36.

[126] W. Hu, Z. Wang, Y. Xiao, S. Zhang, J. Wang, Advances in crosslinking strategies of biomedical hydrogels, Biomater Sci, 7 (2019) 843-855.

1

[127] K. Saini, Preparation method, Properties and Crosslinking of hydrogel: a review, PharmaTutor, 5 (2017) 27-36.

[128] J. Kim, Y.P. Kong, S.M. Niedzielski, R.K. Singh, A.J. Putnam, A. Shikanov, Characterization of the crosslinking kinetics of multi-arm poly(ethylene glycol) hydrogels formed via Michael-type addition, Soft Matter, 12 (2016) 2076-2085.

[129] C.M. Nimmo, M.S. Shoichet, Regenerative biomaterials that "click": simple, aqueous-based protocols for hydrogel synthesis, surface immobilization, and 3D patterning, Bioconjug Chem, 22 (2011) 2199-2209.

[130] Y. Song, N. Nagai, S. Saijo, H. Kaji, M. Nishizawa, T. Abe, In situ formation of injectable chitosan-gelatin hydrogels through double crosslinking for sustained intraocular drug delivery, Mater Sci Eng C Mater Biol Appl, 88 (2018) 1-12.

[131] C. Huin-Amargier, P. Marchal, E. Payan, P. Netter, E. Dellacherie, New physically and chemically crosslinked hyaluronate (HA)-based hydrogels for cartilage repair, J Biomed Mater Res A, 76 (2006) 416-424.

[132] R. Censi, P.J. Fieten, P. di Martino, W.E. Hennink, T. Vermonden, In Situ Forming Hydrogels by Tandem Thermal Gelling and Michael Addition Reaction between Thermosensitive Triblock Copolymers and Thiolated Hyaluronan, Macromolecules, 43 (2010) 5771-5778.

[133] S. Chatterjee, Hui, P. C, Stimuli-Responsive Hydrogels: An Interdisciplinary Overview, London: IntechOpen, 2018.

[134] P. Mahlumba, Y.E. Choonara, P. Kumar, L.C. du Toit, V. Pillay, Stimuli-Responsive Polymeric Systems for Controlled Protein and Peptide Delivery: Future Implications for Ocular Delivery, Molecules, 21 (2016).

[135] F.J. Otero-Espinar, A. Fernández-Ferreiro, M. González-Barcia, J. Blanco-Méndez, A. Luzardo, Chapter 6 - Stimuli sensitive ocular drug delivery systems, in: A.M. Grumezescu (Ed.) Drug Targeting and Stimuli Sensitive Drug Delivery Systems, William Andrew Publishing, 2018, pp. 211-270.

[136] H.M. El-Husseiny, E.A. Mady, L. Hamabe, A. Abugomaa, K. Shimada, T. Yoshida, T. Tanaka, A. Yokoi, M. Elbadawy, R. Tanaka, Smart/stimuli-responsive hydrogels: Cutting-edge platforms for tissue engineering and other biomedical applications, Mater Today Bio, 13 (2022) 100186.

[137] S.R. Van Tomme, G. Storm, W.E. Hennink, In situ gelling hydrogels for pharmaceutical and biomedical applications, Int J Pharm, 355 (2008) 1-18.

[138] S. Awwad, A. Abubakre, U. Angkawinitwong, P.T. Khaw, S. Brocchini, In situ antibody-loaded hydrogel for intravitreal delivery, Eur J Pharm Sci, 137 (2019) 104993.

[139] J. Kaur, M. Saxena, N. Rishi, An Overview of Recent Advances in Biomedical Applications of Click Chemistry, Bioconjug Chem, 32 (2021) 1455-1471.

[140] A. Battigelli, B. Almeida, A. Shukla, Recent Advances in Bioorthogonal Click Chemistry for Biomedical Applications, Bioconjug Chem, 33 (2022) 263-271.

[141] M. van Dijk, D.T.S. Rijkers, R.M.J. Liskamp, C.F. van Nostrum, W.E. Hennink, Synthesis and Applications of Biomedical and Pharmaceutical Polymers via Click Chemistry Methodologies, Bioconjugate Chemistry, 20 (2009) 2001-2016.

[142] M.A. Tasdelen, Diels–Alder "click" reactions: recent applications in polymer and material science, Polymer Chemistry, 2 (2011) 2133-2145.

[143] N.H. Dimmitt, M.R. Arkenberg, M.M. de Lima Perini, J. Li, C.C. Lin, Hydrolytically Degradable PEG-Based Inverse Electron Demand Diels-Alder Click Hydrogels, ACS Biomater Sci Eng, 8 (2022) 4262-4273.

[144] L.J. Smith, S.M. Taimoory, R.Y. Tam, A.E.G. Baker, N. Binth Mohammad, J.F. Trant, M.S. Shoichet, Diels-Alder Click-Cross-Linked Hydrogels with Increased Reactivity Enable 3D Cell Encapsulation, Biomacromolecules, 19 (2018) 926-935.

[145] S.M. Morozova, Recent Advances in Hydrogels via Diels-Alder Crosslinking: Design and Applications, Gels, 9 (2023).

[146] V. Froidevaux, M. Borne, E. Laborbe, R. Auvergne, A. Gandini, B. Boutevin, Study of the Diels–Alder and retro-Diels–Alder reaction between furan derivatives and maleimide for the creation of new materials, RSC Advances, 5 (2015) 37742-37754.

[147] S. Kirchhof, A. Strasser, H.-J. Wittmann, V. Messmann, N. Hammer, A.M. Goepferich, F.P. Brandl, New insights into the cross-linking and degradation mechanism of Diels–Alder hydrogels, J. Mater. Chem. B, 3 (2015) 449-457.

[148] S. Kirchhof, M. Gregoritza, V. Messmann, N. Hammer, A.M. Goepferich, F.P. Brandl, Diels-Alder hydrogels with enhanced stability: First step toward controlled release of bevacizumab, Eur J Pharm Biopharm, 96 (2015) 217-225.

[149] M. Gregoritza, V. Messmann, K. Abstiens, F.P. Brandl, A.M. Goepferich, Controlled Antibody Release from Degradable Thermoresponsive Hydrogels Cross-Linked by Diels-Alder Chemistry, Biomacromolecules, 18 (2017) 2410-2418.

[150] U.B. Kompella, A.C. Amrite, R. Pacha Ravi, S.A. Durazo, Nanomedicines for back of the eye drug delivery, gene delivery, and imaging, Prog Retin Eye Res, 36 (2013) 172-198.

[151] C.H. Tsai, P.Y. Wang, I.C. Lin, H. Huang, G.S. Liu, C.L. Tseng, Ocular Drug Delivery: Role of Degradable Polymeric Nanocarriers for Ophthalmic Application, Int J Mol Sci, 19 (2018) 2830.

[152] N. Omerović, E. Vranić, Application of nanoparticles in ocular drug delivery systems, Health and Technology, 10 (2020) 61-78.

[153] R. Gurny, T. Boye, H. Ibrahim, Ocular therapy with nanoparticulate systems for controlled drug delivery, J Controlled Release, 2 (1985) 353-361.

[154] A. Sadeghi, M. Ruponen, J. Puranen, S. Cao, R. Ridolfo, S. Tavakoli, E. Toropainen, T. Lajunen, V.P. Ranta, J. van Hest, A. Urtti, Imaging, quantitation and kinetic modelling of intravitreal nanomaterials, Int J Pharm, 621 (2022) 121800.

[155] A. Mandal, R. Bisht, I.D. Rupenthal, A.K. Mitra, Polymeric micelles for ocular drug delivery: From structural frameworks to recent preclinical studies, J Controlled Release, 248 (2017) 96-116.

[156] H. Cabral, K. Miyata, K. Osada, K. Kataoka, Block Copolymer Micelles in Nanomedicine Applications, Chem Rev, 118 (2018) 6844-6892.

[157] A. Varela-Moreira, Y. Shi, M.H.A.M. Fens, T. Lammers, W.E. Hennink, R.M. Schiffelers, Clinical application of polymeric micelles for the treatment of cancer, Materials Chemistry Frontiers, 1 (2017) 1485-1501.

[158] Y. Lu, K. Park, Polymeric micelles and alternative nanonized delivery vehicles for poorly soluble drugs, Int J Pharm, 453 (2013) 198-214.

[159] S. Kotta, H.M. Aldawsari, S.M. Badr-Eldin, A.B. Nair, K. Yt, Progress in Polymeric Micelles for Drug Delivery Applications, Pharmaceutics, 14 (2022).

[160] M. Bagheri, J. Bresseleers, A. Varela-Moreira, O. Sandre, S.A. Meeuwissen, R.M. Schiffelers, J.M. Metselaar, C.F. van Nostrum, J.C.M. van Hest, W.E. Hennink, Effect of Formulation and Processing Parameters on the Size of mPEG- b-p(HPMA-Bz) Polymeric Micelles, Langmuir, 34 (2018) 15495-15506.

[161] M. Najafi, N. Kordalivand, M.A. Moradi, J. van den Dikkenberg, R. Fokkink, H. Friedrich, N. Sommerdijk, M. Hembury, T. Vermonden, Native Chemical Ligation for Cross-Linking of Flower-Like Micelles, Biomacromolecules, 19 (2018) 3766-3775.

[162] K.T. Oh, Y.T. Oh, N.M. Oh, K. Kim, D.H. Lee, E.S. Lee, A smart flower-like polymeric micelle for pH-triggered anticancer drug release, Int J Pharm, 375 (2009) 163-169.

[163] E.S. Lee, K.T. Oh, D. Kim, Y.S. Youn, Y.H. Bae, Tumor pH-responsive flower-like micelles of poly(L-lactic acid)-b-poly(ethylene glycol)-b-poly(L-histidine), J Control Release, 123 (2007) 19-26.

[164] M. Talelli, M. Barz, C.J.F. Rijcken, F. Kiessling, W.E. Hennink, T. Lammers, Core-crosslinked polymeric micelles: Principles, preparation, biomedical applications and clinical translation, Nano Today, 10 (2015) 93-117.

[165] C.J.F. Rijcken, F. De Lorenzi, I. Biancacci, R. Hanssen, M. Thewissen, Q. Hu, F. Atrafi, R.M.J. Liskamp, R.H.J. Mathijssen, I.H.C. Miedema, C.W. Menke-van der Houven van Oordt, G. van Dongen, D.J. Vugts, M. Timmers, W.E. Hennink, T. Lammers, Design, development and clinical translation of CriPec(R)-based core-crosslinked polymeric micelles, Adv Drug Deliv Rev, 191 (2022) 114613.

[166] I. Pepic, J. Lovric, J. Filipovic-Grcic, Polymeric micelles in ocular drug delivery: rationale, strategies and challenges, Chemical and Biochemical Engineering Quarterly, 26 (2012) 365-377.
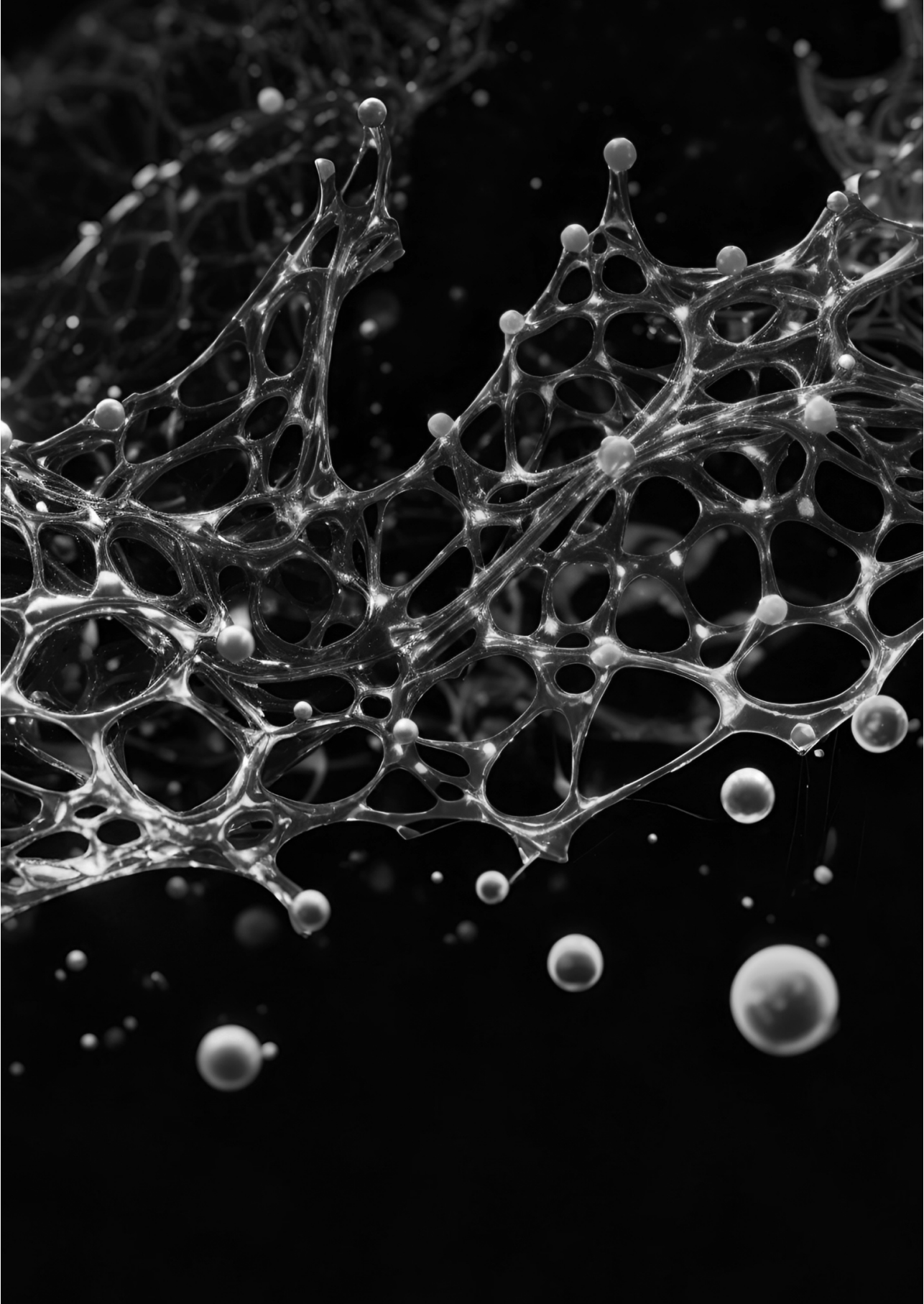
Chapter 2

Intravitreal Hydrogels for Sustained Release of Therapeutic Proteins

Blessing C. Ilochonwu[1], Arto Urtti [2,3], Wim E. Hennink[1], Tina Vermonden[1]

[1]Department of Pharmaceutics, Utrecht Institute for Pharmaceutical Sciences, Faculty of Science, Utrecht University, Universiteitsweg 99, 3584 CG Utrecht, the Netherlands. [2]Centre for Drug Research, Division of Pharmaceutical Biosciences, University of Helsinki, Helsinki, Finland. [3]School of Pharmacy, University of Eastern Finland, Kuopio, Finland.

ABSTRACT

This review highlights how hydrogel formulations can improve intravitreal protein delivery to the posterior segment of the eye in order to increase therapeutic outcome and patient compliance. Several therapeutic proteins have shown excellent clinical successes for the treatment of various intraocular diseases. However, drug delivery to the posterior segment of the eye faces significant challenges due to multiple physiological barriers preventing drugs from reaching the retina, among which intravitreal protein instability and rapid clearance from the site of injection. Hence, frequent injections are required to maintain therapeutic levels. Moreover, because the world population ages, the number of patients suffering from ocular diseases, such as age-related macular degeneration (AMD) and diabetic retinopathy (DR) is increasing and causing increased health care costs. Therefore, there is a growing need for suitable delivery systems able to tackle the current limitations in retinal protein delivery, which also may reduce costs. Hydrogels have shown to be promising delivery systems capable of sustaining release of therapeutic proteins and thus extending their local presence. Here, an extensive overview of preclinically developed intravitreal hydrogels is provided with attention to the rational design of clinically useful intravitreal systems. The currently used polymers, crosslinking mechanisms, in vitro/in vivo models and advancements are discussed together with the limitations and future perspective of these biomaterials.

Keywords: Therapeutic proteins, ocular diseases, retina, anti-VEGF's, sustained protein release

Graphical abstract:
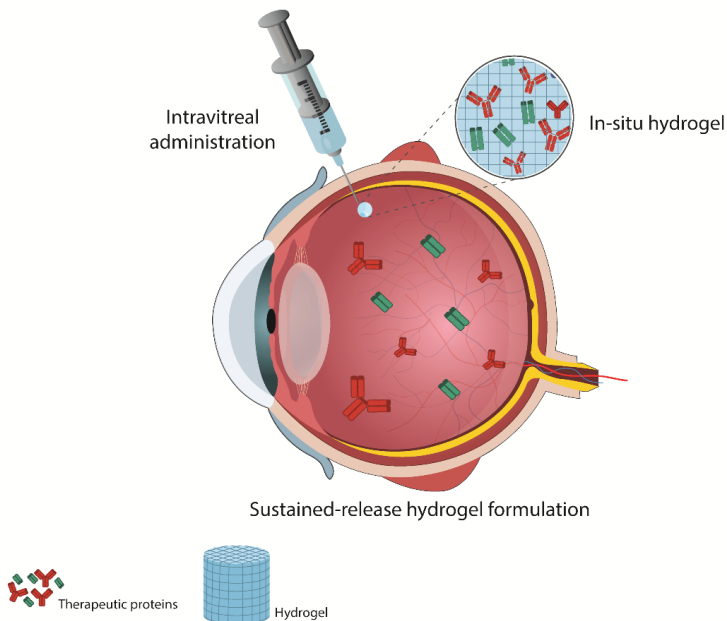
1 INTRODUCTION

Drug delivery to intraocular tissues is one of the major challenges faced by ophthalmologists and formulation scientists because the eye is a highly complex, isolated and specialized organ of the human body. The challenge of drug delivery to this organ is related to the presence of different barriers that prevent exogenous and harmful substances from entering the posterior chamber, in particular, the retina and optic nerve. Vision-threatening disorders are mostly related to abnormalities in intraocular tissues, especially in the retina. The occurrence of such diseases is rapidly increasing in industrialized countries, not only in the ageing populations but also in younger individuals, causing a substantial health problem in modern society. It is estimated that approximately 285 million people worldwide are visually impaired, and 39 million are completely blind.[1, 2] These numbers are expected to double by 2050, representing a significant public health burden.[3, 4]

Conventional eye drops containing low molecular weight drugs are the most commonly used ophthalmic drug formulations. Although they are not suitable for the delivery of therapeutic proteins, they represent 90% of the ocular products present in the market, which is due to ease of manufacturing and scale-up, stability and cost-effectiveness[5]. However, after topical instillation into the lacrimal fluid, drugs are rapidly removed from the ocular surface due to solution drainage and systemic drug absorption across the conjunctiva that lines the inner side of eyelids. Furthermore, the epithelia of the cornea and bulbar conjunctiva are major barriers for drug absorption into the eye. Therefore, only a minimal amount (< 5%) of the administered drug dose reaches the anterior part of the eye, and even a much smaller fraction (<< 1%) reaches the posterior eye segment after topical administration of the drug formulations.[6, 7]. Thus, frequent administration is needed to maintain drug concentrations within the therapeutic window.[4, 8]

A wide range of posterior segment eye pathologies severely impacts vision. These disorders include neovascular age-related macular degeneration (AMD), diabetic retinopathy (DR), diabetic macular edema (DME), retinal vein occlusions (RVO) and diseases that originate from the alteration in the vasculature system of the retina, genetic disorders and eye tumours[9, 10]. Many studies have demonstrated that vascular endothelial growth factor (VEGF) plays a crucial role in the pathogenesis of retinal diseases.[11, 12] Therefore, many therapeutic approaches aim at blocking VEGF signalling by the delivery of intravitreally injected anti-VEGF proteins.[13, 14] The effectiveness of antibodies (bevacizumab, Avastin®), antibody fragments (ranibizumab, Lucentis®), and soluble receptors (aflibercept, Eylea®) have been shown in the treatment of patients with neovascular AMD.[15] However, maintaining sufficient concentrations in the retina after intravitreal injection for an extended period is an important challenge. Monthly injections are burdensome and have resulted in impaired patient compliance[16, 17].

In the past decades, tremendous efforts have been made to improve the disposition of drugs, especially bioactive proteins, in the retina by using different routes of administration and drug delivery vehicles. Several drug delivery technologies such as *in-situ* forming hydrogels, micelles, liposomes, nanoparticles and ocular implants have been developed for ocular applications.[18, 19] *In-situ* forming hydrogels are considered attractive biomaterials, which can be engineered to

offer several benefits, including less frequent administrations, patient comfort and cost reduction. Furthermore, hydrogels that jellify *in-situ* allow loading of therapeutically active compounds during network formation facilitating local delivery and release through a minimally invasive procedure. In the past years, the use of hydrogel has received increased attention as ophthalmic formulation that deliver drugs to the posterior segments.[20-24]

This present review discusses and highlights the clinical success of therapeutic proteins in the treatments for posterior eye diseases and the major limitations in protein delivery to the posterior segment of the eye. Anatomical and physiological barriers in ocular protein delivery are summarized and discussed. It is further conferred how *in-situ* forming hydrogels can improve the long-term release and subsequent exposure of protein-based therapeutics to the posterior segment of the eye, especially to the retina. Different, biodegradable, natural and synthetic hydrogels are presented together with diverse functional groups and crosslinking mechanisms employed to obtain hydrogels with suitable drug release profiles. Guidance on the rational design of ideal drug delivery systems to the posterior segment of the eye is provided in addition to the critical issues related to these delivery technologies.

2 Drug administration to the posterior segment of the eye

2.1 Anatomical and physiological components of the eye

The eye is a highly complex, isolated and specialized organ of the human body. The structure can be classified into two segments: anterior and posterior. The main structures in the anterior chamber are the cornea, conjunctiva, iris, ciliary body, aqueous humour, lens and supporting structures. The posterior chamber encompasses the sclera, choroid, retina, and vitreous body (figure 1). The vitreous cavity contains the vitreous body, which is a transparent, gelatinous mass located between the lens and the retina. The vitreous humour body is a highly hydrated three-dimensional network of hyaluronic acid (HA) ~0.5% and collagen ~0.5% with a water content of ~99%.[25, 26] In order to perceive and recognize objects, light passes through the anterior chamber to the posterior chamber. Light 'travels' the eye through the cornea, the pupil and hits the lens, a convex and transparent disc that focuses and projects the light onto the retina, which is located in the inner layer of the back of the eyeball. The retina is loaded with millions of photoreceptors, which convert light energy into electrical signals that, in turn, the brain receives as impulses to produce images. Drug delivery to the retina can be achieved by various routes such as topical, systemic, intravitreal, sub-retinal, subconjunctival, intracameral and periocular administration. Unfortunately, most patient-friendly administration routes, among which topical and systemic, often result in poor drug bioavailability. Drugs administered to the eye can be restricted by various static and dynamic barriers, as discussed in section 2.2. Particularly, conventional formulations are unable to efficiently deliver proteins into the eye owing to these complex barriers and elimination mechanisms. Therefore, intravitreal injectable depot formulations may solve these limitations by bypassing these barriers and providing a sustained release of proteins reaching intraocular tissues.

2.2 Anatomical and physiological barriers in ocular drug delivery

In-depth knowledge of ocular barriers and pharmacokinetics is essential for the development of effective delivery technologies to the retina. Generally, two types of barriers can be distinguished: 1) anatomical/static barriers representing the different layers of cornea, sclera, conjunctiva, and retina blood-aqueous and blood-retinal barriers. 2) physiological/dynamic barriers including choroidal and conjunctival blood flow, lymphatic clearance, efflux transport, nasolacrimal drainage and tear turnover.

2.2.1 Topical administration

Topically administered eye drops are frequently used to treat anterior segment diseases therapeutically. However, this mode of drug administration is associated with low ocular bioavailability due to dynamic and anatomical barriers.[7] After installation to the eye, the solution drainage in tears and eye blinking results in rapid precorneal drug loss into the nasolacrimal duct, leading to poor absorption of small molecules (< 5%) even into the anterior eye tissues. Importantly, protein drugs have negligible absorption to the anterior eye tissues after topical administration.[22, 27] Most of the dose of small molecular drugs after topical administration is absorbed into the systemic circulation via the highly vascularized nasolacrimal duct, which in turn can result in adverse systemic effects.[5, 28-30] Depending on the drug and the technique of application to the ocular surface, these adverse effects encompasses low blood pressure, reduced heart pulse rate, fatigue, shortness of breath, headaches, allergic reactions and many more.[31] The delivery of topically applied drugs to the posterior eye segment is 1-2 orders of magnitude lower than to the anterior segment due to several reasons.[7, 32] Firstly, the flow of aqueous humor from the posterior to the anterior chamber limits drug access to the intravitreal cavity.[23, 33-34] Also, systemic drug distribution from aqueous humor to the blood circulation of the iris and ciliary body reduces distribution to the posterior eye segment.[7] Finally, the lens forms a dense barrier that limits drug penetration.[35]

2.2.2 Systemic administration

In ophthalmic therapy, systemic administration has been used to deliver antibodies, antibiotics and carbonic anhydrase inhibitors to treat various diseases like endophthalmitis, elevated intraocular pressure and uveitis.[29, 36-38] The presence of the blood-retinal barrier (BRB) regulates the transfer of drugs from the blood circulation to the eye in both directions and can be a major limiting barrier. The blood-ocular barriers consist of a posterior BRB and an anterior blood-aqueous barrier (BAB), and together they represent an impenetrable tight barrier for proteins and other macromolecular therapeutics larger than 2 nm in diameter.[7] The BAB is formed by the inner non-pigmented ciliary epithelium, ciliary muscle capillaries and posterior iris epithelium. The BRB is made up of retinal pigment epithelium (RPE) and inner retinal endothelial capillaries (inner BRB). The RPE is a tight cellular monolayer that is located between the photoreceptors and choroid.[39] It regulates the homeostasis of the neural retina and the outer part of the BRB by controlling, e.g. epithelial transport, secretion, phagocytosis, spatial ion buffering and immune modulation.[40] It is, however, challenging to quantify the permeability of

BAB and BRB separately because, after intravitreal injection or intravenous administration, as drugs can be eliminated from the eye through both of these barriers.[41] Furthermore, because of these physiological barriers, high drug doses and repetitive administration are necessary to achieve adequate therapeutic drug levels with the risk of adverse off-target effects.[42]

2.2.3 Intravitreal administration (IVT)

In clinics, intravitreal drug delivery is the only successful route of administration for proteinaceous drugs (such as anti-VEGF compounds) to the posterior segment of the eye, because of the proximity of the vitreous to the retina.[27, 43-45] Intravitreal administration results in high retinal bioavailability since the drug is directly injected into the vitreous in the vicinity of the retina. After intravitreal injection, protein drugs distribute by Fickian diffusion from the vitreous over the surrounding ocular tissues, reaching the target sites in the retina.[7] The vitreous body does not act as a severe barrier for the diffusion of soluble proteins. However, it might limit the mobility of the administered delivery systems (e.g. drug-loaded nanoparticles) depending on their physicochemical properties and design to deliver proteins to the posterior segment.[46] As mentioned before, one of the main components of the vitreous body, besides water, is hyaluronic acid, a hydrophilic polysaccharide with a molecular weight up to $2-3*10^6$ Da.[7, 47] The vitreous humour has a loose and open structure that allows rapid diffusion of low molecular weight drug molecules since the mesh size in the vitreous network has been estimated to be ~500 nm.[7, 48, 49] Biologics generally administered through intravitreal injections do not exceed a diameter of 10 nm, e.g. bevacizumab (6.5 nm) and ranibizumab (4.1 nm), and therefore based on size only they should not display restricted mobility in the vitreous.[47, 50] The diffusion of aggregates of self-assembled polymers, and nanoparticulate carriers can be restricted.[51] Additionally, positively charged molecules and particles can also be restricted because these cationic entities can bind to the negatively charged hyaluronic acid matrix.[52] Importantly, the movement of macroscopic hydrogels, microspheres and drug-loaded implants are significantly restricted or even absent in the vitreous as they are bigger than the average mesh size in the vitreous network of hyaluronic acid (500 nm). These systems can, therefore, be used as localized reservoirs for sustained drug delivery to the retina. Drug elimination from the vitreous cavity takes place either via anterior or posterior clearance. The anterior route involves drug diffusion in the vitreous to the posterior chamber, followed by convective elimination in the aqueous humor outflow.[33, 53, 54] The posterior route involves drug diffusion to the retina, followed by permeation across the blood-retina barriers into the systemic blood circulation.[33, 55, 40] Pharmacokinetic studies suggest that intravitreally administered biologicals are mostly eliminated from the eye by the anterior route, while a smaller fraction of the dose (≈10%) escapes across the blood-retina barrier. [41]

The posterior clearance is only relevant for therapeutic compounds that can cross the endothelial and epithelial of blood-ocular barriers (typically only small molecular drugs).[55] These barriers are selective, allowing passage of small molecules with lipophilic properties (smaller than 2 nm in diameter) while restricting the permeation of large molecules.[7] For this reason, the half-lives of low molecular weight molecules in the vitreous are typically in the range of 1-10 h, while those of proteins and other macromolecules are in the range of several days.[55] Unfortunately, ocular intravitreal therapies of therapeutic proteins presently applied in the clinics are associated with

serious risks due to their frequent injections. This recurrence results in an increased risk of hemorrhage, retinal detachment, persistent discomfort, degeneration of photoreceptors (PRs), cataract formation, bacterial endophthalmitis and increased intraocular pressure (IOP).[7] New delivery systems are, therefore, urgently needed to prolong the injection intervals for improved treatments of retinal diseases and to reduce side effects. Particularly, tolerability and biocompatibility issues, biodegradability, sterility, reproducible manufacturing and eventually preclinical and clinical performance must be taken into consideration when developing such delivery systems for clinical translation.

2.2.4 Other administration strategies.

Besides topical, systemic and IVT administration, some of the most actively investigated routes to bypass barrier functions in the eye and promote localization of drugs to the back of the eye are periocular, subretinal, intrascleral and suprachoroidal routes.[56-58] Drug and gene delivery through each of these routes of administration can be limited by various static/dynamic barriers, as discussed by del Amo et al.[7] and Rowe-Rendleman et al.[59] Briefly, depending on the exact location, drug diffusion to the posterior segment after injections of drug formulations can be limited by static barriers such as sclera, choroid, Bruch's membrane, RPE tight junctions and retina. At the same time, dynamic restrictions can include choroidal circulation, retinal circulation, subconjunctival-episcleral lymph and blood vessels.[60-62] Despite these limiting barriers, many innovative drug delivery systems and strategies (such as nanoparticles, hydrogels, dendrimers, adenovirus, microspheres and microneedles) are being investigated in animal studies and clinical trials using periocular, subretinal, intrascleral, and suprachoroidal routes of administration.[46, 63-67]

Minimally invasive microneedle-based ocular delivery is worth mentioning as it has the potential to revolutionize the way drug formulations are administered within ocular tissues. Solid and hollow microneedles were initially developed for drug delivery to the skin, where they are used to form micron-sized pores on body surfaces through which drugs can directly enter tissue layers and therefore increase drug permeation. In recent years this technology has been designed to be applied on the ocular surface (e.g. cornea, sclera and suprachoroidal space) to treat diseases in the anterior and posterior segments avoiding complications associated with ocular injections with conventional needles as discussed by Thakur Singh et al.[68] Importantly, this delivery strategy can significantly minimize damage to the ocular tissues, reduce patient discomfort/pain due to its micron-sized needle (typically 25-2000 µm in height) and allow precise localization of drug formulations, as shown by Park et al.[69] and Song et al.[70] Microneedles have been used together with drug delivery systems (e.g. gel formulations, nanoparticle and microparticle suspension) for sustained delivery.[71, 72] The delivery of low molecular weight drugs via microneedles to the anterior segment and the posterior segment has been extensively investigated.[69, 70, 72] While delivery of therapeutic proteins has been developed primarily for the anterior segment, especially in the treatment of corneal neovascularization with limited information about the treatment of posterior eye diseases.[63, 73] Furthermore, it is essential to note that drug distribution to the posterior segment after intrascleral or suprachoroidal microneedle injection can still be limited by the

previously mentioned barriers. Issues concerning forces of injection, IOP, method of injection/retraction and the overall safety of the technology are to be systematically studied together with long term delivery of therapeutic proteins to examine the full benefits of microneedles for ocular applications.[68]
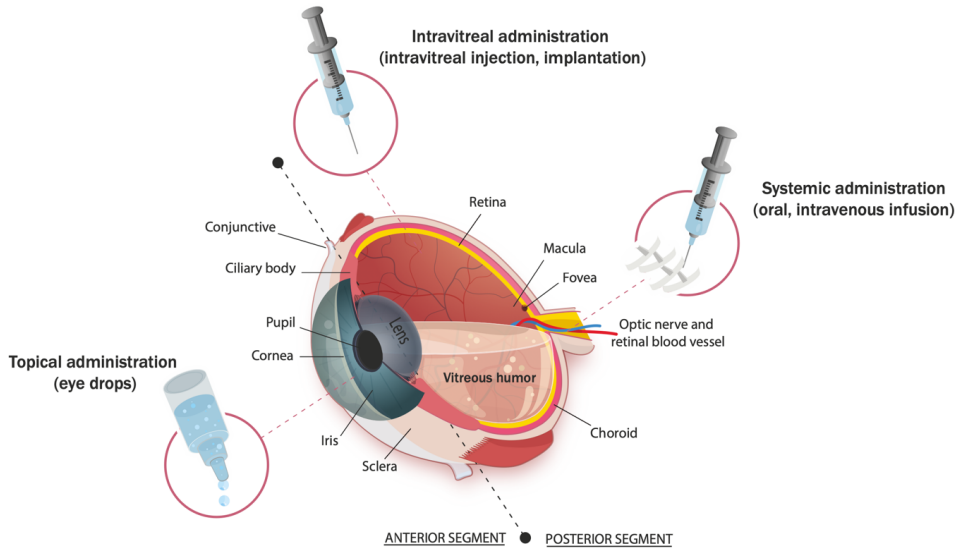
Figure 1 Anatomical components of the eye and frequently used routes of drug administration.

2.3   Clinical success of therapeutic proteins for intraocular diseases

During the last decade, the market of ophthalmic biologicals such as monoclonal antibodies, peptides, aptamers and recombinant proteins has been growing enormously. In 2017, the worldwide sales of monoclonal antibodies for various biomedical applications were estimated to be over 98 billion US$.[74] The success of these biologicals became possible due to the tremendous advances in the fields of genetic engineering, innovative biotechnology, pharmaceutics, identification of druggable targets, formulation and GMP production.[75, 76] Particularly, attention has been given to the pharmaceutical development of anti-VEGF agents to rescue vision in retinal vascular diseases after the validation of the importance of the elevated intraocular levels of vascular endothelial growth factor (VEGF-A). These growth factors are responsible for the angiogenesis and neovascularization in the retina and, therefore, involved in the modulation of posterior segment eye diseases. These diseases include age-related macular degeneration (AMD), diabetic retinopathy (DR),[77] retinal vein occlusion with cystoid macular edema (CME), posterior uveitis.[78] AMD and DR are the leading causes of visual impairment worldwide.[1] The prevalence of these diseases is likely to increase with the rapid growth of the ageing population representing a major public health burden.[1, 79]

AMD is an abnormality of the retinal pigment epithelium (RPE) that leads to the degeneration of the photoreceptors in the macula and consequent loss of central vision in elderly individuals. There are two main forms of AMD: neovascular (wet) and non-neovascular (dry), which affect over

16 million people in Europe and the United States.[80] The wet form represents 90% of cases of severe sight loss in AMD patients and usually affects both eyes. Wet AMD is known as abnormal neovascularization in the central region of the retina.[79] This abnormality results in vision loss due to retinal damage caused by fluid leakage and scar formation. The global cost of wet age-related macular degeneration (AMD) market is estimated to be $6.9 billion in 2018, and in the near future, it is expected to reach $10.4 billion by 2024.[81]

Diabetic retinopathy is the leading cause of blindness in diabetic patients and in working-age adults.[2] It results from damages of blood vessels in the retina, resulting in leakage of blood and other fluids into the retinal tissue followed by cloudy or blurred vision.[2, 82] Diabetic macular edema (DME) is a swelling of the macula and a direct consequence of diabetic retinopathy. In order to cure or slow down the progression of these conditions, bolus intravitreal injections of therapeutic proteins and oligonucleotides such as bevacizumab, ranibizumab, infliximab, aflibercept, pegaptanib are administered.[83] These drugs are generally administered for the neutralization of cytokines and growth factors (Table 1). In this way, photoreceptors in the retina are protected, and angiogenesis caused by the overexpression of vascular endothelial growth factor (VEGF) is prevented. In 2004, the first oligonucleotide-based anti-VEGF aptamer (Macugen®; Pegaptanib; Eyetech, Pfizer) received FDA-approval for neovascular AMD and choroidal neovascularization (CNV) treatments.[84] The monoclonal antibody Avastin® (Bevacizumab; Genentech) received FDA approval in 2004 for metastatic colon cancer treatment. Importantly, bevacizumab is currently used in ophthalmology as an off-label drug for AMD, although not yet FDA approved for these indications. Subsequently, in June 2006, a more effective monoclonal antibody (Lucentis®; ranibizumab; Genentech) was FDA-approved for neovascular AMD and DME therapy. Ranibizumab (48 kDa) is a Fab fragment of IgG1 and has a 17-fold higher binding affinity for the VEGF receptor when compared to bevacizumab (149 kDa). In recent years, ranibizumab has shown to prevent further vision loss in approximately 95% of patients and to improve vision in 40% of the patients suffering from wet AMD.[85] Likewise, in 2011, Eylea® (VEGF-TRAP-Eye; aflibercept; Regeneron)[86] received FDA approval for the treatment of CNV and wet AMD.[79] Aflibercept (97 kDa) is a recombinant fusion protein (decoy receptor for VEGF) that has a 200-fold higher affinity for VEGF than ranibizumab.[76] Moreover, anti-TNFα agents are also used in intraocular inflammation, edematous neurodegenerative and neovascularization diseases as TNF's play an essential role in the pathogenesis of these diseases.[87] Adalimumab (Humira®), a monoclonal anti-TNFα for uveitis, was FDA approved in 2016 and binds specifically to TNFα (pro-inflammatory cytokine produced by macrophages and T-cells) and therefore results in inhibition of the inflammatory response. Infliximab (INF) is also a monoclonal, chimeric IgG antibody that binds circulating and membrane-bound TNFα, but this antibody is not yet FDA approved for uveitis or ocular inflammation.[88-90] Beovu® (brolucizumab) developed by Novartis recently received FDA approval (October 2019) for the treatment of wet AMD (see table 1) by intravitreal injection. The protein is a potent anti-VEGF, which has a high affinity to all VEGF-A isoforms. Clinical studies by randomly used intravitreal doses of brolucizumab 6mg and 3mg versus aflibercept 2 mg demonstrate that Beovu was non-inferior to aflibercept in visual function after 48 weeks.[91] Patients treated with Beovu overall showed a good improvement in their vision and health of the eye within one year.[92] Summarizing, anti-VEGF and anti-TNFα therapies

2

have been very successful in the field of ophthalmology after their FDA-approval, changing the way vision-threatening diseases are currently treated in clinics.

Table 1: FDA approved and off-label (*) proteins/biologics for intraocular medications and dosages.

Biologics	Type of biologics	Route	Clinical phase	Therapy Indications	Mw (kDa)	Half-life after administration	Stand. Dose	Ref.
Bevacizumab (Avastin®)	Anti - VEGF	Ivt	Off-label drug (2004)	Wet AMD*, DR*, DM*	149	4.9 days human 4.3 days in rabbit	1.25mg /50µl	[45, 93]
Ranibizumab (Lucentis®)	Anti-VEGF	Ivt	FDA-approved (2006)	Wet AMD, DME, DR*	48	2.88 days rabbit 9 days human	0.5mg/ 50µl	[93, 94]
Aflibercept (Eylea®)	Anti-VEGF (VEGF Trap-eye)	Ivt	FDA-approved (2011)	Wet AMD, DME, CNV, DR	115	7.1 days human 3.63 days rabbit	2mg/ 50µl	[95, 96]
Pegaptanib sodium (Macugen®)	VEGF inhibitor	Ivt	FDA approved (2004)	Wet AMD, DR*, DME*	50	10 days human	0.3mg /90µl	[96-98]
Adalimumab (Humira®)	Anti-TNFα	SC	FDA-approved (July 2016)	Uveitis	148	2 weeks in human serum	40mg	[99]
Infliximab	Anti-TNFα	Iv/Ivt	Off-label for Iv	Chronic non-infectious uveitis*	149	8.5 days (rabbit vitreous), 7–12 days (systemic human)	1-1.7mg/ 100 µl (Ivt), 3-5mg/kg (Iv)	[89, 90, 100, 101]
Brolucizumab (Beovu®)	anti-VEGF	Ivt	FDA-approved (October 2019)	Wet AMD	26	2.4 days (cynomolgus monkeys) in ocular compartments	1.0 or 6.0mg/ eye	[91, 92]

Abbreviations: Intravitreal (Ivt) injections; suprachoroidal (SC); intravenous (Iv) infusion.

2.4   Limitations of protein delivery to the posterior segment of the eye

Despite the tremendous clinical success of several novel therapeutic proteins for the treatment of vision-threatening disorders, frequent injection of these formulations cause discomfort and adversely affect patient compliance.[102] Importantly, this class of therapeutics is hard to formulate into long-acting delivery systems because of their structural complexity and undesired interactions with the delivery vehicle. For instance, functional groups present in the hydrogel

crosslinks can potentially react with OH, COOH, SH and NH_2 groups of the loaded protein. Further, there are protein stability issues due to protein unfolding, denaturation and aggregation, leading to loss of activity and even unwanted immune responses.[103-107] Intravitreal injection is the only route of administrations used today in clinics to deliver protein-based drugs to the posterior segment of the eye and eventually to the retina. However, this approach is painful, and often monthly repeats of injections are needed depending on the drug and disease progression.[16, 108] Furthermore when delivering proteins using other routes of administration (e.g. topical, systemic), the poor bioavailability to intraocular target sites is caused by their inability to cross biological membranes as most of the therapeutic proteins are highly hydrophilic and have a high molecular weight.[46, 109] Moreover, pharmacokinetic and cell studies have shown that the retina, cornea and sclera have tight junctions that limit the free diffusion of large hydrophilic molecules through these cell layers.[76, 110] So far, various attempts have been made by formulation scientists to develop drug delivery systems that can bypass these intraocular restrictions. However, non-targeted delivery of biologicals into the ocular tissues by any route of administration may lead to drug distribution to other tissues, primarily through the circulatory system. Therefore, drugs eliminated from the eye to other tissues due to ocular barriers may eventually result in unwanted side effects and toxicity.[109]

2.5 Current delivery technologies for the posterior segment of the eye

Currently, in clinics, medical doctors have the choice between treating patients with intravitreal bolus injections (solutions and suspensions) or drug-loaded implants to treat posterior eye diseases.[111, 112] Nevertheless, ophthalmologists consider current drug therapeutic options insufficient regarding effective delivery and reaching sustained therapeutic dose levels to the retina. Intravitreal pharmacokinetics data show relatively rapid ocular clearance of most intraocularly administered drugs. As a consequence of that, drug concentrations in the vitreous is oscillating above and below therapeutic levels in time with multiple bolus injections (Figure 2).[113-115] Intraocular implants are currently the only delivery vehicles approved by the FDA for sustained release of intravitreally administered (small molecular) drugs to the retina. Monolithic (polymer matrix with homogeneous drug dispersion) and reservoir (drug particles loaded in a core with an outer shell of a certain polymer) type of intraocular implants have been produced, to treat both anterior and posterior segment eye diseases. For the fabrication of these implants, both biodegradable and non-biodegradable polymers have been employed. Biodegradable implants are generally based on poly(lactic-co-glycolic acid) (PLGA), poly(lactic acid) (PLA), or poly(glycolic acid) (PGA), while non-biodegradable implants are mostly made of poly(dimethylsiloxane) (PDMS), poly(vinyl alcohol) (PVA), or poly(ethylene-co-vinyl acetate) (pEVA).[112, 116-118] These formulations are used for the controlled release of low molecular-weight drugs, including hydrophobic steroids and hydrophilic drugs (e.g. ganciclovir), to yield therapeutic levels for an extended period of time. The currently FDA approved slow-release reservoir implants for intravitreal administration are summarized in table 2.

Table 2: FDA approved intraocular implants.

Implants	Year of approval	Description	Ref
Yutiq™	2018	Non-biodegradable intravitreal implant using durasert™ delivery technology and loaded with fluocinolone acetonide (0.18mg) for posterior uveitis, engineered to release fluocinolone acetonide over 36 months at an initial rate of 0.25 µg/day	[119, 120]
Dexycu™	2018	Biodegradable intravitreal implant based on the Virisome® sustained delivery technology for the treatment of postoperative eye inflammation. This injectable implant provides sustained release of dexamethasone (103.4mg/mL in a single-dose vial) over 1-6 months.	[121]
Iluvien®	2014	Non-biodegradable intravitreal implant made of PVA matrix encased in a polyimide tube and loaded with fluocinolone acetonide (0.19mg) for the treatment of DME over 36 months.	[122-124]
Ozurdex®	2009	Biodegradable intravitreal PLGA implant loaded with dexamethasone (0.7mg) for DME and non-infectious uveitis with a six months release profile.	[125-128]
Retisert®	2005	intravitreal non-biodegradable (silicone/PVA) implant loaded with fluocinolone acetonide (0.59mg) to treat chronic non-infectious posterior uveitis used up to 3 years	[127, 129]
Vitrasert®	1996	non-biodegradable (PVA/EVA) implant loaded with ganciclovir (4.5mg) for the treatment of viral retinitis, developed to release the drug over a 5 to 8 month period	[23, 130]

Unfortunately, most of these intraocular implants are generally not suitable as matrices for the sustained release of therapeutic proteins. The polymeric matrix's (e.g. EVA, PDMS) used to produce such intraocular implants have a high permeability for a variety of lipophilic drugs due to their hydrophobic characteristics.[111] However, therapeutic proteins are not easily released from these devices due to their relatively large size and hydrophilicity. Furthermore, interactions of the protein with these polymers may adversely affect protein stability.[103] In addition, the majority of these intraocular implants require invasive administration methods to place the devices at the target site, and subsequent surgical procedures are needed to remove non-biodegradable implants. This unmet clinical need triggered research towards innovative drug delivery products such as nanocarriers (NCs),[65, 131] encapsulated cell technologies (cells embedded in a matrix that secrete therapeutic proteins)[132, 133] and stimuli-responsive delivery systems.[19, 134, 135] These novel drug delivery systems are currently preclinically as well as clinically studied, particularly for protein/peptide delivery to the retina (Figure 3). Mandal *et al.* discuss the major advantages and disadvantages of various preclinically/clinically developed implants and stimuli-response delivery systems for therapeutic proteins/peptides to treat ocular diseases.[76] Several products have shown the potential to prolong the residence time of proteins in the eye, thereby overcoming some of the limitations of ocular drug delivery. Biodegradable products are highly favored because these systems do not need to be removed surgically after treatment, and their
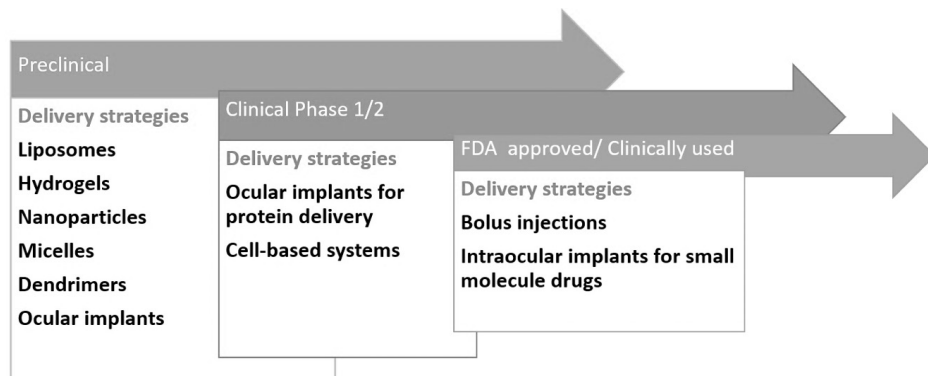
release profiles can be engineered to reach therapeutic levels over prolonged periods. (Figure 2) Currently, many efforts are made by both pharmaceutical companies and academic groups to develop intravitreal implants for the sustained delivery of proteins.[136] Genentech reported the positive phase 2 outcome of a newly developed ranibizumab port delivery system (R-PDS),[137, 138], which consists of a refillable permanent silicone-coated implant surgically inserted through a small incision in the sclera and pars plana. The loaded ranibizumab is released into the vitreous cavity by passive diffusion through a porous release control element based on stainless steel or titanium.[139] This implant was able to provide sustained VEGF inhibition during 9 months of clinical observation in neovascular age-related macular degeneration (nAMD) patients. Interestingly, R-PDS gave visual acuity in patients comparable with monthly intravitreal injection of ranibizumab while maintains the same anatomical results.[140] The product has the potential of being the first device for incorporating a therapeutic protein for posterior eye delivery.
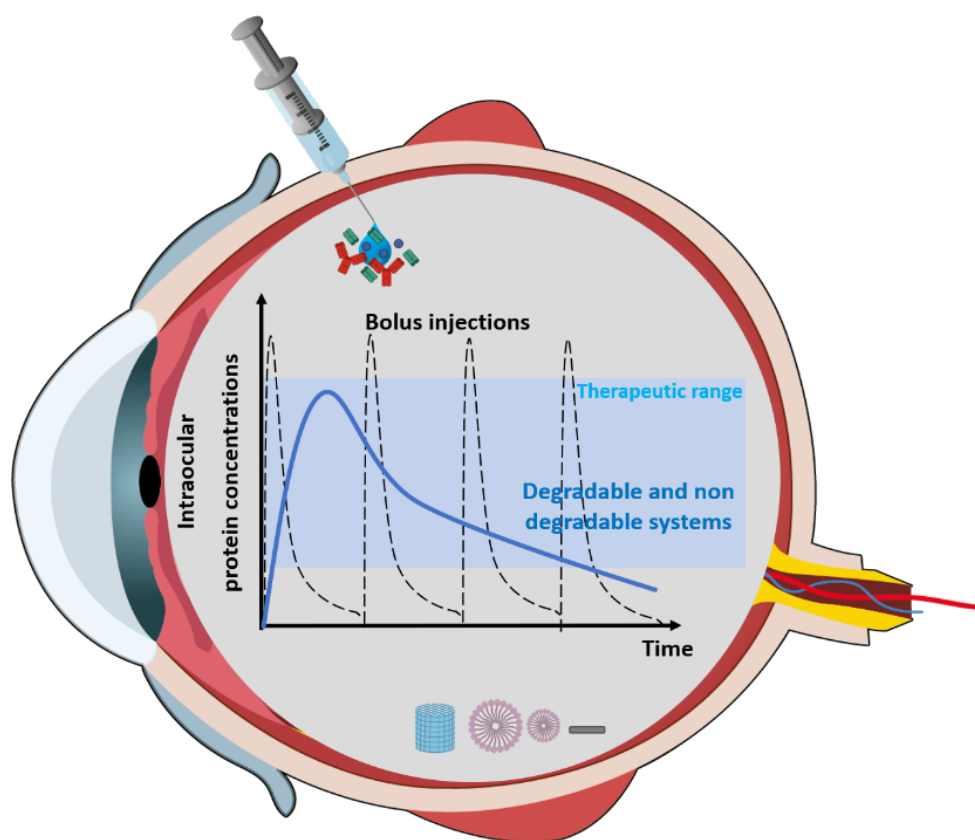
Figure 2 Schematic representation of intraocular pharmacokinetics of drugs delivered by non-degradable and degradable sustained delivery systems compared to frequent bolus intraocular injections.

Although there is a high demand for ground-breaking drug delivery technologies for ocular treatments, most of the developed and investigated technologies remain at preclinical levels and very few at the early clinical stage (Figure 3). The slow progress of these technologies is due to

challenges in reproducibility, safety, large scale production, long term stability. The design of an effective preclinical/clinical sustained release system that will be able to achieve regulatory approval is imperative to move from "Bench to Bedside."

Preclinical

Delivery strategies

Liposomes

Hydrogels

Nanoparticles

Micelles

Dendrimers

Ocular implants

Clinical Phase 1/2

Delivery strategies

Ocular implants for protein delivery

Cell-based systems

FDA approved/ Clinically used

Delivery strategies

Bolus injections

Intraocular implants for small molecule drugs

Figure 3 Schematic representation of currently developed drug delivery strategies to the posterior segment of the eye. Many drug delivery systems are being investigated preclinically, and some technologies have even reached clinical evaluations. However, bolus injection and intraocular implants for small molecule drugs are still the most used therapy to treat posterior eye diseases.

3 Hydrogels for sustained intravitreal release of therapeutic proteins

3.1 Hydrogels: general features

Hydrogels are three-dimensional networks of synthetic or natural polymer chains crosslinked by physical and/or chemical bonds. Compared to other delivery systems that have been developed for posterior eye diseases such as colloidal nanocarriers (NCs) or polymeric implants, hydrogels offer several compelling advantages. Firstly, hydrogels embrace numerous biomedical and pharmaceutical applications due to their tissue-mimicking properties and desirable soft nature.[141-144] Secondly, hydrogels are able to absorb large amounts of water (up to 99% of their weight) while maintaining their structure due to the presence of the crosslinks between the hydrophilic polymer chains.[145] Therefore, hydrogels can serve as scaffolds that provide structural integrity to tissue constructs,[146-148] and can also serve as adhesives[149, 150] or barriers between tissues.[151] Finally, as discussed in this review, hydrogels can be designed to control and/or sustain drug and protein release to tissues due to their network structure of crosslinked polymer chains.[152, 153]

Interestingly, the first publication on hydrogels for biomedical applications was in the early 1950s, when Wichterle and Lim reported on crosslinked poly(hydroxyethyl methacrylate) (pHEMA). The aim was to create a new biomaterial for ophthalmic applications, which led later to the first soft contact lens.[154, 155] Since this breakthrough, hydrogels have been of great interest to biomaterial scientists, and a great variety of hydrogels with interesting and tailor-made properties for different applications (drug delivery, wound dressing, tissue engineering, and hygiene products) have been developed until today as recently summarized by Cascone et al.[156]

Hydrogels can be classified according to different criteria depending on preparation methods, source, physical properties, biodegradation and nature of crosslinking.[157] Additionally, hydrogels can consist of homopolymers, copolymers, and/or interpenetrating networks with different physical properties[158-160] and can also be designed using both charged and non-charged polymers. The net charge of the network might affect the release kinetics of the loaded drug due to electrostatic interactions between the polymeric matrix and the loaded protein.[161-163] Different types of ocular hydrogels with varying polymer architectures and crosslinking chemistry have been studied preclinically to deliver proteins to the posterior segment of the eye. (Table 3) In this review, we classify intraocular hydrogels based on the origin of the polymers and present how the studied hydrogels sustain the release of therapeutic proteins to treat intraocular diseases. The main advantages and disadvantages of polymer-based hydrogels that are currently evaluated in preclinical studies are presented and discussed.

3.2   Hydrogels under preclinical development for sustained intravitreal delivery of therapeutic proteins

To improve the current strategies of intraocular delivery of pharmaceutically active proteins, suitable delivery technologies should have the following characteristics:

1. Provide controlled and sustained release of therapeutic proteins for at least two to three months, therefore, resulting in reduced administration frequency.
2. Easy to administer (minimally invasive).
3. Safe and compatible with intraocular tissues with no or very minimal irritation.
4. Do not obstruct the vision after injection and allow patient comfort.
5. Maintain effective local drug concentration with none to very low systemic effects compared to currently used delivery strategies in the clinic.
6. Maintain protein stability and activity during preparation, storage and release.
7. Undergo biodegradation; the degradation process can modulate the release of entrapped proteins.
8. Possess physical crosslinking and/or bioorthogonal crosslinking chemistry.
9. Allow easy manufacturing in terms of sterilization procedures, scaling up and GMP production.

Hydrogels are considered as one of the most promising preclinically ophthalmic biomaterials for the sustained release of bioactive proteins to intraocular tissues. One of the most interesting features of hydrogels is their physicochemical similarities with native tissues because they are generally very soft and have an elastic texture with high water content. Further, mild crosslinking conditions of polymers are presently available for preserving the activity of entrapped biopharmaceuticals such as proteins and peptides in the hydrogels.[152, 164] The safety of intraocular hydrogels has been evaluated in different animal models (rabbit, rat, mouse) by using different techniques. Evaluation of the intraocular pressure after injection, fundus examination by ophthalmoscope imaging, histological analysis and assessment of retinal function (by electroretinogram analyses) have shown that generally speaking hydrogels are safe for intraocular use.[165-167] Furthermore, different cell lines have been used to investigate the

cytocompatibility of hydrogels and their building blocks, and generally, no toxic effects have been observed with the used polymers (see Table 3).

To bypass the intraocular barriers that drugs have to pass after, e.g. topical or Iv administration (see section 2.2), drug-loaded hydrogels can be administered by intravitreal injection in a minimally invasive way. Importantly, hydrogels can be administered as "*in-situ*" forming formulations by injection using small gauge needles into the vitreous cavity. After intravitreal injection, the polymeric solution undergoes a sol-to-gel phase transition, entrapping and stabilizing therapeutic proteins in their hydrated network.[157, 168] The gelation time, preferably, is in the order of seconds to minutes to limit the rapid and unwanted distribution of proteins and uncrosslinked polymers due to Fickian diffusion in the vitreous body. After gelation, the formed hydrogel functions as a reservoir, providing sustained release of the loaded protein for a prolonged period of time due to the polymer network that restricts protein mobility. Therefore, when properly designed, this reservoir can maintain effective local concentrations of the loaded pharmaceutically active protein in the vitreous and retina. Hydrogels have been successfully used for the controlled release of anti-VEGF (ranibizumab, bevacizumab), anti-TNFα (infliximab), and ciliary neurotrophic factor (CNTF) in the vitreous to protect vision as discussed in details below in section 3.3 and section 3.4.[21, 153, 165, 169, 170] Also, insulin has been released from hydrogel systems after subconjunctival injection to treat diabetic retinopathy.[171] Model proteins (BSA, Fab antibody fragment, IgG) have also been extensively used to study the tunability of hydrogel systems for release characteristics and possible unwanted or wanted interactions with hydrogel building blocks.[172-174] Therapeutic proteins have also been loaded together with low molecular weight drugs in hydrogels to obtain synergic effects.[152, 175, 176] To mention, the anti-metabolic agent 5-fluorouracil (5FU) has been co-released with bevacizumab from *N,O*-carboxymethyl chitosan (CMCS) hydrogels to modulate wound healing and prevent scar formation after glaucoma filtration surgery[177] as discussed in section 3.3.2. In another study, dexamethasone (Dex) was released in combination with bevacizumab (Avastin®) from supramolecular PEG-PCL micelles and α-cyclodextrin (α-CD) hydrogel to treat inflammatory corneal neovascularization in a rat model.[178] The hydrogel was obtained by mixing MPEG-PCL micelles with an aqueous solution of α-CD due to the "host-guest" interaction between MPEG and α-CD.[178, 179] It was shown that 70% of the loaded Avastin® was released within 5 days, and 70% of Dex was released in 1 day. Despite the rapid drug release, this Dex/Avastin® hydrogel medication suppressed the corneal neovascularization in the studied rat model.[178]

Proteins loaded into a hydrogel can be released through different mechanisms, including diffusion-controlled and degradation-controlled release.[180-182] Formulation scientists have designed hydrogels capable of releasing proteins intraocularly from a hydrogel network in a predictable and controlled manner by tailoring the crosslink density, which depends on the polymer concentration, molecular weight, polymer architecture, and degree of polymer modification with reactive species.[152, 183, 184] In ophthalmology and other biomedical applications, biodegradable hydrogels are favored over non-degradable ones. Degradable ocular hydrogels have been designed in the last decades by using both natural and synthetic polymers and combinations thereof, selecting their building blocks as well as the applied crosslinking

strategy with particular attention.[152] The degradation rate can be tuned by the crosslink density and the nature of degradable linkers (by chemical and/or enzymatic hydrolysis) in the polymer chains[183] (Figure 4). Formulation scientists exploit these parameters to design hydrogels with predictable and controlled protein release profiles, as recently described in a review by Chang *et al*.[20]
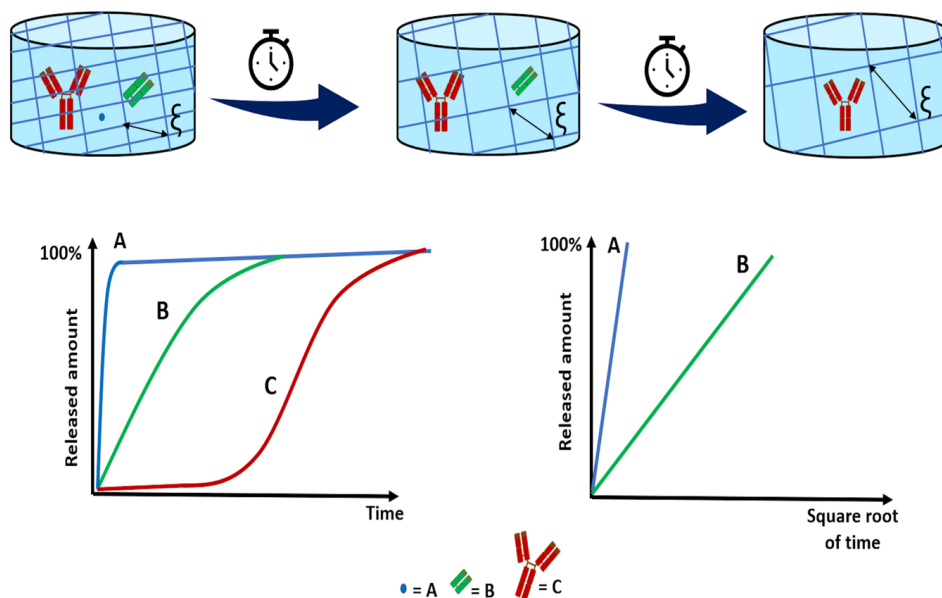
Figure 4 Schematic representation of the correlation between the release rate of protein therapeutics and the mesh size (ξ) of the hydrogel network, as illustrated by the three hydrogels. The curves A, B and C show different release profiles depending on the drug molecular weight and changes in hydrogel pore size over time due to swelling and degradation. Low molecular weight drugs are generally released from hydrogels by Fickian diffusion because their size is much smaller than the hydrogel mesh-size. On the other hand, the release rate of larger molecules such as pharmaceutical proteins is determined by degradation and swelling rate of the hydrogel when the protein is entrapped in the hydrogels matrix, meaning that their hydrodynamic size is larger than the hydrogel mesh size.[185, 186] The blue A curve represents a fast first-order release of a loaded small drug, whereas the green B curve indicates sustained first-order release of a loaded therapeutic with a relatively low molecular weight (e.g. a Fab fragment). The release follows first-order kinetics since the released amount is proportional to the square root of time, meaning that the size of the loaded therapeutics is smaller than the pore size of the hydrogel and that the hydrogel is dimensionally stable during the release time. The red C curve represents delayed-release kinetics of a loaded therapeutic (e.g. a full IgG type antibody). Here the protein is initially entrapped in the pores of the hydrogel and only releases when the crosslink density decreases (and thus pore size increases) over time due to degradation.[174, 183]

**Table 3** Hydrogels for sustained and controlled release of intraocular proteins.

HYDROGEL COMPOSITION	CROSSLINKING METHOD	DRUG/PROTEIN ENCAPSULATED	THERAPEUTIC INDICATIONS	IN VITRO/VIVO RELEASE	ANIMAL TESTED	TOXICITY TEST	REF
POLY (NIPAAM-CO-DEX-LACTATEHEMA)	UV Photopoly-merization	Insulin	DR	5 months (vivo)	Rat	R28 retinal cells and rat eyes	[171]
PLGA-PEG-PLGA	Thermo-gelation	Bevacizumab	DR, DME, AMD	20% in 14 days (vitro) 6 weeks (Vivo)	Rat		[187]
N, O-CARBOXYMETHYL CHITOSAN (CMCS)	CMCS crosslinked with genipin	5FU, bevacizumab	Glaucoma filtration surgery	5FU 8h, 20% Bev. after 53h (in vitro)	Rabbit	Corneal endothelial cells	[177]
PNIPAAMPEG-DA	Free radical polymerization, thermo-gelation	(BSA), IgG, bevacizumab, ranibizumab	AMD, DR, DME	3 weeks (in vitro)	Rat	HUVECs	[173]
4-ARM PEG-MAL & 4-ARM PEG-SH	Thiol-maleimide reaction	Bevacizumab	CNV, AMD, DR, DME	14 days (in vitro)	-	L-929 cells	[188]
4, 8-ARM POLOXAMINE-MALEIMIDE & FURAN	Diels-Alder thermo-gelation	Bevacizumab	AMD, DR, DME	115 days (in vitro)	-	Mouse fibroblast L-929 cells	[189]
MPEG-PCL MICELLES & A-CYCLODEXTRIN(A-CD)	Inclusion complexation	Bevacizumab, dexamethasone Sodium Phosphate	CNV	5 days (65% Bev) and 1day (70% dex) (in vitro)	Rat and albino rabbit	L-929 cells, HCEC	[178]
HA-TZ & PEG-BISNOR-BORNENE	Diels-Alder (tetrazine & norbornene)	Fab1 protein	-	90% in 27 days	-	-	[172]
PEOZ-PCL-PEOZ	Thermo-gelation	Bevacizumab	AMD, DR, DME	40 μg/day for 11 days with 80% in 20 days (in vitro)	-	Human retinal pigment epithelial cells	[190]
HA-VS & DEX-SH	Thiol-ene reaction	Bevacizumab	AMD, DR, DME	6 months (vivo)	Rabbit	ARPE-19 cells	[165]
HA-TYR-INF/ PEGDA-PNIPAAM-HA-INF.	Enzymatically & Thermo-responsive	Infliximab	Ocular inflammation	25% in 9 days (in vitro)	-	-	[169]

	Method	Protein	Posterior eye diseases	On-Off release	Model	Cells	Ref
AUNPS & AGAROSE	Photo-modulation	IgG, BSA, bevacizumab, ranibizumab, conbercept	Posterior eye diseases	On-Off release	-	RCE, HCEC, HRPE	[170]
ESHU	Thermo-gelation	Bevacizumab	AMD, DR, DME	17 weeks *in vitro* 9 weeks *in vivo*	Rabbit	Primary bovine CE and ARPE-19 cells	[191, 192]
DEX-GMA	Radical polymerization	IgG	-	250 days (no dextranase) 5-10 days (0.001–0.03 U/g gel dextranase)	-	-	[174]
HAMC	Thermo-gelation	CNTF	Neuro-protection	7 days	Mouse	-	[153]
SILK BASED HYDROGELS	Physically crosslinked silk fibroin chains	Bevacizumab	AMD, DR, DME	3 months (in vitro & in vivo)	Rabbits	-	[21]
ICNPH (hybrid delivery system)	Thermo-gelation	Insulin (subconjunctival)	DR	2 weeks (in vivo)	Rat	-	[167]
PEG-PLLA-DA/NIPAAM (hybrid delivery system)	Thermo gel loaded with microspheres	Aflibercept	AMD, CNV	6 months (in vitro)	-	HUVECs	[193]
GLYCOL CHITOSAN AND OXIDIZED ALGINATE	Dynamic covalent Schiff-base linkage	Bevacizumab	AMD, DR, DME	3 days	-	-	[194]
PCM-HEMA GEL	Light-activated copolymerization	Bevacizumab (suprachoroidal space)	AMD, DR, DME	20% burst release, ~ 4 months.	Rabbit	ARPE (in vitro), rats (in vivo)	[195]

Abbreviations: (poly(ethylene glycol)-poly-(serinol hexamethylene urethane) (ESHU), rabbit corneal endothelium (RCE) primary cells, human corneal epithelial cell lines (HCEC), human retinal pigment epithelial cell lines (HRPE), glycidyl methacrylate-derivatized dextran (dex-GMA), thermal of hyaluronan and methylcellulose (HAMC), Chitosan nanoparticles/poly(lactic-co-glycolic acid)-poly(ethylene glycol)-poly(lactic-co-glycolic acid) hydrogel (ICNPH), Polycaprolactone dimethacrylate (PCM)- hydroxyethyl methacrylate (HEMA), Ciliary neurotrophic factor (CNTF), Human Umbilical Cells (HUVECs), Human corneal endothelial cells (HCEC), thermal of hyaluronan and methylcellulose (HAMC), Adult Retinal Pigment Epithelial cell line-19 (ARPE 19), diabetic retinopathy (DR), age-related macular degeneration (AMD) choroidal neovascularization (CNV).

2

3.3 Intravitreal hydrogels based on natural polymers as matrices for the controlled release of therapeutic proteins

Natural polymers display multiple advantages and have been used to develop drug delivery systems.[196, 197] These advantages are related to the fact that natural polymers often display good cell adhesion properties, and most of them are biodegradable. Specifically, polysaccharide-based hydrogels have often been used for the development of ocular drug delivery systems and formulations. The most frequently used polysaccharides are hyaluronic acid, alginate, semisynthetic chitosan and dextran.[198-203] Although natural polymers display many advantages, they also have several drawbacks related to the possible risk of infections and immunogenicity due to complexity in their purifications from natural sources.[160] However, both natural and synthetic polymers allow tailoring of hydrogel properties by changing the polymer architecture and composition (Figure 5), initial water content and crosslink density, as well as their degradation mechanism and kinetics which will reflect on their release profiles.
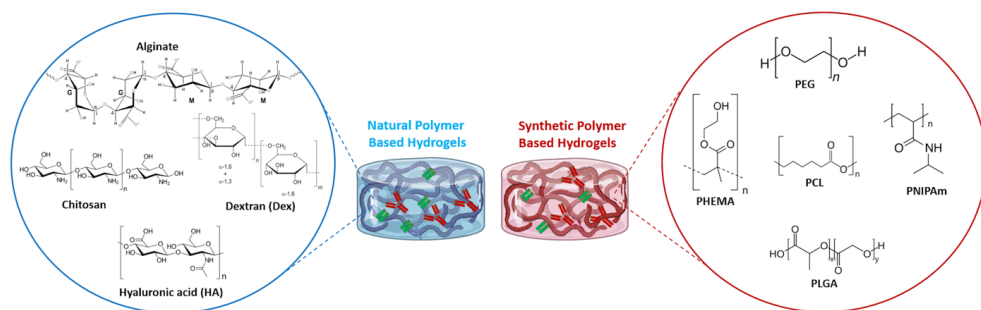
Figure 5 Schematic representation of hydrogel design for protein delivery to the back of the eye using natural synthetic polymers.

3.3.1 Hyaluronic acid-based hydrogels for protein delivery

Hyaluronic acid (HA) is a negatively charged, naturally occurring polysaccharide with molecular weights up to 10^7 Da, which is abundantly present in the human vitreous body. Importantly, HA can presently be produced via biotechnological routes reducing the risks associated with the use of animal sources for this polymer.[204] HA, also known as hyaluronan, is a glycosaminoglycan composed of repeating disaccharide units of D-glucuronic acid and *N*-acetylglucosamine. HA-based materials have been investigated for different biomedical [205] and pharmaceutical applications.[200, 206-208] Often, the carboxylic acids or primary hydroxyl groups are chemically modified to obtain crosslinking functionalities.[208-211] In the field of ophthalmic protein delivery, a few intraocular HA-based gels have been developed including enzymatically crosslinked HA–tyramine conjugates, vinyl sulfone functionalized hyaluronic acid (HA–VS) crosslinked with thiolated dextran (Dex-SH) using a thiol-ene reaction, and HA-tetrazine crosslinked by catalyst-free inverse-demand Diels–Alder reaction with PEG-bisnorbornene (Table 3). Protein release from HA hydrogels can be sustained up to a few months, depending on the

protein net charge and size, hydrogel crosslink density and degradation kinetics. As mentioned, HA is negatively charged, and cationic proteins (pI>7.4) can be retained in the polymer network by electrostatic interactions.[163] In addition, protein release can also be controlled by enzymatic degradation of HA hydrogels by hyaluronidases,[212] which are present in most human tissues, including the vitreous.[25]

An injectable transparent *in-situ* forming hydrogel based on HA-VS/Dex-SH was formulated for intravitreal delivery of bevacizumab.[165] The controlled release performance of this *in situ* forming hydrogel formulation was evaluated *in vivo* in a rabbit eye model, and the formulation released bevacizumab (pI ~8.3).[213] After vitreous aspiration from the rabbit eye at different time points, the concentration of released protein was measured by using an enzyme-linked immunosorbent assay (ELISA). Specifically, the assay determines the amount of bevacizumab that can still bind to VEGF after being released in the vitreous. Six months after intravitreal injection of the hydrogel formulation (40 µl) into a rabbit eye, it was shown that the gel maintained intravitreal protein concentration above the therapeutic level (>50 ng/ml).[165] Egbu *et al.* reported the sustained release of infliximab (INF; MW:149.100Da pI:8.25) from two gel systems based on crosslinked HA for the treatment of intraocular inflammation. Tyramine-substituted HA (HA-Tyr, 4.8 kDa) was enzymatically crosslinked in the presence of INF to form a drug-loaded gel (HA-Tyr, INF). A second gel was prepared by the polymerization and crosslinking of NIPAM with poly(ethylene glycol) diacrylate (PEGDA) in the presence of unmodified HA (50 kDa) and INF to form a thermosensitive PEGDA-pNIPAAM/HA semi-interpenetrating polymer network. *In vitro* release of INF from these hydrogels was studied by using a two-compartment *in vitro* outflow model of the human eye, called the PK-Eye. This model was previously developed by Awwad *et al.* to estimate the clearance of ocular drugs by the anterior aqueous outflow pathway. [214] The model is made of an anterior and posterior cavity, which are separated by a cellulose membrane. This model previously showed clearance values for the studied drugs (ranibizumab, bevacizumab, triamcinolone acetonide) that were comparable to that observed in humans.[214] Egbu *et al.* showed that the two hydrogel formulations had a controlled release of INF, with the slowest release rate being ~25% of the loaded protein in 9 days.[169] However, important issues among which the *in vitro* hydrogel cytotoxicity, *in vivo* biocompatibility, possible interference of protein functional groups in the crosslinking reaction and protein activity after release from the hydrogels were not addressed in this study. Tetrazine-modified HA and norbornene-modified poly(ethene glycol) were used to obtain an HA-Tz/PEG-bisnorbornene hydrogel for *in-situ* encapsulation of a Fab fragment (Fab1) as a model protein.[172] In this hydrogel system, a catalyst-free inverse-demand Diels–Alder reaction between tetrazine and norbornene groups was used to exploit the bio-orthogonal nature and protein friendly conditions of this crosslinking method (Figure 6). At room temperature, the gelation of the soluble hydrogel precursors occurred within 3 min.[172] Protein release kinetics showed that the hydrogels formed from 20 and 50mg/mL HA showed a sustained release of Fab1 with a daily release rate >1µg for 7 and 27 days, respectively (Figure 6A-B). Importantly, more than 95% of the loaded Fab1 was released from the hydrogels suggesting that the protein was physically entrapped and had not undergone covalent bond formation with the hydrogel matrix.[172] The integrity of the released protein was analyzed by size-exclusion chromatography (SEC), ion-exchange chromatography (IEC) and by liquid

chromatography-mass spectrometry (LC-MS). The proteins maintained their structure during their residence time within the hydrogel network at 37°C and did not carry fragments of hydrogel precursors. Although the authors had not investigated this system for intraocular protein delivery, the *in vitro* release data are encouraging and suggest that intraocular release of ranibizumab may be achievable as well with this system. Furthermore, additional *in vitro, in vivo* studies, degradability studies and protein bioactivity after been released from the gel are necessary to ascertain whether this delivery system is indeed safe and suitable for intraocular use.
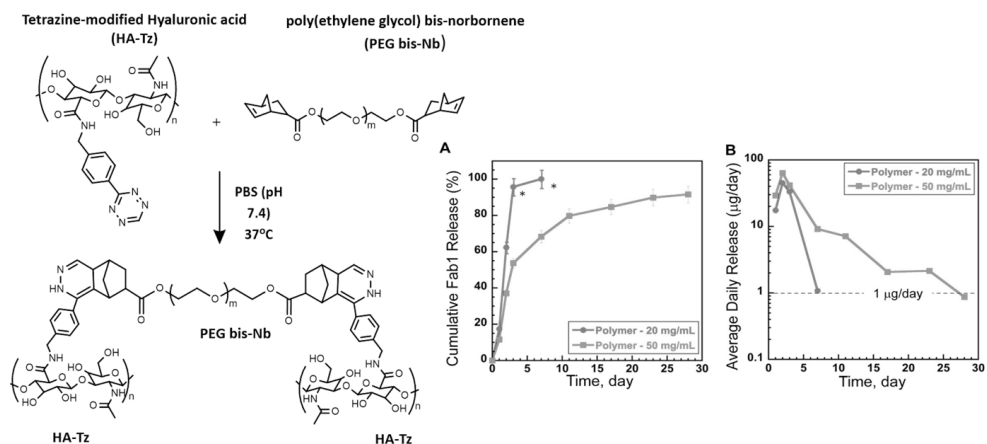
Figure 6 Schematic representation of the reaction between tetrazine-modified hyaluronic acid and poly(ethylene glycol) bis-norbornene at physiological conditions reported by Famili et al.[172] to form an *in situ* hydrogel network. A) Release of a model Fab1 protein from an *in-situ* formed gel based on HA-TZ, PEG-bisnorbornene hydrogel in PBS at 37°C. Both high (50mg/ml) and low (20mg/ml) starting polymer concentrations resulted in hydrogels, which showed a quantitative release of Fab1, suggesting that the protein has not undergone unwanted reaction with the functional groups present in the hydrogel building blocks. B) Hydrogels formed from 20 and 50mg/mL HA showed a sustained release of the loaded Fab1 protein > 1 µg/day for 7 and 27 days, respectively. Data points represent mean ± standard deviation of n = 3 replicates. Adapted and reprinted with permission from [172] Copyright © 2017 American Chemical Society.

3.3.2 Intravitreal hydrogels based on chitosan

Both natural (alginate, dextran, hyaluronic acid and gelatin) and semi-synthetic polymers (chitosan) have been successfully used to prepare different drug delivery systems for ophthalmological applications.[215] These polymers are primarily used in the preparation of nano- or micro technology-based drug carriers but also for the development of in situ gels for the delivery of low molecular weight drugs such as corticosteroids, antibiotics, antimetabolites and siRNA mainly for topical therapy.[216-224] In contrast, fewer studies are showing the potential use of these natural polymer based materials for ocular delivery of pharmaceutical proteins.[225-227]

Chitosan is a cationic polysaccharide that is prepared from the natural polymer chitin after partial or complete deacetylation. In ophthalmic applications, chitosan-based nanocarriers and in situ forming gels have been extensively investigated for the delivery of low molecular weight drugs mostly to prolong the release of topically administered drugs.[228-230] There are some promising examples of chitosan-based drug delivery strategies to deliver pharmaceutical proteins, using nano- or micro particles and hydrogels.[194, 231] The in vitro sustained release of bevacizumab and ranibizumab from chitosan-PLGA nano- or micro- particles have been studied by Pandit et al.[232] and Elsaid et al.[233] for posterior eye therapy. The studied chitosan PLGA nano- or micro- particles release 15% of loaded bevacizumab within 72h of the study, while ranibizumab showed a biphasic release profile with an initial 20% burst release followed by a second dose after ~135 days. Although chitosan is not soluble in water at a pH of 7.4, chitosan can be dissolved in acidic solution, and because of the charged amino groups, it is able to interact spontaneously with anionic polymers to form a hydrogel network.[234-236] Chitosan hydrogel systems are being studied for the delivery of small drugs such as ciprofloxacin [237], chloramphenicol [238], and latanoprost [239]) for ocular applications.[240-242]

Xu et al. studied the sustained release of bevacizumab from an alginate-chitosan hydrogel.[194] Specifically, the hydrogel network was formed by glycol chitosan crosslinked by oxidized alginate. The hydrogel completely released the protein within three days. This release rate is too fast for long term ocular treatments; therefore, more extended release profiles should be investigated. The in vitro and in vivo toxicity in relevant models were not reported in this study.

Carboxymethyl chitosan is a water-soluble polysaccharide with good biocompatibility used to prepare hydrogels for pharmaceutical applications. Li-Qun Yang *et al.* described O-carboxymethyl chitosan (CMCS) *in-situ* forming hydrogels for intraocular delivery of 5-fluorouracil (5-FU) or bevacizumab using genipin as the water-soluble crosslinker.[177] After subconjunctival injection, the effect of this drug-loaded CMCS hydrogel in modulating wound healing and reducing postoperative IOP values following glaucoma filtration surgery on rabbits was evaluated. As expected, based on the molecular weight of the drugs, it was shown that that bevacizumab was released slower (20% after 53h, by anomalous transport) from the hydrogel than 5FU (8h, by Fickian diffusion). *In vivo* evaluation showed that the CMCS hydrogels were compatible with the cornea and gradually biodegraded in the rabbit's eye. However, the mechanism that governs the degradation was not studied. Drug-loaded CMCS hydrogels effectively delayed subconjunctival scar formation after glaucoma filtration surgery and controlled postoperative IOP.[177] However, it is essential to consider that genipin can readily react with primary amines present in lysine residues of proteins that could potentially alter the structure of the protein and its function.[243] This hydrogel system has shown to increase the therapeutic efficacy of glaucoma filtration surgery, and in future studies, it would be interesting to investigate their potential use as long term protein release depot for ocular applications.

3.4 Intravitreal hydrogels based on synthetic polymers as matrices for the controlled release of therapeutic proteins

Hydrogels based on synthetic polymers have been used as release systems of bioactives into the eye. Poly(ethylene glycol) (PEG), poly(2-hydroxyethyl methacrylate) (pHEMA), poly(vinyl alcohol) (PVA), polyacrylamide (PAM), poly(D,L-lactide-*co*-glycolide) (PLGA), poly(ε-caprolactone) (PCL) are the most commonly used synthetic polymers to prepare ocular drug delivery systems.[215, 244, 245] PEG is a frequently used synthetic polymer for biomedical and pharmaceutical applications, also in ophthalmology. It is a water-soluble polymer that can be eliminated from the circulation by the kidneys up to a molecular weight of 50 kDa.[246] Since 1990, several PEG-based pharmaceutical products have been approved by the FDA for clinical use.[244, 247, 248] Jing Yu *et al.* used an *in-situ* covalently crosslinked PEG hydrogel for the intraocular delivery of Avastin® (bevacizumab).[188] The PEG hydrogels were formed via a thiol-maleimide reaction between 4-arm PEG-Mal and 4-arm PEG-SH at physiological conditions. Variation of polymer concentrations yielded PEG hydrogels with differences in gelation time, the extent of swelling, pore size and mechanical properties. These PEG hydrogels and their leachables were non-toxic to L-929 cells after seven days of cell culture. Importantly, L-929 cells on the surface of this PEG hydrogel showed a different morphology and did not proliferate because of poor cell adhesion. Since the system is aimed to function as a long-term intravitreal reservoir, the fact that cells do not adhere to the hydrogel surface might be beneficial to prevent undesired cell adhesion and proliferation on the hydrogel depot. The PEG hydrogel formulation showed *in vitro* (PBS buffer of pH 7.4 and at 37 °C) release of 25% encapsulated bevacizumab within 1 day and subsequently released 70% of the loaded protein for the subsequent 14 days. Further, sodium dodecyl sulfate-polyacrylamide gel electrophoresis (SDS-PAGE) showed that no fragments with molecular weights smaller than that of the native protein were detected. However, the authors did not show whether the activity of the released protein was retained.[188] Besides the examples given above, many other *in-situ* forming PEG hydrogels have been investigated to deliver both pharmaceutical proteins and low-molecular-weight drugs with promising results for ophthalmic application. [173, 188, 249-251] Imperiale et al. summarized the use of synthetic and natural polymers for ophthalmic drug delivery.[215] Synthetic and natural polymers can be engineered to stimuli-responsive hydrogels, meaning that they jellify or release drugs from their network in response to external stimuli (for example, changes in temperature, oxidation, light intensity, pH, ionic strength). These hydrogels are very attractive for ophthalmic applications as they can be formed in situ in the ocular tissues. However, the majority of currently developed stimuli-sensitive hydrogels are focused on the topical delivery of small molecular drugs. [218, 252-255] While, in protein delivery, light-activated gels (section 3.4.1) and temperature-sensitive hydrogels (described in section 3.4.2), are the most commonly developed systems for intraocular medications.

3.4.1 Photosensitive synthetic hydrogels:

Light-activated in situ forming gels are an attractive concept for intraocular delivery mainly because light can travel to the posterior segment from the anterior segment, causing the formation of an in situ hydrogel network. Thus, after injection or deposition of hydrogel precursors in the eye, light can be used together with a photoinitiator to photocrosslink the gel in situ.

Furthermore, the release of therapeutic proteins from the hydrogel depot can also be photo-modulated, as described in section 3.5. Tyagi et al. reported about a light-activated, in situ forming gel based on polycaprolactone dimethacrylate and hydroxyethyl methacrylate.[195] The gel network was formed in the presence of a photoinitiator 2-dimethoxy-2-phenylacetophenone (DMPA) and 365 nm UV light. After 10 minutes of crosslinking, the gel network was able to sustain the delivery of bevacizumab up to 4 months in vitro after an initial 20% burst release. In vivo studies showed sustained release in the suprachoroidal space for at least 60 days in a rat model. Williams et al. investigated the extended-release of bevacizumab by embedding protein containing microparticles into hydrogel matrices (based on photocurable PEG).[256] The in vitro release profile from this system showed a zero-order release of active bevacizumab over 90 days.

Although photosensitive hydrogels may represent an interesting delivery strategy for ocular application, several drawbacks could limit the clinical translation. The use of photoinitiators that form free radicals upon exposure to light could potentially harm ocular tissues or the encapsulated protein cargo. Long crosslinking times may also be an issue as the use of specific laser light and wavelengths may not be well tolerated by the eye.

3.4.2   Temperature-sensitive synthetic hydrogels

Due to the fast *in-situ* gelation properties, temperature-sensitive hydrogels have been frequently investigated as systems that slowly release therapeutic proteins to the back of the eye. After the administration of the formulation, the change from room to body temperature triggers its gelation. These systems are characterized by a phase transition at a certain temperature in aqueous solutions, which is known as "lower critical solution temperature (LCST) behavior."[257] Thermo-responsive polymers most commonly used in the pharmaceutical field for the formulation of injectable hydrogels are characterized by an LCST between room and body temperature. Formulations based on this type of polymers can be used as injectable release systems since they are liquid at room temperature and jellify rapidly at body temperature after administration. Therapeutics can be easily loaded in these gels by dissolving/dispersing them in the hydrogel precursor solution. After crosslinking, the encapsulated drugs will be released in a controlled manner with kinetics depending amongst others on the size of the therapeutic agent, hydrogel pore size and swelling/degradation. Temperature-sensitive polymers can be either synthetic or natural origin. However, in this review, we focus on synthetic thermosensitive polymers since they have been predominantly used to deliver and release proteins to the retina. The most frequently investigated thermosensitive polymers are poly-(*N*-isopropylacrylamide) (PNIPAM), poloxamers (Pluronics®), poloxamines (Tetronics®), poly(methacrylamide hydroxylpropyl lactate) (pHPMAm-lac), poly(2-ethyl-2-oxazoline)-b-poly(ε-caprolactone)-b-poly(2-ethyl-2-oxazoline) (PEOz-PCL-PEOz), and poly(DL-lactic acid-co-glycolic acid) (PLGA)–polyethylene glycol (PEG)–PLGA (PLGA-PEG-PLGA). These polymers can be derivatized with functional groups that allow chemical crosslinking for further stabilization of the hydrogel network. Hydrogels obtained by covalent crosslinking of thermosensitive polymers swell below the LCST but collapse (shrink) above the LCST.[257] Xie *et al.* reported the use of a thermosensitive PLGA-PEG-PLGA hydrogel for sustained release of Avastin® to treat posterior segment diseases.[187] The sol-gel transition of the system occurred at 26°C, as demonstrated by

rheological studies. However, the Avastin® loaded PLGA-PEG-PLGA hydrogel showed lower gelation temperatures of 22-24°C depending on the concentration of the protein. The authors suggest that hydrophobic regions of the protein might interact with hydrophobic polymer segments of PLGA-PEG-PLGA, resulting in a lower gel formation temperature. The authors also mentioned that a similar result was reported by Park *et al.*[258] It should be remarked that these hydrophobic interactions might cause undesired protein unfolding resulting in loss of its biological activity. Furthermore, although a fast thermal transition is observed at these temperatures (22-26°C), the LCST temperature close to room temperature might cause unwanted gelation prior to the intravitreal injection. The authors claimed that the system slowly releases the protein up to 14 days *in vitro*. However, reported data showed a 10-13% release within 8 hours, followed by marginal release (<2.5% of the loaded amount of protein) for two weeks.[187] Nevertheless, *in vivo* pharmacokinetic studies (formulations were injected in rat eyes) showed that the PLGA-PEG-PLGA hydrogel could extend the presence of Avastin® in the vitreous humor and retina for 4 weeks (35 ± 14 ng/mL) compared with bolus injection (no Avastin® was detected in the vitreous humor after 4 weeks).[187]

PNIPAm gained substantial attention for biomedical and pharmaceutical applications after being described by Heskins and Guillet as a temperature-dependent phase transition polymer in aqueous solution.[259-261] This phase transition (LCST) occurs at 32°C and is suitable for the design of *in-situ* gelling systems.[262, 263] PNIPAM has isopropyl $(CH(CH_3)_2)$ and amide $(CONH)$ moieties in its structure. Below the LCST, the polymer is soluble in water because of hydration of the amide bonds, whereas above this temperature, the hydrophobic characteristics of the isopropyl groups dominate the properties in water, resulting in polymer precipitation.[261] The incorporation of hydrophilic monomers in the polymer chains results in an increased LSCT, while more hydrophobic units decrease the LCST. [264] Because of its attractive characteristics, PNIPAm based hydrogels have been studied as drug delivery systems for various applications, including ocular therapy.[173, 265-268] However, PNIPAM based hydrogels can be very fragile and unstable, resulting in the relatively fast release of the loaded drugs.[265, 269] Furthermore, at high concentrations, both physically and chemically crosslinked PNIPAM-based hydrogels often show a common phenomenon known as syneresis due to the shrinking of gel size with the expulsion of water from the network.[270] This dehydration of the network will mediate the rapid expulsion and release of proteins and/or cause undesired gel-protein interactions.[265] There are different ways to enhance the mechanical stability of PNIPAM hydrogels, as reviewed by Haq *et al.*[269] For instance, an interpenetrating polymer network can be formed by the incorporation of another polymer in the hydrogel matrix to obtain a multicomponent polymeric system.[271-273] PNIPAM can be co-polymerized with different monomers, e.g. acrylic acid (AA),[274] N, N-dimethylacrylamide (DMA)[275] to prevent syneresis.[276, 277] Alternatively, PNIPAM copolymerized with functional monomers can be covalently crosslinked with other complementary polymers by, e.g. azide/alkene click chemistry, Michael addition, photopolymerization and thiol-ene reactions to form stable hydrogels. [278-280] It should be mentioned that pNIPAM and its copolymers with hydrophilic and/or hydrophobic monomers are generally not biodegradable, which represents a major limitation for its use as a drug delivery system for the eye. Nevertheless, several PNIPAM copolymers have been engineered to obtain

networks that are degradable under physiological conditions. For example, PNIPAM copolymers with hydrolyzable side groups can, in time, result in the formation of soluble polymer chains, which can be eliminated by the kidneys when the molecular weight is sufficiently low.[7, 281] Neradovic et al. developed an AB block copolymer of PEG (A block) and a random copolymer of NIPAM and *N*-(2-hydroxypropyl) methacrylamide lactate (HPMAm-lactate) (B block).[282] Interestingly, these block copolymers formed micelles at 37 °C which is above the LCST of the B block, but after hydrolysis of the lactate side groups, the cloud point (CP) increased above 37°C resulting in the dissolution of the polymers. Since then, other copolymers of NIPAM with hydrolytically labile monomers have been developed.[283-287] Vernon *et al.* reported on the hydrolysis-dependent degradation of NIPAM copolymerized with dimethyl-γ-butyrolactone acrylate (DBA). As shown in figure 7, after hydrolysis of DBA, the overall polymer becomes more hydrophilic due to the formation of hydroxyl and carboxyl groups that will then promote polymer dissolution.[285, 286] The suitability of NIPAM and DBA copolymers for injectable hydrogels for biomedical applications was demonstrated for example by Vo *et al.* and Boere *et al.*[287, 288]
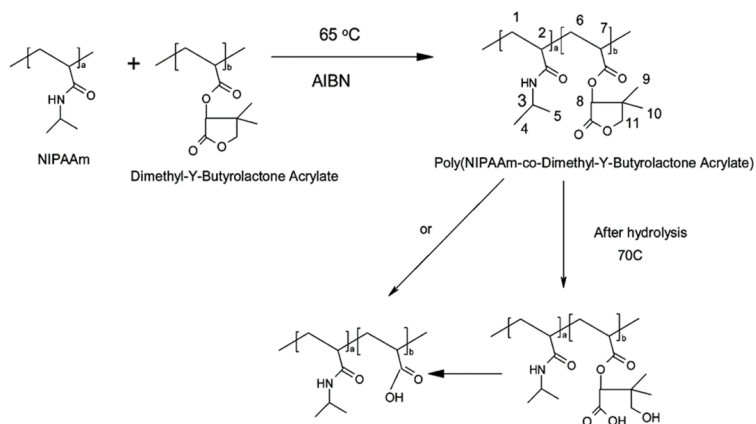
Figure 7 Synthesis and hydrolysis of poly(NIPAAM-co-dimethyl-γ-butyrolactone). Adapted and reprinted with permission from [285] Copyright © 2007, American Chemical Society.

Imai *et al.* reported on a synthetic subconjunctival implanted hydrogel for sustained release of insulin to rescue retinal neurons from apoptosis in diabetic rats.[171] The hydrogel was synthesized by UV photopolymerization of *N*-isopropylacrylamide and a dextran macromer containing oligolactate-(2-hydroxyethyl methacrylate) units. FITC-insulin was dissolved in *N, N*-dimethylformamide (DMF) together with hydrogel precursors and upon UV polymerization in a Teflon mold, FITC-insulin–loaded hydrogels were obtained. This protein was released from this gel *in vitro* for least five months by a combination of degradation and diffusion, depending on the hydrogel composition.[171] Interestingly, FITC-insulin released from the hydrogel after subconjunctival injection could be detected on the target site (euthanized retina model) by confocal imaging. *In vivo,* biosafety studies showed normal retinal histology after two months post blank hydrogel implantation in Sprague-Dawley rats. The developed poly(NIPAm-Dex-lactate HEMA) hydrogels showed the capacity to release biologically active insulin for 1 month to the retina via subconjunctival implantation with the potential to minimize DR without the risk

of hypoglycemia. Although the authors showed that there was no toxicity in the animal model, possible residual of DMF present after preparation and purification of the hydrogel may pose a risk for toxicity in the eye.[171] Derwent *et al.* developed thermoresponsive hydrogels as drug delivery systems for ocular applications.[173] Poly(ethylene glycol) diacrylate (PEG-DA) was polymerized with NIPAM to obtain a non-degradable hydrogel, which was used to encapsulate bovine serum albumin (BSA) and immunoglobulin G (IgG) as model proteins. The crosslinked PNIPAm–PEG-DA hydrogel showed a phase transition at 32°C and was injectable using a 27-30 gauge needle below this temperature. This injection was possible because, at room temperature, the formulation is liquid but rapidly gelated within 1 minute at 37°C. The release kinetics of the loaded proteins could be tuned by varying the ratio of PEG-DA/NIPAM and, therefore, the crosslink density. The different hydrogels showed a rapid release within 48 hours of the loaded proteins, which might be due to the initial volume collapse of the hydrogel in response to temperature. Thereafter, the loaded proteins were released for three weeks. *In vivo* tests confirmed hydrogel formation in the vitreous of a rat model after intravitreal injections of a FITC-labeled hydrogel formulation. A fluorescein angiography image of the FITC-hydrogel showed the localized formation of the gel in vitreous, and no adverse effects on the retina were observed in histological studies.[173] Furthermore, a test on retinal function after the injection of PEG-DA crosslinked PNIPAm hydrogel showed a limited transient effect on retinal function without any long-term adverse effects.[166] However, the clinical translation of this formulation is unlikely because the gel system does not degrade under physiological conditions. Wang *et al.* developed a thermosensitive and biodegradable hydrogel based on a triblock copolymer of poly(2-ethyl-2-oxazoline)-b-poly(caprolactone)-b-poly(2-ethyl-2-oxazoline)(PEOz-PCL-PEOz) which was used as an intraocular controlled release system for bevacizumab (Figure 8).[190] The aqueous solution of the polymer showed a reversible sol (room temperature) –gel (physiological temperature) phase transition to yield a hydrogel. The protein was loaded in the hydrogel by the dissolution of bevacizumab with the PEOz-PCL-PEOz triblock copolymer at low temperature, and subsequently, the temperature of the obtained solution was increased to 37°C. The formed hydrogel was incubated in balanced salt solution as the standard saline for intraocular use (BSS) at 37 °C, and the released protein was detected by enzyme immunoassay (ELISA). During the first 11 days, a diffusion-controlled release was observed, while from day 12 to 20, the release was controlled by a combination of diffusion and erosion. Overall, 80% of the loaded bevacizumab was released from the hydrogel network in 20 days (Figure 8A), and the released protein was able to bind to VEGF, demonstrating that the biological activity of the protein was preserved. However, longer-term release profiles should be aimed as currently soluble bevacizumab is typically administered once a month. The hydrogel hydrolytic degradation was conducted at 37°C in BSS and analyzed by scanning electron microscope. Initially, the hydrogel surface morphology was smooth and became more and more porous over time due to hydrogel erosion. After ten days of degradation, pores of 10–20 μm in size were seen, and channels were observed through which the protein could have been released. *In vivo* studies demonstrated that the hydrogel was formed in a localized position in the vitreous after intravitreal injection. Histomorphology and electrophysiology were studied on rabbit neuroretina, and normal functions were preserved two months after injection and thus showing the safety of this system in the rabbit eye. Gregoritza *et*

al. investigated the controlled release of bevacizumab from a degradable thermoresponsive hydrogel crosslinked by Diels-alder chemistry (see figure 9).[189] The hydrogel was prepared by reacting maleimide modified four, and eight-armed poloxamines with furyl modified four and eight-armed poloxamines. This thermal gel showed a rapid sol-gel transition at 37°C due to its thermosensitivity, which was stabilized by the Diels-Alder click reaction between the maleimide and furyl groups. The obtained gels released > 90% of the loaded protein over a period of 7, 21 and 115 days, depending on the used ratios between four- and eight-armed polymers at a fixed polymer total concentration. Furthermore, binding studies of the released antibody at 7 and 30 days demonstrated that the structural integrity of the released protein was almost fully preserved. The hydrogel might be beneficial for the treatment of ocular neovascularization.

Rauck *et al.* investigated the *in vivo* release of bevacizumab from poly(ethylene glycol)-poly-(serinol hexamethylene urethane) thermal hydrogels (ESHU) after intravitreal injection in a rabbit eye.[192] Rheological studies on ESHU solution in phosphate-buffered saline showed a phase transition at 32°C with a maximum elastic modulus at 37°C as previously described by Park *et al.*[289] Rauck and co-workers analyzed samples obtained from the anterior chamber paracentesis to quantify the concentrations of released protein using ELISA.[192] Compared to bolus bevacizumab injections, ESHU hydrogels were able to sustain therapeutically active bevacizumab intravitreal concentrations for nine weeks, which is ~4-5 times longer than observed after the injection of the free protein (~2 weeks).[192]
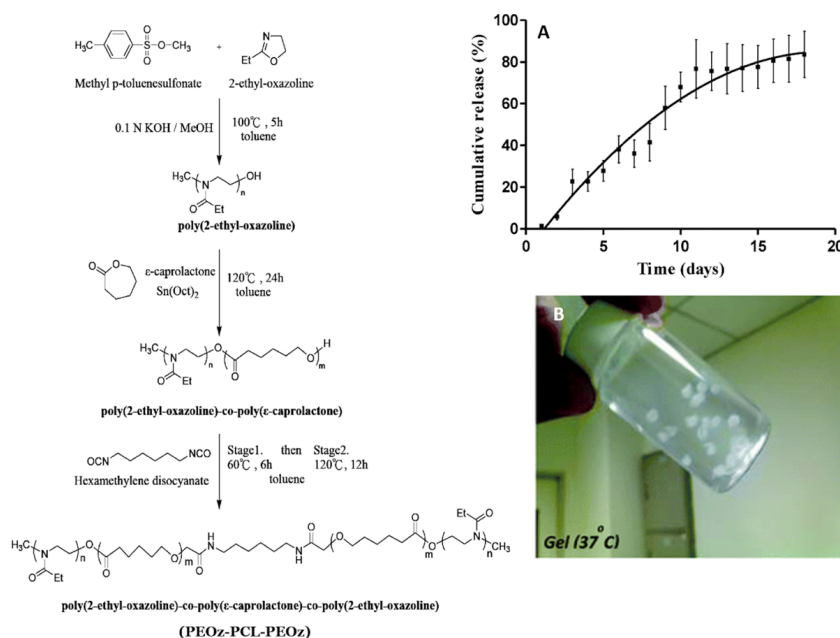
Figure 8 Schematic representation of the synthesis method of amphiphilic PEOz-PCL-PEOz triblock copolymer. A) In vitro cumulative release of bevacizumab from 20 wt % ECE hydrogel. B) Crosslinked PEOz-PCL-PEOz hydrogel particles at 37°C in a viscous solution (B). Adapted and reprinted with permission from [190] Copyright © 2012, American Chemical Society.
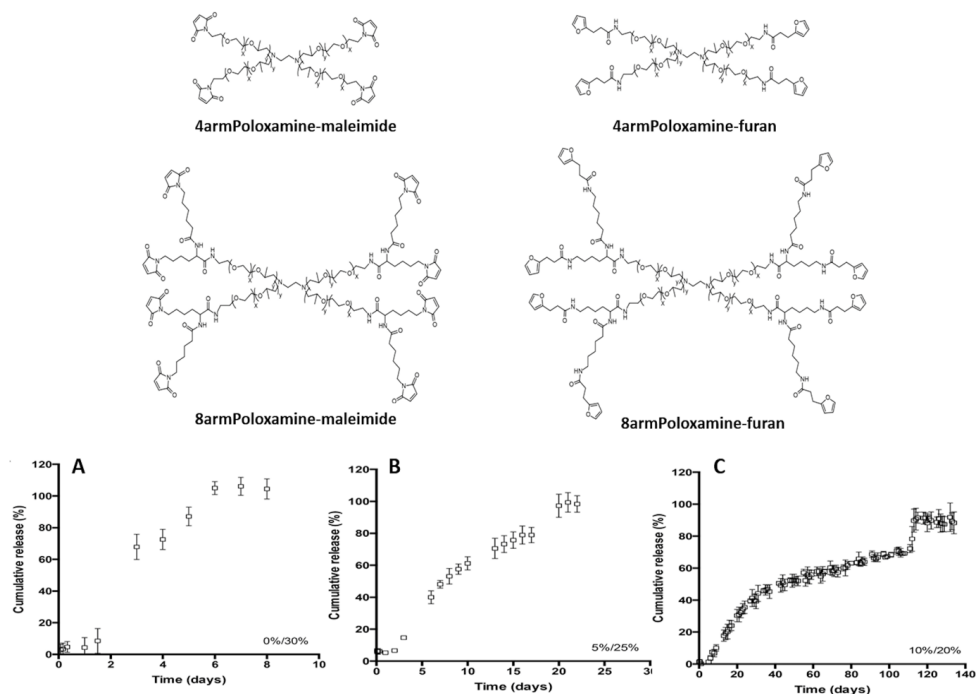
Figure 9 Schematic representation of poloxamines with multiple maleimide or furyl groups used for hydrogel formation by Diels-Alder reaction. In vitro release of bevacizumab from 0%/30% (A), 5%/25% (B), and 10%/20% (C) 8armPoloxamine to 4armPoloxamine ratios Diels-Alder hydrogels in phosphate buffer, pH 7.4 at 37°C. Adapted and reprinted with permission from [189] Copyright © 2017 American Chemical Society.

3.5 Hybrid-delivery hydrogel technologies

Besides the dispersion/dissolution of a proteinaceous drug in a hydrogel matrix, sustained release can also be obtained by incorporating drug-loaded polymeric nanoparticles, microparticles, micelles and liposomes in a hydrogel network, which is named hybrid-delivery technology.[134, 226, 290] As previously discussed in section 2.2.3, drug delivery particles with size <500nm generally diffuse rapidly in the vitreous and are rapidly cleared from the posterior segment, especially if neutrally or negatively charged. Therefore, once loaded in hydrogels, drug-loaded particles are immobile and thus retained at the site of administration. Rong *et al.* recently evaluated the use of insulin-loaded chitosan nanoparticles/PLGA-PEG-PLGA hydrogel (ICNPH) for a neuroprotective effect in a diabetic retinopathy rat model.[167] The primary objective of the study was to provide evidence for its potential clinical application for DR. After subconjunctival injection of ICNPH in diabetic rats, retinal histological and functional changes were evaluated at different time points. The authors showed that the system was able to protect retinal function, reduced cell apoptosis and decreased VEGF expressions compared to controls.[167] Another intraocular hybrid nanoparticles/hydrogel delivery technology was studied by Basuki *et al.*[170], who described the use of polymer-coated gold nanoparticles (AuNPs) loaded in an agarose

hydrogel as a depot for intraocular delivery of both model proteins (BSA, IgG) and therapeutic proteins (bevacizumab, ranibizumab, conbercept). The system was engineered to release the proteins to the retina by a visible light-trigger with an "on-off" release mechanism for non-invasive repetitive dosing. The exposure of visible light (400-500 nm, 508 mW/cm^2, 10 min) caused a localized temperature increase of the hydrogel depot (up to 50 °C) due to the conversion of photons to thermal energy by gold nanostructures. As a result, the agarose matrix underwent a reversible reduction of the storage modulus (G') that resulted in the triggered release of the pre-loaded proteins. This reduction of G' is associated with lower crosslink density, increased swelling and thus larger mesh size of the network. The authors showed the *in vitro* "on-off" release of the loaded proteins from a 2% agarose 0.01% polymer-coated gold nanoparticles (AuNPs) agarose hydrogel (AuNPs hydrogel), and the rates were generally comparable.[170] The system showed photo-thermal modulation after implantation of the depot loaded with FITC-BSA in the anterior chamber of an isolated bovine eye since high intensity of the FITC-BSA was measured in the aqueous humor after light exposure compared to suitable controls. It would be interesting to study the photo-thermal modulation of this system after intravitreal implantation, as released protein from the hydrogel matrix can easily diffuse to the retina. The system may have good potential as an on-demand release of therapeutics for the treatment of various chronic diseases. Further, the authors did neither discuss nor show data regarding the biodegradability and elimination of the delivery system after the complete release of the loaded proteins. No toxicity was shown to L929 (mouse fibroblasts) after 2 minutes of exposure to blue light (400-500 nm) with increasing light intensity at a fixed distance. However, blue light can cause loss of mitochondrial respiratory activity and therefore result in a decrease of retinal cells viability, as shown by Godley *et al.*[291] Therefore, parameters such as blue light exposure time, light intensity and wavelength should be investigated carefully and optimized to prevent undesired toxicity to retinal tissues.

4   Current challenges for ocular protein delivery by hydrogels

Despite the many advantages of hydrogel-based protein delivery systems, several important issues have to be addressed to develop an effective intraocular drug delivery system suitable for clinical translation and application.

4.1   Protein stability

The physical and chemical stability of the encapsulated and released proteins is crucial at the different stages of drug delivery system development. Ideally, the protein should retain its complex secondary and tertiary structure and biological activity during loading, storage and release, because the loss of structural integrity can result in unwanted immunological responses.[104-106, 292] Hydrogels have proven to stabilize proteins by limiting their mobility in the network structure.[293-295] However, the development of *in-situ* forming hydrogel formulations with crosslinking mechanisms that do not interfere with different functional groups in proteins (e.g. NH$_2$ and SH groups) is a major challenge. Some of the developed crosslinking methods make use of thiol-ene, thiol-maleimide, and Diels-Alder reactions, which can result in highly unwanted chemical immobilization of the protein molecules onto the hydrogel

network.[296-298] The grafted proteins will only be released upon degradation of the network. Moreover, the released proteins may still carry fragments of the network, which in turn may compromise protein activity and might even induce immunogenicity.[106] Double-bonds, present in compounds carrying vinyl sulfone (VS), (metha)crylate, and maleimide groups are reactive towards thiols and amines present in proteins. Yu *et al.* reported that the formation of covalent bonds between bevacizumab and HA-VS of hydrogel networks results in an incomplete release of the encapsulated protein (less than 20% of the loaded protein was released).[296] The authors suggest the use of De Gennes's blob theoretical model for polymers at the semi-dilute state[299] as guidance to reduce the chemical grafting of proteins to the vinylsulfone-thiol (VS-SH) hydrogel network.[296] According to this blob model, polymer chains in semi-dilute solutions can interact with each other at the entanglement points. The authors compared such polymers to the *in-situ* crosslinked hydrogel state from the blob perspective in which the VS-SH hydrogel is formed by chemically crosslinking at the entanglement points. They discussed that the covalent grafting of proteins in the hydrogel network via reaction of, e.g. SH in the protein and VS groups of the polymer is due to the mismatch between reactive groups and the entanglement points, leaving many unreacted VS and SH groups. Therefore, protein grafting to the polymer chains was reduced by using a higher degree of modification (DM) and a higher concentration of SH polymers compared to VS polymers. This strategy was used to decrease the number of unreacted VS groups to achieve extended-release profiles of approximately 60% unmodified proteins for 3 months.[296] As previously discussed Gregoritza *et al.[189]* reported that bevacizumab released from a Diels-Alder (furan-maleimide) *in-situ* forming hydrogel had the same affinity for the VEGF receptor as native bevacizumab by using ELISA assay. However, the authors did not analyze whether the released protein contained fragments of the degraded polymer network, which might, as mentioned before, induce unwanted immune responses. Nevertheless, the potential and unwanted protein reactions with groups present in hydrogel precursors remain one of the major hurdles faced today. Famili *et al.*[172] report the development of bio-orthogonal crosslinking chemistries that enable *in-situ* protein encapsulation without competing reactions with protein functional groups to provide sustained and complete release, as discussed in detail in section 3.3.1. The pH of the formulation is another critical parameter to consider as both very low and high pH values can be detrimental for protein stability and activity due to irreversible conformational changes. Further, the pH, concentration and type of buffering salt can influence many degradation pathways such as deamidation, disulfide bond formation/exchange, isomerization, and fragmentation.[300-302] The optimum pH value varies largely depending on the type of protein. Generally, a weak acidic buffer is optimal for the storage of most antibodies.[300] For example, some of the presently used antibodies such as adalimumab, ranibizumab, and bevacizumab are formulated in slightly acidic buffers (pH 5.2, 5.5 and 6.2, respectively, below their isoelectric points (~8.3- 8.8)[50, 303, 304] for ocular treatments.[189]

4.2   Hydrogel turbidity and viscosity

Hydrogels for intraocular delivery are often designed to be thermosensitive hydrogels. However, some of these hydrogels (based on, e.g. PNIPAM, PLGA-PEG-PLGA, PEOz-PCL-PEOz), become turbid at physiological temperature resulting in non-transparent hydrogels. (Figure 8B) This

phenomenon raises the question of whether hydrogels injected in the vitreous body need to be transparent. There are no restrictions on whether a formulation or device injected into the eye has to be transparent or not.[164] Nevertheless, from the patient's viewpoint, transparency would be beneficial, and accordingly, some formulation scientists conclude that transparency is a significant asset,[165, 173, 226] Nevertheless, the human eye vitreous volume (~4 ml) is relatively large in comparison with the typically injected formulation volume (50 μl). Therefore, hydrogel turbidity does not seem to represent a major obstacle-when the hydrogel is injected and localized outside of the visual path (e.g. behind the iris). Derwent *et al.* reported the localized presence of a thermosensitive FITC-labeled hydrogel in an adult rat model after intravitreal injection. Laser ophthalmoscope images demonstrated that the hydrogel formed locally, and no fluorescence from any other location in the vitreous was observed, and thus the injected hydrogel might not interfere with the vision. Interestingly, after two months, the hydrogel had not moved from the site at which it was initially injected.[173] In addition, it is essential to highlight that opaque FDA approved implants are successfully used in the clinic to treat ocular diseases.[305] However, it is clear that bulky opaque materials/implants are not ideal for intravitreal drug delivery as they could prevent light from reaching the retina. Therefore, since that hydrogels are swellable materials, it is important that opaque gels do not obscure the vision by increasing in size due to swelling and/or degradation after intravitreal implantation. Moreover, small opaque materials should not be injected in the middle of the vitreous body to prevent any discomfort for the patient.

The viscosity of polymeric solutions during injection needs to be considered when developing an injectable *in-situ*, forming hydrogel as the needle diameter used for intraocular delivery is very small (~22-31G).[165, 190] Generally, hydrogels developed for ocular delivery have a relatively high polymeric concentration to achieve extended-release profiles. This high concentration, in turn, may render the injectable solution very viscous and, therefore, do not allow the use of small needles. For this reason, research has been focused on hydrogels that have low initial viscosity, which can increase quickly upon a sol-gel transition at the site of injection. The sol-gel change should occur shortly after injection but not instantaneously to prevent gelation and thus clogging in the needle during the injection procedure.

4.3 Sterilization methods, safety issues, and industrial production

The sterilization methods and safety issues are parameters that need to be taken into consideration for the design and development of intraocular hydrogels that aim to receive approval by registration authorities. The sterilization process of polymeric biomaterials is often challenging, as many sterilization methods have shown to affect the properties of biodegradable polymers profoundly.[306] The sterilization processes among which radiation, chemical sterilization and exposure to high temperatures can cause unwanted polymer degradation and structural changes.[306-308] Also, undesirable effects of the applied sterilization method on the loaded proteins may be a significant issue. Therefore, preferred sterilization methods may differ depending on the polymer/hydrogel composition and drug properties. Importantly, aseptic production technologies and sterile filtration represent an attractive method to pharmaceutically produce sterile hydrogel products. Saher *et al.* used thermosensitive (poloxamer 407 and 188) and ion-activated Gelrite polymers (phytagel) to formulate an ocular *in-situ* forming gel. The authors

concluded that for this system, sterile filtration via a 0.22-μm membrane filter was a more effective sterilization method than gamma sterilization.[309]

Hydrogel degradability is a crucial issue to consider when developing intraocular hydrogel formulations. As previously discussed, hydrogels can be engineered to degrade by enzymatic hydrolysis, photolytic cleavage, *via* ester hydrolysis or a combination of these mechanisms with different degradation rates, depending on the desired drug release rate and specific application. Hydrogels are generally designed to degrade into non-toxic soluble products, which can be either be metabolized and eliminated from the body. It should be mentioned that, so far, there are very limited studies describing the long-term *in vivo* hydrogel degradation in vitreous. However, during material design, it is essential to scrutinize the elimination pathways of molecules used or generated during hydrogel chemical crosslinking or degradation (such as unreacted monomer, initiator, reactive groups and crosslinkers), as such molecules could cause local or systemic toxicity. For example, photo-initiators, such as 2,2-dimethoxy-2-phenyl-acetophenone (mentioned in section 3.4.1), can potentially be cytotoxic and they produce potentially harmful free radicals.[310] Unreacted functional groups (e.g. maleimide, thiols) and polymer fragments can leak out of the hydrogel network during swelling and degradation to the surrounding tissues triggering undesired side reactions. [311] To overcome these issues, research should focus on crosslinking strategies that do not require toxic catalysts and do not generate toxic by-products (e.g. copper-free strain-promoted azide-alkyne cycloaddition[210], inverse-electron demand Diels-alder[312] and Staudinger ligation).[297, 313] Ideally, hydrogel network degradation should generate biologically inert molecules or polymer fragments that can be quickly eliminated from the eye and body. (e.g. small and hydrophilic fragments with non-reactive functional groups).

In addition, more information on intravitreal clearance of molecules with different properties (such as size, charge, and composition) in relevant animal models that can allow animal-to-human translation are considered valuable for the development of intravitreal dosage forms. In 2015, Del Amo et al. analyzed data found in the literature on intravitreal pharmacokinetics in rabbits and humans and concluded that the rabbit animal model could provide a useful prediction for clinical translation.[314] This study did not evaluate disease state effects, which might complement the understanding of intravitreal pharmacokinetics.

Furthermore, other safety issues that are to be considered when designing injectable *in-situ* forming hydrogels for prolonged intraocular release of biotherapeutics are IOP and hydrogel toxicity. As mentioned, hydrogels are swellable materials, and it is important that the swelling properties of the designed hydrogels do not cause IOP. Therefore, efforts should be made to systematically study the correlation between hydrogel swelling ratios and the risk of IOP, as not much information has been reported until now. The toxicity of hydrogels to ocular tissues has been tested both in animal models (rat, mouse, rabbit) and cell models (e.g. RPE cell; L-929 cells) (Table 3). Overall, no significant toxicity has been observed using these models for many hydrogel formulations. However, efforts should be made to evaluate the cytocompatibility of new polymer building blocks and formulations also on other ocular cells, especially those that are relatively in close proximity to the vitreous cavity (e.g. Ganglion cells, Muller cell, and photoreceptors). Yu *et al.* demonstrated that an HA-VS/Dex-SH hydrogel was relatively safe using *in vitro*

cytocompatibility tests on ARPE19 cells and "*in vivo*" compatibility on female New Zealand White rabbit's eye. Further, IOP measurement, ophthalmoscope, full-field electroretinography (ERG), and histological studies showed that the system was compatible with the rabbit's eye after ~ 3 months of evaluation. [165] Other *in vitro* and *in vivo* safety tests of different intraocular hydrogel formulations suggest that many of them are potentially safe for intraocular applications.[177, 188, 190, 289] Nevertheless, long term safety on the human eye has to be investigated. Furthermore, despite the promising preclinical results and the economic potential of intravitreal hydrogels, issues in industrial scale-up and production need to be adequately tackled in the development stage. The manufacturing process and quality control should all match with the standards of GMP and Pharmacopeia. Unfortunately, during the early preclinical research, these crucial aspects are generally insufficiently studied as a result of lacking information in the literature regarding scalability and process development toward GMP manufacturing of hydrogels for ocular applications. The novelty of the approach might be the primary reason for this gap in knowledge. This challenge is even more prominent due to the complex chemistry required to design in situ forming hydrogel for intravitreal protein delivery. The production of polymeric hydrogels is generally accomplished by polymerization of different monomers (mainly hydrophilic) or by modification or functionalization of existing polymers (natural or synthetic). In some cases, multiple synthetic steps are required first to produce the monomers or the functional linkers and then proceed with polymerization or functionalization and crosslinking. This long and complicated synthesis route might limit industrial production as it may not be cost-effective. Unfortunately, another critical challenge that needs to be addressed is the issue of batch-to-batch variation seen on the polymer synthesis (e.g. molecular weight, degree of substitution of functional groups) and hydrogel crosslinking density which could then cause unpredictable release profiles. Finally, it is essential to consider that intraocular polymer depot systems can potentially be contaminated with endotoxins during the polymer production or packaging processes. According to FDA guidelines (issued in 2015, "endotoxin testing recommendations for single-use intraocular ophthalmic devices''), the recommended endotoxin limit for ophthalmic devices is ≤0.2 EU/mL for the anterior and posterior segment of the eye.[315] Endotoxins cannot be easily removed after contamination, and thus the recommended limit value should be taken into account in starting materials and processes. Natural polymer materials may be more prone to endotoxin contamination when compared to synthetic polymers due to difficulties in optimal purification from natural sources.

5   CONCLUSION AND PERSPECTIVES

Intraocular drug delivery is an important challenge, considering that retinal diseases are the leading cause of visual impairment worldwide. So far, the treatments with therapeutic proteins still face significant limitations, including frequent intraocular injections, related adverse effects, relatively high clearance, and high costs of the treatments. The efficiency of intraocularly injected proteins such as bevacizumab, ranibizumab, aflibercept and infliximab has been shown, but despite the clinical successes, sustaining sufficient concentrations in the target tissue for an extended period is still challenging. This review describes the ideal features of hydrogels that could solve these major limitations. In the last years, tremendous efforts have been made to

develop injectable, fast gelling, biocompatible and biodegradable gels. However, challenges regarding initial gel viscosity, hydrogel turbidity, crosslinking strategies, sterilization procedures, storage conditions and long-term intraocular safety need to be addressed by formulation scientists and ophthalmologists to facilitate their clinical translation.

The next generation of intravitreal hydrogels for improved sustained protein delivery should move towards biorthogonal crosslinking to preserve the stability of the encapsulated bioactive and also improve the safety profile of the used materials. Furthermore, the continuous down-regulation of VEGF in the eye due to the prolonged release of anti-VEGF from the hydrogel depot, might, in the long run, cause undesired side effects. Therefore, the next generation of hydrogels depot ideally should focus on disease state triggered sustained release of anti-VEGF so that the depot will release the drug only when there is an up-regulation of the growth factor. Hydrogel depots that provide co-delivery of low molecular weight drugs (e.g. anti-inflammatory corticosteroids) together with therapeutic proteins for a synergic effect might offer an attractive platform for intraocular therapy. Overall, from a clinical standpoint, injectable hydrogels have shown to be attractive tools for sustained protein delivery to the back of the eye. Their administration is similar to the current clinical procedures for intravitreal injections of anti-VEGF, but less frequent injections are potentially needed. Therefore, hydrogels may represent a useful tool to solve the unmet needs in intraocular protein delivery to the retina in the near future.

6   REFERENCES

[1] V. Delplace, S. Payne, M. Shoichet, Delivery strategies for treatment of age-related ocular diseases: From a biological understanding to biomaterial solutions, Journal of Controlled Release, 219 (2015) 652-668.

[2] J.B. Saaddine, A.A. Honeycutt, K.M.V. Narayan, X. Zhang, R. Klein, J.P. Boyle, Projection of Diabetic Retinopathy and Other Major Eye Diseases Among People With Diabetes Mellitus: United States, 2005-2050, Archives of Ophthalmology, 126 (2008) 1740-1747.

[3] N. Congdon, B. O'Colmain, C.C.W. Klaver, R. Klein, B. Munoz, D.S. Friedman, J. Kempen, H.R. Taylor, P. Mitchell, L. Hyman, E.D.P.R. Group, Causes and Prevalence of Visual Impairment Among Adults in the United States, Arch Ophthalmol., 122 (2004) 477-485.

[4] K. Wang, Z. Han, Injectable hydrogels for ophthalmic applications, Journal of Controlled Release, 268 (2017) 212-224.

[5] A. Patel, K. Cholkar, V. Agrahari, A.K. Mitra, Ocular drug delivery systems: An overview, World J Pharmacol, 2 (2013) 47-64.

[6] V. Agrahari, A. Mandal, V. Agrahari, H.M. Trinh, M. Joseph, A. Ray, H. Hadji, R. Mitra, D. Pal, A.K. Mitra, A comprehensive insight on ocular pharmacokinetics, Drug delivery and translational research, 6 (2016) 735-754.

[7] E.M. Del Amo, A.K. Rimpela, E. Heikkinen, O.K. Kari, E. Ramsay, T. Lajunen, M. Schmitt, L. Pelkonen, M. Bhattacharya, D. Richardson, A. Subrizi, T. Turunen, M. Reinisalo, J. Itkonen, E. Toropainen, M. Casteleijn, H. Kidron, M. Antopolsky, K.S. Vellonen, M. Ruponen, A. Urtti, Pharmacokinetic aspects of retinal drug delivery, Prog Retin Eye Res, 57 (2017) 134-185.

[8] J.J. Kang-Mieler, E. Dosmar, W. Liu, W.F. Mieler, Extended ocular drug delivery systems for the anterior and posterior segments: biomaterial options and applications, Expert Opin Drug Deliv, 14 (2017) 611-620.

[9] R. Ehrlich, A. Harris, N.S. Kheradiya, D.M. Winston, T.A. Ciulla, B. Wirostko, Age-related macular degeneration and the aging eye, Clin Interv Aging, 3 (2008) 473-482.

[10] U.N. Das, Diabetic macular edema, retinopathy and age-related macular degeneration as inflammatory conditions, Arch Med Sci, 12 (2016) 1142-1157.

[11] J.S. Penn, A. Madan, R.B. Caldwell, M. Bartoli, R.W. Caldwell, M.E. Hartnett, Vascular endothelial growth factor in eye disease, Prog Retin Eye Res, 27 (2008) 331-371.

[12] T.A. Ciulla, P.J. Rosenfeld, Anti-vascular endothelial growth factor therapy for neovascular ocular diseases other than age-related macular degeneration, Curr Opin Ophthalmol, 20 (2009) 166-174.

[13] V. Agrahari, V. Agrahari, A. Mandal, D. Pal, A.K. Mitra, How are we improving the delivery to back of the eye? Advances and challenges of novel therapeutic approaches, Expert Opin Drug Deliv, 14 (2017) 1145-1162.

[14] M. Amadio, S. Govoni, A. Pascale, Targeting VEGF in eye neovascularization: What's new?: A comprehensive review on current therapies and oligonucleotide-based interventions under development, Pharmacol Res, 103 (2016) 253-269.

2

[15] P.A. Keane, S.R. Sadda, Development of Anti-VEGF Therapies for Intraocular Use: A Guide for Clinicians, J Ophthalmol, 2012 (2012) 483034.

[16] K. Radhakrishnan, N. Sonali, M. Moreno, J. Nirmal, A.A. Fernandez, S. Venkatraman, R. Agrawal, Protein delivery to the back of the eye: barriers, carriers and stability of anti-VEGF proteins, Drug Discov Today, 22 (2017) 416-423.

[17] Z. Elgundi, M. Reslan, E. Cruz, V. Sifniotis, V. Kayser, The state-of-play and future of antibody therapeutics, Adv Drug Deliv Rev, 122 (2017) 2-19.

[18] A. Mandal, R. Bisht, I.D. Rupenthal, A.K. Mitra, Polymeric micelles for ocular drug delivery: From structural frameworks to recent preclinical studies, J Controlled Release, 248 (2017) 96-116.

[19] M.N. Yasin, D. Svirskis, A. Seyfoddin, I.D. Rupenthal, Implants for drug delivery to the posterior segment of the eye: a focus on stimuli-responsive and tunable release systems, Journal of Controlled Release, 196 (2014) 208-221.

[20] D. Chang, K. Park, A. Famili, Hydrogels for sustained delivery of biologics to the back of the eye, Drug Discov Today, 24 (2019) 1470-1482.

[21] M.L. Lovett, X. Wang, T. Yucel, L. York, M. Keirstead, L. Haggerty, D.L. Kaplan, Silk hydrogels for sustained ocular delivery of anti-vascular endothelial growth factor (anti-VEGF) therapeutics, Eur J Pharm Biopharm, 95 (2015) 271-278.

[22] A.K. Rimpela, I. Kiiski, F. Deng, H. Kidron, A. Urtti, Pharmacokinetic Simulations of Intravitreal Biologicals: Aspects of Drug Delivery to the Posterior and Anterior Segments, Pharmaceutics, 11 (2018) 9.

[23] P. Bansal, S. Garg, Y. Sharma, P. Venkatesh, Posterior Segment Drug Delivery Devices: Current and Novel Therapies in Development, J Ocul Pharmacol Ther, 32 (2016) 135-144.

[24] E.B. Souto, J. Dias-Ferreira, A. Lopez-Machado, M. Ettcheto, A. Cano, A. Camins Espuny, M. Espina, M.L. Garcia, E. Sanchez-Lopez, Advanced Formulation Approaches for Ocular Drug Delivery: State-Of-The-Art and Recent Patents, Pharmaceutics, 11 (2019) 460.

[25] S. Shuster, M.D. Jumper, A. Chang, R. Stern, Human vitreous hyaluronidase: isolation and characterization AU - Schwartz, Daniel M, Current Eye Research, 15 (1996) 1156-1162.

[26] M. Bond-Taylor, G. Jakobsson, M. Zetterberg, Posterior vitreous detachment - prevalence of and risk factors for retinal tears, Clin Ophthalmol, 11 (2017) 1689-1695.

[27] H. Nomoto, F. Shiraga, N. Kuno, E. Kimura, S. Fujii, K. Shinomiya, A.K. Nugent, K. Hirooka, T. Baba, Pharmacokinetics of bevacizumab after topical, subconjunctival, and intravitreal administration in rabbits, Invest Ophthalmol Vis Sci, 50 (2009) 4807-4813.

[28] T. Carreon, E. van der Merwe, R.L. Fellman, M. Johnstone, S.K. Bhattacharya, Aqueous outflow - A continuum from trabecular meshwork to episcleral veins, Prog Retin Eye Res, 57 (2017) 108-133.

[29] A. Urtti, L. Salminen, Minimizing systemic absorption of topically administered ophthalmic drugs, Survey of ophthalmology 37 (1993) 435-456.

[30] J.B. Christoforidis, K. Briley, K. Binzel, P. Bhatia, L. Wei, K. Kumar, M.V. Knopp, Systemic Biodistribution and Intravitreal Pharmacokinetic Properties of Bevacizumab, Ranibizumab, and Aflibercept in a Nonhuman Primate Model, Invest Ophthalmol Vis Sci, 58 (2017) 5636-5645.

[31] J. Ali, M. Fazil, M. Qumbar, N. Khan, A. Ali, Colloidal drug delivery system: amplify the ocular delivery, Drug Deliv, 23 (2016) 710-726.

[32] A. Urtti, J.D. Pipkin, G. Rork, T. Sendo, U. Finne, A.J. Repta, Controlled drug delivery devices for experimental ocular studies with timolol 2. Ocular and systemic absorption in rabbits, International Journal of Pharmaceutics, 61 (1990) 241-249.

[33] D.M. Maurice, S. Mishima, Ocular pharmacology, Pharmacology of the Eye (1984) pp. 16-119.

[34] P.J. Missel, Simulating intravitreal injections in anatomically accurate models for rabbit, monkey, and human eyes, Pharm Res, 29 (2012) 3251-3272.

[35] E.M. Heikkinen, S. Auriola, V.P. Ranta, N.J. Demarais, A.C. Grey, E.M. Del Amo, E. Toropainen, K.S. Vellonen, A. Urtti, M. Ruponen, Distribution of Small Molecular Weight Drugs into the Porcine Lens: Studies on Imaging Mass Spectrometry, Partition Coefficients, and Implications in Ocular Pharmacokinetics, Mol Pharm, 16 (2019) 3968-3976.

[36] T.E. Duncan, Side Effects of Topical Ocular Timolol, American Journal of Ophthalmology, 95 (1983) 562-563.

[37] J.A. Anderson, Systemic Absorption of Topical Ocularly Applied Epinephrine and Dipivefrin, JAMA Ophthalmology, 98 (1980) 350-353.

[38] K. Inoue, Managing adverse effects of glaucoma medications, Clin Ophthalmol, 8 (2014) 903-913.

[39] R.D. Bachu, P. Chowdhury, Z.H.F. Al-Saedi, P.K. Karla, S.H.S. Boddu, Ocular Drug Delivery Barriers-Role of Nanocarriers in the Treatment of Anterior Segment Ocular Diseases, Pharmaceutics, 10 (2018).

[40] O. Strauss, The retinal pigment epithelium in visual function, Physiol Rev, 85 (2005) 845-881.

[41] G.Raviola, The Structural Basis of the Blood-Ocular Barriers, Exp. Eye Res., (1977) 27-63.

[42] Y. Shirasaki, Molecular design for enhancement of ocular penetration, J Pharm Sci, 97 (2008) 2462-2496.

[43] J.J. Kang-Mieler, C.R. Osswald, W.F. Mieler, Advances in ocular drug delivery: emphasis on the posterior segment, Expert Opin Drug Deliv, 11 (2014) 1647-1660.

[44] J. Ahn, H. Kim, S.J. Woo, J.H. Park, S. Park, D.J. Hwang, K.H. Park, Pharmacokinetics of intravitreally injected bevacizumab in vitrectomized eyes, J Ocul Pharmacol Ther, 29 (2013) 612-618.

[45] E. Moisseiev, M. Waisbourd, E. Ben-Artsi, E. Levinger, A. Barak, T. Daniels, K. Csaky, A. Loewenstein, I.S. Barequet, Pharmacokinetics of bevacizumab after topical and intravitreal administration in human eyes, Graefes Arch Clin Exp Ophthalmol, 252 (2014) 331-337.

2

[46] J. Barar, A.R. Javadzadeh, Y. Omidi, Ocular novel drug delivery: impacts of membranes and barriers, Expert Opin Drug Deliv, 5 (2008) 567-581.

[47] C. Durairaj, Ocular Pharmacokinetics, Handb Exp Pharmacol, 242 (2017) 31-55.

[48] Q. Xu, N.J. Boylan, J.S. Suk, Y.Y. Wang, E.A. Nance, J.C. Yang, P.J. McDonnell, R.A. Cone, E.J. Duh, J. Hanes, Nanoparticle diffusion in, and microrheology of, the bovine vitreous ex vivo, Journal of Controlled Release, 167 (2013) 76-84.

[49] L. Peeters, N.N. Sanders, K. Braeckmans, K. Boussery, J. Van de Voorde, S.C. De Smedt, J. Demeester, Vitreous: A Barrier to Nonviral Ocular Gene Therapy, Invest Ophthalmol Vis Sci, 46 (2005) 3553-3561.

[50] S.K. Li, M.R. Liddell, H. Wen, Effective electrophoretic mobilities and charges of anti-VEGF proteins determined by capillary zone electrophoresis, J Pharm Biomed Anal, 55 (2011) 603-607.

[51] A.K.M. Clapton S. Dias, Vitreal Elimination Kinetics of Large Molecular Weight FITC-Labeled Dextrans in Albino Rabbits Using a Novel Microsampling Technique, Journal of pharmaceutical sciences, 89 (2000) 572–578.

[52] B.T. Kasdorf, F. Arends, O. Lieleg, Diffusion Regulation in the Vitreous Humor, Biophys J, 109 (2015) 2171-2181.

[53] M. Lamminsalo, E. Taskinen, T. Karvinen, A. Subrizi, L. Murtomaki, A. Urtti, V.P. Ranta, Extended Pharmacokinetic Model of the Rabbit Eye for Intravitreal and Intracameral Injections of Macromolecules: Quantitative Analysis of Anterior and Posterior Elimination Pathways, Pharm Res, 35 (2018) 153.

[54] L.A. Hutton-Smith, E.A. Gaffney, H.M. Byrne, P.K. Maini, D. Schwab, N.A. Mazer, A Mechanistic Model of the Intravitreal Pharmacokinetics of Large Molecules and the Pharmacodynamic Suppression of Ocular Vascular Endothelial Growth Factor Levels by Ranibizumab in Patients with Neovascular Age-Related Macular Degeneration, Mol Pharm, 13 (2016) 2941-2950.

[55] E.M. del Amo, K.S. Vellonen, H. Kidron, A. Urtti, Intravitreal clearance and volume of distribution of compounds in rabbits: In silico prediction and pharmacokinetic simulations for drug development, Eur J Pharm Biopharm, 95 (2015) 215-226.

[56] S. Raghava, M. Hammond, U.B. Kompella, Periocular routes for retinal drug delivery, Expert Opin Drug Deliv, 1 (2004) 99-114.

[57] Y. Peng, L. Tang, Y. Zhou, Subretinal Injection: A Review on the Novel Route of Therapeutic Delivery for Vitreoretinal Diseases, Ophthalmic Res, 58 (2017) 217-226.

[58] R.R. Hartman, U.B. Kompella, Intravitreal, Subretinal, and Suprachoroidal Injections: Evolution of Microneedles for Drug Delivery, J Ocul Pharmacol Ther, 34 (2018) 141-153.

[59] C.L. Rowe-Rendleman, S.A. Durazo, U.B. Kompella, K.D. Rittenhouse, A. Di Polo, A.L. Weiner, H.E. Grossniklaus, M.I. Naash, A.S. Lewin, A. Horsager, H.F. Edelhauser, Drug and gene delivery to the back of the eye: from bench to bedside, Invest Ophthalmol Vis Sci, 55 (2014) 2714-2730.

[60] A.C. Amrite, H.F. Edelhauser, S.R. Singh, U.B. Kompella, Effect of circulation on the disposition and ocular tissue distribution of 20 nm nanoparticles after periocular administration, Mol Vis, 14 (2008) 150-160.

[61] V.P. Ranta, E. Mannermaa, K. Lummepuro, A. Subrizi, A. Laukkanen, M. Antopolsky, L. Murtomaki, M. Hornof, A. Urtti, Barrier analysis of periocular drug delivery to the posterior segment, J Control Release, 148 (2010) 42-48.

[62] C. Loch, S. Zakelj, A. Kristl, S. Nagel, R. Guthoff, W. Weitschies, A. Seidlitz, Determination of permeability coefficients of ophthalmic drugs through different layers of porcine, rabbit and bovine eyes, Eur J Pharm Sci, 47 (2012) 131-138.

[63] J. Jiang, H.S. Gill, D. Ghate, B.E. McCarey, S.R. Patel, H.F. Edelhauser, M.R. Prausnitz, Coated microneedles for drug delivery to the eye, Invest Ophthalmol Vis Sci, 48 (2007) 4038-4043.

[64] S. Jiang, Y.L. Franco, Y. Zhou, J. Chen, Nanotechnology in retinal drug delivery, Int J Ophthalmol, 11 (2018) 1038-1044.

[65] U.B. Kompella, A.C. Amrite, R. Pacha Ravi, S.A. Durazo, Nanomedicines for back of the eye drug delivery, gene delivery, and imaging, Prog Retin Eye Res, 36 (2013) 172-198.

[66] R. Bisht, A. Mandal, J.K. Jaiswal, I.D. Rupenthal, Nanocarrier mediated retinal drug delivery: overcoming ocular barriers to treat posterior eye diseases, Wiley Interdiscip Rev Nanomed Nanobiotechnol, 10 (2018).

[67] R. Varela-Fernandez, V. Diaz-Tome, A. Luaces-Rodriguez, A. Conde-Penedo, X. Garcia-Otero, A. Luzardo-Alvarez, A. Fernandez-Ferreiro, F.J. Otero-Espinar, Drug Delivery to the Posterior Segment of the Eye: Biopharmaceutic and Pharmacokinetic Considerations, Pharmaceutics, 12 (2020).

[68] R.R. Thakur Singh, I. Tekko, K. McAvoy, H. McMillan, D. Jones, R.F. Donnelly, Minimally invasive microneedles for ocular drug delivery, Expert Opin Drug Deliv, 14 (2017) 525-537.

[69] S.H. Park, D.H. Jo, C.S. Cho, K. Lee, J.H. Kim, S. Ryu, C. Joo, J.H. Kim, W. Ryu, Depthwise-controlled scleral insertion of microneedles for drug delivery to the back of the eye, Eur J Pharm Biopharm, 133 (2018) 31-41.

[70] H.B. Song, K.J. Lee, I.H. Seo, J.Y. Lee, S.M. Lee, J.H. Kim, J.H. Kim, W. Ryu, Impact insertion of transfer-molded microneedle for localized and minimally invasive ocular drug delivery, J Control Release, 209 (2015) 272-279.

[71] R.R. Thakur, S.J. Fallows, H.L. McMillan, R.F. Donnelly, D.S. Jones, Microneedle-mediated intrascleral delivery of in situ forming thermoresponsive implants for sustained ocular drug delivery, J Pharm Pharmacol, 66 (2014) 584-595.

[72] S.R. Patel, A.S. Lin, H.F. Edelhauser, M.R. Prausnitz, Suprachoroidal drug delivery to the back of the eye using hollow microneedles, Pharm Res, 28 (2011) 166-176.

[73] A. Than, C. Liu, H. Chang, P.K. Duong, C.M.G. Cheung, C. Xu, X. Wang, P. Chen, Self-implantable double-layered micro-drug-reservoirs for efficient and controlled ocular drug delivery, Nat Commun, 9 (2018) 4433.

[74] A.L. Grilo, A. Mantalaris, The Increasingly Human and Profitable Monoclonal Antibody Market, Trends Biotechnol, 37 (2019) 9-16.

[75] G. Walsh, Biopharmaceutical benchmarks 2014, Nature Biotechnology, 32 (2014) 992.

[76] A. Mandal, D. Pal, V. Agrahari, H.M. Trinh, M. Joseph, A.K. Mitra, Ocular delivery of proteins and peptides: Challenges and novel formulation approaches, Adv Drug Deliv Rev, (2018).

[77] I. Bravo-Osuna, V. Andres-Guerrero, A. Arranz-Romera, S. Esteban-Perez, I.T. Molina-Martinez, R. Herrero-Vanrell, Microspheres as intraocular therapeutic tools in chronic diseases of the optic nerve and retina, Adv Drug Deliv Rev, 126 (2018) 127-144.

[78] W.H. Wu, Y.T. Tsai, S. Justus, T.T. Lee, L. Zhang, C.S. Lin, A.G. Bassuk, V.B. Mahajan, S.H. Tsang, CRISPR Repair Reveals Causative Mutation in a Preclinical Model of Retinitis Pigmentosa, Mol Ther, 24 (2016) 1388-1394.

[79] A. Kato, T. Yasukawa, Y. Ogura, Antivascular endothelial growth factor therapies for neovascular age-related macular degeneration: Search for the optimized treatment regimen, Taiwan J. Ophthalmol, 4 (2014) 3-8.

[80] B.A. Syed, J.B. Evans, L. Bielory, Wet AMD market, Nature Reviews Drug Discovery, 11 (2012) 827.

[81] ResearchAndMarkets.com, Global $10.4 Bn Wet Age-Related Macular Degeneration Market to 2024 - Rising Prevalence of AMD, Lack of a Specific Treatment, and Increasing Aging Population, in, GlobeNewswire https://www.globenewswire.com/news-release/2019/05/15/1824402/0/en/Global-10-4-Bn-Wet-Age-Related-Macular-Degeneration-Market-to-2024-Rising-Prevalence-of-AMD-Lack-of-a-Specific-Treatment-and-Increasing-Aging-Population.html, 2019.

[82] A.W. Stitt, T.M. Curtis, M. Chen, R.J. Medina, G.J. McKay, A. Jenkins, T.A. Gardiner, T.J. Lyons, H.P. Hammes, R. Simo, N. Lois, The progress in understanding and treatment of diabetic retinopathy, Prog Retin Eye Res, 51 (2016) 156-186.

[83] C.H. Meyer, F.G. Holz, Preclinical aspects of anti-VEGF agents for the treatment of wet AMD: ranibizumab and bevacizumab, Eye (Lond), 25 (2011) 661-672.

[84] J. Ambati, B.J. Fowler, Mechanisms of age-related macular degeneration, Neuron, 75 (2012) 26-39.

[85] C. Thetford, S. Hodge, S. Harding, S. Taylor, P.C. Knox, Living with age-related macular degeneration treatment: Patient experiences of being treated with ranibizumab (Lucentis)(R) intravitreal injections, British Journal of Visual Impairment, 31 (2013) 89-101.

[86] R. Sophie, A. Akhtar, Y.J. Sepah, M. Ibrahim, M. Bittencourt, D.V. Do, Q.D. Nguyen, Aflibercept: a Potent Vascular Endothelial Growth Factor Antagonist for Neovascular Age-Related Macular Degeneration and Other Retinal Vascular Diseases, Biol Ther, 2 (2012) 3.

[87] G. Levy-Clarke, D.A. Jabs, R.W. Read, J.T. Rosenbaum, A. Vitale, R.N. Van Gelder, Expert panel recommendations for the use of anti-tumor necrosis factor biologic agents in patients with ocular inflammatory disorders, Ophthalmology, 121 (2014) 785-796 e783.

[88] H. Khalili, R.W. Lee, P.T. Khaw, S. Brocchini, A.D. Dick, D.A. Copland, An anti-TNF-alpha antibody mimetic to treat ocular inflammation, Sci Rep, 6 (2016) 36905.

[89] M.E.C.K. Lucia Sobrin, MD; William Christen, PhD; Thekla Papadaki, MD; Erik Letko, MD; C. Stephen Foster, MD, Infliximab Therapy for the Treatment of Refractory Ocular Inflammatory Disease, Arch Ophthalmol., 125(7) (2007) 895-900.

[90] J.N. Kruh, P. Yang, A.M. Suelves, C.S. Foster, Infliximab for the treatment of refractory noninfectious Uveitis: a study of 88 patients with long-term follow-up, Ophthalmology, 121 (2014) 358-364.

[91] P.U. Dugel, A. Koh, Y. Ogura, G.J. Jaffe, U. Schmidt-Erfurth, D.M. Brown, A.V. Gomes, J. Warburton, A. Weichselberger, F.G. Holz, Hawk, H.S. Investigators, HAWK and HARRIER: Phase 3, Multicenter, Randomized, Double-Masked Trials of Brolucizumab for Neovascular Age-Related Macular Degeneration, Ophthalmology, 127 (2020) 72-84.

[92] Q.D. Nguyen, A. Das, D.V. Do, P.U. Dugel, A. Gomes, F.G. Holz, A. Koh, C.K. Pan, Y.J. Sepah, N. Patel, H. MacLeod, P. Maurer, Brolucizumab: Evolution through Preclinical and Clinical Studies and the Implications for the Management of Neovascular Age-Related Macular Degeneration, Ophthalmology, 127 (2020) 963-976.

[93] T.A. Moreno, S.J. Kim, Ranibizumab (Lucentis) versus Bevacizumab (Avastin) for the Treatment of Age-Related Macular Degeneration: An Economic Disparity of Eye Health, Seminars in Ophthalmology, 31 (2016) 378-384.

[94] L. Xu, T. Lu, L. Tuomi, N. Jumbe, J. Lu, S. Eppler, P. Kuebler, L.A. Damico-Beyer, A. Joshi, Pharmacokinetics of ranibizumab in patients with neovascular age-related macular degeneration: a population approach, Invest Ophthalmol Vis Sci, 54 (2013) 1616-1624.

[95] A. Moradi, Y.J. Sepah, M.A. Sadiq, H. Nasir, S. Kherani, R. Sophie, D.V. Do, Q.D. Nguyen, Vascular endothelial growth factor trap-eye (Aflibercept) for the management of diabetic macular edema, World J Diabetes, 4 (2013) 303-309.

[96] F. Semeraro, F. Morescalchi, S. Duse, F. Parmeggiani, E. Gambicorti, C. Costagliola, Aflibercept in wet AMD: specific role and optimal use, Drug Des Devel Ther, 7 (2013) 711-722.

[97] A.S. Basile, M.M. Hutmacher, K.G. Kowalski, K.Y. Gandelman, D.J. Nickens, Population pharmacokinetics of pegaptanib sodium (Macugen ®) in patients with diabetic macular edema, Clin Ophthalmol, 9 (2015) 323-335.

[98] S.A. Vinores, Pegaptanib in the treatment of wet, age-related macular degeneration, International Journal of Nanomedicine 1(2006) 263–268.

[99] P. Neri, M. Lettieri, C. Fortuna, M. Zucchi, M. Manoni, S. Celani, A. Giovannini, Adalimumab (Humira™) in Ophthalmology: A Review of the Literature, Middle East African Journal of Ophthalmology, 17 (2010) 290-296.

[100] U. Klotz, A. Teml, M. Schwab, Clinical Pharmacokinetics and Use of Infliximab, Clinical Pharmacokinetics, 46 (2007) 645-660.

[101] F. Giansanti, M. Ramazzotti, L. Vannozzi, E. Rapizzi, T. Fiore, B. Iaccheri, D. Degl' Innocenti, D. Moncini, U. Menchini, A pilot study on ocular safety of intravitreal infliximab in a rabbit model, Invest Ophthalmol Vis Sci, 49 (2008) 1151-1156.

[102] S.J. Shire, Z. Shahrokh, J. Liu, Challenges in the development of high protein concentration formulations, J Pharm Sci, 93 (2004) 1390-1402.

[103] S. Frokjaer, D.E. Otzen, Protein drug stability: a formulation challenge, Nature Reviews Drug Discovery, 4 (2005) 298.

2

[104] K.D. Ratanji, J.P. Derrick, R.J. Dearman, I. Kimber, Immunogenicity of therapeutic proteins: influence of aggregation, J Immunotoxicol, 11 (2014) 99-109.

[105] E.M. Moussa, J.P. Panchal, B.S. Moorthy, J.S. Blum, M.K. Joubert, L.O. Narhi, E.M. Topp, Immunogenicity of Therapeutic Protein Aggregates, J Pharm Sci, 105 (2016) 417-430.

[106] W. Jiskoot, T.W. Randolph, D.B. Volkin, C.R. Middaugh, C. Schoneich, G. Winter, W. Friess, D.J. Crommelin, J.F. Carpenter, Protein instability and immunogenicity: roadblocks to clinical application of injectable protein delivery systems for sustained release, J Pharm Sci, 101 (2012) 946-954.

[107] J. den Engelsman, P. Garidel, R. Smulders, H. Koll, B. Smith, S. Bassarab, A. Seidl, O. Hainzl, W. Jiskoot, Strategies for the assessment of protein aggregates in pharmaceutical biotech product development, Pharm Res, 28 (2011) 920-933.

[108] A.M. Schauwvlieghe, G. Dijkman, J.M. Hooymans, F.D. Verbraak, C.B. Hoyng, M.G. Dijkgraaf, T. Peto, J.R. Vingerling, R.O. Schlingemann, Comparing the Effectiveness of Bevacizumab to Ranibizumab in Patients with Exudative Age-Related Macular Degeneration. The BRAMD Study, PLoS One, 11 (2016) e0153052.

[109] S.P. Vyas, R. Paliwal, S.R. Paliwal, Chapter 5 - Ocular Delivery of Peptides and Proteins, in: C. Van Der Walle (Ed.) Peptide and Protein Delivery, Academic Press, Boston, 2011, pp. 87-103.

[110] M. El Sanharawi, L. Kowalczuk, E. Touchard, S. Omri, Y. de Kozak, F. Behar-Cohen, Protein delivery for retinal diseases: from basic considerations to clinical applications, Prog Retin Eye Res, 29 (2010) 443-465.

[111] T. Yasukawa, Y. Ogura, H. Kimura, E. Sakurai, Y. Tabata, Drug delivery from ocular implants, Expert Opin. Drug Delivery, 3 (2006) 261-273.

[112] J.L. Bourges, C. Bloquel, A. Thomas, F. Froussart, A. Bochot, F. Azan, R. Gurny, D. BenEzra, F. Behar-Cohen, Intraocular implants for extended drug delivery: therapeutic applications, Adv Drug Deliv Rev, 58 (2006) 1182-1202.

[113] R.L. Avery, D.J. Pieramici, M.D. Rabena, A.A. Castellarin, M.A. Nasir, M.J. Giust, Intravitreal bevacizumab (Avastin) for neovascular age-related macular degeneration, Ophthalmology, 113 (2006) 363-372 e365.

[114] M.W. Stewart, P.J. Rosenfeld, Predicted biological activity of intravitreal VEGF Trap, Br J Ophthalmol, 92 (2008) 667-668.

[115] S.J. Bakri, M.R. Snyder, J.M. Reid, J.S. Pulido, M.K. Ezzat, R.J. Singh, Pharmacokinetics of intravitreal ranibizumab (Lucentis), Ophthalmology, 114 (2007) 2179-2182.

[116] J.A. Haller, P. Dugel, D.V. Weinberg, C. Chou, S.M. Whitcup, Evaluation of the safety and performance of an applicator for a novel intravitreal dexamethasone drug delivery system for the treatment of macular edema, Retina, 29 (2009) 46-51.

[117] S.S. Lee, P. Hughes, A.D. Ross, M.R. Robinson, Biodegradable implants for sustained drug release in the eye, Pharm Res, 27 (2010) 2043-2053.

[118] N. Haghjou, M. Soheilian, M.J. Abdekhodaie, Sustained release intraocular drug delivery devices for treatment of uveitis, Journal of ophthalmic & vision research, 6 (2011) 317-329.

[119] ClinicalTrials.gov, Safety and Efficacy of an Injectable Fluocinolone Acetonide Intravitreal Insert, in, https://clinicaltrials.gov/ct2/show/NCT01694186, 2012.

[120] ClinicalTrials.gov, Safety and Efficacy Study of a Fluocinolone Acetonide Intravitreal (FAI) Insert in Subjects With Chronic Non-infectious Posterior Uveitis, in, https://clinicaltrials.gov/ct2/show/NCT02746991, 2016.

[121] E. Donnenfeld, E. Holland, Dexamethasone Intracameral Drug-Delivery Suspension for Inflammation Associated with Cataract Surgery: A Randomized, Placebo-Controlled, Phase III Trial, Ophthalmology, 125 (2018) 799-806.

[122] L.F. Weber, S. Marx, G.U. Auffarth, A.F. Scheuerle, T. Tandogan, C. Mayer, R. Khoramnia, Injectable 0.19-mg fluocinolone acetonide intravitreal implant for the treatment of non-infectious uveitic macular edema, J Ophthalmic Inflamm Infect, 9 (2019) 3.

[123] F.E. Kane, J. Burdan, A. Cutino, K.E. Green, Iluvien: a new sustained delivery technology for posterior eye disease, Expert Opin Drug Deliv, 5 (2008) 1039-1046.

[124] ClinicalTrials.gov, Iluvien Registry Safety Study (IRISS) in, https://clinicaltrials.gov/ct2/show/NCT01998412, 2013.

[125] D.S. Boyer, Y.H. Yoon, R. Belfort, Jr., F. Bandello, R.K. Maturi, A.J. Augustin, X.Y. Li, H. Cui, Y. Hashad, S.M. Whitcup, M.S.G. Ozurdex, Three-year, randomized, sham-controlled trial of dexamethasone intravitreal implant in patients with diabetic macular edema, Ophthalmology, 121 (2014) 1904-1914.

[126] A. Chan, L.S. Leung, M.S. Blumenkranz, Critical appraisal of the clinical utility of the dexamethasone intravitreal implant (Ozurdex) for the treatment of macular edema related to branch retinal vein occlusion or central retinal vein occlusion, Clin Ophthalmol, 5 (2011) 1043-1049.

[127] L.L. Lim, J.R. Smith, J.T. Rosenbaum, Retisert (Bausch & Lomb/Control Delivery Systems), Curr Opin Investig Drugs, 6 (2005) 1159-1167.

[128] ClinicalTrials.gov, Effect of Intravitreal Long Acting Dexamethasone Implant, Ozurdex in Patients With Diabetic Macular Edema, in, https://clinicaltrials.gov/ct2/show/NCT01698749, 2012.

[129] G.J. Jaffe, D. Martin, D. Callanan, P.A. Pearson, B. Levy, T. Comstock, G. Fluocinolone Acetonide Uveitis Study, Fluocinolone acetonide implant (Retisert) for noninfectious posterior uveitis: thirty-four-week results of a multicenter randomized clinical study, Ophthalmology, 113 (2006) 1020-1027.

[130] D.S. Boyer, J. Posalski, Potential complication associated with removal of ganciclovir implants, American Journal of Ophthalmology, 127 (1999) 349-350.

[131] C.H. Tsai, P.Y. Wang, I.C. Lin, H. Huang, G.S. Liu, C.L. Tseng, Ocular Drug Delivery: Role of Degradable Polymeric Nanocarriers for Ophthalmic Application, Int J Mol Sci, 19 (2018) 2830.

[132] F.S.Y. Wong, K.K. Tsang, A.C.Y. Lo, Delivery of therapeutics to posterior eye segment: cell-encapsulating systems, Neural Regener. Res., 12 (2017) 576-577.

2

[133] B. Annamalai, N. Parsons, M. Belhaj, C. Brandon, J. Potts, B. Rohrer, Encapsulated Cell Technology-Based Delivery of a Complement Inhibitor Reduces Choroidal Neovascularization in a Mouse Model, Transl Vis Sci Technol, 7 (2018) 3.

[134] V. Agrahari, V. Agrahari, W.T. Hung, L.K. Christenson, A.K. Mitra, Composite Nanoformulation Therapeutics for Long-Term Ocular Delivery of Macromolecules, Mol Pharm, 13 (2016) 2912-2922.

[135] F.J. Otero-Espinar, A. Fernández-Ferreiro, M. González-Barcia, J. Blanco-Méndez, A. Luzardo, Chapter 6 - Stimuli sensitive ocular drug delivery systems, in: A.M. Grumezescu (Ed.) Drug Targeting and Stimuli Sensitive Drug Delivery Systems, William Andrew Publishing, 2018, pp. 211-270.

[136] N. Kuno, S. Fujii, Recent Advances in Ocular Drug Delivery Systems, Polymers, 3 (2011) 193-221.

[137] ClinicalTrials.gov, Study of the efficacy and safety of the ranibizumab port delivery system (RPDS) for sustained delivery of ranibizumab in participants with subfoveal neovascular age-related macular degeneration (LADDER), 2015 https://clinicaltrials.gov/ct2/show/NCT02510794 (accessed May 05, 2021)

[138] ClinicalTrials.gov, Extension Study for the Port Delivery System With Ranibizumab (Portal) (Portal), in, https://clinicaltrials.gov/ct2/show/NCT03683251 (accessed May 22, 2021), 2018.

[139] J.C. Boyette, Randolph E.; Erickson, Signe; Farinas, Kathleen Cogan; Sacherman, Kevin W, Patent: Porous structure for sustained release drug delivery device, in: https://patents.google.com/patent/CN108430405A/en, China, 2016.

[140] P.A. Campochiaro, D.M. Marcus, C.C. Awh, C. Regillo, A.P. Adamis, V. Bantseev, Y. Chiang, J.S. Ehrlich, S. Erickson, W.D. Hanley, J. Horvath, K.F. Maass, N. Singh, F. Tang, G. Barteselli, The Port Delivery System with Ranibizumab for Neovascular Age-Related Macular Degeneration: Results from the Randomized Phase 2 Ladder Clinical Trial, Ophthalmology, 126 (2019) 1141-1154.

[141] Y. Liu, J. Liu, S. Chen, T. Lei, Y. Kim, S. Niu, H. Wang, X. Wang, A.M. Foudeh, J.B. Tok, Z. Bao, Soft and elastic hydrogel-based microelectronics for localized low-voltage neuromodulation, Nat Biomed Eng, 3 (2019) 58-68.

[142] S. Gharazi, B.C. Zarket, K.C. DeMella, S.R. Raghavan, Nature-Inspired Hydrogels with Soft and Stiff Zones that Exhibit a 100-Fold Difference in Elastic Modulus, ACS Appl Mater Interfaces, 10 (2018) 34664-34673.

[143] N. Contessi Negrini, M. Bonnetier, G. Giatsidis, D.P. Orgill, S. Fare, B. Marelli, Tissue-mimicking gelatin scaffolds by alginate sacrificial templates for adipose tissue engineering, Acta biomaterialia, 87 (2019) 61-75.

[144] Y. Zhang, J. Yu, K. Ren, J. Zuo, J. Ding, X. Chen, Thermosensitive Hydrogels as Scaffolds for Cartilage Tissue Engineering, Biomacromolecules, 20 (2019) 1478-1492.

[145] A.S. Hoffman, Hydrogels for biomedical applications, Adv Drug Delivery Rev, 64 (2002) 18-23.

[146] M. Castilho, G. Hochleitner, W. Wilson, B. van Rietbergen, P.D. Dalton, J. Groll, J. Malda, K. Ito, Mechanical behavior of a soft hydrogel reinforced with three-dimensional printed microfibre scaffolds, Sci Rep, 8 (2018) 1245.

[147] J.L. Drury, D.J. Mooney, Hydrogels for tissue engineering: scaffold design variables and applications, Biomaterials, 24 (2003) 4337-4351.

[148] L. Saunders, P.X. Ma, Self-Healing Supramolecular Hydrogels for Tissue Engineering Applications, Macromol Biosci, 19 (2019) e1800313.

[149] C. Ghobril, M.W. Grinstaff, The chemistry and engineering of polymeric hydrogel adhesives for wound closure: a tutorial, Chem Soc Rev, 44 (2015) 1820-1835.

[150] J. Sueda, T. Fukuchi, N. Usumoto, T. Okuno, M. Arai, T. Hirose, Intraocular use of hydrogel tissue adhesive in rabbit eyes, Jpn J Ophthalmol, 51 (2007) 89-95.

[151] Z. Zhang, J. Ni, L. Chen, L. Yu, J. Xu, J. Ding, Biodegradable and thermoreversible PCLA-PEG-PCLA hydrogel as a barrier for prevention of post-operative adhesion, Biomaterials, 32 (2011) 4725-4736.

[152] T. Vermonden, R. Censi, W.E. Hennink, Hydrogels for protein delivery, Chem Rev, 112 (2012) 2853-2888.

[153] V. Delplace, A. Ortin-Martinez, E.L.S. Tsai, A.N. Amin, V. Wallace, M.S. Shoichet, Controlled release strategy designed for intravitreal protein delivery to the retina, Journal of Controlled Release, 293 (2019) 10-20.

[154] O. Wichterle, D. LÍM, Hydrophilic Gels for Biological Use, Nature, 185 (1960) 117-118.

[155] M.F. Passos, D.R.C. Dias, G.N.T. Bastos, A.L. Jardini, A.C.B. Benatti, C.G.B.T. Dias, R. Maciel Filho, pHEMA hydrogels, Journal of Thermal Analysis and Calorimetry, 125 (2016) 361-368.

[156] S. Cascone, G. Lamberti, Hydrogel-based commercial products for biomedical applications: A review, Int J Pharm, 573 (2020) 118803.

[157] S.J. Buwalda, T. Vermonden, W.E. Hennink, Hydrogels for Therapeutic Delivery: Current Developments and Future Directions, Biomacromolecules, 18 (2017) 316-330.

[158] R. Censi, P. Di Martino, T. Vermonden, W.E. Hennink, Hydrogels for protein delivery in tissue engineering, J Controlled Release, 161 (2012) 680-692.

[159] E. Caló, V.V. Khutoryanskiy, Biomedical applications of hydrogels: A review of patents and commercial products, European Polymer Journal, 65 (2015) 252-267.

[160] E.M. Ahmed, Hydrogel: Preparation, characterization, and applications: A review, J Adv Res, 6 (2015) 105-121.

[161] C.C.L. Schuurmans, A. Abbadessa, M.A. Bengtson, G. Pletikapic, H.B. Eral, G. Koenderink, R. Masereeuw, W.E. Hennink, T. Vermonden, Complex coacervation-based loading and tunable release of a cationic protein from monodisperse glycosaminoglycan microgels, Soft Matter, 14 (2018) 6327-6341.

2

[162] Y. Tabata, Y. Ikada, Protein release from gelatin matrices, Advanced Drug Delivery Reviews, 31 (1998) 287-301.

[163] E. Jooybar, M.J. Abdekhodaie, A. Mousavi, B. Zoetebier, P.J. Dijkstra, Enzymatically crosslinked hyaluronic acid microgels as a vehicle for sustained delivery of cationic proteins, European Polymer Journal, 115 (2019) 234-243.

[164] S. Kirchhof, A.M. Goepferich, F.P. Brandl, Hydrogels in ophthalmic applications, Eur J Pharm Biopharm, 95 (2015) 227-238.

[165] Y. Yu, L.C. Lau, A.C. Lo, Y. Chau, Injectable Chemically Crosslinked Hydrogel for the Controlled Release of Bevacizumab in Vitreous: A 6-Month In Vivo Study, Translational Vision Science & Technology, 4 (2015) 5.

[166] S.B. Turturro, M.J. Guthrie, A.A. Appel, P.W. Drapala, E.M. Brey, V.H. Perez-Luna, W.F. Mieler, J.J. Kang-Mieler, The effects of cross-linked thermo-responsive PNIPAAm-based hydrogel injection on retinal function, Biomaterials, 32 (2011) 3620-3626.

[167] X. Rong, Y. Ji, X. Zhu, J. Yang, D. Qian, X. Mo, Y. Lu, Neuroprotective effect of insulin-loaded chitosan nanoparticles/PLGA-PEG-PLGA hydrogel on diabetic retinopathy in rats, Int J Nanomedicine, 14 (2019) 45-55.

[168] K.H. Bae, L.-S. Wang, M. Kurisawa, Injectable biodegradable hydrogels: progress and challenges, Journal of Materials Chemistry B, 1 (2013) 5371.

[169] R. Egbu, S. Brocchini, P.T. Khaw, S. Awwad, Antibody loaded collapsible hyaluronic acid hydrogels for intraocular delivery, European Journal of Pharmaceutics and Biopharmaceutics, 124 (2018) 95-103.

[170] F.Q. Johan S. Basuki, Xavier Mulet, Randy Suryadinata, Aditya V. Vashi, Yong Y. Peng,Lingli Li, Xiaojuan Hao,Tianwei Tan, and Timothy C. Hughes, Photo-Modulated Therapeutic Protein Release from aHydrogel Depot Using Visible Light, Angewandte Chemie, 56 (2017) 966-971.

[171] G.P.M. Hisanori Imai, Linfeng Wu, Dileep R. Janagam, Thomas W. Gardner, and Tao L. Lowe, Subconjunctivally Implanted Hydrogels for Sustained Insulin Release to Reduce Retinal Cell Apoptosis in Diabetic Rats, The Association for Research in Vision and Ophthalmology, Inc., 56 (2015) 7839–7846.

[172] A. Famili, K. Rajagopal, Bio-Orthogonal Cross-Linking Chemistry Enables In Situ Protein Encapsulation and Provides Sustained Release from Hyaluronic Acid Based Hydrogels, Mol Pharm, 14 (2017) 1961-1968.

[173] J.J.K.D.P.W.F.M. MD, Thermoresponsive hydrogels as a new ocular drug delivery platform to the posterior segment of the eye., Trans Am Ophthalmol Soc, 106 (2008) 206-214.

[174] O.P.V. O. Franssen , W.E. Hennink, Delayed release of a model protein from enzymatically-degrading dextran hydrogels, Journal of Controlled Release, 44 (1997) 237–245.

[175] M.F. Akhtar, M. Hanif, N.M. Ranjha, Methods of synthesis of hydrogels … A review, Saudi Pharm J, 24 (2016) 554-559.

[176] G. Turco, I. Donati, M. Grassi, G. Marchioli, R. Lapasin, S. Paoletti, Mechanical spectroscopy and relaxometry on alginate hydrogels: a comparative analysis for structural characterization and network mesh size determination, Biomacromolecules, 12 (2011) 1272-1282.

[177] L.Q. Yang, Y.Q. Lan, H. Guo, L.Z. Cheng, J.Z. Fan, X. Cai, L.M. Zhang, R.F. Chen, H.S. Zhou, Ophthalmic drug-loaded N,O-carboxymethyl chitosan hydrogels: synthesis, in vitro and in vivo evaluation, Acta Pharmacol Sin, 31 (2010) 1625-1634.

[178] J. Huang, W. Wang, J. Yu, X. Yu, Q. Zheng, F. Peng, Z. He, W. Zhao, Z. Zhang, X. Li, Q. Wang, Combination of dexamethasone and Avastin((R)) by supramolecular hydrogel attenuates the inflammatory corneal neovascularization in rat alkali burn model, Colloids Surf B Biointerfaces, 159 (2017) 241-250.

[179] F. van de Manakker, T. Vermonden, C.F. van Nostrum, W.E. Hennink, Cyclodextrin-Based Polymeric Materials: Synthesis, Properties, and Pharmaceutical/Biomedical Applications, Biomacromolecules, 10 (2009) 3157-3175.

[180] O. Franssen, L. Vandervennet, P. Roders, W.E. Hennink, Degradable dextran hydrogels: controlled release of a model protein from cylinders and microspheres, Journal of Controlled Release, 60 (1999) 211-221.

[181] S.J. Buwalda, A. Bethry, S. Hunger, S. Kandoussi, J. Coudane, B. Nottelet, Ultrafast in situ forming poly(ethylene glycol)-poly(amido amine) hydrogels with tunable drug release properties via controllable degradation rates, Eur J Pharm Biopharm, 139 (2019) 232-239.

[182] R. Censi, T. Vermonden, M.J. van Steenbergen, H. Deschout, K. Braeckmans, S.C. De Smedt, C.F. van Nostrum, P. di Martino, W.E. Hennink, Photopolymerized thermosensitive hydrogels for tailorable diffusion-controlled protein delivery, Journal of Controlled Release, 140 (2009) 230-236.

[183] S. Kirchhof, M. Abrami, V. Messmann, N. Hammer, A.M. Goepferich, M. Grassi, F.P. Brandl, Diels-Alder Hydrogels for Controlled Antibody Release: Correlation between Mesh Size and Release Rate, Mol Pharm, 12 (2015) 3358-3368.

[184] C.C. Lin, A.T. Metters, Hydrogels in controlled release formulations: network design and mathematical modeling, Adv Drug Deliv Rev, 58 (2006) 1379-1408.

[185] P.L. Ritger, N.A. Peppas, A simple equation for description of solute release I. Fickian and non-fickian release from non-swellable devices in the form of slabs, spheres, cylinders or discs, Journal of Controlled Release, 5 (1987) 23-36.

[186] P.L. Ritger, N.A. Peppas, A simple equation for description of solute release II. Fickian and anomalous release from swellable devices, Journal of Controlled Release, 5 (1987) 37-42.

[187] B. Xie, L. Jin, Z. Luo, J. Yu, S. Shi, Z. Zhang, M. Shen, H. Chen, X. Li, Z. Song, An injectable thermosensitive polymeric hydrogel for sustained release of Avastin(R) to treat posterior segment disease, Int J Pharm, 490 (2015) 375-383.

[188] J. Yu, X. Xu, F. Yao, Z. Luo, L. Jin, B. Xie, S. Shi, H. Ma, X. Li, H. Chen, In situ covalently cross-linked PEG hydrogel for ocular drug delivery applications, Int J Pharm, 470 (2014) 151-157.

[189] M. Gregoritza, V. Messmann, K. Abstiens, F.P. Brandl, A.M. Goepferich, Controlled Antibody Release from Degradable Thermoresponsive Hydrogels Cross-Linked by Diels-Alder Chemistry, Biomacromolecules, 18 (2017) 2410-2418.

[190] C.H. Wang, Y.S. Hwang, P.R. Chiang, C.R. Shen, W.H. Hong, G.H. Hsiue, Extended release of bevacizumab by thermosensitive biodegradable and biocompatible hydrogel, Biomacromolecules, 13 (2012) 40-48.

[191] D. Park, V. Shah, B.M. Rauck, T.R. Friberg, Y. Wang, An anti-angiogenic reverse thermal gel as a drug-delivery system for age-related wet macular degeneration, Macromol Biosci, 13 (2013) 464-469.

[192] T.R.F. Britta M. Rauck, Carlos A. Medina Mendez, Daewon Park, Veeral Shah, Richard A. Bilonick and Yadong Wang, Biocompatible Reverse Thermal Gel Sustains the Release of Intravitreal Bevacizumab In Vivo, The Association for Research in Vision and Ophthalmology, 55 (2014) 469–476.

[193] W. Liu, B.S. Lee, W.F. Mieler, J.J. Kang-Mieler, Biodegradable Microsphere-Hydrogel Ocular Drug Delivery System for Controlled and Extended Release of Bioactive Aflibercept In Vitro, Curr Eye Res, 44 (2019) 264-274.

[194] X. Xu, Y. Weng, L. Xu, H. Chen, Sustained release of Avastin(R) from polysaccharides cross-linked hydrogels for ocular drug delivery, Int J Biol Macromol, 60 (2013) 272-276.

[195] P. Tyagi, M. Barros, J.W. Stansbury, U.B. Kompella, Light-activated, in situ forming gel for sustained suprachoroidal delivery of bevacizumab, Mol Pharm, 10 (2013) 2858-2867.

[196] P. Pahuja, S. Arora, P. Pawar, Ocular drug delivery system: a reference to natural polymers, Expert Opin Drug Deliv, 9 (2012) 837-861.

[197] J.M. Dang, K.W. Leong, Natural polymers for gene delivery and tissue engineering, Advanced Drug Delivery Reviews, 58 (2006) 487-499.

[198] Y. Lu, N. Zhou, X. Huang, J.W. Cheng, F.Q. Li, R.L. Wei, J.P. Cai, Effect of intravitreal injection of bevacizumab-chitosan nanoparticles on retina of diabetic rats, Int J Ophthalmol, 7 (2014) 1-7.

[199] X. Kong, W. Xu, C. Zhang, W. Kong, Chitosan temperature-sensitive gel loaded with drug microspheres has excellent effectiveness, biocompatibility and safety as an ophthalmic drug delivery system, Exp Ther Med, 15 (2018) 1442-1448.

[200] C. Li, R. Chen, M. Xu, J. Qiao, L. Yan, X.D. Guo, Hyaluronic acid modified MPEG-b-PAE block copolymer aqueous micelles for efficient ophthalmic drug delivery of hydrophobic genistein, Drug Deliv, 25 (2018) 1258-1265.

[201] M. de la Fuente, B. Seijo, M.J. Alonso, Novel hyaluronic acid-chitosan nanoparticles for ocular gene therapy, Invest Ophthalmol Vis Sci, 49 (2008) 2016-2024.

[202] S.B. Makwana, V.A. Patel, S.J. Parmar, Development and characterization of in-situ gel for ophthalmic formulation containing ciprofloxacin hydrochloride, Results Pharma Sci, 6 (2016) 1-6.

[203] T.K. Giri, 5 - Nanoarchitectured Polysaccharide-Based Drug Carrier for Ocular Therapeutics, in: A.M. Holban, A.M. Grumezescu (Eds.) Nanoarchitectonics for Smart Delivery and Drug Targeting, William Andrew Publishing, 2016, pp. 119-141.

[204] J.H. Sze, J.C. Brownlie, C.A. Love, Biotechnological production of hyaluronic acid: a mini review, 3 Biotech, 6 (2016) 67.

[205] J.A. Burdick, G.D. Prestwich, Hyaluronic acid hydrogels for biomedical applications, Adv Mater, 23 (2011) H41-56.

[206] A. Darr, A. Calabro, Synthesis and characterization of tyramine-based hyaluronan hydrogels, J Mater Sci Mater Med, 20 (2009) 33-44.

[207] W. Liang, Y. Huang, D. Lu, X. Ma, T. Gong, X. Cui, B. Yu, C. Yang, C. Dong, S. Shuang, β-Cyclodextrin–Hyaluronic Acid Polymer Functionalized Magnetic Graphene Oxide Nanocomposites for Targeted Photo-Chemotherapy of Tumor Cells, Polymers, 11 (2019) 133.

[208] C.B. Rodell, A.L. Kaminski, J.A. Burdick, Rational design of network properties in guest-host assembled and shear-thinning hyaluronic acid hydrogels, Biomacromolecules, 14 (2013) 4125-4134.

[209] A. Takahashi, Y. Suzuki, T. Suhara, K. Omichi, A. Shimizu, K. Hasegawa, N. Kokudo, S. Ohta, T. Ito, In situ cross-linkable hydrogel of hyaluronan produced via copper-free click chemistry, Biomacromolecules, 14 (2013) 3581-3588.

[210] S. Fu, H. Dong, X. Deng, R. Zhuo, Z. Zhong, Injectable hyaluronic acid/poly(ethylene glycol) hydrogels crosslinked via strain-promoted azide-alkyne cycloaddition click reaction, Carbohydr Polym, 169 (2017) 332-340.

[211] G.D. Prestwich, D.M. Marecak, J.F. Marecek, K.P. Vercruysse, M.R. Ziebell, Controlled chemical modification of hyaluronic acid: synthesis, applications, and biodegradation of hydrazide derivatives, Journal of Controlled Release, 53 (1998) 93-103.

[212] F. Lee, J.E. Chung, M. Kurisawa, An injectable hyaluronic acid-tyramine hydrogel system for protein delivery, Journal of Controlled Release, 134 (2009) 186-193.

[213] M. Vlckova, F. Kalman, M.A. Schwarz, Pharmaceutical applications of isoelectric focusing on microchip with imaged UV detection, J Chromatogr A, 1181 (2008) 145-152.

[214] S. Awwad, A. Lockwood, S. Brocchini, P.T. Khaw, The PK-Eye: A Novel In Vitro Ocular Flow Model for Use in Preclinical Drug Development, J Pharm Sci, 104 (2015) 3330-3342.

[215] J.C. Imperiale, G.B. Acosta, A. Sosnik, Polymer-based carriers for ophthalmic drug delivery, J Controlled Release, 285 (2018) 106-141.

[216] A. Hafner, J. Lovric, M.D. Romic, M. Juretic, I. Pepic, B. Cetina-Cizmek, J. Filipovic-Grcic, Evaluation of cationic nanosystems with melatonin using an eye-related bioavailability prediction model, Eur J Pharm Sci, 75 (2015) 142-150.

[217] M.M. Ibrahim, A.H. Abd-Elgawad, O.A. Soliman, M.M. Jablonski, Natural Bioadhesive Biodegradable Nanoparticle-Based Topical Ophthalmic Formulations for Management of Glaucoma, Transl Vis Sci Technol, 4 (2015) 12.

[218] P. Upadhayay, M. Kumar, K. Pathak, Norfloxacin Loaded pH Triggered Nanoparticulate in-situ Gel for Extraocular Bacterial Infections: Optimization, Ocular Irritancy and Corneal Toxicity, Iran J Pharm Res, 15 (2016) 3-22.

2

[219] S.E. Leucuț̦a, The kinetics of in vitro release and the pharmacokinetics of miotic response in rabbits of gelatin and albumin microspheres with pilocarpine, International Journal of Pharmaceutics, 54 (1989) 71-78.

[220] A. Mahor, S.K. Prajapati, A. Verma, R. Gupta, A.K. Iyer, P. Kesharwani, Moxifloxacin loaded gelatin nanoparticles for ocular delivery: Formulation and in-vitro, in-vivo evaluation, J Colloid Interface Sci, 483 (2016) 132-138.

[221] S. Liu, M.D. Dozois, C.N. Chang, A. Ahmad, D.L. Ng, D. Hileeto, H. Liang, M.M. Reyad, S. Boyd, L.W. Jones, F.X. Gu, Prolonged Ocular Retention of Mucoadhesive Nanoparticle Eye Drop Formulation Enables Treatment of Eye Diseases Using Significantly Reduced Dosage, Mol Pharm, 13 (2016) 2897-2905.

[222] R.C. Nagarwal, R. Kumar, J.K. Pandit, Chitosan coated sodium alginate-chitosan nanoparticles loaded with 5-FU for ocular delivery: in vitro characterization and in vivo study in rabbit eye, Eur J Pharm Sci, 47 (2012) 678-685.

[223] M.A. Kalam, Development of chitosan nanoparticles coated with hyaluronic acid for topical ocular delivery of dexamethasone, Int J Biol Macromol, 89 (2016) 127-136.

[224] M.A. Kalam, The potential application of hyaluronic acid coated chitosan nanoparticles in ocular delivery of dexamethasone, Int J Biol Macromol, 89 (2016) 559-568.

[225] S.M. Jay, W.M. Saltzman, Controlled delivery of VEGF via modulation of alginate microparticle ionic crosslinking, J Control Release, 134 (2009) 26-34.

[226] W. Liu, M. Griffith, F. Li, Alginate microsphere-collagen composite hydrogel for ocular drug delivery and implantation, J Mater Sci Mater Med, 19 (2008) 3365-3371.

[227] J. Zhang, R. Bi, W. Hodge, P. Yin, W.H. Tse, A nanocomposite contact lens for the delivery of hydrophilic protein drugs, J Mater Chem B, 1 (2013) 4388-4395.

[228] R. Zhao, J. Li, J. Wang, Z. Yin, Y. Zhu, W. Liu, Development of Timolol-Loaded Galactosylated Chitosan Nanoparticles and Evaluation of Their Potential for Ocular Drug Delivery, AAPS PharmSciTech, 18 (2017) 997-1008.

[229] S. Katiyar, J. Pandit, R.S. Mondal, A.K. Mishra, K. Chuttani, M. Aqil, A. Ali, Y. Sultana, In situ gelling dorzolamide loaded chitosan nanoparticles for the treatment of glaucoma, Carbohydrate Polymers, 102 (2014) 117-124.

[230] Z.M. Fathalla, K.A. Khaled, A.K. Hussein, R.G. Alany, A. Vangala, Formulation and corneal permeation of ketorolac tromethamine-loaded chitosan nanoparticles, Drug Dev Ind Pharm, 42 (2016) 514-524.

[231] S. Wassmer, M. Rafat, W.G. Fong, A.N. Baker, C. Tsilfidis, Chitosan microparticles for delivery of proteins to the retina, Acta Biomater, 9 (2013) 7855-7864.

[232] J. Pandit, Y. Sultana, M. Aqil, Chitosan-coated PLGA nanoparticles of bevacizumab as novel drug delivery to target retina: optimization, characterization, and in vitro toxicity evaluation, Artif Cells Nanomed Biotechnol, 45 (2017) 1397-1407.

[233] N. Elsaid, T.L. Jackson, Z. Elsaid, A. Alqathama, S. Somavarapu, PLGA Microparticles Entrapping Chitosan-Based Nanoparticles for the Ocular Delivery of Ranibizumab, Mol Pharm, 13 (2016) 2923-2940.

[234] P.I.-S. M. A. Mateescu, and E. Assaad, Chitosan and its derivatives as self-assembled systems for drug delivery, in: M.A. Mateescu, P. Ispas-Szabo, E. Assaad (Eds.) Controlled Drug Delivery, Woodhead Publishing, 2015, pp. 85-125.

[235] S. Supper, N. Anton, J. Boisclair, N. Seidel, M. Riemenschnitter, C. Curdy, T. Vandamme, Chitosan/glucose 1-phosphate as new stable in situ forming depot system for controlled drug delivery, Eur J Pharm Biopharm, 88 (2014) 361-373.

[236] E. Szymańska, K. Winnicka, Stability of chitosan-a challenge for pharmaceutical and biomedical applications, Mar Drugs, 13 (2015) 1819-1846.

[237] J. Varshosaz, M. Tabbakhian and Z. Salmani, Designing of a Thermosensitive Chitosan/Poloxamer In Situ Gel for Ocular Delivery of Ciprofloxacin, The Open Drug Delivery Journal, 2 (2008) 61-70.

[238] J. Hurler, N. Skalko-Basnet, Potentials of chitosan-based delivery systems in wound therapy: bioadhesion study, J Funct Biomater, 3 (2012) 37-48.

[239] Y.H. Cheng, T.H. Tsai, Y.Y. Jhan, A.W. Chiu, K.L. Tsai, C.S. Chien, S.H. Chiou, C.J. Liu, Thermosensitive chitosan-based hydrogel as a topical ocular drug delivery system of latanoprost for glaucoma treatment, Carbohydr Polym, 144 (2016) 390-399.

[240] L. Popa, M.V. Ghica, C.E. Dinu-Pîrvu, T. Irimia, Chitosan: A Good Candidate for Sustained Release Ocular Drug Delivery Systems, (2018).

[241] X. Chen, X. Li, Y. Zhou, X. Wang, Y. Zhang, Y. Fan, Y. Huang, Y. Liu, Chitosan-based thermosensitive hydrogel as a promising ocular drug delivery system: preparation, characterization, and in vivo evaluation, J Biomater Appl, 27 (2012) 391-402.

[242] D. Jain, Newer Trends in In Situ Gelling Systems for Controlled Ocular Drug Delivery, Journal of Analytical & Pharmaceutical Research, 2 (2016).

[243] H.-W. Sung, I.L. Liang, C.-N. Chen, R.-N. Huang, H.-F. Liang, Stability of a biological tissue fixed with a naturally occurring crosslinking agent (genipin), Journal of Biomedical Materials Research, 55 (2001) 538-546.

[244] A.S.H. B.S. Lele, Mucoadhesive drug carriers based on complexes of poly(acrylic acid) and PEGylated drugs having hydrolysable PEG–anhydride–drug linkages, Journal of Controlled Release, 69 (2000) 237–248.

[245] A.M. Alhalafi, Applications of polymers in intraocular drug delivery systems, Oman J Ophthalmol, 10 (2017) 3-8.

[246] T. Yamaoka, Y. Tabata, Y. Ikada, Distribution and Tissue Uptake of Poly(ethylene glycol) with Different Molecular Weights after Intravenous Administration to Mice, Journal of Pharmaceutical Sciences, 83 (1994) 601-606.

[247] A. D'Souza A, R. Shegokar, Polyethylene glycol (PEG): a versatile polymer for pharmaceutical applications, Expert Opin Drug Deliv, 13 (2016) 1257-1275.

2

[248] S.N.S. Alconcel, A.S. Baas, H.D. Maynard, FDA-approved poly(ethylene glycol)–protein conjugate drugs, Polymer Chemistry, 2 (2011) 1442.

[249] C. Lu, P. Zahedi, A. Forman, C. Allen, Multi-arm PEG/silica hydrogel for sustained ocular drug delivery, J Pharm Sci, 103 (2014) 216-226.

[250] Y.J. Yang, D.J. Mai, T.J. Dursch, B.D. Olsen, Nucleopore-Inspired Polymer Hydrogels for Selective Biomolecular Transport, Biomacromolecules, 19 (2018) 3905-3916.

[251] Z. Luo, L. Jin, L. Xu, Z.L. Zhang, J. Yu, S. Shi, X. Li, H. Chen, Thermosensitive PEG-PCL-PEG (PECE) hydrogel as an in situ gelling system for ocular drug delivery of diclofenac sodium, Drug Deliv, 23 (2016) 63-68.

[252] S.K. Kushwaha, P. Saxena, A. Rai, Stimuli sensitive hydrogels for ophthalmic drug delivery: A review, Int J Pharm Investig, 2 (2012) 54-60.

[253] B. Srividya, R.M. Cardoza, P.D. Amin, Sustained ophthalmic delivery of ofloxacin from a pH triggered in situ gelling system, Journal of Controlled Release, 73 (2001) 205-211.

[254] G. Horvat, B. Gyarmati, S. Berko, P. Szabo-Revesz, B.A. Szilagyi, A. Szilagyi, J. Soos, G. Sandri, M.C. Bonferoni, S. Rossi, F. Ferrari, C. Caramella, E. Csanyi, M. Budai-Szucs, Thiolated poly(aspartic acid) as potential in situ gelling, ocular mucoadhesive drug delivery system, Eur J Pharm Sci, 67 (2015) 1-11.

[255] Y. Cao, C. Zhang, W. Shen, Z. Cheng, L. Yu, Q. Ping, Poly(N-isopropylacrylamide)–chitosan as thermosensitive in situ gel-forming system for ocular drug delivery, Journal of Controlled Release, 120 (2007) 186-194.

[256] S. Williams, K. Herlihy, G. Owens, J. Savage, L. Gardner, J. Tully, B. Maynor, T. Navratil, B.R. Yerxa, Photocurable Hydrogel Implants for the Extended Release of Bevacizumab for the Treatment of Age Related Macular Degeneration, Investigative Ophthalmology & Visual Science, 55 (2014) 471-471.

[257] N. Shimada, A. Maruyama, Thermoresponsive Polymers with Functional Groups Selected for Pharmaceutical and Biomedical Applications, in: Tailored Polymer Architectures for Pharmaceutical and Biomedical Applications, American Chemical Society, 2013, pp. 235-241.

[258] M.R. Park, C. Chun, S.W. Ahn, M.H. Ki, C.S. Cho, S.C. Song, Sustained delivery of human growth hormone using a polyelectrolyte complex-loaded thermosensitive polyphosphazene hydrogel, Journal of Controlled Release, 147 (2010) 359-367.

[259] H.G. Schild, Poly(N-isopropylacrylamide): experiment, theory and application, Progress in Polymer Science, 17 (1992) 163-249.

[260] E.H. Marzieh Najafi, WimE. Hennink, and Tina Vermonden, Poly(N-isopropylacrylamide): Physicochemical Properties and Biomedical Applications, in: V.V.K.a.T.K. Georgiou. (Ed.) Temperature-Responsive Polymers, 2018.

[261] M. Heskins, J.E. Guillet, Solution Properties of Poly(N-isopropylacrylamide), Journal of Macromolecular Science: Part A - Chemistry, 2 (1968) 1441-1455.

[262] P.Y. Chou, S.H. Chen, C.H. Chen, S.H. Chen, Y.T. Fong, J.P. Chen, Thermo-responsive in-situ forming hydrogels as barriers to prevent post-operative peritendinous adhesion, Acta biomaterialia, 63 (2017) 85-95.

[263] X.-Y. Zhang, Y. Zheng, C.-H. Liu, P.-H. Wang, Y.-Y. Zhu, Facile and large scale in situ synthesis of the thermal responsive fluorescent SiNPs/PNIPAM hydrogels, RSC Advances, 6 (2016) 55666-55670.

[264] H. Feil, Y.H. Bae, J. Feijen, S.W. Kim, Effect of comonomer hydrophilicity and ionization on the lower critical solution temperature of N-isopropylacrylamide copolymers, Macromolecules, 26 (1993) 2496-2500.

[265] J.Y. Wu, S.Q. Liu, P.W. Heng, Y.Y. Yang, Evaluating proteins release from, and their interactions with, thermosensitive poly (N-isopropylacrylamide) hydrogels, Journal of Controlled Release, 102 (2005) 361-372.

[266] P.W. Drapala, E.M. Brey, W.F. Mieler, D.C. Venerus, J.J. Kang Derwent, V.H. Perez-Luna, Role of Thermo-responsiveness and Poly(ethylene glycol) Diacrylate Cross-link Density on Protein Release from Poly(N-isopropylacrylamide) Hydrogels, J Biomater Sci Polym Ed, 22 (2011) 59-75.

[267] S. Ashraf, H.-K. Park, H. Park, S.-H. Lee, Snapshot of phase transition in thermoresponsive hydrogel PNIPAM: Role in drug delivery and tissue engineering, Macromolecular Research, 24 (2016) 297-304.

[268] X. Huang, T.L. Lowe, Biodegradable Thermoresponsive Hydrogels for Aqueous Encapsulation and Controlled Release of Hydrophilic Model Drugs, Biomacromolecules, 6 (2005) 2131-2139.

[269] M.A. Haq, Y. Su, D. Wang, Mechanical properties of PNIPAM based hydrogels: A review, Mater Sci Eng C Mater Biol Appl, 70 (2017) 842-855.

[270] C.K. Han, Y.H. Bae, Inverse thermally-reversible gelation of aqueous N-isopropylacrylamide copolymer solutions, Polymer, 39 (1998) 2809-2814.

[271] Y. Jiang, Y. Wu, Y. Huo, Thermo-responsive hydrogels with N-isopropylacrylamide/acrylamide interpenetrating networks for controlled drug release, J Biomater Sci Polym Ed, 26 (2015) 917-930.

[272] J.-T. Zhang, S.-X. Cheng, R.-X. Zhuo, Poly(vinyl alcohol)/poly(N-isopropylacrylamide) semi-interpenetrating polymer network hydrogels with rapid response to temperature changes, Colloid and Polymer Science, 281 (2003) 580-583.

[273] S.P. Rwei, H.N.A. Tuan, W.Y. Chiang, T.F. Way, Synthesis and Characterization of pH and Thermo Dual-Responsive Hydrogels with a Semi-IPN Structure Based on N-Isopropylacrylamide and Itaconamic Acid, Materials (Basel), 11 (2018).

[274] T. Gan, Y. Guan, Y. Zhang, Thermogelable PNIPAM microgel dispersion as 3D cell scaffold: effect of syneresis, Journal of Materials Chemistry, 20 (2010) 5937.

[275] M.K. Gupta, J.R. Martin, T.A. Werfel, T. Shen, J.M. Page, C.L. Duvall, Cell protective, ABC triblock polymer-based thermoresponsive hydrogels with ROS-triggered degradation and drug release, J Am Chem Soc, 136 (2014) 14896-14902.

[276] S. Lanzalaco, E. Armelin, Poly(N-isopropylacrylamide) and Copolymers: A Review on Recent Progresses in Biomedical Applications, Gels, 3 (2017).

[277] A. Alexander, Ajazuddin, J. Khan, S. Saraf, S. Saraf, Polyethylene glycol (PEG)-Poly(N-isopropylacrylamide) (PNIPAAm) based thermosensitive injectable hydrogels for biomedical applications, Eur J Pharm Biopharm, 88 (2014) 575-585.

[278] N. Nasongkla, B. Chen, N. Macaraeg, M.E. Fox, J.M. Frechet, F.C. Szoka, Dependence of pharmacokinetics and biodistribution on polymer architecture: effect of cyclic versus linear polymers, J Am Chem Soc, 131 (2009) 3842-3843.

[279] X.D. Xu, C.S. Chen, Z.C. Wang, G.R. Wang, S.X. Cheng, X.Z. Zhang, R.X. Zhuo, "Click" chemistry forin situformation of thermoresponsive P(NIPAAm-co-HEMA)-based hydrogels, Journal of Polymer Science Part A: Polymer Chemistry, 46 (2008) 5263-5277.

[280] S. Tang, M. Floy, R. Bhandari, M. Sunkara, A.J. Morris, T.D. Dziubla, J.Z. Hilt, Synthesis and Characterization of Thermoresponsive Hydrogels Based on N-Isopropylacrylamide Crosslinked with 4,4'-Dihydroxybiphenyl Diacrylate, ACS Omega, 2 (2017) 8723-8729.

[281] E. Markovsky, H. Baabur-Cohen, A. Eldar-Boock, L. Omer, G. Tiram, S. Ferber, P. Ofek, D. Polyak, A. Scomparin, R. Satchi-Fainaro, Administration, distribution, metabolism and elimination of polymer therapeutics, Journal of Controlled Release, 161 (2012) 446-460.

[282] D. Neradovic, C.F. Van Nostrum, W.E. Hennink, Thermoresponsive Polymeric Micelles with Controlled Instability Based on Hydrolytically Sensitive N-Isopropylacrylamide Copolymers, Macromolecules, 34 (2001) 7589-7591.

[283] B.M. Watson, F.K. Kasper, P.S. Engel, A.G. Mikos, Synthesis and characterization of injectable, biodegradable, phosphate-containing, chemically cross-linkable, thermoresponsive macromers for bone tissue engineering, Biomacromolecules, 15 (2014) 1788-1796.

[284] O. Soga, C.F. van Nostrum, W.E. Hennink, Poly(N-(2-hydroxypropyl) Methacrylamide Mono/Di Lactate): A New Class of Biodegradable Polymers with Tuneable Thermosensitivity, Biomacromolecules, 5 (2004) 818-821.

[285] Z. Cui, B.H. Lee, B.L. Vernon, New Hydrolysis-Dependent Thermosensitive Polymer for an Injectable Degradable System, Biomacromolecules, 8 (2007) 1280-1286.

[286] Z. Cui, B.H. Lee, C. Pauken, B.L. Vernon, Degradation, cytotoxicity, and biocompatibility of NIPAAm-based thermosensitive, injectable, and bioresorbable polymer hydrogels, J Biomed Mater Res A, 98 (2011) 159-166.

[287] T.N. Vo, A.K. Ekenseair, F.K. Kasper, A.G. Mikos, Synthesis, physicochemical characterization, and cytocompatibility of bioresorbable, dual-gelling injectable hydrogels, Biomacromolecules, 15 (2014) 132-142.

[288] K. Boere, J. Van den Dikkenberg, Y. Gao, J. Visser, W. Hennink, T. Vermonden, Thermogelling and Chemoselectively Cross-Linked Hydrogels with Controlled Mechanical Properties and Degradation Behavior, 2015, 16, 9, 2840–2851

[289] D. Park, W. Wu, Y. Wang, A functionalizable reverse thermal gel based on a polyurethane/PEG block copolymer, Biomaterials, 32 (2011) 777-786.

[290] Y.H. Cheng, Y.C. Ko, Y.F. Chang, S.H. Huang, C.J. Liu, Thermosensitive chitosan-gelatin-based hydrogel containing curcumin-loaded nanoparticles and latanoprost as a dual-drug delivery system for glaucoma treatment, Exp Eye Res, 179 (2019) 179-187.

[291] B.F. Godley, F.A. Shamsi, F.Q. Liang, S.G. Jarrett, S. Davies, M. Boulton, Blue light induces mitochondrial DNA damage and free radical production in epithelial cells, J Biol Chem, 280 (2005) 21061-21066.

[292] T. Laptos, J. Omersel, The importance of handling high-value biologicals: Physico-chemical instability and immunogenicity of monoclonal antibodies, Exp Ther Med, 15 (2018) 3161-3168.

[293] F. Raza, H. Zafar, Y. Zhu, Y. Ren, A. Ullah, A.U. Khan, X. He, H. Han, M. Aquib, K.O. Boakye-Yiadom, L. Ge, A Review on Recent Advances in Stabilizing Peptides/Proteins upon Fabrication in Hydrogels from Biodegradable Polymers, Pharmaceutics, 10 (2018) 16.

[294] T.R. Hoare, D.S. Kohane, Hydrogels in drug delivery: Progress and challenges, Polymer, 49 (2008) 1993-2007.

[295] A.M. Jonker, D.W.P.M. Löwik, J.C.M. van Hest, Peptide- and Protein-Based Hydrogels, Chemistry of Materials, 24 (2012) 759-773.

[296] Y. Yu, Y. Chau, Formulation of in situ chemically cross-linked hydrogel depots for protein release: from the blob model perspective, Biomacromolecules, 16 (2015) 56-65.

[297] C.M. Madl, S.C. Heilshorn, Bioorthogonal Strategies for Engineering Extracellular Matrices, Adv Funct Mater, 28 (2018).

[298] C.M. Nimmo, M.S. Shoichet, Regenerative biomaterials that "click": simple, aqueous-based protocols for hydrogel synthesis, surface immobilization, and 3D patterning, Bioconjug Chem, 22 (2011) 2199-2209.

[299] P.G.d. Gennes, Scaling concepts in polymer physics, Cornell University Press, Ithaca, New York, 1979.

[300] W. Wang, S. Singh, D.L. Zeng, K. King, S. Nema, Antibody structure, instability, and formulation, J Pharm Sci, 96 (2007) 1-26.

[301] W. Wang, Instability, stabilization, and formulation of liquid protein pharmaceuticals, International Journal of Pharmaceutics, 185 (1999) 129-188.

[302] M.C. Manning, D.K. Chou, B.M. Murphy, R.W. Payne, D.S. Katayama, Stability of protein pharmaceuticals: an update, Pharm Res, 27 (2010) 544-575.

[303] S. Kaja, J.D. Hilgenberg, E. Everett, S.E. Olitsky, J. Gossage, P. Koulen, Effects of dilution and prolonged storage with preservative in a polyethylene container on Bevacizumab (Avastin) for topical delivery as a nasal spray in anti-hereditary hemorrhagic telangiectasia and related therapies, Hum. Antibodies, 20 (2011) 95-101.

[304] L. Magnenat, A. Palmese, C. Fremaux, F. D'Amici, M. Terlizzese, M. Rossi, L. Chevalet, Demonstration of physicochemical and functional similarity between the proposed biosimilar adalimumab MSB11022 and Humira(R), MAbs, 9 (2017) 127-139.

2

[305] T. Sherman, V. Raman, Incomplete scleral penetration of dexamethasone (Ozurdex) intravitreal implant, BMJ Case Rep, 11 (2018).

[306] D. Kanjickal, S. Lopina, M.M. Evancho-Chapman, S. Schmidt, D. Donovan, Effects of sterilization on poly(ethylene glycol) hydrogels, J Biomed Mater Res A, 87 (2008) 608-617.

[307] B. Singh, L. Varshney, V. Sharma, Design of sterile mucoadhesive hydrogels for use in drug delivery: effect of radiation on network structure, Colloids Surf B Biointerfaces, 121 (2014) 230-237.

[308] E. Eljarrat-Binstock, A. Bentolila, N. Kumar, H. Harel, A.J. Domb, Preparation, characterization, and sterilization of hydrogel sponges for iontophoretic drug-delivery use, Polymers for Advanced Technologies, 18 (2007) 720-730.

[309] O. Saher, D.M. Ghorab, N.M. Mursi, Preparation and in vitro/in vivo evaluation of antimicrobial ocular in situ gels containing a disappearing preservative for topical treatment of bacterial conjunctivitis, Pharm Dev Technol, 21 (2016) 600-610.

[310] V.A. Liu, S.N. Bhatia, Three-Dimensional Photopatterning of Hydrogels Containing Living Cells, Biomedical Microdevices, 4 (2002) 257-266.

[311] P.M. Kharkar, K.L. Kiick, A.M. Kloxin, Designing degradable hydrogels for orthogonal control of cell microenvironments, Chem Soc Rev, 42 (2013) 7335-7372.

[312] H. Zhang, K.T. Dicker, X. Xu, X. Jia, J.M. Fox, Interfacial Bioorthogonal Cross-Linking, ACS Macro Lett, 3 (2014) 727-731.

[313] C.M. Madl, S.C. Heilshorn, Tyrosine-Selective Functionalization for Bio-Orthogonal Cross-Linking of Engineered Protein Hydrogels, Bioconjug Chem, 28 (2017) 724-730.

[314] E.M. Del Amo, A. Urtti, Rabbit as an animal model for intravitreal pharmacokinetics: Clinical predictability and quality of the published data, Exp Eye Res, 137 (2015) 111-124.

[315] FDA, Endotoxin Testing Recommendations for Single-Use Intraocular Ophthalmic Devices. Guidance for Industry and Food and Drug Administration Staff, in, https://www.fda.gov/regulatory-information/search-fda-guidance-documents/endotoxin-testing-recommendations-single-use-intraocular-ophthalmic-dev, 2015.

2

Chapter 3

Hyaluronic Acid-PEG-Based Diels−Alder in Situ Forming Hydrogels for Sustained Intraocular Delivery of Bevacizumab

Blessing C. Ilochonwu[1], Marko Mihajlovic[1], Roel F. Maas-Bakker[1], Charis Rousou[1], Miao Tang[2], Mei Chen[2], Wim E. Hennink[1], Tina Vermonden[1]

[1]Department of Pharmaceutics, Utrecht Institute for Pharmaceutical Sciences, Faculty of Science, Utrecht University, PO box 80082, 3508 TB Utrecht, the Netherlands. [2]Wellcome-Wolfson Institute for Experimental Medicine, School of Medicine, Dentistry & Biomedical Sciences, Queen's University Belfast, UK.

ABSTRACT

Retinal diseases are the leading cause of visual impairment worldwide. The effectiveness of antibodies for the treatment of retinal diseases has been demonstrated. Despite the clinical success, achieving sufficiently high concentrations of these protein therapeutics at the target tissue for an extended period is challenging. Patients suffering from macular degeneration often receive injections once per month. Therefore, there is a growing need for suitable systems that can help reduce the number of injections and adverse effects while improving patient complacency. This study systematically characterized degradable "in situ" forming hydrogels that can be easily injected into the vitreous cavity using a small needle (29G). After intravitreal injection, the formulation is designed to undergo a sol-gel phase transition at the administration site to obtain an intraocular depot system for long-term sustained release of bioactives. A Diels–Alder reaction was exploited to crosslink hyaluronic acid-bearing furan groups (HAFU) with 4 arm-PEG10K-maleimide (4APM), yielding stable hydrogels. Here, a systematic investigation of the effects of polymer composition and the ratio between functional groups on the hydrogels physicochemical properties was performed to select the most suitable formulation for protein delivery. Rheological analysis showed rapid hydrogel formation, with the fastest gel-formation within 5 min after mixing the hydrogel precursors. In this study, the mechanical properties of an ex vivo intravitreally formed hydrogel were investigated and compared to the in vitro fabricated samples. Swelling and degradation studies showed that the hydrogels are biodegradable by retro Diels-Alder reaction at physiological conditions. The 4APM-HAFU (ratio 1:5) hydrogel formulation showed sustained release of bevacizumab > 400 days by a combination of diffusion, swelling and degradation. A bioassay showed that the released bevacizumab remained bioactive. The hydrogel platform described in this study offers high potential for the sustained release of therapeutic antibodies to treat ocular diseases.

Keywords: Anti-VEGF; Ocular drug delivery; Mechanical Properties; Hyaluronic Acid; Injectable Hydrogels

Graphical abstract:
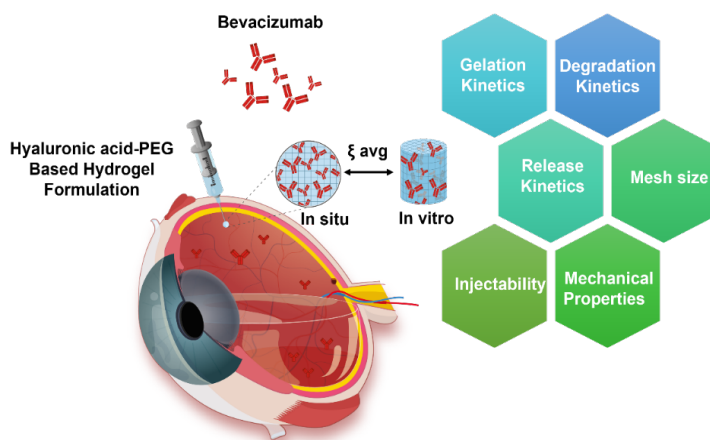
1   INTRODUCTION

According to the world health organization, in 2019, approximately 2.2 billion people lived with some sort of vision impairment worldwide. Of those, 1 billion have a preventable vision impairment and, 39 million are entirely blind.[1] Ocular vascular diseases are among the leading causes of vision loss at the global level. The most prevalent ones include diabetic retinopathy (DR), diabetic macular edema (DME), and age-related macular degeneration (AMD). The number of patients suffering from these diseases is rapidly increasing in both low and high-income countries, not only in the ageing populations but also in younger individuals, representing a significant public health burden. DR is a retinal disease causing vision impairment or vision loss in diabetic patients.[2] Over one-third of diabetic patients have signs of DR, with or without DME, making this condition one of the leading causes of visual impairment in working-age adults aged 20-71. AMD is the leading cause of irreversible blindness in elderly Europeans. Around 30-50 million people worldwide are affected by AMD, which is expected to increase in the ageing population.[3]

Many studies have demonstrated that elevated levels of vascular endothelial growth factor (VEGF) play a critical role in these retinal diseases' pathogenesis, resulting in neovascularization and vaso-permeability.[4, 5] Therefore, besides photodynamic therapy and photocoagulation, many clinical approaches aim to block VEGF signaling by delivering intravitreally injected anti-VEGF proteins.[6] The current treatment for ocular vascular diseases includes full-length VEGF antibody (bevacizumab, Avastin®), antibody fragments (ranibizumab, Lucentis®), and soluble receptors (aflibercept, Eylea®).[7]

Various studies have shown the effectiveness of antibodies in significantly slowing down DR and AMD progression by bolus intravitreal injections.[8, 9] This administration route's advantage is related to rapid drug distribution to the back of the eye, increased therapeutic effect and reduced systemic adverse events compared to other administration routes. Nevertheless, ophthalmologists consider current treatment options insufficient, as repeated injections are required to control these chronic diseases. These injections can be given at a maximum frequency of once a month because repeated intravitreal administrations result in poor patient compliance and are associated with several risks, such as bacterial endophthalmitis, retinal detachment, and hemorrhage.[10, 11] Intravitreal pharmacokinetics (PK) data show relatively rapid ocular clearance of the anti-VEGF agents (half-life around 2-14 days).[12-14] Consequently, a high drug dose is injected into the eye, and the drug concentration in the vitreous is oscillating above and below therapeutic levels in time when multiple bolus injections are administered. Therefore, there is a growing need for suitable delivery systems to tackle the current limitations of conventional drug formulations by providing sustained release of the therapeutic agents to the back of the eye for an extended period of time, thus improving patient compliance and reducing healthcare costs.

In the past decades, tremendous efforts have been made to improve the disposition of drugs, especially bioactive proteins, in the retina by using different drug delivery vehicles.[15]

3

Several drug delivery technologies, such as in-situ forming hydrogels, micelles, liposomes, nanoparticles, dendrimers, microneedles and ocular implants, are currently being investigated for ocular applications.[16-18] However, despite these efforts, antibody-carrying implants are still currently limited on the market.[7] Genentech's Susvimo, previously called Port Delivery System[19, 20], is the first and currently only FDA approved refillable ranibizumab implant used for the treatment of neovascular age-related macular degeneration[21]. The system allows continuous diffusion of the protein from the reservoir into the vitreous.[22]

Although this implant can significantly prolong drug release to the posterior segment of the eye, it requires invasive methods to insert the device (2.6 mm in width and 8.4 mm in length) at the target site and also to remove it. Furthermore, during phase 1 and phase 2 clinical evaluations, the occurrence of vitreous hemorrhage in a significant number of cases was noticed. Although this limitation was overcome in phase 3 evaluation by modifying the surgical technique, time will tell how practical such a system will be in ocular therapy.[23]

The use of hydrogels has received increased attention as ophthalmic formulations that deliver drugs to the posterior segments. Hydrogels are three-dimensional hydrophilic polymeric networks with versatile and tunable characteristics such as biocompatibility, mechanical flexibility, tailorable release properties and transparency.[24-28] This type of delivery system offers several benefits for ocular drug delivery compared to the current bolus injections, including less frequent administrations, patient comfort and potentially also cost reduction. Furthermore, hydrogels that jellify in-situ allow entrapment of therapeutically active antibodies during network formation, facilitating local delivery and release through a minimally invasive procedure. To obtain a formulation that releases the loaded antibody for a prolonged time, its initial mobility in the gel matrix should be limited and increase in time due to swelling and degradation of the hydrogel matrix.

In this study, furan-modified hyaluronic acid (HAFU) was crosslinked with 4 arm-PEG10kDa-maleimide (4APM), yielding stable hydrogels due to Diels-Alder reaction (DA). Similar hydrogel formulations have previously been used to enable the controlled release of extracellular vesicles, and for the encapsulation and 3D culture of cells in tissue engineering.[29-34] Hyaluronic acid (HA) is a polysaccharide that is abundantly present in the vitreous of the eye.[35] Therefore, HA has been used in vitreous substitution and to replace fluid during certain eye surgeries.[36-40] Furthermore, HA has also been used in many ocular products designed to cleanse the eyes and offer relief from dryness in the form of eye drops.[41] HAFU was therefore selected as a building block because of its expected compatibility with the posterior and anterior segments of the eye. Furthermore, poly(ethylene glycol) (PEG) is one of the most used polymers in drug delivery systems.[42, 43] After the first approved PEGylated products around 30 years ago[44], a vast amount of clinical experience has since been gained with this polymer, making it an ideal building block for hydrogels for biomedical applications. In addition, solely PEG hydrogel formulations crosslinked with DA or Micheal type reactions have also been investigated for sustained protein release [32, 33] and potential ocular applications [45].

Different types of crosslinking chemistry have been studied in hydrogel systems to deliver proteins to the posterior segment of the eye, as previously reviewed by Ilochonwu et al.[15] However, slow crosslinking mechanism, permanent crosslinks and the need for toxic catalysts and radical initiators still limit the clinical use of such systems. A major advantage of DA chemical crosslinking is that it occurs at physiological conditions avoiding the use of potentially toxic catalysts and initiators, commonly used in many existing crosslinking strategies for controlled-release hydrogel delivery systems.[46, 47] However, maleimide functional groups present in the furan-maleimide DA crosslinks can potentially react with SH and NH_2 groups of the loaded protein[48], creating protein conjugates. Despite this limitation, the unique properties and advantages of DA chemistry has been gaining increasing recognition, especially when applied in biomedical applications.[46] Although some DA-based hydrogels for ocular drug delivery have been previously studied as long- acting sustained delivery system for bevacizumab[31, 32] with release profiles up to 100 days, there is limited information available on the influence of hydrogel composition on material's physicochemical and structural properties and how that relates to the release profiles of therapeutic proteins.

This study aims to fill this gap by systematically examining the effects of hydrogel polymer composition and the ratio of functional groups on a series of material's properties, such as gelation kinetics, injectability, mechanical properties, mesh size, degradation, and drug release kinetics for intraocular therapy. Specifically, the present work investigates a DA crosslinked hydrogel based on HA and PEG polymers with potential application as a long-acting sustained delivery system for bevacizumab (and potentially for other anti-VEGF therapeutics). The formulation was designed and aimed to be injectable into the vitreous cavity using a small needle (29G). After injection, the aqueous polymeric solution formed a crosslinked hydrogel at the administration site, entrapping the antibody dissolved in the same solution to obtain an intraocular depot system.

Furthermore, the potential prospect of HAFU-4APM hydrogels for intraocular protein therapy was examined by testing *in situ* gel formation in porcine eye explants. Uniquely to this study, the elastic moduli (E) of *in vitro* and *ex vivo* formed hydrogels were determined to calculate the hydrogel mesh size. Considering the size of the used intraocular model protein, the average mesh size (ξ_{avg}) of the hydrogels were designed to allow controlled release of the antibody due to a combination of swelling, diffusion and degradation. The cytocompatibility of the formed hydrogel and its building blocks was evaluated using retinal Müller cells (QMMUC-1).

2   MATERIAL & METHODS

2.1   Materials

Lyophilized sodium hyaluronate (HA; 24 kDa) was obtained from Lifecore Biomedical (Chaska, MN, U.S.A.). The 4-arm PEG maleimide crosslinker (4APM; 10kDa) was purchased from JenKem Technology USA Inc. (Beijing, China). Stock Phosphate buffered saline 10x (PBS) pH 7.4 (1.37 M NaCl, 0.027 M KCl and 0.119 M phosphates) BioReagents were purchased from B. Braun (Melsungen,   Germany).   4-(4,6-Dimethoxy-1,3,5triazin-2-yl)-4-methylmorpholiniumchloride

(DMTMM) was purchased from TCI EUROPE N.V. Alexa Fluor™ 750 C5 maleimide dye was obtained from Thermo Fisher Scientific (Massachusetts, United States). All other commercial chemicals were purchased from Sigma-Aldrich (Zwijndrecht, the Netherlands) and used as received unless indicated otherwise. Dialysis tube membranes (molecular weight cut-off (MWCO) 10 kDa) were purchased from Fisher Scientific (Bleiswijk, the Netherlands). Avastin100 mg/4ml Roche (100 mg of Bevacizumab, 240 mg trehalose dehydrate, 4.8 mg sodium phosphate, 1.6 mg polysorbate 20 (tween 20) and injection water; (pH 6.2) were kind gifts from the UMC Utrecht.

2.2 Functionalization of hyaluronic acid with furfuryl-amine (HAFU)

Furan-modified HA (HAFU) derivatives were prepared by functionalizing hyaluronic acid with furfuryl-amine groups by means of two methods. HAFU with a low degree of substitution (DS) (30%) was synthesized by dissolving sodium hyaluronate (24 kDa; 1 g; 2.5 mmol disaccharide units) in Milli-Q-water at a concentration of 3.2 wt/v%. After dissolution, 1 ml (1.09 g; 11.2 mmol) of furfuryl amine was added to the solution while stirring. The pH was adjusted with 5 M HCl to 4.75, and subsequently, 1.35 g (7.0 mol) of 1-ethyl-3-(3-dimethylaminopropyl)carbodiimide (EDC) was added. Next, 724 mg (6.0 mmol) N-hydroxysuccinimide (NHS) was added while keeping the pH at 4.75. The solution was stirred at room temperature for 48 h, and the reaction was stopped by increasing the pH to 7 using 5 M NaOH. The mixture was purified by dialysis (Mw cut-off= 14 kDa) against dilute HCl (pH 3.5) containing 100-150 mM of NaCl and finally against water at 4 °C. The final product was obtained as a fluffy white powder after freeze-drying with a yield of 70-80%. To obtain HA with a higher DS (50 and 83 %), HAFU was synthesized according to the procedure described by Nimmo et al. [29] with modifications. Briefly, HA (0.40 g, 1.01 mmol disaccharide units) was dissolved in 40 ml of MES buffer (100 mM, pH 5.51) to which DMTMM was added at 6 (1.7 g, 6.0 mmol), or 2 (0.60 g, 2.0 mmol) molar ratio (relative to the -COOH groups in HA) and stirred for 10 min. Furfurylamine was subsequently added dropwise at a 2 (188.8 µL, 2.04 mmol), or 1 (90 µL, 0.97 mmol) molar ratio relative to the -COOH groups in HA. The reaction was conducted at room temperature for 24 h, and afterwards, the pH was raised to 7 (using 5 M NaOH) to stop the reaction. Compared to EDC coupling, it was possible to quickly isolate the HAFU polymer produced by DMTMM coupling through precipitation in ethanol/water as the reaction byproduct remained soluble. Briefly, the products were precipitated in water/ethanol at RT with a ratio of 1:7.5 (reaction mixture H$_2$O: ethanol) and washed 3 times with ethanol. The precipitate was vacuum dried to obtained HAFU derivatives as a solid white powder with a yield of 84-88%. The different HAFU polymers were characterized with ^{1}H NMR spectroscopy using an Agilent 400MR-NMR spectrometer (Agilent Technologies, Santa Clara, CA). Data analysis was performed using MestReNova, and the chemical shifts were calibrated against the residual solvent peak (4.79 ppm for H$_2$O). The ratios of the integrals of the N-acetyl glucosamine peak on the HA-backbone were compared with the aromatic furan peaks to determine the degree of substitution. ^{1}H-NMR δ (ppm): 7.5 (OCH; 1H), 6.4 (CHCH; 2H), 4.10-3.0 (protons of HA disaccharide), 2.0 (NHCOCH$_3$; 3H).

2.3 Preparation of hydrogels and bevacizumab-loaded hydrogels

Cylindrically shaped empty HAFU-4APM hydrogels of 100 mg were prepared at 37 °C in a plastic mould (diameter 4 mm, 5 mm height). Specifically, equal amount of HAFU and 4APM-crosslinker

were weighed and dissolved separately in PBS buffer (0.13 M NaCl, 2.7 mM KCl and 11.9 mM phosphates, pH 7.4) and mixed to obtain a total polymer concentration of 5, 10, 20 or 25 wt% unless indicated otherwise. Different molar ratios between the 4 APM crosslinker and HAFU polymers corresponding to 1:1.9; 1:3.1; 1:5.2 approximated to 1:2; 1:3; 1:5 ratios of maleimide: furan, respectively (calculated based on the DS of the functional groups present in the HA polymers) were used to prepare hydrogels with different properties. Subsequently, the samples were incubated at 37 °C for 4 hours to allow crosslinking of the hydrogels.

Bevacizumab-loaded HAFU-4APM hydrogels were prepared as described above with a slight modification. HAFU polymers were dissolved in a mixture of PBS (0.13 M NaCl, 2.7 mM KCl and 11.9 mM phosphates, pH 7.4) and bevacizumab solution (50 ml; 25 mg/ml), while the 4APM crosslinker was separately dissolved in PBS. Upon dissolution, the 4APM crosslinker solution was mixed with the HAFU-bevacizumab solution and incubated at 37 °C for 4 hours to enable crosslinking and protein entrapment. The HAFU-4APM hydrogels were loaded with either 1.25 or 1.50 mg of bevacizumab in the 100 mg hydrogels.

2.4   In vitro swelling and degradation

Crosslinked empty hydrogels (100 mg) were prepared as described in section 2.3 and placed in a 2 ml glass vial to perform the swelling and degradation test. The exact weight of the gel was measured (W_0), after which 1 ml PBS buffer (pH 7.4) was added to the vial, which was subsequently incubated at 37 °C. At regular intervals, hydrogel weight was determined (W_t) after removal of the PBS. Subsequently, 1 ml of fresh PBS (0.13 M NaCl, 2.7 mM KCl and 11.9 mM phosphates, pH 7.4) was added for further incubation at 37 °C. The swelling ratio (SR) is defined as the weight at a particular time point (W_t) divided by the initial hydrogel weight: $SR = W_t/W_0$.

2.5   Rheological characterization

The rheological properties of the hydrogel were analyzed using a Discovery HR-2 Rheometer (TA Instruments New Castle, DE) with a Peltier plate for temperature control. The samples were measured using a 20 mm diameter aluminum plate-plate geometry at a loading gap of 3000 μm and gap value of 200 μm. For each analysis, samples of 180 μl of different liquid hydrogel formulations were prepared as described in section 2.3 and pipetted under the geometry on the rheometer Peltier plate. The system was covered with a solvent trap. The data were acquired at strain values within the linear viscoelastic regime (LVR). Storage (G') and loss (G") moduli of the different hydrogel formulations were measured during a time sweep at 37 °C with a frequency of 0.1 Hz and 1% strain. The gelation time (defined as the crossover point between G' and G") of the different hydrogel formulations was measured at different temperatures (4, 20 and 37 °C). Hydrogel average mesh size (ξ) was calculated from the G' using the following equation [49-52] :

$\xi = (G' N_A / RT)^{-1/3}$

where N_A is Avogadro's constant, R is the molar gas constant (8.3 J/K.mol), and T is the absolute temperature in K.

2.6 Synthesis of dye labelled HAFU-polymer

HAFU DS 30% (150 mg) was dissolved in 800 µl of PBS. Subsequently, 160 µl of an Alexa Fluor 750 C5 maleimide solution in DMSO (0.5 mg/ml) was added and left to react overnight at room temperature by means of Diels-Alder reaction. Next, the solution was dialyzed against DMSO/water (1/14) for 16 hours with 3 times solvent exchange. The product was lyophilized to obtain fluorescently labelled hyaluronic acid-furan (HAFU-750dye) polymer as a glassy light green powder. The covalent conjugation of the dye to HA was analyzed by Shimadzu UV 2450 Spectrophotometer. The HAFU-750dye polymer (10.5 mg/ml) and the Alexa Fluor 750 C5 maleimide dye standards (0.001-0.005 mg/ml) were dissolved in 1:9 DMSO/PBS (0.13 M NaCl, 2.7 mM KCl and 11.9 mM phosphates, pH 7.4) and the absorbance UV/VIS spectra were recorded from 200 to 1000 nm with 0.5 nm resolution. Size exclusion chromatography (SEC) was used to discriminate the presence of free dye in obtained HAFU-750dye polymer, as shown in SI-Figure4A.

2.7 *Ex vivo* intravitreal injection and in-situ hydrogel formation

The enucleation of porcine eyes were performed according to the previously reported protocol by Rousou et al.[53] Briefly, enucleation is the surgical procedure by which the entire eye is removed, including the sclera and the muscles that control eye movement are left intact. HAFU-750dye (synthesized as described in section 2.6)-4APM hydrogels were prepared as follows: 20 mg HAFU-750dye (furan DS 30%) and 20 mg 4APM crosslinker were dissolved separately in 100 µl and 60µl PBS (0.13 M NaCl, 2.7 mM KCl and 11.9 mM phosphates, pH 7.4), respectively. Next, the hydrogel precursors were mixed to obtain a 20wt% polymer solution (1:2 molar ratio of maleimide: furan). This solution (160 µl, 200 mg) was subsequently injected into the vitreous of an *ex vivo* porcine eye to allow *in situ* hydrogel formation. The mixture was placed in the barrel of a 1 ml insulin syringe (needle size 29G) through a pipette after removing the plunger. Before the injection, the eyes were brought at 37 °C in a water bath for 30 min. Next, the formulation was injected into the eye (vitreous body). Images of the *ex vivo* porcine eye were taken before and 5 min after intravitreal injection using an LI-COR Pearl® impulse imager (LICOR, Lincoln, Nebraska, USA) at 37 °C. The *in situ* formed hydrogel was collected from the vitreous as follows, the eyeball was held firmly with the use of a gillies forceps, after making a small incision with a sharp blade, a spring scissor was used to cut the sclera around the cornea starting from the opening of the incision. Subsequently, the lens was removed, and the vitreous was carefully transferred into a container. The hydrogels were isolated from the vitreous body, and the mechanical properties were compared with the *in vitro* formed hydrogel (prepared in a plastic mould, section 2.3) after 1-hour incubation at 37 °C as described below.

2.8 DMA characterization of in vitro and *ex vivo* formed hydrogels

DMA 2980 Dynamic Mechanical Analyzer (TA Instruments, New Castle, DE) was used to determine Young's modulus of the hydrogels. Hydrogel samples *in vitro* were prepared as described in section 2.3, at 20wt% (corresponding to 1:2, 1:5 molar ratios of maleimide: furan moieties in the polymers), wheres the same concentration and ratios of the *ex vivo* hydrogels were formed in vitreous, as described in section 2.7. After extracting the hydrogels from the porcine eye vitreous

body, the gels were cut to allow mechanical tests. All hydrogels (*ex vivo* and in vitro) were prepared with approximately 3x4 mm in height and diameter. The gels were placed between parallel plates, and a force ramp was applied at a rate of 0.5 N/min up to a total force of 8 N at room temperature. The raw data were analyzed using TA Universal Analysis software, and Young's modulus (E) was calculated from the slope of the linear section (from 0-22% strain) of the stress-strain curve. Data are represented as mean ± standard deviation (n=3 for *in vitro* gel and n=6 in 2 porcine eyes for the *ex vivo* formed gels).

2.9 *In vitro* release from hydrogel network

To determine the release of bevacizumab from the different hydrogels, bevacizumab-loaded hydrogels (10, 16, 20 wt% with molar ratio 1:2, 1:3 or 1:5 ratios of maleimide : furan) were prepared as described in section 2.3. The release studies were performed at 37 °C, and the *in vitro* release buffer (IVR buffer) consisted of PBS (0.13 M NaCl, 2.7 mM KCl and 11.9 mM phosphates, pH 7.4) supplemented with 0.02 % NaN_3. Bevacizumab-loaded hydrogels (100 mg) were first immersed in 500 μL of PBS. After incubation, the release samples of 200 μl were taken at predetermined time points, and 200 μl fresh IVR buffer was added. The release samples were stored at 4 °C until analysis of protein content by size exclusion ultra-performance liquid chromatography (SE-ULPC) on an Acquity UPLC (Waters Corporation, Milford, USA) with an FLR-detector, operated at λ_{ex} and λ_{em} of 276 and 310 nm, respectively. BEH SEC column (200A, 1.7μm, 4.6 mm x 150 mm; Waters) was attached to the system and used for all measurements at room temperature. The filtered (0.2 μm) mobile phase consisted of an aqueous solution of sodium phosphate 100 mM, sodium sulfate 300 mM at pH 6.7 and was operated at a flow rate of 0.3 ml/min. Sample aliquots of 7.5 μl were injected, and the retention time of bevacizumab was 4.90 min under these conditions. The bevacizumab calibration curve's linear range was from 7.8 μg/ml (detection limit) to 1250 μg/ml.

2.10 SDS-PAGE electrophoresis

To study possible structural modifications of the protein with hydrogel precursors, sodium dodecyl sulphate polyacryl amide gel electrophoresis (SDS-PAGE) was performed. One ml of a bevacizumab PBS (0.13 M NaCl, 2.7 mM KCl and 11.9 mM phosphates, pH 7.4) solution (1 mg/ml) was incubated with 5 mg of hydrogel precursors, either HAFU (DS 30 %, 83 %) or 4APM for 1 hour and 5 days. Bevacizumab solution (1 mg/ml) was used as a control, and Precision Plus Protein™ Unstained Protein Standards 10-250 kDa (Bio-Rad, Hercules, CA) were used for calibration. Possible grafting of the hydrogel polymer precursors to the antibody was studied under both reducing and non-reducing conditions. Specifically, 2 μl samples (bevacizumab-polymer solutions or bevacizumab solution) were mixed with 7.5 μl of solution of 250 mM Tris-HCl pH6.5; 8 % SDS; 0,008 % Bromophenol Blue; 40 % glycerol with and without β-mercaptoethanol 5 % (100 mM), and PBS was added to obtain a final volume of 30 μl. The prepared solutions were heated to 90-100 °C for 10 min. Subsequently, samples (25 μl) and standard (3 μl) were loaded into the Bolt™ 4-12 % Bis-Tris Gel (Invitrogen Thermo-Fisher Scientific, Waltham, MA) and run at 90 V for 65 minutes. Bolt MES (2-(N-morpholino)ethanesulfonic acid) was used as a running buffer. The gels were stained with Coomassie blue (Thermo Fisher, Waltham, MA) overnight and washed 3 times to remove excess stain. Photos were captured with the ChemiDoc (Bio-Rad, Hercules, CA).

2.11 Bioactivity of released bevacizumab by endothelial cell proliferation assay

The bioactivity of released bevacizumab was evaluated with a previously described cell proliferation assay[54, 55]. Human umbilical vein endothelial cells (HUVECs) were stimulated with 20 ng/ml VEGF. At this concentration, proliferation is maximal and enhanced approximately six times compared to not stimulated cells.[55] The ability of released bevacizumab relative to that of the native protein to inhibit HUVECs VEGF-induced cell proliferation was determined. HUVECs (Lonza, Switzerland) were cultured until passage 2–5 in Endothelial Cell Basal Medium 2 (Promocell C-22211) supplemented with Endothelial Cell Growth Medium 2 Supplement Mix (Promocell C-39216). Proliferation inhibition experiments were performed in assay medium (M199 medium supplemented with 2.5 % fetal bovine serum) in 96-well plates coated with rat tail collagen (Greiner Bio-One, the Netherlands).

Specifically, wells were filled with 50 µl of 25 times diluted in vitro release IVR sample and 50 µL of assay buffer supplemented with 80 ng/ml VEGF (final concentration 20 ng/ml) and preincubated at 37 °C and 5 % CO_2 for 1 hour. Next, 4000 cells dispersed in 100 µL assay medium were added resulting in a final volume of 200 µL per well (corresponding to 100 times IVR sample dilution). Wells without cells and filled with 200 µL of assay medium served as blank. Wells with cells stimulated with 0, 5, 10, 20, 30, 50, 100 ng/ml (final concentrations) VEGF were included as a reference to show that a VEGF concentration of 20 ng/ml, proliferation was maximal.

Polymer solutions (3 mg/ml) of HAFU (DS 30 and 83 %) and 4APM were used as controls. Cell proliferation was assessed after 92 hours of incubation at 37 °C / 5 % CO_2 by adding 20 µL of the Alamar Blue reagent and another four hours of incubation.[56] Fluorescence was measured (λ_{ex} 530 nm and λ_{em} 600 nm) with a microplate reader (Berthold Mithras LB 940, Germany). Results are expressed as relative cell proliferation, which is the proliferation normalized by the proliferation of unstimulated cells. The concentration of bioactive bevacizumab was calculated from the bevacizumab dose-dependent inhibition of VEGF stimulated HUVEC proliferation at a fixed concentration (20 ng/ml) of VEGF stimulated HUVEC proliferation.

2.12 Cytotoxicity on Retinal Muller cells (QMMUC-1)

Possible cytotoxicity of hydrogels and hydrogel precursors in contact with cells was evaluated using Queen's University Murine Müller glia Clone-1 (QMMUC-1 cells)[57]. Cells were cultured in Dulbecco's modified eagle medium (DMEM, low glucose) (Life Technologies, USA, Cat. No: 41965039) supplemented with 10% Foetal calf serum (Life Technologies, USA, Cat. No: 10270106) and 1% penicillin/streptomycin (PS) (Life Technologies, USA, Cat. No: 15140122). Cells were maintained in a humidified atmosphere with 5% CO_2 at 37 °C. HAFU (5 mg) with DS 30% and 5 mg 4APM crosslinker were dissolved separately in 50 µl and 40 µl PBS, respectively. After dissolution, the hydrogel precursors were mixed to obtain a 10wt% hydrogel (1:2 molar ratio of maleimide: furan, respectively). The formulation mixture was transferred into a 48-well plate, partly covering the bottom of the well. After 3 hours of incubation at 37 °C, the formed hydrogel adhered to the well's bottom. Next, QMMUC-1 cells suspended in DMEM were seeded into the

wells at 3000 cells/well. After 1 and 5 days of incubation, pictures of the cells were taken with a Leica DMi1 inverted microscope (Leica Microsystems, Germany) to investigate their morphology.

AlamarBlue® Cell Viability Assay was used to evaluate the effect of polymers and hydrogel leachables on QMMUC-1 cells. Hydrogels were prepared by mixing 4APM aqueous solution and HAFU (DS- 50%) aqueous solution (10 and 20 wt%) as described in section 2.3. After crosslinking, 1 ml PBS buffer was added to the hydrogel and incubated at 37 ℃ for 9 days to extract possible soluble products that were released from the hydrogel network. Furthermore, HAFU (DS 30%, 50% and 83%) and 4armPEGmalemide crosslinker were dissolved in cell culture medium to obtain different polymer concentration (0-5 mg/ml and 50 mg/ml). The QUMMC-1 cells were seeded in Costar® 96-well assay plates (Costar 3904, Corning Inc., NY, USA) at a concentration of 3000 cells/ml. After 24 h, the cell medium was removed, 20µl PBS solution with either possible leachables plus 100 µl cell medium or the polymers disolved in cell medium were added to the cells and incubated over another 24 h. After the treatment, a medium containing 1% Alamar Blue® (Life Technologies Inc., Gaithersburg, MD, USA) was added to the cells after washing the cells twice with the same medium, and the plates were incubated at 37 °C for 2 hours after which the resulting fluorescence was measured using a Glomax multi detection system (Promega, Southampton, UK) at 544/590 nm. Control samples containing media and Alamar Blue® solution without cells were also run as an assay control. For each test material, the results were averaged from six wells at the same time (n=6).

3   RESULTS & DISCUSSION

3.1   Hydrogel preparation and characterization:

HA 24 kDa was chosen over higher HA molecular weights, as it is important that the final formulations have an initially low viscosity to allow injectability through a small G needle. A HAFU derivate with a low degree of substitution was prepared by the activation of carboxyl groups of HA with EDC and NHS, followed by reaction of the formed activated NHS ester with the primary amine of furfurylamine. The degree of furan substitution of HA (DS) is defined as the number of furan-groups residues per 100 HA disaccharide units (see equation in supporting information, SI-Figure 1). ^{1}H NMR analysis showed that HAFU with DS 30% was successfully obtained with this method, as shown in SI-Figure 1. However, using this EDC/NHS method, the extent of the derivation of HA with furfurylamine is limited due to some drawbacks, such as the necessity of accurate pH control of the reaction mixture and short half-life of EDC (~4 h) in water at pH 5.0 when compared to DMTMM which provides superior yields, as reported by D'este et al. [58] Therefore, in order to obtain a HAFU derivative with a high DS, DMTMM was used as activation agent. By varying the molar ratios of HA (disaccharide units)/furfurylamine/DMTMM, HAFU with different DS were synthesized. Molar ratios of 1:2:6 and 1:1:2 yielded HAFU with DS of 83 and 50%, respectively, as shown by ^{1}H NMR analysis (SI-Figure 1). The conjugation of furfurylamine to the carboxylic acid on HA was further demonstrated by FTIR spectroscopic analysis as shown in SI-Figure 2. The successful grafting of the furan groups to HA is demonstrated by the increase and shift of the peaks at 741, 1652 and 1541 cm^{-1} corresponding to =C-H- bend of furan moiety, amide I stretching and amide II bending, respectively.

Transparent (see SI-Figure 10) and cylindrically shaped hydrogels were formed after mixing a solution of HAFU and 4APM in PBS (pH 7.4) in a plastic mold at 37 °C due to Diels-Alder (DA) reaction between the furan and the maleimide moieties [59] (Figure 1, reaction 1). The presence of DA crosslinks in the hydrogel network was confirmed by FTIR of the dried hydrogel, as shown in SI-Figure 3. The appearance of a new peak at 1459 cm^{-1} corresponding to the C=C bond in the Diels-Alder adduct confirms the proposed crosslinking chemistry. Hydrogels of different compositions were obtained using different polymers at varying concentrations in buffer, as shown in Table 1.

Table 1: Composition of the different hydrogel's formulation

Name Formulation	Exact molar ratio (Maleimide/Furan)	Polymer composition	Used total polymer concentrations (wt%)
4APM-HAFU (1:2)	1 : 1.9	4APM / HAFU DS 30%	10-20-25 %
4APM-HAFU (1:3)	1 : 3.1	4APM / HAFU DS 50%	5-10-15-30 %
4APM-HAFU (1:5)	1 : 5.2	4APM / HAFU DS 83 %	10-20-25 %

3.2   Swelling and degradation behavior

Hydrogel swelling and degradation properties are essential factors to evaluate when developing long-lasting hydrogels for ocular/biomedical applications. Swelling and degradation of different hydrogels during incubation in PBS buffer (pH 7.4) and at 37 °C were measured gravimetrically. All gel formulations first absorbed water, which caused a mass increase in time up to a maximum swelling ratio followed by a gradual decrease in gel weight until they completely dissolved in the buffer (Figure 2). This increase in the gel mass and thus swelling ratio is caused by the progressive degradation of the polymer network by hydrolysis of the crosslinks by retro Diels-Alder (rDA) reaction and subsequent water uptake (Figure 1, reaction 2). The degradation mechanism is based on the ring-opening hydrolysis of the generated maleimide after rDA to form unreactive maleamic acid (Figure 1, reaction 3), causing the removal of maleimide groups from the DA/rDA equilibrium and, therefore, consequent permanent cleavage of the crosslinks. This mechanism was confirmed by ^{1}H-NMR of the hydrogel degradation products (see SI-Figure 7). The presence of the hydrolyzed (ring-open) maleimide was identified, in line with previous reports by Kirchhof et al.[60]
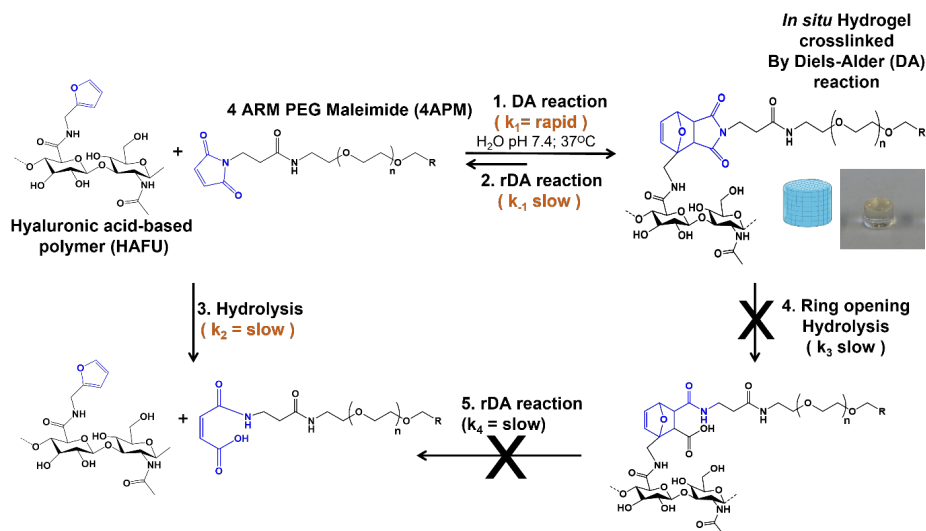
Figure 1 Schematic representation of hydrogel DA crosslinking reaction and potential degradation pathways. A total of 6 reactions involved in a dynamic equilibrium in which the first step is faster than the other reactions. There are 5 rate constants: k_1, k_{-1}, k_2, k_3, and k_4. The k_1 and k_{-1} rate constants represent the reversible steps between reactants (HAFU and 4APM) and intermediate (DA-adduct in crosslinked gel). k_1 is the forward step (1 DA reaction) and k_{-1} is the reverse step (2 rDA reaction). k_2 is the rate constant for the irreversible hydrolysis of the maleimide in the 4APM to unreactive maleamic acid. k_3 and k_4 describe the ring-opening rection of the DA adducts to eventually form HAFU and hydrolyzed maleamic acid in the 4APM.

Another possible pathway is caused by the direct hydrolysis of the carbonyl moiety and ring opening of the DA adduct (Figure 1 reaction 4) with subsequent rDA reaction yielding furan and unreactive maleic acid (Figure 1 reaction 5). However, as previously reported by Kirchhof et al.[61] hydrogel degradation through this second pathway is not likely to occur. Gregoritza et al. and Kirchhof et al. showed that DA hydrogels based on PEG or Poloxamine can be completely degraded under physiological conditions by retro-Diels Alder at 37 °C.[31, 60, 61]

Figure 2A shows that, as expected, 4APM-HAFU (molar ratio of maleimide and furan 1:2, respectively) hydrogels with 10 wt% polymer degrades faster (30 days) when compared to the formulations with 20 and 25 wt% (100 and 120 days, respectively). Hydrogels with an equal overall concentration of the HAFU and 4APM building blocks and crosslinked at a molar ratio of maleimide and furan of 1:5 showed lower swelling compared the hydrogel crosslinked at a molar ratio 1:2 (Figure 2A and 2B). Specifically, the mass of the hydrogels prepared with maleimide-furan ratio 1:5 steadily increased in weight, after which they displayed a dissolution phase which ended at 120 days (10wt%), 300 days (20wt%), and 360 days (25wt%) of incubation. This suggests that with increasing furan moieties concentration, the reaction DA/rDA equilibrium shifts towards the formation of DA crosslinks (Figure 1, reaction 1), resulting in higher hydrogel stability and thus longer degradation time. The hydrogels of crosslinked 4APM-HAFU ratio 1:2 DA degraded approximately three times faster than 1:5 DA hydrogels, independent of the initial polymer

concentration (Figure 2 D) and all investigated hydrogels were found to be fully degradable. Images of the hydrogels after 26 days of incubation at 37 °C (Figure 2C) clearly show that the gels with ratio 1:2 lose their shape faster compared to gels prepared at ratio 1:5, due to their faster degradation kinetics.

It is important to note that hydrogel swelling, and degradation behavior might differ in vivo due to surrounding ocular tissue, ocular clearance and the presence of hydrolytic enzymes. In follow-up studies, hydrogel degradation and intraocular pressure should be systematically studied in vivo settings to rule out excessive swelling effects in the presently studied 4APM-HAFU hydrogel formulation.
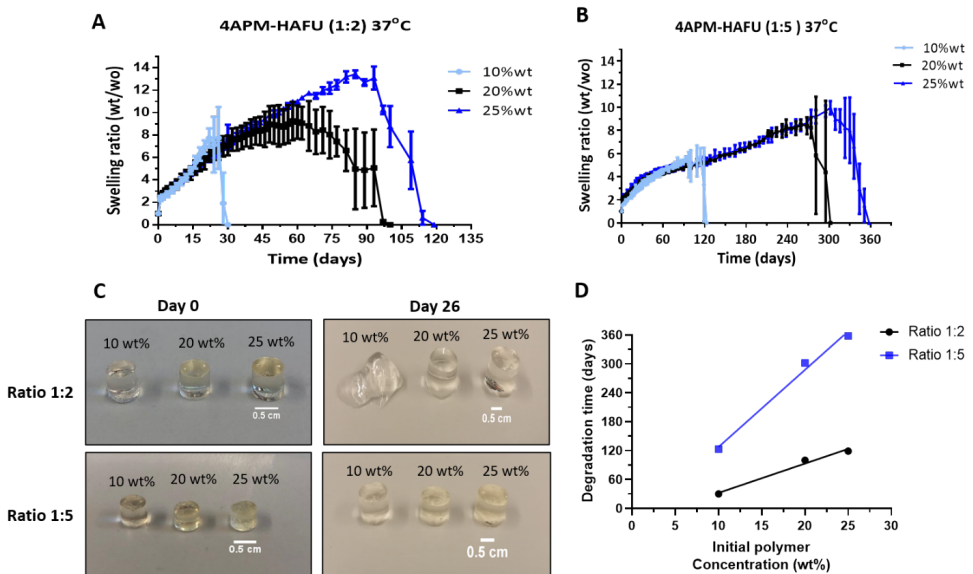
Figure 2 Swelling and degradation characteristics of different 4APM-HAFU DA hydrogels. A) swelling ratio of 10, 20, 25 initial wt% hydrogels prepared at ratio 1: 2 4APM-HAFU incubated at 37 °C in PBS pH 7.4. B) swelling ratio of 10 ,20, 25 initial wt% hydrogels prepared at ratio 1: 5 4APM-HAFU incubated at 37 °C in PBS pH 7.4. C) Pictures of 4APM-HAFU hydrogel (ratio 1:2 and 1:5) on day 26 of incubation at 37 °C in PBS (pH 7.4) in comparison with hydrogel after formation. D) 4APM-HAFU (ratio 1:2 and 1:5) hydrogel degradation time as a function the initial polymer concentration.

3.3   Rheological analysis

In order to be used as injectable, *in situ* forming hydrogel for intraocular drug delivery, the formulation should possess appropriate flow during injection and gelation properties, such as kinetics and stiffness, after injection. Rheological analysis was used to monitor the evolution of the storage (G') and loss moduli (G") as a function of time at different temperatures in relation to hydrogel compositions. A formulation composed of 15wt% polymers (molar ratio 1:3; maleimide: furan respectively) was prepared with and without bevacizumab (1.25 mg/ml) and analyzed for gel formation using a rheometer. This formulation (15 wt% polymers (ratio 1:3)) was chosen as a

model formulation with intermediate gelation kinetics in order to verify if there are any interactions of the protein with the hydrogel network.

The G', G", and complex viscosity (η^*) were monitored over time, as shown in Figure 3 A-B. Initially, the G' and G" were low with a complex viscosity (η^*) of 0.07 Pa.s indicating a free-flowing liquid solution. Both moduli subsequently increased in time, and a crossover between G' and G" (defined here as the gelation time and corresponding to tan(δ) = 1, SI-Figure 9) demonstrated network formation due to the reaction of the maleimide and furan functionalities. Figure 3 A and B show that the gelation time of the formulation with and without protein loading was around 17 min, indicating that the protein did not affect the gelation kinetics. Also, the final stiffness (34-38 kPa) was not affected by the presence of the protein. The G' increase is dependent on the polymer concentration (Figure 3C), as higher concentrations lead to faster gelling (Figure 3D) and stiffer gels. As expected, the Diels-Alder crosslinking occurred faster at higher temperatures Figure 3E. This means that depending on the composition the formulation can be kept in the fridge (4 °C) for 1 to 3 hours, before administration to a patient. In addition, formulations with a higher furan to maleimide molar ratio (5:1) resulted in faster gelation (within 5 min) at 37 °C, as compared to the formulation with a 2 to 1 molar ratio of these groups (16 min). This faster gelation can be explained by the higher probability of the furan to react with the available maleimide groups. The relatively good stability upon storage at low temperature and the rapid and tailorable gelation time after intravitreal administration is a substantial advantage for possible clinical use of the formulation. The observed decrease in gelation time with an increase of temperature (from 4 to 37 °C) can be ascribed to the increased reaction rate of furan and maleimide groups. Interestingly, it was observed that at the gelation point, 20 wt% 4APM-HAFU hydrogel formulations (molar ratio 1:2 and 1:5 maleimide: furan) had lower storage modulus with an increasing temperature, see SI-Figure 8. This observation indicates that overall fewer cross-links are formed at higher temperatures, which can be attributed to a slight shift in the equilibrium of forming and breaking of DA adducts [62-65].
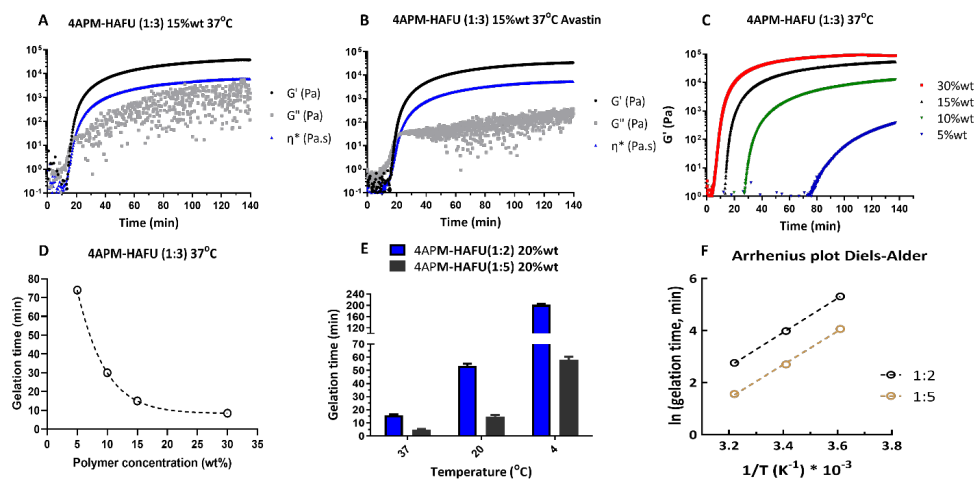
Figure 3 Time and temperature dependent rheological characteristics of 4APM-HAFU hydrogel formulation. A-B) storage (G') and loss moduli (G") as a function of time of 15wt% 4APM-HAFU (molar ratio 1:3) hydrogel formulation with and without bevacizumab. C) G' as a function of time of 4APM-HAFU formulation with different polymer concentrations. D) Gelation time of 4APM-HAFU hydrogels as a function of polymer concentration. E) gelation time of 20wt% 4APM-HAFU hydrogel formulations at molar ratio 1:2 and 1:5 maleimide: furan at 37, 20, and 4 °C. F) Arrhenius plot of the natural logarithm of the gelation time as a function of the reciprocal absolute temperature for formulations with two different maleimide: furan ratios, 1:2 (black) and 1:5 (gold). The dashed lines represent the fit of the data and the activation energy was calculated from the slopes of the fitted lines.

The temperature-dependent gelation time of the hydrogels (Figure 3F) was used to calculate the activation energy for the Diels-Alder adduct formation in the hydrogel system, as previously reported for other hydrogel forming systems. [66] [67]

$$g_t = A \exp(E_a/RT)$$

Where g_t is the gelation time, A is the pre-exponential factor, E_a is the activation (kJ/mol), R and T are the universal gas constant (8.314 J/K.mol) and the reaction temperature (in K), respectively. The calculated activation energy was 54.5 ±1.1 kJ/mol and 53.4 ±1.9 kJ/mol for 1:2 and 1:5 maleimide: furan ratios, respectively, used in the hydrogel formulations. The calculated activation energy is in agreement with previously reported values for furan-maleimide Diels-Alder systems (51.9 kJ/mol and 48.4 kJ/mol). [68, 69]

3.4 *Ex vivo* injection and mesh size determination of *in situ* formed hydrogels

In order to localize the formulation in the vitreous after injection, HAFU was labelled with Alexa Fluor 750 C5 maleimide by means of Diels-Alder reaction, resulting in the formation of HAFU-750 dye conjugate. The absence of free dye was demonstrated by SEC, as shown in SI-Figure 4A. The chromatogram of the synthesized HAFU-750 dye polymer showed a UV signal at 750 nm,

which corresponds to the dye fluorophore (SI-Figure 4B). From the spectrum, it is calculated that ~0.01% of the disaccharide units were labelled with the fluorophore showing a coupling efficiency of around 50%. The injectability of HA-PEG formulations was investigated by intravitreal injection into vitreous humor of an *ex vivo* porcine eye at 37 °C, using a 29-gauge needle. After injection (5 min), the localized presence of the formulation (in green) was observed in the vitreous at the site of injection (Figure 4C). The constrained presence within the vitreous might be due to the differences in viscosity between the vitreous body and the gel formulation. Shafaie et al.[70] reported the complex viscosity [η^*] of vitreous humor samples from the porcine eye and human eye was approximately 0.30 Pa.s at oscillatory stress of 1 Hz. The η^* of 20wt% 4APM-HAFU formulation was measured at a time sweep of 1 Hz frequency. As shown in SI-Figure 5D, the hydrogel with a ratio maleimide: furan of 1:2 give a complex viscosity of 0.23 ± 0.12 Pa.s, while the hydrogel with a ratio of 1:5 showed 0.75 ± 0.36 Pa.s around 3 mins after mixing of the hydrogel building blocks. These values progressively increased in time due to further network formation, reaching final viscosities of 6.0 kPa.s and 7.2 kPa.s, respectively SI-Figure 5C. This relatively rapid increase in the viscosity after *in situ* crosslinking explains why after injection, the gel formulation did not significantly spread in the vitreous. Furthermore, after injection of 4APM-HAFU-750dye hydrogel formulation (160 ml, 20 wt%) and 1 hour incubation at 37 °C, the vitreous was isolated from the porcine eye to allow extraction of the formed hydrogel (in light blue), as shown in Figure 4D. The hydrogel formed *in situ* upon injection in the eye showed an irregular, bean-like shape after administration of the liquid formulation through a 29 G needle. It was found that the *ex vivo* formed hydrogel had a width of 0.73 cm and a length of 0.83 cm, whereas as a comparison, a hydrogel prepared *in vitro* took the shape of the mold (Figure 4E). Intravitreal injection of hydrogel formulations has been previously investigated in *ex vivo* and *in vivo* models[71-73]. However, no attempts have been made to rheologically characterize *ex vivo* formed gels. Therefore, in this study, the mechanical properties of *ex vivo* intravitreally formed hydrogel were investigated for the first time. Moreover, the mesh size of the formed hydrogel was calculated and compared to that of the *in vitro* formed hydrogels. The average mesh size is an important parameter that characterizes the hydrogel network density.[74] Therefore, the hydrogel mesh size gives information on macromolecules' (such as therapeutic proteins) diffusivity in the gel network,[75] a crucial aspect to consider when developing an ocular drug delivery reservoir.
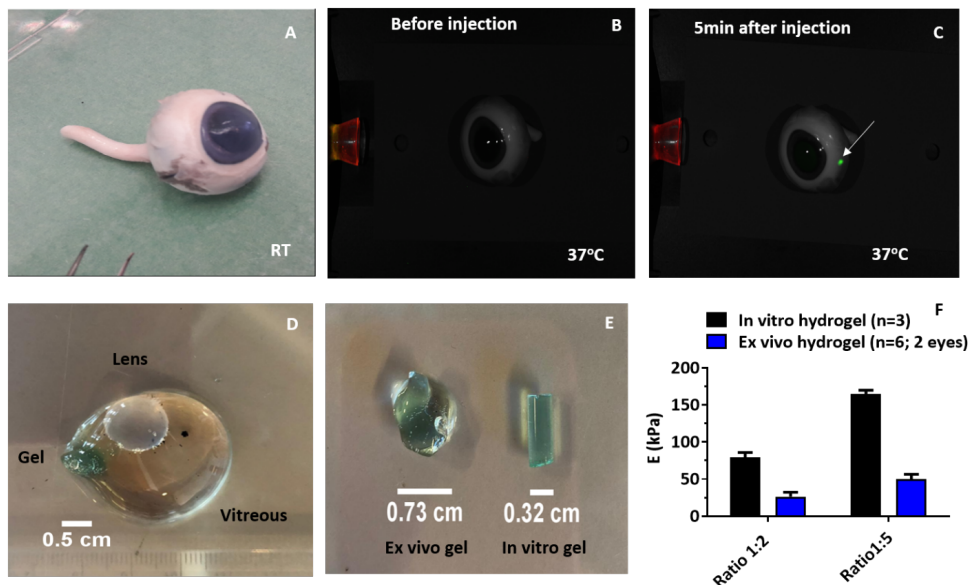
Figure 4 *In situ* hydrogel formation in the vitreous body after intravitreal injection. A) Clean enucleated porcine eye at room temperature. B-C) Fluorescent image of a porcine eye before and 5 min after intravitreal injection at 37 °C (20 wt% HAFU-750dye/4APM ratio 1:3). D) Vitreous image after extraction from ocular tissues, with *in situ* formed 4APM-HAFU hydrogel visible in green within the vitreous body. E) Representative image of *ex vivo* and *in vitro* formed hydrogels. F) E (kPa) of *in vitro* (n=3) and *ex vivo* (n=6; 2 eyes) formed 20 wt% 4APM-HAFU hydrogels at ratio 1:2 and 1:5.

To calculate the average mesh size (ξ) of *in vitro* and the isolated *ex vivo* formed hydrogels, their Young's moduli (E) were determined experimentally by compression tests (Figure 4F).[76] Furthermore, the shear modulus values (G') taken at the plateau region of a time sweep curve was also experimentally determined for 20 wt% *in vitro* formed hydrogels (SI-Figure 5A, B). The ratio between the elastic (E) and shear (G') moduli for the *in vitro* formed hydrogels was used to calculate the G' of the *ex vivo* formed hydrogel, as shown in Table 2. Specifically, it was found that for the *in vitro* hydrogels, a factor of 2.5 ± 0.2 was experimentally determined for E and G' at a frequency of 1 Hz. This value is close to the theoretical ratio, with E being three times G' [77]. Considering that the G' of the *ex vivo* prepared hydrogels could not be experimentally determined, the same factor for the *in vitro* formed hydrogels was used. As expected, *in vitro* and *ex vivo* gels formed at molar a ratio 1:5 maleimide/furan had higher E (in vitro: 165±3 kPa; *ex vivo* 50±3 kPa) and G' (in vitro: 62.4± 4kPa; *ex vivo* 20 kPa) when compared to formulations of a molar ratio 1:2, E (in vitro: 79±3.5 kPa; *ex vivo* 26±2 kPa) and G' (in vitro: 32±3 kPa; *ex vivo* 10.5 kPa) see Table 2. The higher E and G' values for the *in vitro* formed hydrogels (approximately 3 times higher than the ex vivo gels) indicate a higher crosslinking density. The obtained G' values were used to calculate the average mesh sizes (see equation in section 2.5) of the different *in vitro* and *ex vivo* hydrogels by applying the rubber elasticity theory with the assumption of an affine network model, neglecting end effects of single chains and excluding physical entanglements.[52, 78] The

ex vivo hydrogels mesh size at molar ratio of 1:5 (5.9 nm) was calculated to be smaller than at the ratio of 1:2 (7.4 nm), as shown in Table 2.

The calculated mesh sizes of the *ex vivo* hydrogels are about 1.5 times greater than that of the *in vitro* formed gels, which might be because when injecting the hydrogel precursors into the eye, the polymers are diluted in the vitreous humor, which is a gelatinous tissue mainly composed of water with small amounts of hyaluronic acid, glucose, anions, cations and collagen[79]. The determined mesh sizes can be used to evaluate what polymer composition is suitable for releasing a therapeutic protein of a given size. The present paper reports for the fist time examples of a direct comparison of average mesh size (ξ_{avg}) between *in vitro* and *ex vivo* formed hydrogels. Although the ex-vivo eye is not entirely comparible to the in vivo situation, it provides a valuable method for preclinical intraocular hydrogel characterization.

Table 2 Mesh size of in vitro and ex vivo 20 wt% 4APM-HAFU hydrogels as determined by rheological and mechanical measurements.

Gel samples	G' (kPa)	E (kPa)	Mesh size (nm)
In vitro ratio (1:2)	32 ± 3	79 ± 4	5.1
In vitro ratio (1:5)	62.4 ± 4	165 ± 3	3.9
Ex vivo ratio (1:2)	*10.5	26 ± 2	7.4
Ex vivo ratio (1:5)	*20	50 ± 3	5.9

The E values of ex vivo formed hydrogels were determined as n=6 using two porcine eyeballs, while the E values of the in vitro produced hydrogels are presented as the mean of n=3 independent experiments using DMA. The G' value of the in vitro gel was obtained from the mean of the plateau region of a time sweep curve measured at a frequency of 1 Hz and a strain of 0.1 %. *Determined from the experimentally obtained E divided by 2.5.

3.5   In vitro release and structural integrity of Bevacizumab

The in vitro release of bevacizumab from the hydrogels was studied in PBS (pH 7.4) at 37 °C. The chosen bevacizumab dose (1.25 and 1.5 mg) corresponds to the typical amount administered in clinics by bolus injection of 50 µl Avastin (1.25 mg bevacizumab).[80, 81] Figure 5 shows that the release of bevacizumab from the 4APM-HAFU hydrogels is generally speaking dependent on the hydrogel composition, and sustained release was observed for all investigated hydrogel formulations. The release of bevacizumab from 4APM-HAFU hydrogels prepared with molar ratios of maleimide/furan 1:2 and 1:3 lasted for 70 days, after which no protein could be detected in the release samples. Specifically, hydrogels prepared at ratio 1:2 maleimide/furan released approximately 55% of the incorporated bevacizumab during 70 days. In the first 13 days, the 10 wt% gel released ~29% of loaded protein while 20 wt% and 25 wt% released ~17 % of loaded protein also during 13 days, after which the release profile was independent of the initial polymer weight fraction of the hydrogels. This observation suggests that in the first 13 days, the mesh size of the 10 wt% gel was larger than the protein size, and therefore, faster release was observed from this network compared to the 20 and 25wt% gels. After 13 days, the mesh sizes of both the low and high concentration gels are larger than the protein diameter due to significant swelling

of the hydrogels. No significant differences in release rate were observed after day 13 as the free volume fraction, which determines the release of proteins from hydrogels when the mesh size is greater than the protein hydrodynamic diameter [82] as well as the gel geometries after swelling is not very different for these gels. From these results, it can be concluded that although the gelation time and the degradation kinetics largely depend on the initial polymer concentration for the gels formed based on a 1:2 maleimide/ furan ratio, the release kinetics are hardly affected by these parameters. On the other hand, 4APM-HAFU hydrogels prepared at a molar ratio of 1:3 maleimide/furan showed a two-phase release profile. The 10% gel released approximately 46% of the loaded protein in ~16 days in an almost linear way, followed by a slower release of up to 74% of the loaded protein during the next ~54 days. The 16 wt% 4APM-HAFU hydrogel (ratio 1:3 maleimide/furan) released ~60% of the loaded protein within the first 30 days, followed by slower release kinetics of up to 77% of loaded bevacizumab to 70 days. Interestingly, bevacizumab was released from 4APM-HAFU hydrogels prepared at a molar ratio of 1:5 for more than 329 days, also with a two-phase release kinetics. In the first phase, 34% of the loaded protein was released from the 10wt% gel during 30 days and from the 20wt % gel during 50 days, while 40 % was released from 25 wt% gel during 60 days. This was followed by the second phase of slower protein release. After 329 days, approximately 53% of bevacizumab was released from the 10wt % gel, while 64% was released from the 20wt% gel after 427 days. Remarkably, the 25 wt% gel prepared at a ratio 1:5 4APM-HAFU showed nearly complete bevacizumab release over the measured time frame of 427 days. For comparison, previously Kirchhof et al.[61] Gregoritza et al.[31] reported up to ~100 days of sustained bevacizumab release from DA-based hydrogels.

As reported in Table 2, the *in vitro* and *ex vivo* formed hydrogels' mesh size is between 3.9 and 7.4 nm, and these values increase during hydrogel swelling and degradation. Therefore, it is expected and also in agreement with the *in vitro* data, that the release of a monoclonal antibody such as bevacizumab with a hydrodynamic radius of around 6.5 nm[83] is likely controlled by a combination of swelling, degradation and diffusion and subsequently multiple phase release profiles can be observed. However, for the *ex vivo* formed 4APM-HAFU (molar ratio 1:2) hydrogel, the calculated average ξ_{avg} is around 7.4 nm (Table 2), which means that after 2 times swelling the loaded protein will released mainly by diffusion from regions with mesh size above the size of the protein while part of the loaded protein molecules might be entrapped in the hydrogel in regions with mesh sizes < 2x6.52 nm and can therefore only be released upon swelling and degradation of the hydrogel.

In general, other proteins administered through intravitreal injections do not exceed a hydrodynamic radius of 10 nm, e.g. aflibercept (5.20 nm); ranibizumab (4.1 nm).[84, 85] Therefore, knowing the difference in hydrogel initial mesh size in vitro (5.1 -3.9 nm) and ex-vivo (7.4-5.9 nm), protein release kinetics could be potentially be predicted based on their diameter. Nevertheless, it is essential to note that protein-network interactions might also affect drug release rate.

The release curves of Figure 5 span a much longer time frame as compared to the degradation curves in Figure 2 for the empty hydrogels. Noteworthy, the protein loaded hydrogels were visually discernable in the release medium over the complete release period. This observation

means that the protein loaded hydrogels degrade much slower compared to the empty hydrogels. Specifically, we observed a factor 2-3 slower degradation rate for the protein loaded 4APM-HAFU hydrogels compared to the corresponding empty hydrogels. The retarded degradation of the protein-loaded gels may have a number of reasons. Firstly, electrostatic interactions between the negatively charged hydrogel network and the slightly cationic bevacizumab (isoelectric point 8.3) may play a role in retaining the protein in the gel[86]. Secondly, the encapsulated protein can act as a chemical crosslinker when one protein molecule reacts with two or more maleimide groups present in the polymer network. Amine and thiol residues of proteins can react with maleimides by a Michael-type addition.[87] For bevacizumab , reactivity with amines is more likely since thiol functionalities are disulfide bridged in this protein.[88] Free maleimide moieties available during the formation of Diels-Alder crosslinks can potentially react with the protein both during and after hydrogel formation. These grafted proteins can only be released upon the network's degradation. The occurrence of these grafting reactions, leading to protein-polymer conjugates, were indeed confirmed by SDS PAGE analysis under reducing and nonreducing conditions. Incubation of bevacizumab for one hour with 4APM polymer resulted in the coupling of around one PEG chain after 1 hour, and more extensive modification was observed after five days of incubation, and approximately on the average three PEG chains were coupled to the protein as shown in SI-Figure 6A. As expected, the HAFU DS30 and 83 did not react with the protein even after 5 days of incubation at 37 °C, justifying the choice to dissolve HAFU in the protein solution.

When preparing a hydrogel at a molar ratio of maleimide and furan groups of 1:1, in principle, 100% conversion of both reactants is possible. However, crosslinks are formed randomly, and the mismatched reactive groups can result in the presence of free reactive maleimide groups in the polymer network.[89] For this reason, bevacizumab was loaded in hydrogel formulations containing higher ratios of furan functional groups compared to maleimide groups to minimize the presence of the latter and thus limiting protein modification. The excess furan was also chosen to minimize possible side reactions of the maleimide with biological systems as furan is considered to be more safe. During the release study, a significant extent of modification was still seen for the protein released after 21 days from the 1:2 4APM-HAFU hydrogels. Nevertheless, when proteins are linked to the hydrogels, quantitative release of modified protein from a hydrogel matrix can still occur upon complete degradation of the network. However, complete release was not observed in this study, likely, because large soluble conjugates composed of multiple PEG chains and protein molecules linked together are formed, which are captured by the precolumn in the analysis method, and consequently they are not detected. Importantly, the extent of modification was substantially reduced by using a higher concentration of furan polymer than maleimide polymer in a molar ratio of 5:1 respectively (SI-Figure 6B). In this hydrogel the concentration of free maleimide groups is low and thus unwanted reaction with bevacizumab is minimized and prolonged-release of approximately 90% native protein after 3 months was achieved. Figure 5C shows that by increasing the furan/maleimide molar ratios of the formulations, nearly complete release of protein was obtained (88% for 25wt% 4APM-HAFU molar ratio of 1:5). Overall, in agreement with the swelling and degradation study, the initial polymer concentration has a relatively small effect on the release rate when compared to the furan/maleimide ratio.
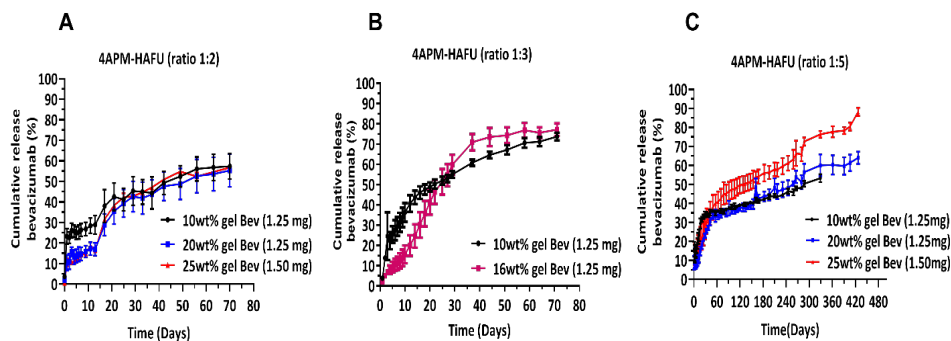
Figure 5 Cumulative release of bevacizumab from A) 10, 20, 25wt% ratio 1:2 4APM-HAFU hydrogels. B) 10, 16 wt% ratio 1:3 4APM-HAFU hydrogels. C) 10, 20, 25wt% ratio 1:5 4APM-HAFU hydrogels as determined by the SEC UPLC.

The bioactivity of released bevacizumab was analyzed by a cell proliferation assay as shown in Figure 6. The bioactivity of the released protein from 4APM-HAFU hydrogels (ratio 1:2 and 1:5) after days 7, 29 and 60 was studied. The bioactivity of bevacizumab after longer release time points was not measured as time-related unspecific effects, such as oxidation, deamidation, aggregation, and adsorption to the vial surfaces are likely to occur.

Figure 6A shows that the relative cell proliferation increases approximately six times compared to non-treated HUVECs with VEGF concentration up to 20 ng/ml and levels off at higher concentration. Therefore, the inhibitory effect of bevacizumab was investigated for cells in the presence of 20 ng/ml VEGF and a sigmoidal dose-response curve was observed (figure 6B). As shown in Figure 6C, after dilution of the in vitro release (IVR) samples a 100 times to reach concentrations within the descending range of the dose-dependent inhibition curve (0.1-0.01 µg/ml), proliferation of HUVECs was measured. All groups showed a significant reduction ($p < 0.05$) of cell proliferation compared to the maximal cell proliferation (Figure 6C), except for the formulation 20 wt% ratio 1:2 IVR day 60, probably due to dilution close to the detection limit. This reduction can be explained by the inactivation of VEGF due to bevacizumab in the release samples and as expected polymer precursors (which can be present in the IVR) did not inactivate VEGF Figure 6D. Quantitative correlation between the released bevacizumab concentration (detected by SEC) and reduction in HUVEC proliferation cannot be directly obtained due to the relatively high inaccuracy of the biological assay. Nevertheless, after 60 days, the released bevacizumab from the hydrogel formulations was still able to reduce the activity of VEGF stimulated proliferative HUVECs indicating that the released proteins were still active.
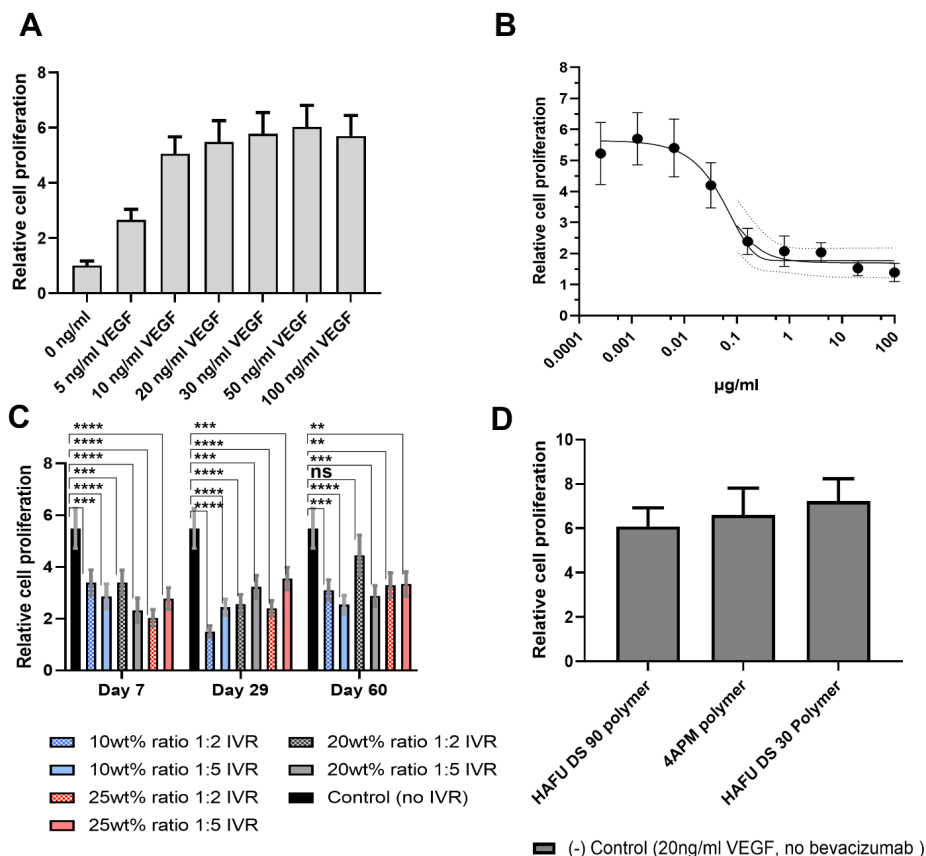
Figure 6 Bioactivity of released bevacizumab from 4APM-HAFU hydrogel networks. A) Relative cell proliferation of HUVECs stimulated by VEGF (0-100 ng/ml). B) Bevacizumab dose-dependent inhibition of VEGF (20 ng/ml.) stimulated HUVEC proliferation. C) Bioactivity of 100 times diluted IVR samples (on days 7, 29, 60) on cell proliferation of HUVECs treated with 20 ng/ml VEGF; * p < 0.05, ** p < 0.01, *** p < 0.001, **** p < 0.0001 and ns for p > 0.05 compared to control treated with 20 ng/ml VEGF (One-way ANOVA, multiple comparison test) D) The effect of the polymer precursors on proliferation (cells were treated with 20 ng/ml VEGF). Data are presented as the mean ±SD of three independent

3.6   Cytocompatibility studies

Possible cytotoxicity of the hydrogel polymer precursors and hydrogel on contacting cells was evaluated using the QMMUC-1 cell line. Müller glial are a primary retinal glial cell type and contribute to maintaining retinal structure and homeostasis.[57] Furthermore, Müller glia are known to play a role in the pathogenesis of diabetic retinopathy and hypoxia retinal vascular disorders as they produce VEGF, which plays an important role in retinal inflammation and vascular leakage in diabetic retinopathy.[90] Clearly, damage to these cells will drastically disrupt normal retinal function. Figure 7A shows that the QMMUC-1 cells surrounding the gels adhered

to, spread and grew on the cell culture dish with normal morphology and proliferation after 24 hours and 5 days of culture. This observation indicates that the hydrogels do not release toxic leachables for these cells. QMMUC-1 cells located on top of the hydrogel's surface did not spread and grow, and they were found floating with different morphology compared to the control. This poor cell adhesion on the surface of the hydrogel might be due to the presence of a 4-arm PEG crosslinker in the hydrogel network, as also discussed by Yu et al.[45] In another study, Nimmo et al.[29] showed that MDA-MB-231 cells (human breast cancer cell line) placed on top of HA-PEG hydrogels remained round for the first 24 h, after which the cells began to adopt a flattened morphology, suggesting cell attachment. The authors discussed this was due to the expression of CD44 cell surface antigen, a receptor for HA[91], allowing for cell interaction and potential adhesion to the gel surface; however, a significant number of cells did not adhere to the gels and were removed during media exchange. Nevertheless, although CD44 cell surface antigen is expressed on mature Müller glial cells,[92] the cells did not attach on top of the gel surface but were found in direct contact with the gel after the 5 days of study. It is essential to note that intravitreally implanted hydrogels are not required to have cell adhesion properties when used as drug reservoirs, as they are developed to have limited interaction with cellular tissue surrounding the vitreous environment.

Alamar Blue® cell viability assay was used to evaluate the effect of hydrogel leachables and polymer precursors on QMMUC-1 cells. Figure 7B shows that hydrogel leachables (from 10 and 20 wt% gel) did not affect cell viability (approximately 100% of the cells were metabolically active after 24h exposure). This result is in accordance with the direct contact experiments.

As discussed in section 3.2, the HA-PEG hydrogels studied are fully degradable by retro-Diels Alder reaction. This means that the hydrogel precursors could gradually detach from the network and diffuse in the vitreous with potential toxicity to the surrounding tissues. Therefore, different polymer concentrations of 4APM crosslinker and HAFU DS 30%, 50%, 83% (0.125-50mg/ml) were used to evaluate cytocompatibility with QMMUC-1 cells. From the results shown in Figure 7C, it is clear that the polymers were well tolerated by the cells up to the concentration of 5 mg/ml. However, at a polymer concentration of 50 mg/ml, cell viability was significantly ($p < 0.0001$) reduced to 75, 59, 77% for HAFU polymer with DS of 30, 50 and 83%, respectively, while more pronounced toxicity was observed for the 4APM crosslinker, reducing the viability to 21%. Considering that the volume of the vitreous humor in the adult human eye is approximately 4 ml [93], it is expected that after intravitreal injection of 50 µl of PEG-HA hydrogel polymer precursors, the concentration of the individual components in the eye would be maximally between 0.625 to 1.25 mg/ml, which is shown to be well tolerated by the QMMUC-1 cells.
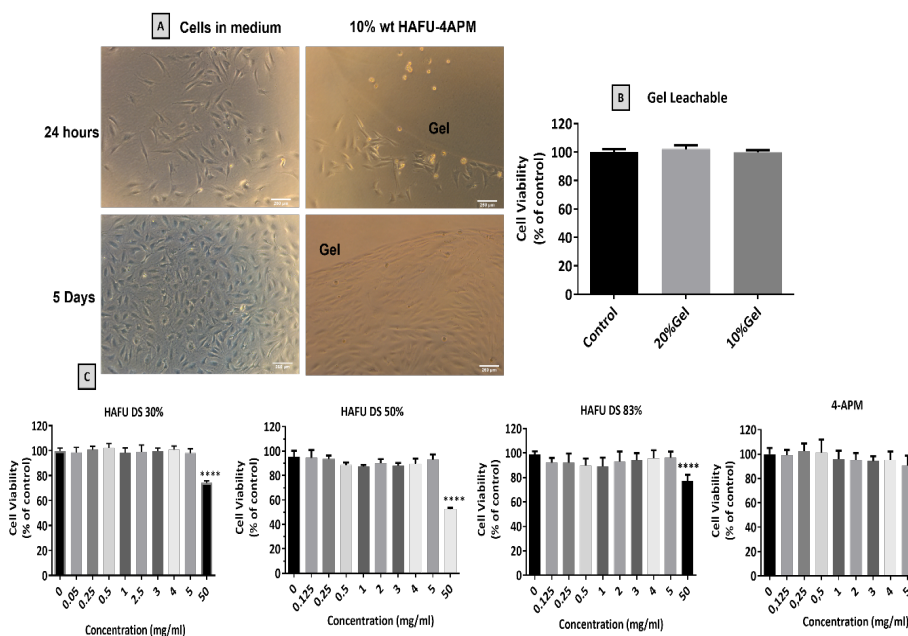
Figure 7 Cytocompatibility of hydrogel and hydrogel precursors on QMMUC-1 cells. A) The morphology of QMMUC-1 cells after 24 hours and 5 days co-incubated in direct contact with 10wt% 4APM-HAFU hydrogel; The location of the hydrogels and the scale bar (260 μm) are indicated in the images. (B) QMMUC-1 cell viability in the presence of hydrogel leachables from 10, 20 wt% 4APM-HAFU hydrogels after 24h incubation. C) Cell viability (Alamar blue) of QMMUC-1 cells after 24h incubation with polymers (HAFU DS 30, 50,83% & 4APM) across concentration range of 0.125-50 mg/ml. **** $p < 0.0001$ compared to control untreated cells (One-way ANOVA, multiple comparison test), (n=6).

4 CONCLUSIONS

In this study, an intravitreal *in situ* forming DA crosslinked hydrogel based on HA and PEG polymers with potential application as a long-acting sustained delivery system for bevacizumab and potentially for other anti-VEGF therapeutics was investigated. The prospect of the system for treating retinal diseases was examined step-by-step by testing hydrogel gelation kinetics, mechanical properties, injectability, biodegradability, sustained release of bevacizumab and cytocompatibility to retinal cells. In summary, we showed that gelation time and hydrogel final stiffness are strongly dependent on temperature and ratios of the reacting furan and maleimide groups present on HA and PEG respectively. The obtained hydrogels were fully degradable at physiological conditions due to retro Diels-Alder reaction. Formulations could be easily injected into the vitreous body of an ex-vivo porcine eye through a 29G needle, and crosslinked hydrogels were obtained of which the mesh size was determined mechanical analysis. To the best of our knowledge, the reported method was the first example of a direct comparison of hydrogel mesh size in vitro and *ex vivo*, providing a valuable tool for preclinical intraocular hydrogel

characterization. The hydrogels showed no toxicity to QMMUC-1 at the used concentrations in vitro. Concluding, 4APM-HAFU hydrogels formed at a maleimide/furan molar ratio 1:3 provide sustained release of bevacizumab for two months. This formulation can therefore potentially be used for therapy to replace the monthly injection by an injection every two months. For prolonging chronic therapy, the hydrogel formulation with a maleimide/furan molar ratio of 1:5 could be considered as this formulation showed sustained release of bevacizumab for up to a year. However, further research whether indeed bioactive protein is released during this timeframe is needed.

5   ACKNOWLEDGEMENTS

6   REFERENCES

[1] W.H. Organization, World Report on Vision in, WHO, ISBN: 978-92-4-151657-0, 2019.

[2] R. Cheloni, S.A. Gandolfi, C. Signorelli, A. Odone, Global prevalence of diabetic retinopathy: protocol for a systematic review and meta-analysis, BMJ Open, 9 (2019) e022188.

[3] J.M. Colijn, G.H. Buitendijk, M.A. Meester, J.R. Vingerling, A. Hofman, C.C.W. Klaver, The prevalence of Age-related Macular Degeneration in Europe. The E3 Consortium, Invest. Ophthalmol. Visual Sci., 57 (2016) 11-11.

[4] J.L. Kovach, S.G. Schwartz, H.W. Flynn, Jr., I.U. Scott, Anti-VEGF Treatment Strategies for Wet AMD, J Ophthalmol, 2012 (2012) 786870.

[5] A. Kato, T. Yasukawa, Y. Ogura, Antivascular endothelial growth factor therapies for neovascular age-related macular degeneration: Search for the optimized treatment regimen, Taiwan J. Ophthalmol, 4 (2014) 3-8.

[6] P.P. Yip, C.F. Woo, H.H. Tang, C.K. Ho, Triple therapy for neovascular age-related macular degeneration using single-session photodynamic therapy combined with intravitreal bevacizumab and triamcinolone, Br J Ophthalmol, 93 (2009) 754-758.

[7] A. Mandal, D. Pal, V. Agrahari, H.M. Trinh, M. Joseph, A.K. Mitra, Ocular delivery of proteins and peptides: Challenges and novel formulation approaches, Adv. Drug Delivery Rev., 126 (2018) 67-95.

[8] P.A. Keane, S.R. Sadda, Development of Anti-VEGF Therapies for Intraocular Use: A Guide for Clinicians, J Ophthalmol, 2012 (2012) 483034.

[9] K. Radhakrishnan, N. Sonali, M. Moreno, J. Nirmal, A.A. Fernandez, S. Venkatraman, R. Agrawal, Protein delivery to the back of the eye: barriers, carriers and stability of anti-VEGF proteins, Drug Discov Today, 22 (2017) 416-423.

[10] M. Papadia, M. Misteli, B. Jeannin, C.P. Herbort, The influence of anti-VEGF therapy on present day management of macular edema due to BRVO and CRVO: a longitudinal analysis on visual function, injection time interval and complications, Int. Ophthalmol., 34 (2014) 1193-1201.

[11] K.M. Sampat, S.J. Garg, Complications of intravitreal injections, Curr Opin Ophthalmol, 21 (2010) 178-183.

[12] H. Nomoto, F. Shiraga, N. Kuno, E. Kimura, S. Fujii, K. Shinomiya, A.K. Nugent, K. Hirooka, T. Baba, Pharmacokinetics of bevacizumab after topical, subconjunctival, and intravitreal administration in rabbits, Invest Ophthalmol Vis Sci, 50 (2009) 4807-4813.

[13] E. Moisseiev, M. Waisbourd, E. Ben-Artsi, E. Levinger, A. Barak, T. Daniels, K. Csaky, A. Loewenstein, I.S. Barequet, Pharmacokinetics of bevacizumab after topical and intravitreal administration in human eyes, Graefes Arch Clin Exp Ophthalmol, 252 (2014) 331-337.

[14] L. Xu, T. Lu, L. Tuomi, N. Jumbe, J. Lu, S. Eppler, P. Kuebler, L.A. Damico-Beyer, A. Joshi, Pharmacokinetics of ranibizumab in patients with neovascular age-related macular degeneration: a population approach, Invest Ophthalmol Vis Sci, 54 (2013) 1616-1624.

3

[15] B.C. Ilochonwu, A. Urtti, W.E. Hennink, T. Vermonden, Intravitreal hydrogels for sustained release of therapeutic proteins, J. Controlled Release, 326 (2020) 419-441.

[16] C.H. Tsai, P.Y. Wang, I.C. Lin, H. Huang, G.S. Liu, C.L. Tseng, Ocular Drug Delivery: Role of Degradable Polymeric Nanocarriers for Ophthalmic Application, Int J Mol Sci, 19 (2018) 2830.

[17] F.S.Y. Wong, K.K. Tsang, A.C.Y. Lo, Delivery of therapeutics to posterior eye segment: cell-encapsulating systems, Neural Regener. Res., 12 (2017) 576-577.

[18] T. Yasukawa, Y. Ogura, H. Kimura, E. Sakurai, Y. Tabata, Drug delivery from ocular implants, Expert Opin. Drug Delivery, 3 (2006) 261-273.

[19] ClinicalTrials.gov, Extension Study for the Port Delivery System With Ranibizumab (Portal) (Portal), in, https://clinicaltrials.gov/ct2/show/NCT03683251 (accessed May 22, 2021), 2018.

[20] ClinicalTrials.gov, Study of the efficacy and safety of the ranibizumab port delivery system (RPDS) for sustained delivery of ranibizumab in participants with subfoveal neovascular age-related macular degeneration (AMD) (LADDER), (accessed May 05, 2021)2015. In, https://clinicaltrials.gov/ct2/show/NCT02510794

[21] ClinicalTrials.gov, A Phase III Study to Evaluate the Port Delivery System With Ranibizumab Compared With Monthly Ranibizumab Injections in Participants With Wet Age-Related Macular Degeneration (Archway), 2021.(accessed May 22, 2021) in https://clinicaltrials.gov/ct2/show/NCT03677934?term=archway&rank=1

[22] A.M. Khanani, A.A. Aziz, C.Y. Weng, W.V. Lin, J. Vannavong, J. Chhablani, C.J. Danzig, P.K. Kaiser, Port delivery system: a novel drug delivery platform to treat retinal diseases, Expert Opin Drug Deliv, 18 (2021) 1571-1576.

[23] A. Sharma, N. Parachuri, N. Kumar, B.D. Kuppermann, F. Bandello, The Port Delivery System with ranibizumab-journey of mitigating vitreous hemorrhage, Eye (Lond), 36 (2022) 488-489.

[24] S.J. Buwalda, T. Vermonden, W.E. Hennink, Hydrogels for Therapeutic Delivery: Current Developments and Future Directions, Biomacromolecules, 18 (2017) 316-330.

[25] S. Cascone, G. Lamberti, Hydrogel-based commercial products for biomedical applications: A review, Int J Pharm, 573 (2020) 118803.

[26] S. Kirchhof, A.M. Goepferich, F.P. Brandl, Hydrogels in ophthalmic applications, Eur J Pharm Biopharm, 95 (2015) 227-238.

[27] T. Vermonden, R. Censi, W.E. Hennink, Hydrogels for protein delivery, Chem Rev, 112 (2012) 2853-2888.

[28] M.I. Rial-Hermida, A. Rey-Rico, B. Blanco-Fernandez, N. Carballo-Pedrares, E.M. Byrne, J.F. Mano, Recent Progress on Polysaccharide-Based Hydrogels for Controlled Delivery of Therapeutic Biomolecules, ACS Biomater Sci Eng, 7 (2021) 4102-4127.

[29] C.M. Nimmo, S.C. Owen, M.S. Shoichet, Diels-Alder Click cross-linked hyaluronic acid hydrogels for tissue engineering, Biomacromolecules, 12 (2011) 824-830.

[30] L.J. Smith, S.M. Taimoory, R.Y. Tam, A.E.G. Baker, N. Binth Mohammad, J.F. Trant, M.S. Shoichet, Diels-Alder Click-Cross-Linked Hydrogels with Increased Reactivity Enable 3D Cell Encapsulation, Biomacromolecules, 19 (2018) 926-935.

[31] M. Gregoritza, V. Messmann, K. Abstiens, F.P. Brandl, A.M. Goepferich, Controlled Antibody Release from Degradable Thermoresponsive Hydrogels Cross-Linked by Diels-Alder Chemistry, Biomacromolecules, 18 (2017) 2410-2418.

[32] S. Kirchhof, M. Gregoritza, V. Messmann, N. Hammer, A.M. Goepferich, F.P. Brandl, Diels-Alder hydrogels with enhanced stability: First step toward controlled release of bevacizumab, Eur J Pharm Biopharm, 96 (2015) 217-225.

[33] S. Kirchhof, M. Abrami, V. Messmann, N. Hammer, A.M. Goepferich, M. Grassi, F.P. Brandl, Diels-Alder Hydrogels for Controlled Antibody Release: Correlation between Mesh Size and Release Rate, Mol Pharm, 12 (2015) 3358-3368.

[34] Y. Yang, Z. Zhu, R. Gao, J. Yuan, J. Zhang, H. Li, Z. Xie, Y. Wang, Controlled release of MSC-derived small extracellular vesicles by an injectable Diels-Alder crosslinked hyaluronic acid/PEG hydrogel for osteoarthritis improvement, Acta Biomater, 128 (2021) 163-174.

[35] J.S. Ng, Ocular Anatomy and Physiology (2nd ed.), Optometry and Vision Science, 86 (2009) 1208.

[36] C. Schramm, M.S. Spitzer, S. Henke-Fahle, G. Steinmetz, K. Januschowski, P. Heiduschka, J. Geis-Gerstorfer, T. Biedermann, K.U. Bartz-Schmidt, P. Szurman, The cross-linked biopolymer hyaluronic acid as an artificial vitreous substitute, Invest Ophthalmol Vis Sci, 53 (2012) 613-621.

[37] T.T. Kleinberg, R.T. Tzekov, L. Stein, N. Ravi, S. Kaushal, Vitreous substitutes: a comprehensive review, Surv. Ophthalmol., 56 (2011) 300-323.

[38] M. Thacker, C.L. Tseng, F.H. Lin, Substitutes and Colloidal System for Vitreous Replacement and Drug Delivery: Recent Progress and Future Prospective, Polymers (Basel), 13 (2020) 121.

[39] A.E.G. Baker, H. Cui, B.G. Ballios, S. Ing, P. Yan, J. Wolfer, T. Wright, M. Dang, N.Y. Gan, M.J. Cooke, A. Ortin-Martinez, V.A. Wallace, D. van der Kooy, R. Devenyi, M.S. Shoichet, Stable oxime-crosslinked hyaluronan-based hydrogel as a biomimetic vitreous substitute, Biomaterials, 271 (2021) 120750.

[40] H. Barth, S. Crafoord, S. Andreasson, F. Ghosh, A cross-linked hyaluronic acid hydrogel (Healaflow((R))) as a novel vitreous substitute, Graefes Arch Clin Exp Ophthalmol, 254 (2016) 697-703.

[41] T. Kojima, T. Nagata, H. Kudo, W.G.K. Muller-Lierheim, G.B. van Setten, M. Dogru, K. Tsubota, The Effects of High Molecular Weight Hyaluronic Acid Eye Drop Application in Environmental Dry Eye Stress Model Mice, Int J Mol Sci, 21 (2020) 3516.

[42] C.C. Lin, K.S. Anseth, PEG hydrogels for the controlled release of biomolecules in regenerative medicine, Pharm Res, 26 (2009) 631-643.

[43] A. D'Souza A, R. Shegokar, Polyethylene glycol (PEG): a versatile polymer for pharmaceutical applications, Expert Opin Drug Deliv, 13 (2016) 1257-1275.

3

[44] A.S. Hoffman, The early days of PEG and PEGylation (1970s-1990s), Acta Biomater, 40 (2016) 1-5.

[45] J. Yu, X. Xu, F. Yao, Z. Luo, L. Jin, B. Xie, S. Shi, H. Ma, X. Li, H. Chen, In situ covalently cross-linked PEG hydrogel for ocular drug delivery applications, Int J Pharm, 470 (2014) 151-157.

[46] F. Cadamuro, L. Russo, F. Nicotra, Biomedical Hydrogels Fabricated Using Diels–Alder Crosslinking, Eur. J. Org. Chem., 2021 (2020) 374-382.

[47] Y. Jiang, J. Chen, C. Deng, E.J. Suuronen, Z. Zhong, Click hydrogels, microgels and nanogels: emerging platforms for drug delivery and tissue engineering, Biomaterials, 35 (2014) 4969-4985.

[48] W.A. Wall A, Forte N, Bahou C, Bonin L, Nicholls K, one-pot-thiol-amine-bioconjugation-to-maleimides-simultaneous-stabilisation-and-dual-functionalisation., Chemical Science Source: RSC Gold excluding archive 2019, 11 (2020) 11455–11460.

[49] P. Atallah, L. Schirmer, M. Tsurkan, Y.D. Putra Limasale, R. Zimmermann, C. Werner, U. Freudenberg, In situ-forming, cell-instructive hydrogels based on glycosaminoglycans with varied sulfation patterns, Biomaterials, 181 (2018) 227-239.

[50] P.J. Flory, Principles of Polymer Chemistry, Ithaca, N.Y. : Cornell University Press, 1953., 1953.

[51] L. Pescosolido, L. Feruglio, R. Farra, S. Fiorentino, I. Colombo, T. Coviello, P. Matricardi, W.E. Hennink, T. Vermonden, M. Grassi, Mesh size distribution determination of interpenetrating polymer network hydrogels, Soft Matter, 8 (2012) 7708–7715.

[52] M. Rubinstein, R.H. Colby, Polymer physics, Oxford university press New York, 2003.

[53] C. Rousou, P. Hoogenboom, K.A. van Overdam, G. Storm, J. Dorrestijn, E. Mastrobattista, A technical protocol for an experimental ex vivo model using arterially perfused porcine eyes, Exp Eye Res, 181 (2019) 171-177.

[54] K.C. Scheiner, R.F. Maas-Bakker, T.T. Nguyen, A.M. Duarte, G. Hendriks, L. Sequeira, G.P. Duffy, R. Steendam, W.E. Hennink, R.J. Kok, Sustained Release of Vascular Endothelial Growth Factor from Poly(epsilon-caprolactone-PEG-epsilon-caprolactone)-b-Poly(l-lactide) Multiblock Copolymer Microspheres, ACS Omega, 4 (2019) 11481-11492.

[55] Y. Wang, D. Fei, M. Vanderlaan, A. Song, Biological activity of bevacizumab, a humanized anti-VEGF antibody in vitro, Angiogenesis, 7 (2004) 335-345.

[56] S. Ansar Ahmed, R.M. Gogal, J.E. Walsh, A new rapid and simple non-radioactive assay to monitor and determine the proliferation of lymphocytes: an alternative to [3H]thymidine incorporation assay, J. Immunol. Methods, 170 (1994) 211-224.

[57] J. Augustine, S. Pavlou, M. O'Hare, K. Harkin, A. Stitt, T. Curtis, H. Xu, M. Chen, Characterization of a Spontaneously Immortalized Murine Muller Glial Cell Line QMMuC-1, Invest Ophthalmol Vis Sci, 59 (2018) 1666-1674.

[58] M. D'Este, D. Eglin, M. Alini, A systematic analysis of DMTMM vs EDC/NHS for ligation of amines to hyaluronan in water, Carbohydr. Polym., 108 (2014) 239-246.

[59] A. Oluwasanmi, C. Hoskins, Potential use of the Diels-Alder reaction in biomedical and nanomedicine applications, Int J Pharm, 604 (2021) 120727.

[60] S. Kirchhof, F.P. Brandl, N. Hammer, A.M. Goepferich, Investigation of the Diels-Alder reaction as a cross-linking mechanism for degradable poly(ethylene glycol) based hydrogels, J Mater Chem B, 1 (2013) 4855-4864.

[61] S. Kirchhof, A. Strasser, H.-J. Wittmann, V. Messmann, N. Hammer, A.M. Goepferich, F.P. Brandl, New insights into the cross-linking and degradation mechanism of Diels–Alder hydrogels, J. Mater. Chem. B, 3 (2015) 449-457.

[62] D. Ehrhardt, K. Van Durme, J.F.G.A. Jansen, B. Van Mele, N. Van den Brande, Self-healing UV-curable polymer network with reversible Diels-Alder bonds for applications in ambient conditions, Polymer, 203 (2020) 122762.

[63] J. Mangialetto, A. Cuvellier, R. Verhelle, J. Brancart, H. Rahier, G. Van Assche, N. Van den Brande, B. Van Mele, Diffusion- and Mobility-Controlled Self-Healing Polymer Networks with Dynamic Covalent Bonding, Macromolecules, 52 (2019) 8440-8452.

[64] M.M. Diaz, G. Van Assche, F.H.J. Maurer, B. Van Mele, Thermophysical characterization of a reversible dynamic polymer network based on kinetics and equilibrium of an amorphous furan-maleimide Diels-Alder cycloaddition, Polymer, 120 (2017) 176-188.

[65] B. Strachota, A. Morand, J. Dybal, L. Matějka, Control of Gelation and Properties of Reversible Diels-Alder Networks: Design of a Self-Healing Network, Polymers, 11 (2019) 930.

[66] A.A. Adewunmi, S. Ismail, A.S. Sultan, Study on strength and gelation time of polyacrylamide/polyethyleneimine composite gels reinforced with coal fly ash for water shut-off treatment, J. Appl. Polym. Sci., 132 (2015) 41392.

[67] B. Sengupta, V.P. Sharma, G. Udayabhanu, Gelation studies of an organically cross-linked polyacrylamide water shut-off gel system at different temperatures and pH, J. Pet. Sci. Eng., 81 (2012) 145-150.

[68] B.J. Adzima, H.A. Aguirre, C.J. Kloxin, T.F. Scott, C.N. Bowman, Rheological and Chemical Analysis of Reverse Gelation in a Covalently Cross-Linked Diels–Alder Polymer Network, Macromolecules, 41 (2008) 9112-9117.

[69] Z. Stirn, A. Rucigaj, M. Krajnc, Characterization and kinetic study of Diels-Alder reaction: Detailed study on N-phenylmaleimide and furan based benzoxazine with potential self-healing application, eXPRESS Polym. Lett., 10 (2016) 537-547.

[70] S. Shafaie, V. Hutter, M.B. Brown, M.T. Cook, D.Y.S. Chau, Diffusion through the ex vivo vitreal body - Bovine, porcine, and ovine models are poor surrogates for the human vitreous, Int J Pharm, 550 (2018) 207-215.

[71] T.R.F. Britta M. Rauck, Carlos A. Medina Mendez, Daewon Park, Veeral Shah, Richard A. Bilonick and Yadong Wang, Biocompatible Reverse Thermal Gel Sustains the Release of Intravitreal Bevacizumab In Vivo, The Association for Research in Vision and Ophthalmology, 55 (2014) 469–476.

[72] Y. Yu, L.C. Lau, A.C. Lo, Y. Chau, Injectable Chemically Crosslinked Hydrogel for the Controlled Release of Bevacizumab in Vitreous: A 6-Month In Vivo Study, Translational Vision Science & Technology, 4 (2015) 5.

3

[73] J.J.K. Derwent, W.F. Mieler, Thermoresponsive hydrogels as a new ocular drug delivery platform to the posterior segment of the eye, Trans. Am. Ophthalmol. Soc. , 106 (2008) 206-214.

[74] G.W. Scherer, Hydraulic radius and mesh size of gels, J. Sol-Gel Sci. Technol, 1 (1994) 285-291.

[75] N.R. Richbourg, A. Ravikumar, N.A. Peppas, Solute Transport Dependence on 3D Geometry of Hydrogel Networks, Macromol Chem Phys, 222 (2021) 1022-1352.

[76] J.G. Williams, C. Gamonpilas, Using the simple compression test to determine Young's modulus, Poisson's ratio and the Coulomb friction coefficient, Int. J. Solids Struct., 45 (2008) 4448-4459.

[77] J.B. Choi, R.S. Lakes, Analysis of elastic modulus of conventional foams and of re-entrant foam materials with a negative Poisson's ratio, Int. J. Mech. Sci., 37 (1995) 51-59.

[78] P.J. Flory, J.R. Jr., Statistical Mechanics of Cross-Linked Polymer Networks I. Rubberlike Elasticity, J. Chem. Phys., 11 (1943) 512-520.

[79] M.M. Le Goff, P.N. Bishop, Adult vitreous structure and postnatal changes, Eye (Lond), 22 (2008) 1214-1222.

[80] R. Ehrlich, D. Weinberger, E. Priel, R. Axer-Siegel, Outcome of bevacizumab (Avastin) injection in patients with age-related macular degeneration and low visual acuity, Retina, 28 (2008) 1302-1307.

[81] M. Modarres, M. Naseripour, K.G. Falavarjani, A. Nikeghbali, M. Hashemi, M.M. Parvaresh, Intravitreal injection of 2.5 mg versus 1.25 mg bevacizumab (Avastin) for treatment of CNV associated with AMD, Retina, 29 (2009) 319-324.

[82] W.E. Hennink, H. Talsma, J.C.H. Borchert, S.D. Smedt, J. Demeester, Controlled release of proteins from dextran hydrogels, J. Controlled Release, 39 (1996) 47-55.

[83] S.K. Li, M.R. Liddell, H. Wen, Effective electrophoretic mobilities and charges of anti-VEGF proteins determined by capillary zone electrophoresis, J Pharm Biomed Anal, 55 (2011) 603-607.

[84] P. Jakubiak, R. Alvarez-Sanchez, M. Fueth, O. Broders, H. Kettenberger, K. Stubenrauch, A. Caruso, Ocular Pharmacokinetics of Intravitreally Injected Protein Therapeutics: Comparison among Standard-of-Care Formats, Mol Pharm, 18 (2021) 2208-2217.

[85] E.M. Del Amo, A.K. Rimpela, E. Heikkinen, O.K. Kari, E. Ramsay, T. Lajunen, M. Schmitt, L. Pelkonen, M. Bhattacharya, D. Richardson, A. Subrizi, T. Turunen, M. Reinisalo, J. Itkonen, E. Toropainen, M. Casteleijn, H. Kidron, M. Antopolsky, K.S. Vellonen, M. Ruponen, A. Urtti, Pharmacokinetic aspects of retinal drug delivery, Prog Retin Eye Res, 57 (2017) 134-185.

[86] S. Kaja, J.D. Hilgenberg, E. Everett, S.E. Olitsky, J. Gossage, P. Koulen, Effects of dilution and prolonged storage with preservative in a polyethylene container on Bevacizumab (Avastin) for topical delivery as a nasal spray in anti-hereditary hemorrhagic telangiectasia and related therapies, Hum. Antibodies, 20 (2011) 95-101.

[87] N. Hammer, F.P. Brandl, S. Kirchhof, V. Messmann, A.M. Goepferich, Protein compatibility of selected cross-linking reactions for hydrogels, Macromol Biosci, 15 (2015) 405-413.

[88] W.C. Sung, C.W. Chang, S.Y. Huang, T.Y. Wei, Y.L. Huang, Y.H. Lin, H.M. Chen, S.F. Chen, Evaluation of disulfide scrambling during the enzymatic digestion of bevacizumab at various pH values using mass spectrometry, Biochim Biophys Acta, 1864 (2016) 1188-1194.

[89] Y. Yu, Y. Chau, Formulation of in situ chemically cross-linked hydrogel depots for protein release: from the blob model perspective, Biomacromolecules, 16 (2015) 56-65.

[90] E. Vecino, F.D. Rodriguez, N. Ruzafa, X. Pereiro, S.C. Sharma, Glia-neuron interactions in the mammalian retina, Prog. Retinal Eye Res., 51 (2016) 1-40.

[91] J. Lesley, V.C. Hascall, M. Tammi, R. Hyman, Hyaluronan Binding by Cell Surface CD44*, J. Biol. Chem., 275 (2000) 26967-26975.

[92] T. Shinoe, H. Kuribayashi, H. Saya, M. Seiki, H. Aburatani, S. Watanabe, Identification of CD44 as a cell surface marker for Müller glia precursor cells, J. Neurochem., 115 (2010) 1633-1642.

[93] S. Friedrich, Y.-L. Cheng, B. Saville, Drug distribution in the vitreous humor of the human eye: the effects of intravitreal injection position and volume, Curr. Eye Res., 16 (1997) 663-669.

3

7 SUPPORTING INFORMATION

^{1}H-NMR spectra of HAFU DS 30, 50, 83% ; FTIR spectra of HA, HAFU DS 30% and HAFU 83%; FTIR spectra of: 4APM, HAFU DS 83% and HAFU-4APM hydrogel; SEC chromatograms and UV-vis spectra of HAFU-750dye polymer; Rheological and mechanical characterization of 4APM-HAFU hydrogel; SDS-page of bevacizumab and SEC chromatograms of 10-20 wt% 4APM-HAFU hydrogels after 21-63 days of release; ^{1}H-NMR spectra hydrogel degradation product; Storage modulus (Pa) at gelation time of 4APM-HAFU hydrogels; Storage (G') , loss moduli (G") and Tan (δ) in time; Image of transparent HAFU-4APM hydrogels.

In SI-Figure 1, the presence of furan protons on the HA-backbone are shown by the aromatic peak at 6.4 (CHCH, 2 protons) and 7.5 (OCH, 1 proton) ppm. The degree of substitution (DS %) was determined by ^{1}H-NMR using the following equation:

$$\text{DS (\%)}= \frac{I_{7.5}/1}{I_{2.0}/3} \times 100$$

Where $I_{7.5}$ is the integral at 7.5ppm and $I_{2.0}$ integral at 2ppm of N-acetyl glucosamine (NHCOCH$_3$) in native HA.
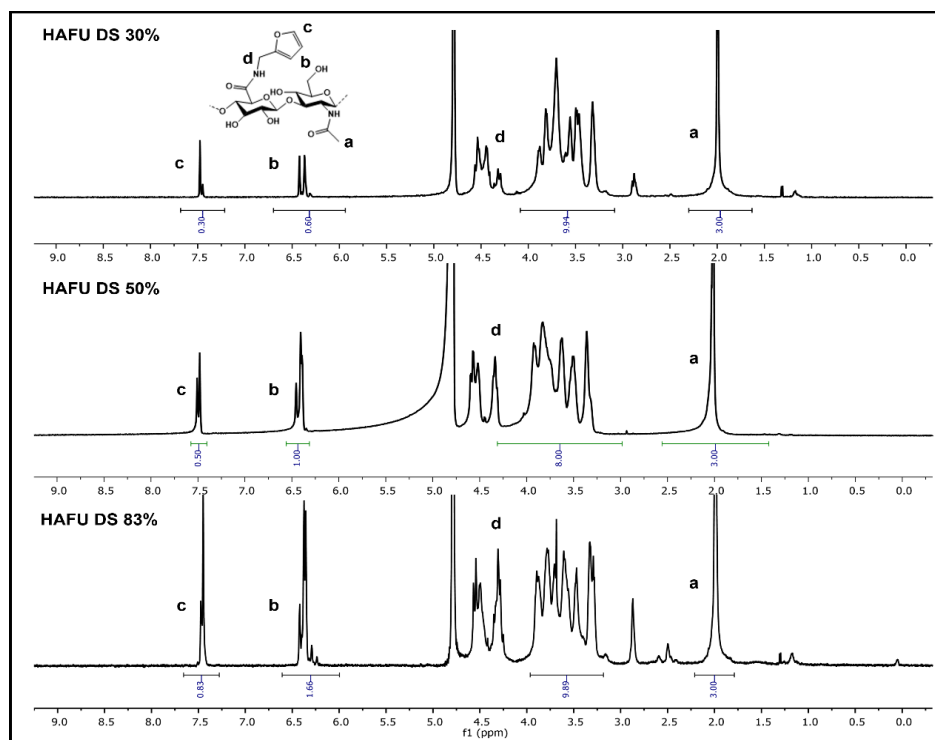
SI-Figure 1 ^{1}*H*-NMR spectra of HAFU DS ~ 30, 50, 83% .D$_2$O was used as solvent.
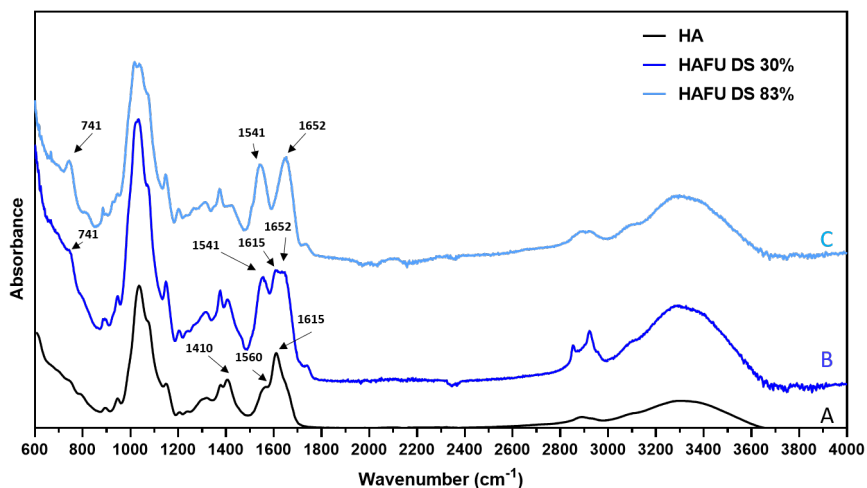
SI-Figure 2 FTIR spectra of A) HA, B) HA-FU DS 30% and C) HAFU 83%. Unmodified HA has spectral bands at 1615 and 1410 cm^{-1}, assigned to the asymmetric and symmetric stretching vibration of the carboxylate anion, respectively. HA spectra are also characterized by an amide II bond at 1560 cm^{-1}. The grafting of furan groups to HA (HAFU) after the reaction of HA with furfurylamine is indicated by shift and increase of the peaks at 741, 1541 and 1652 cm^{-1} from the HAFU DS 30% and even more for HAFU DS 83% derivative corresponding to the furan moieties. The functionalization of HA with furan groups is also demonstrated by the decrease in the absorbance of carboxylate anion (1410 cm^{-1}) peak for the HAFU DS 30% and even more for DS 83%.
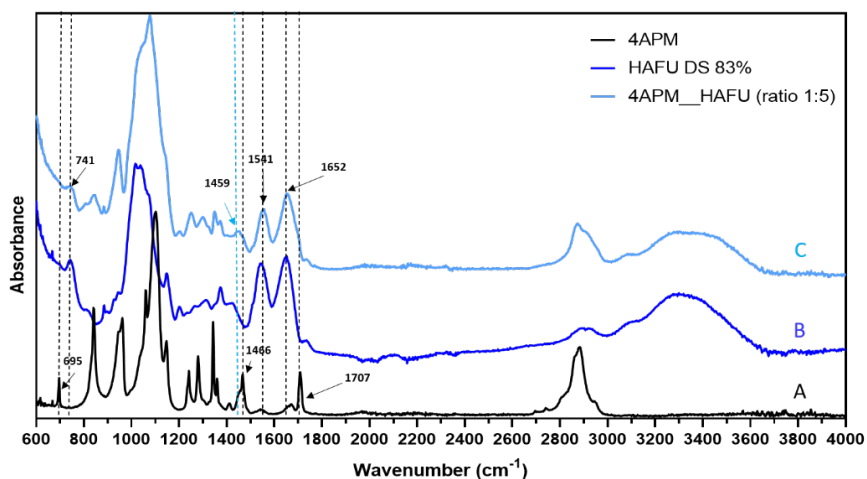
SI-Figure 3 FTIR spectra of: A) 4APM with arrows showing the C=C absorbance at 1466 cm^{-1}, -C=O stretch vibration at 1707 cm^{-1} and the =C-H- bending vibration at 695 cm^{-1} from maleimide. B) HAFU DS 83% with arrows indicating bonds of amide I stretching, amide II bending at 1652, 1541 cm^{-1} respectively, and =C-H-bend of furan moiety 741 cm^{-1}. C) The cross-linked HAFU-4APM hydrogel (molar ratio maleimide: furan 1:5) showing the absence of the 695, 1466 and 1707 cm^{-1} maleimide peaks, decreased 741, 1541 cm^{-1} furan

peak and the appearance of a new peak at 1459 cm^{-1} corresponding to the C=C bond in the Diels-Alder adduct.
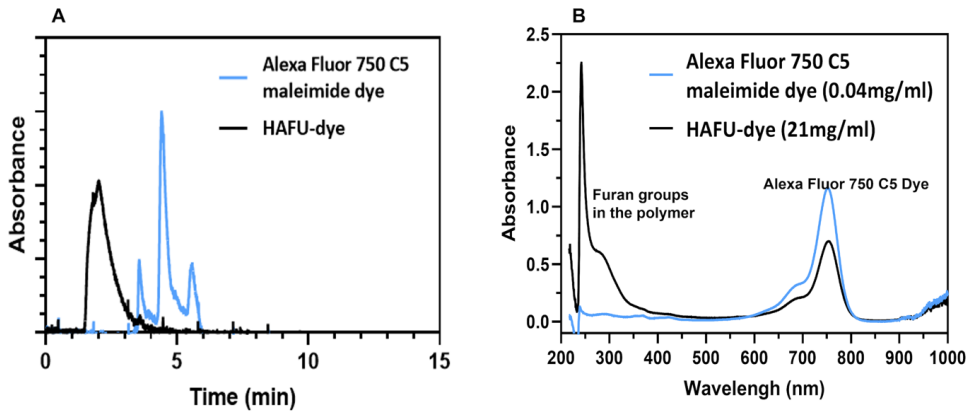
SI-Figure 4 A) SEC chromatograms of HAFU-750dye polymer in black and Alexa fluor 750 C5 maleimide dye in blue. B) UV-vis spectra of HAFU-750dye polymer in black and Alexa fluor 750 C5 maleimide dye in blue.
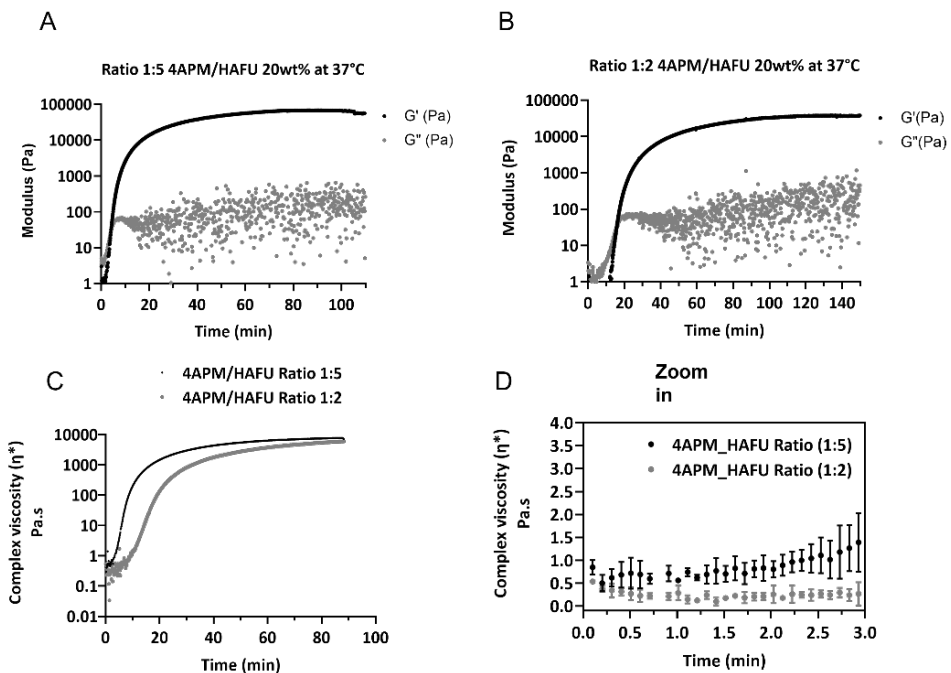
SI-Figure 5 Rheological and mechanical characterization of 4APM-HAFU hydrogel formulations. Evaluation of storage (G') and loss modulus (G") as a function of time in 20 wt% 4APM-HAFU hydrogel, A) molar ratio of maleimide/furan 1:2 and B) molar ratio 1:5. C) Complex viscosity (η*) of 20 wt% 4APM-HAFU hydrogel at 37 °C. D) Complex viscosity (η*) of 20wt% 4APM-HAFU hydrogel at 37°C time (0-3 minutes).
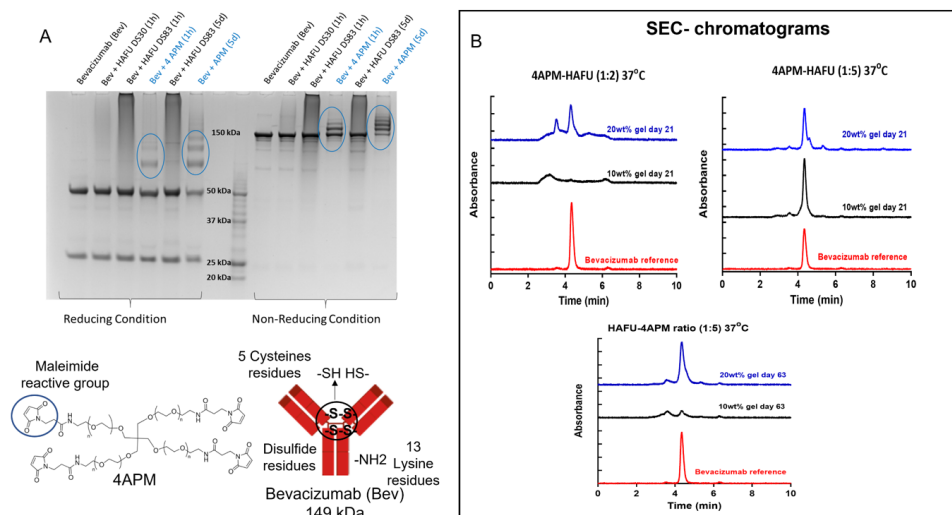
SI-Figure 6 A) SDS-page of bevacizumab after incubation with hydrogel precursors at 37 °C for 1 hour and 5 days. The maleimide present in the 4APM crosslinker conjugated to the proteins, and therefore, its molecular weight was increased. B) SEC chromatograms of 10-20 wt% 4APM-HAFU hydrogels at 1:2 and 1:5 ratio after 21-63 days of release.
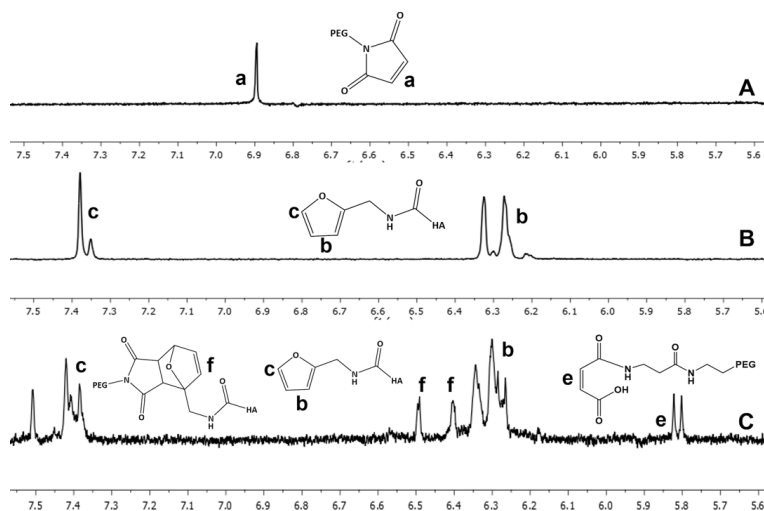
SI-Figure 7 ^{1}H-NMR spectra in D$_2$0 (between 5.6-7.6 ppm) of A) 4APM crosslinker, indicating the presence of maleimide protons (a). B) HAFU polymer, indicating the presence of furan protons (b and c). C) Freeze-dried degradation product obtained during swelling and degradation studies upon the complete dissolution of hydrogel network in aqueous medium. Protons of furan (c and b) and the Diels-Alder adduct (f) are found. No intact maleimide protons are found (a), while the protons of the hydrolyzed maleimide product were identified (e).
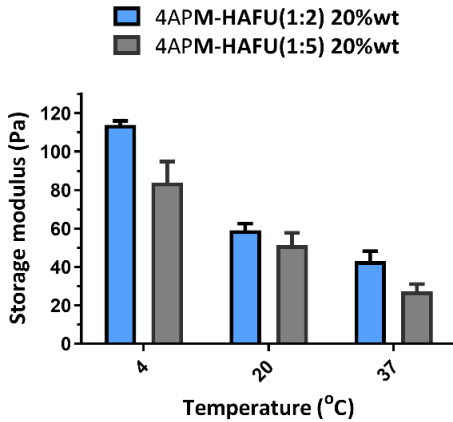
SI-Figure 8 Storage modulus (Pa) at the gelation point (here defined as the time at which G' equals G") of 20wt% 4APM-HAFU hydrogel formulations at molar ratio 1:2 and 1:5 maleimide: furan as a function temperature (37, 20, and 4 °C).
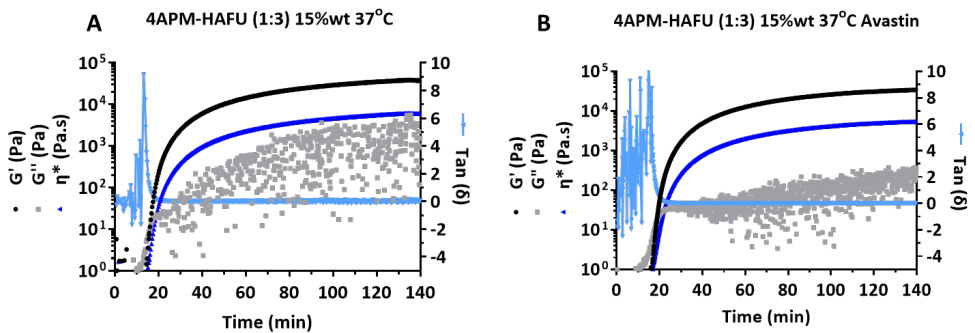
SI-Figure 9 Storage (G'), loss modulus (G") and tan(δ) as a function of time of 15wt% 4APM-HAFU (molar ratio 1:3) hydrogel formulation with and without bevacizumab.

SI-Figure 10 Image of transparent 20 wt% HAFU-4APM hydrogels (diameter 8 mm, 4 mm height) formed at 37 °C with and without loading of bevacizumab.

3

Chapter 4

In Situ Diels-Alder Crosslinked Hydrogel for Controlled Release of Bevacizumab in Rabbit Vitreous: Insights from In Vivo Pharmacokinetics and Safety Evaluation

Blessing C. Ilochonwu[1], Ada Annala[1,2], Amir Sadeghi [2], Elisa Toropainen[2], Wim E. Hennink[1], Jussi Paterno[2], Marika Ruponen[2], Arto Urtti [2,3], Tina Vermonden[1]

[1]Department of Pharmaceutics, Utrecht Institute for Pharmaceutical Sciences, Faculty of Science, Utrecht University, PO box 80082, 3508 TB Utrecht, the Netherlands. [2]School of Pharmacy, University of Eastern Finland, Kuopio, Finland. [3]Centre for Drug Research, Division of Pharmaceutical Biosciences, University of Helsinki, Helsinki, Finland.

ABSTRACT

Purpose:

The pharmaceutical protein bevacizumab is commonly used off-label for treating ocular diseases via intravitreal injections. However, frequent injections can lead to ocular complications and poor patient compliance. To address these issues, pharmaceutical scientists have developed preclinical depot systems for sustained delivery of this biotherapeutic. This study examines the in vivo pharmacokinetic (PK) profile and ocular safety of an injectable, in situ forming Diels-Alder crosslinked hydrogel composed of hyaluronic acid and PEG, loaded with bevacizumab.

Methods:

Intravitreal injections of hydrogel precursors, with and without fluorescently labeled bevacizumab, were administered into the eyes of albino rabbits. Formulations with polymer concentrations of 10 wt% (fast release) and 20 wt% (slow release) were injected. Ex vivo albino rabbit eyes were used to examine the effect of vitreous dilution on hydrogel mechanical properties and its mesh size. Albino rabbit eyes were selected as the in vivo animal model, with five rabbits receiving the 10 wt% formulation in their right eye and the 20 wt% formulation in their left eye. The bevacizumab concentrations were measured in aqueous humor and vitreous samples over time after injection using fluorophotometer analysis, and subsequently the in vivo release rate constants were calculated using a compartmental model. Ocular safety was assessed through analysis of intraocular pressure (IOP), ophthalmic examination, fundus imaging, and microscopic imaging of the anterior eye for empty and bevacizumab loaded hydrogel formulations.

Results:

Consistent with the findings of the ex vivo rabbit eye study, we observed a confined stable hydrogel within the vitreous body in vivo. Furthermore, the mesh sizes of the hydrogels formed ex vivo and based on rheological analysis ranged from 4.0 to 8.6 nm, making them suitable for the sustained release of bevacizumab. In vivo release results showed that the burst release (taken as the amount of protein released during the first 24 hours) of bevacizumab from the 10 and 20 wt% formulation was 53 and 33 % of the loaded drug, respectively. Following this initial burst, the gels gradually released the protein with first order release rate constants of 0.26 ± 0.05 day^{-1} for the 10 wt% and 0.13 ± 0.02 day^{-1} for the 20 wt% formulations, respectively. One-month post-injection, the vitreous concentrations of bevacizumab were 1.7-3.2 times higher for the hydrogel group compared to the rabbits that received bolus injections of the same dose of the protein. Furthermore, the 20 wt% hydrogel formulation resulted in bevacizumab concentrations 20 times above its therapeutic concentration (0.05 µg/ml) for at least 55 days post-injection. Safety evaluation revealed that hydrogels with fluorescently labelled bevacizumab exhibited an inflammatory response in the posterior segment of the eye at 14 days post- injection in 4 out of 10 eyes. However, the empty hydrogels demonstrated no toxicity in the posterior segment, but transient irritation of the anterior segment was observed in the first-week post-injection. The

exact causes of these side-effects are however unclear at present and need further in-depth studies.

Conclusions:

The studied hydrogel prolongs the residence of bevacizumab in the vitreous significantly compared to bolus injection, but the safety concerns require further investigation.

Keywords: Intravitreal; Ocular diseases; AMD; DR

1   INTRODUCTION

Neovascular eye diseases, such as wet age-related macular degeneration (AMD) and proliferative diabetic retinopathy, are recognized as the leading causes of blindness and visual impairment in older patients worldwide.[1] While the mechanisms of ocular neovascularization are not fully understood, studies have shown that up-regulation of vascular endothelial growth factors (VEGFs) plays a critical role in stimulating angiogenesis and vascular permeability in the retina.[2] As a result, anti-VEGF liquid formulations injected into the vitreous have become the standard of care for treatment of wet AMD.[3] Pegaptanib (Macugen®), ranibizumab (Lucentis®), brolucizumab (Beovu®), faricimab (Vabysmo™) and aflibercept (Eylea®) are FDA-approved anti-VEGF therapeutics for the treatment of wet AMD.[4-10] Additionally, bevacizumab (Avastin®), a recombinant humanized monoclonal IgG1 antibody that binds and inhibits VEGF, is widely used off-label for this indication.[11, 12] Bevacizumab is an IgG type monoclonal antibody composed of two identical light chains (214 amino acids) and two heavy chains (453 residues) containing N-linked oligosaccharides with a molecular weight of 149 kDa.[13, 14] A single intravitreal dose of bevacizumab for humans is typically 1.25 mg, which is equivalent to 0.5 mg of ranibizumab having a molecular weight of 49 kDa in clinics.[5, 15, 16] Different dosing schedules, such as monthly injections or as-needed, have been reported in clinical studies.[15] Despite the clinical success of current anti-VEGF therapy, one limitation is the need for repeated monthly or bimonthly intravitreal injections to maintain therapeutic effects, which is due to the relatively fast vitreous elimination half-lives of the used biotherapeutics ranging from a few days up to 12 days in humans.[17, 18] Even though adverse events associated with frequent intravitreal injections are relatively rare, the substantial number of injections (exceeding 20 million per year worldwide[19]) results in a significant number of such events (e.g. endophthalmitis, retinal detachment, hemorrhage).[20-23] Obviously, the frequent injections are burden to the patients and costly to the health care systems. Furthermore, the intravitreal pharmacokinetic profiles of the presently used anti-VEGF proteins are suboptimal, with very high initial concentrations, fast ocular clearance and fluctuating drug concentrations (≈ two orders of magnitude) within the vitreous body and retina.[24] To address these limitations, intraocular drug depots have been developed to provide extended drug delivery, which thus reduce the frequency of intravitreal injections. Genentech's Susvimo, previously called Port Delivery System, is the only FDA-approved (October 2021) ranibizumab implant used to treat neovascular age-related macular degeneration, but this refillable system was voluntarily recalled due to problems of reproducibility in the clinical

use.[25-27] Also, in the phase 2 trials, a notable incidence of vitreous hemorrhage was observed with this system. [28]

Hydrogels are promising ophthalmic biomaterials for vitreous substitution and recent progress in hydrogel design offers excellent opportunities to sustain the release of ophthalmic drugs, potentially improving therapeutic efficacy in ocular therapy.[29, 30] Previously, in vitro/in vivo evaluations of in situ forming hydrogel depots have shown great potential in the controlled and sustained release of proteins.[31-33] Particularly in-situ forming hydrogels can be easily administered by injection using small gauge needles into the vitreous cavity. After intravitreal injection, the polymer solution undergoes a sol-to-gel phase transition, entrapping dissolved therapeutics in their hydrated network. In recent years, different types of intraocular hydrogels based on varying polymer matrices and crosslinking strategies have been employed to achieve desired drug release profiles. [30, 34-37]

The most frequently used polymers for the design of injectable hydrogels include hyaluronic acid, alginate, semi-synthetic chitosan, dextran, poly(ethylene glycol) (PEG), and thermo-responsive synthetic polymers such as poly(N-isopropylacrylamide) (PNIPAM) and block copolymers of poly(lactic-co-glycolic acid) (PLGA)-PEG, etc.[38] Although many polymer-based hydrogel depot systems have demonstrated the ability for the controlled release of therapeutic proteins in vitro, as previously reviewed by Ilochonwu et al.[29], there are only limited studies on their PK profile and safety in in vivo models. [31, 39-41] In the past years, PEG based hydrogels crosslinked exploiting Diels-Alder (DA) or Michael-type reactions have been investigated as matrices for sustained protein release and potential ocular applications were demonstrated in in vitro studies.[32, 42]

Hyaluronic acid (HA) is a natural polymer and an essential component of the extracellular matrix of connective tissues such as vitreous, subcutaneous tissue, umbilical cord, synovial tissue, and synovial fluid [43]. Preclinical and clinical studies have shown that injections of HA solutions/hydrogels with high molecular weight and high viscosity within the vitreous and anterior chamber of monkeys, rabbits and human eyes were well tolerated and demonstrates that this polymer can be used in various intraocular therapeutic modalities to treat vitreoretinal diseases.[44-46] Injectable in situ forming hydrogels based on Diels-Alder crosslinking chemistry between furan and maleimide groups have been previously shown to yield matrices suitable for the sustained release of bevacizumab in ocular therapy.[42, 47, 48] A major advantage of Diels-Alder chemistry is that it occurs under physiological conditions, avoiding potentially toxic catalysts and initiators often used in other crosslinking strategies for the preparation of hydrogel delivery systems.[48, 49] In a previous study, we introduced an HA-PEG-based hydrogel using Diels-Alder chemistry and this research focused on in situ forming hydrogels designed for easy intravitreal injection.[48] We systematically studied the sustained release profile of bevacizumab in relation to gel composition. The hydrogel were formed within minutes and were biodegradable under in vitro physiological conditions.[48] Importantly, the hydrogels exhibited extended release of the bioactive from 30 to 400 days, showcasing potential for ocular disease treatment.[48] The study presented here aimed to investigate the in vivo PK profile and ocular safety of hyaluronic

acid-PEG-based Diels–Alder in situ forming hydrogels for sustained intraocular delivery of bevacizumab to determine the suitability of this formulation for ocular therapies.

2   MATERIALS AND METHODS

Materials

Lyophilized sodium hyaluronate (HA; 24 kDa) was obtained from Lifecore Biomedical (Chaska, MN, USA). The 4-arm PEG maleimide crosslinker (4APM; 10 kDa) was purchased from JenKem Technology USA Inc. (Beijing, China). Phosphate buffered saline 10x (PBS) pH 7.4 (1.37 M NaCl, 0.027 M KCl and 0.119 M phosphates) was purchased from B. Braun (Melsungen, Germany). Zirabev Pfizer, (100 mg of bevacizumab dissolved in 4 ml buffer excipient: sucrose, succinic acid, disodium edetate, polysorbate 80, sodium hydroxide for pH adjustment, water for injections) was a kind gift from the UMC Utrecht. The protein solution was stored at 4 °C util use. BODIPY (BDP) fluorescein (FL) N-hydroxysuccinimide (NHS) ester was obtained from Lumiprobe GmbH (Europe, Maryland, USA).

Methods

2.1   Hydrogel preparation

Furan-modified HA polymers (HAFU) (degree of substitution (DS) 50 and 83 %) were prepared by functionalizing hyaluronic acid with furfuryl-amine according to a previously published protocol by Ilochonwu et al.[48] The 4-arm PEG maleimide (4APM) was used as a crosslinker for reaction with the furan moieties present in HAFU to obtain hydrogels.

2.1.1   Empty hydrogel preparation for in vitro and ex vivo dynamic mechanical analysis (DMA)

In order to gain a better understanding of the influence of vitreous dilution during in vivo evaluation, it is important to assess the mechanical properties and mesh size of hydrogels formed both ex vivo and in vitro. To this end, empty 4APM-HAFU hydrogels were prepared according to a previously published protocol[48] with slight modifications. Specifically, HAFU (DS 50 or 83) and 4APM-crosslinker were dissolved separately in PBS and mixed to obtain a total polymer concentration of 10-20 wt% unless indicated otherwise. Different ratios between the 4APM crosslinker and HAFU polymers corresponding to 1:2, 1:3 and 1:5 molar ratios of maleimide: furan, respectively, were used to prepare different hydrogel formulations. Subsequently, 100 µl of the formulation was either allowed to crosslink in a plastic mold (4 mm and 5 mm in height and diameter, respectively) or injected intravitreally (needle size 29G) into an ex vivo New Zealand rabbit eye (only 20 wt % solution were injected) and kept at 37°C for 1 hour. Before the intravitreal injection, the eyes in a excess volume of PBS were preincubated at 37 °C for 30 minutes using a water bath. The in situ formed hydrogels were isolated from the vitreous body and subsequently cut for further mechanical tests. All hydrogels (ex vivo n=3 and in vitro n=3) were prepared or cut in a cylindrical shape with dimensions of approximately 4 mm and 5 mm in height and diameter, respectively. DMA 2980 Dynamic Mechanical Analyzer (TA Instruments, New Castle, DE) was used to determine Young's modulus of the hydrogels according to previously published protocol.[48]

2.2   Rheological studies (10-20 wt % gel, furan/maleimide molar ratio 1:3)

The rheological properties of the hydrogel were analyzed as previously reported [48] using a Discovery HR-2 Rheometer (TA Instruments Inc., Etten-Leur, NL) with a Peltier plate for temperature control. The samples were measured using a 20 mm diameter aluminum plate-plate geometry. For each analysis, samples of 180 μl of empty hydrogel formulations were prepared as described in section 2.1.1 and placed on the rheometer Peltier plate. The distance between the plates was controlled by the equipment during the measurement to enable a constant normal force. The time needed to reach the crossover point between G' and G'' is defined as gelation time. After reaching the plateau value for G' and G'' indicating complete crosslinking, an angular frequency sweep ranging between 0.1-100 rad/s was performed. Hydrogel mesh size (ξ in m) was calculated from the G' using the following equation[50] :

$$\xi = (G'^{*}N_{av}/\ RT)^{-1/3}$$

where N_{av} is Avogadro's constant, R is the molar gas constant (8.3 J/K.mol), and T is the absolute temperature in K.

2.3   Dye conjugation to bevacizumab

BDP FL NHS-ester (389.2 Da) was conjugated to bevacizumab (149 kDa) following the manufacturer's protocol for labelling proteins (LI-COR, Inc. Biosciences). In brief, BDP FL NHS ester was dissolved in dimethyl sulfoxide (DMSO) to obtain a stock solution of 10 mg/ml and stored at −20°C until use. A sample of the Zirabev protein solution (500 μl, 12.5 mg bevacizumab) was diluted by adding 100 μl PBS (pH 7.4) and adjusted to pH 8.5 by adding 300 μl of 1 M potassium phosphate (pH 9). Subsequently, 10 μl of the dye stock solution was diluted with 90 μl DMSO and this obtained solution was added to the protein solution resulting in a 3:1 dye: bevacizumab molar ratio. The final mixture (1000 μl) was allowed to react at room temperature for 3 h. The unreacted dye was subsequently removed with pyrogen-free water by using Zeba™ spin desalting columns equilibrated with pyrogen-free water. Characterization of labelled bevacizumab was done by size-exclusion chromatography (SEC) using a Waters ARC UPLC Acquity system (Waters Corporation, Milford, USA) equipped with a fluorescence detector. A Yarra 3 μm SEC-3000 (LC column 150 x 4.6 mm) equipped with security guard cartridge was attached to the system and used for the measurements at room temperature. Two detection channels were used to confirm dye conjugation to the protein and discriminate between free BDP dye and labeled bevacizumab. Channel 1 for detecting the protein (excitation at 280 nm and emission at 340 nm), and channel 2 for detecting the BDP signal (excitation at 409 nm and emission at 509 nm). The filtered (0.2 μm) mobile phase consisted of an aqueous solution of sodium phosphate 100 mM and sodium sulfate 300 mM of pH 6.7 with 15% (v/v) DMSO, which was operated at a flow rate of 0.3 mL/min. Samples of 7.5 μl were injected, and the retention time of bevacizumab was 5.2 min under these conditions. The bevacizumab calibration curve's linear range was from 0.16 mg/mL (detection limit) to 2.5 mg/ml and was used to determine the protein yield after labeling. To calculate the dye/bevacizumab molar ratio, the UV spectrum of a bevacizumab BDP dye aqueous solution (diluted to 0.5 mg/ml with 10% DMSO/water) was recorded (Shimadzu 2450, Japan), and

the maximum absorbance values at 283 nm (A_{283} = 0.257) and 505 nm (A_{505} = 0.189) were used to calculate the degree of conjugation according to the following equation 1:

$$\frac{\text{BDP dye}}{\text{Bevacizumab}} = \left[\frac{A_{505}}{\varepsilon_{\text{BDP dye}}}\right] / \left[\frac{A_{283}}{\varepsilon_{\text{Bevacizumab}}}\right]$$

Eq.1

BDP Dye/bevacizumab is the molar ratio of BDP Dye to bevacizumab and the molar extinction coefficient of BDP Dye ($\varepsilon_{\text{BDP Dye}}$) is 92000 L·mol^{-1}·cm^{-1} (according to the manufacturer) and the molar extinction coefficient of bevacizumab ($\varepsilon_{\text{bevacizumab}}$) is 245850 L·mol^{-1}·cm^{-1}.[51]

2.4 Endotoxin tests

The different formulation components (polymers, protein-BDP dye and BDP-dye) were dissolved or dispersed (BDP FL NHS-ester dye) in sterile endotoxin-free water and tested in duplicate for endotoxin content by utilizing Pierce™ chromogenes Endotoxin Quant Kit (Thermo Scientific™) according to the manufacturer's instructions.

2.5 In vivo experiment in rabbits

2.5.1 Type of animals, housing and animal study permit

Nine New Zealand White female rabbits (four to five months old) were used in the studies. The animals were housed under standard white cyclic lighting with free access to food and water. The experiments were designed and conducted in accordance with the guidelines of the ARVO Statement for the Use of Animals in Ophthalmic and Vision Research. The procedures were approved by the Finnish National Animal Experiment Broad (ELLA, Regional State Administrative Agency for Southern Finland), performed under project license (ESAVI-2020-027769) and in compliance with 3R principles (replacement, reduction and refinement) monitored by animal-welfare body of University of Eastern Finland Lab Animal Center (UEF LAC).

2.5.2 Formulation preparation and intravitreal injection for in vivo PK experiments

HAFU (DS 50%) and 4AMP crosslinker were dissolved separately in the protein solution of bevacizumab-BDP dye at two different polymer concentrations (10 or 20 wt%) and molar ratio maleimide/furan 1:3. Specifically, for the preparation of six 10 wt% hydrogels, 24.0 mg of HAFU was dissolved in 0.336 ml of the bevacizumab-BDP dye solution (12 mg/ml), while 23.9 mg of 4APM was dissolved in 0.096 ml of the same solution. For the preparation of six 20 wt% hydrogels, 53.6 mg of HAFU was dissolved in 0.322 ml of the bevacizumab-BDP dye solution, while 52.5 mg of 4APM was dissolved in 0.105 ml of the same solution. The 4APM crosslinker protein solution was then mixed with the HAFU protein solution in the following ratios for each injection. For one 10 wt% hydrogel preparation, 15.5 µl of 4APM-bevacizumab-BDP dye solution was added to 54.5 µl of HAFU DS 50%-bevacizumab-BDP dye solution. For the preparation of six 10 wt% hydrogels, 17.5 µl of 4APM-bevacizumab-BDP dye solution was added to 52.5 µl of HAFU-bevacizumab-BDP dye solution. The mixtures were then immediately pipetted into a 1 ml syringe (BD Micro Fine Insulin syringe, 0.5 ml, 30G, Becton Dickinson, Franklin Lakes, NJ, USA). A volume of 70 µl was

prepared to account for the loss of materials during handling and the dead space in the syringe. Next, 50 µl of the hydrogel precursor solution was immediately injected 4 mm from the limbus trans-sclerally into the vitreous of the rabbits and allowed to crosslink in situ. Topical oxybuprocaine (4 mg/ml) was instilled as a local anesthetic a few minutes before the intravitreal injections. The intravitreal injection volume of the formulation was 50 µl per eye, resulting in a bevacizumab-BDP dose of 600 µg. Six rabbits received the 10 wt% formulation in the right eye, and the left six eyes received the 20 wt% formulation. One animal had to be excluded from the study due to an infection (not necessarily related to the formulation) and the research proceeded with the remaining five rabbits.

2.5.3   Intravitreal injection for in vivo safety evaluation of empty hydrogel formulation

The formulation was prepared according to section 2.5.2 with slight modification. Briefly, HAFU (Ds 83 %) and 4AMP crosslinker were separately dissolved in PBS and the solutions were mixed to obtain 20 wt% solution with a maleimide/furan molar ratio of 1:5. Subsequently, 70 µl of this solution was pipetted into a 1 ml syringe (insulin needle size 30G) and injected 4 mm from the limbus trans-sclerally into the vitreous and allowed the two hydrogel building blocks to crosslink. Oxybuprocaine (4 mg/ml) was instilled topically as a local anesthetic a few minutes before the intravitreal injections. The intravitreal injection volume of the empty formulation was 50 µl per rabbit eye. In total of 6 eyes of three rabbits received the placebo formulation.

2.5.4   Fundus imaging

The pupil was dilated using topical tropicamide (one drop of Oftan Tropicamid 5 mg/mL, Santen, Finland) instilled to each eye 15 min before imaging, and the fundus images were captured by Micron IV Retinal Imaging Microscope (Phoenix Technology Group, Pleasanton, CA, USA) using full color and green fluorescence sets of filters. The rabbits were under anesthesia using subcutaneous injection of ketamine (dose 25/kg) and medetomidine (dose 0.5 mg/kg) during the imaging.

2.5.5   Fluorophotometric studies with rabbits

In vivo PK studies in rabbit eyes were performed using fluorophotometer (Fluorotron, OcuMetrics, Mountain view, CA, USA) as reported previously.[52, 53] Prior to the experiments, the rabbits were anesthetized by s.c. injection of 0.5 mg/kg medetomidine (Domitor vet 1 mg/mL; Orion Pharma, Finland) and ketamine (25 mg/kg; Ketaminol®, 50 mg/mL; Pfizer Oy Animal Health, Finland). The pupils were dilated after topical administration of an eye drop of tropicamide (Oftan Tropicamid 5 mg/mL, Santen, Finland). The baseline autofluorescence for each eye was measured before intravitreal injection of hydrogel formulation loaded with BDP labeled bevacizumab. The post-injection fluorescence signals were measured from the vitreous and aqueous humor. The fluorophotometry scans were performed at different time points for up to 41 days.

Autofluorescence originating from the vitreous and aqueous humor was subtracted from the measured fluorescence values. Subsequently, the remaining fluorescence signals were converted to bevacizumab-BDP dye concentrations using calibration standards ranging from 0.4 to 400

µg/ml. During each scan, the rabbits were under sedation by Domitor (Domitor vet 1 mg/mL; 0.3 mL/kg) given by s.c. injection. The levels of bevacizumab-BDP dye in the vitreous were quantitated by calculating the average concentration within a specific region. This region began at a relative distance of 3 mm from the retina and extended to 13 mm from the retina. Atipamezole (0.2 mL/kg; Antisedan®, 5 mg/mL; Orion Pharma, Finland) was used as an antagonist to reverse the sedation by s.c. injection.

2.6   PK simulations

PK curve fitting was performed to calculate the PK parameters for the released bevacizumab-BDP in the vitreous and aqueous humor after intravitreal injections of 10 and 20 wt% 4APM_HAFU hydrogels. First, the experimental values obtained from Bakri et al.[54] were used to calculate the PK parameters for free bevacizumab (dose 600 µg) in rabbit eyes following intravitreal injections. The model (Figure 1A and Eq 2-3) assumes previously proven anterior elimination route of intravitreal bevacizumab.[19]

Eq.2 $\frac{dM_{vit}}{d_t} = -k_{vit} \times M_{vit}$

Eq.3 $\frac{dM_{aqh}}{d_t} = k_{vit} \times M_{vit} - k_{aqh} \times M_{aqh}$

M_{vit} and M_{aqh} are the masses of bevacizumab in the vitreous and aqueous humor, respectively. The mass of drug in each compartment was calculated as mass = volume × concentration. The vitreous volume of distribution was 2500 µl [54] and the anatomical volume of aqueous humor is 325 µl . [55] K_{vit} and k_{aqh} are the elimination rate constants for bevacizumab from the vitreous and the aqueous humor, respectively. The intravitreal PK parameters of free bevacizumab were obtained with curve fitting using PKSolver software.[56] The fittings are shown in supplement (SI-Figure 2). A compartmental model (Figure 1B) was used to describe the PK after intravitreal injection of the hydrogels. The following differential equations (Eq. 4-6) were used to estimate the burst-released mass and drug release rate by curve fitting.

Eq.4 $\frac{dM_{gel}}{d_t} = -k_{re} \times \left(M_{gel} - M_b\right)$

Eq.5 $\frac{dM_{vit}}{d_t} = -k_{vit} \times (M_{vr} + M_b) + k_{re} \times \left(M_{gel} - M_b\right)$

Eq.6 $\frac{dM_{aqh}}{d_t} = k_{vit} \times (M_{vr} + M_b) - k_{aqh} \times M_{aqh}$

k_{re} is the first order release rate constant for bevacizumab-BDP release from the hydrogel. M_b represents the released amount of bevacizumab during the first day post-injection (arbitrarily taken as burst release). M_{gel} is the initial mass of bevacizumab in the hydrogel. M_{vr} and M_{gel} are the amounts of bevacizumab-BDP released in the vitreous after the burst release and the mass of bevacizumab-BDP dye within the hydrogel, respectively. All the fitting was done using least square method using Levenberg-Marquardt algorithm. R packages (packages FME and deSolve) and RStudio [57-59] were used for fitting.
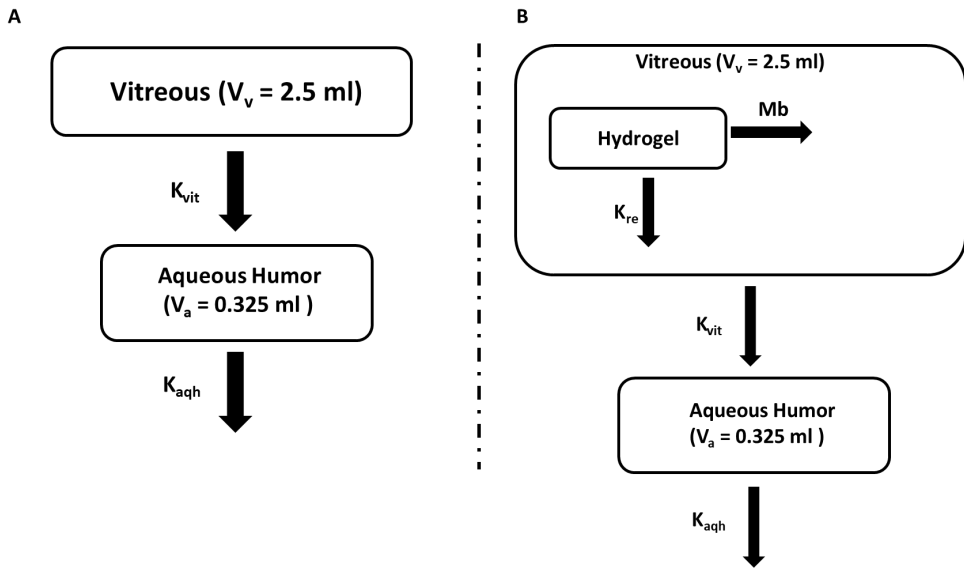
Figure 1 A) Compartmental PK model of intravitreal bevacizumab in rabbits. V_v and V_a are the volumes of the vitreous and anterior chamber, respectively. k_{vit} and k_{aqh} are elimination rate constants of labeled bevacizumab from the vitreous and anterior chamber, respectively. B) Compartmental model for vitreous kinetics of bevacizumab loaded in the hydrogel with first order in vivo release kinetics. M_b is the mass of drug released during the first day after injection. k_{re} is the first order release rate constant of bevacizumab from the hydrogel.

2.7 IOP measurements

The intraocular pressure of the eyes was recorded 30 minutes after 50 µl intravitreal injection of 10 or 20% HAFU-4AMP hydrogel loaded with bevacizumab formulation by using a tonometer (iCare PRO® tonometer, iCare Finland Ltd).

2.8 Aqueous humor samples

Aqueous humor samples were collected from the anterior chamber of the rabbits with Hamilton syringe with G34 needle (Hamilton company, Reno, NV, USA). Anesthesia was performed with s.c. medetomidine (Domitor vet 1 mg/ml, 0.4 ml/kg) and ketamine (Ketaminol vet 50 mg/ml, 0.4 ml/kg). The pupils were dilated with tropicamide eye drops (Oftan Tropicamid 5 mg/ml) and local anesthesia of ocular surface was achieved by oxybuprocaine eye drops (Oftan Obucain 4 mg/ml, Santen, Finland). Carbomer eye gel (Viscotears 2 mg/g, from Dr. Gerhard Mann chem.-pharm. Fabric GmbH, Berlin, Germany) was administered topically to prevent corneal drying. Anesthesia was reversed by s.c. injection of atipamezole (Antisedan vet 5 mg/ml, 0.2 ml/kg). After aqueous humor sampling, the eyes were treated with ocular antibiotics (Oftan Chlora, Santen, Finland; 10 mg/g) and the animals received s.c injection of painkiller carprofen (Rimadyl vet 50 mg/ml, 4 mg/kg; Zoetis, Helsinki, Finland).

The aqueous humor samples were stored at -20 °C until analysis. The fluorescence of the samples was measured using a plate reader (PerkinElmer Wallace, Turku, Finland) with 485/535nm excitation/emission wavelengths and the protein concentration was quantified against calibration curve of bevacizumab BDP prepared in bovine aqueous humor (range of 80– 5000 ng/mL).

3   RESULTS AND DISCUSSION

3.1   Gelation kinetics and hydrogel mesh size of the in vitro and ex vivo formed hydrogels

Figure 2 A-B shows the rheological characteristics of 4APM-HAFU solutions where the evolution of the storage (G') and loss moduli (G″) as a function of time was monitored for hydrogel precursor compositions (10 and 20 polymer wt%). After 3 h of crosslinking, the dependency of the G' as a function of angular frequency was examined as shown in figure 2C. As previously observed[48], the G' and G″ were initially low, indicating a free-flowing liquid solutions. However, both G' and G″ subsequently increased in time, and a crossover between G' and G″ (defined as the gelation time and corresponding with tan(δ) = 1) demonstrated network formation due to the reaction of the maleimide and furan functional groups. As expected, the gelation time of the formulation with a higher polymer concentration of 20 wt% (13 min) was shorter than that of the 10 wt% solution (32 min). As shown in Figure 2C, there was no dependency of angular frequency on G' after 3 h network formation, indicative of the formation of a fully elastic gel. The 10 wt% hydrogel showed a G' of 18.3 kPa, while the G' of the 20 wt% hydrogel was 72.0 kPa confirming the formation of a stiffer gel.

Dynamic Mechanical Analyzer (DMA) was used to determine Young's module (E) of the hydrogels formed in situ in the vitreous body of an ex vivo albino rabbit eye. Figure 2D shows the E of hydrogels isolated from the vitreous body after intravitreal injection of 4APM-HAFU) hydrogel formulation (160 µl, 20 wt %) as a function of the maleimide-furan molar ratio. Figure 2D also shows the E values of in vitro prepared gels. The measured E moduli of the in vitro and ex vivo formed hydrogels were converted to G' by dividing the values with 2.5 as previously reported by Ilochonwu et al. for the same hydrogels.[48] The plateau G' values were used to calculate the average mesh sizes of hydrogel network using the previously mentioned equation of rubber elasticity theory with the assumption of an affine network, neglecting end effects of single chains, and excluding physical entanglements[50] (see equation in section 2.2) As expected, the hydrogel mesh size of the in vitro and ex vivo hydrogels decreased with increasing ratio molar ratio of maleimide/furan groups. To explain, the ex vivo hydrogels mesh size prepared with molar ratios of maleimide/furan 1:2, 1:3, and 1:5 were 8.6, 8.2, and 6.9 nm, respectively (Table 1). The calculated mesh sizes were approximately 1.7 times larger than those of the in vitro-formed gels (Table 1), which is consistent with the previously observed 1.5 fold increase for the same hydrogels formed in porcine eyes (Ilochonwu et al.[48]) .
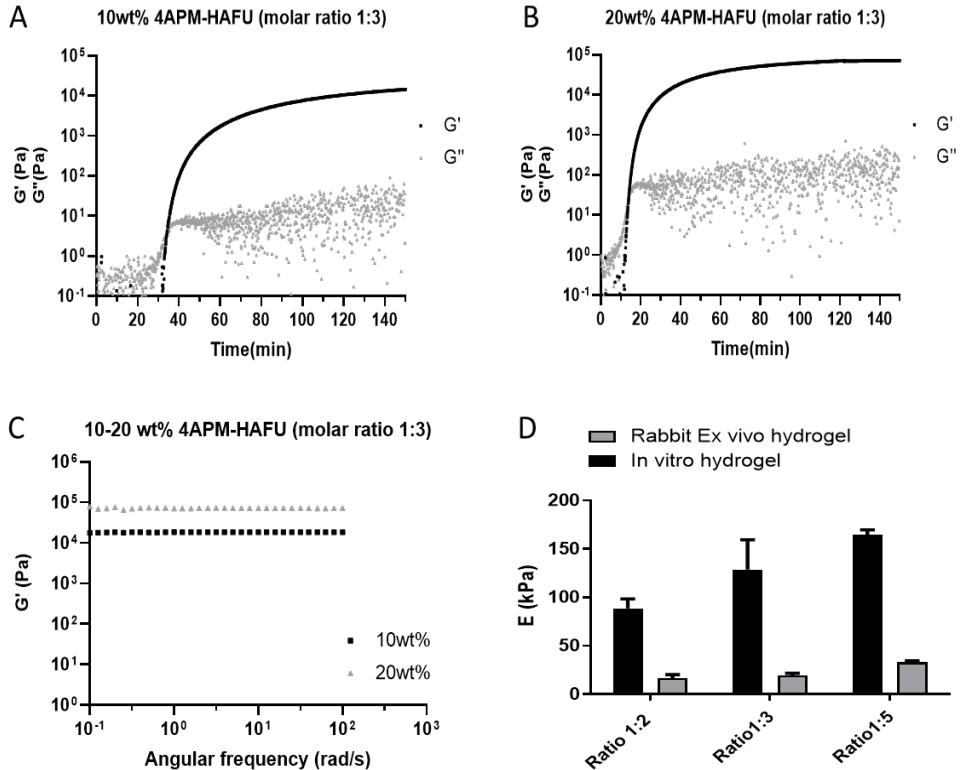
Figure 2 Rheological characteristics of 4APM-HAFU hydrogel formulation. A, B) Storage (G') and loss moduli (G") as a function of time for the 10 and 20 wt % 4APM-HAFU (molar maleimide/furan ratio 1:3) hydrogel formulations. C) Storage (G') as a function of the angular frequency of 10 and 20 wt % 4APM-HAFU (molar ratio 1:3) hydrogel. D) Young's moduli E (kPa) of in vitro (n = 3) and ex vivo (n = 3) formed 20 wt % 4APM-HAFU hydrogels at molar maleimide/furan ratios 1:2, 1:3 and 1:5.

Table 1 Average mesh sizes of in vitro and ex vivo 20 wt % HAFU-4APM hydrogels as calculated from the DMA mechanical measurements, *obtained from the previous publication [48]. Ratio refers to molar maleimide/furan.

Gel samples name	E kPa	G' (kPa)	Mesh size (nm)
In vitro ratio (1:2)	79*	31.6	5.1
in vitro ratio (1:3)	129	51.6	4.4
in vivo ratio (1:5)	165*	66.0	4.0
ex vivo ratio (1:2)	17	6.8	8.6
ex vivo ratio (1:3)	20	8.0	8.2
ex vivo ratio (1:5)	33	13.2	6.9

3.2   Conjugation of BDP to bevacizumab

BDP FL NHS ester dye was conjugated to lysine residues of bevacizumab. An average of 2.0 molecules of BDP FL dye per molecule of bevacizumab were conjugated based on the UV absorbance measurements of the dye at 505 nm and the protein at 283 nm (Figure 3; equation mentioned in section 2.3). SEC analysis of the purified bevacizumab BDP conjugate revealed a trace amount of free BDP dye, accounting for only 0.03% of the protein peak, while achieving an overall protein yield of 64%. The overlapping peaks at retention time of ≈5 min corresponds to bevacizumab (excitation 280 and emission 340 nm; SI Figure 1 A_1) and BDP FL dye (excitation 409 and emission 509 nm; SI Figure 1 C_2) in the chromatogram of the purified bevacizumab BDP Dye (SI Figure 1 B1-B2) confirming that the dye was conjugated to bevacizumab.
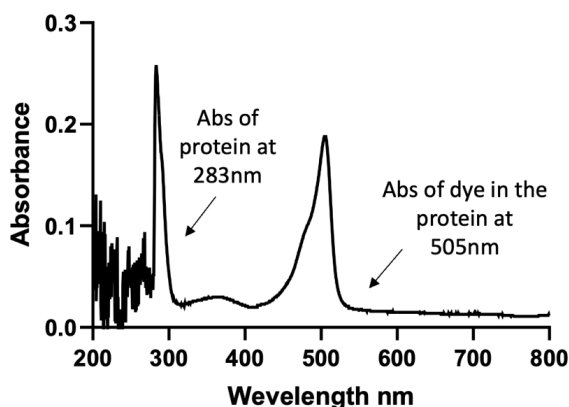
Figure 3 The UV spectrum of Bevacizumab-BDP dye (0.5 mg/ml) dissolved in water with 10% (v/v) DMSO after purification by Zeba™ spin desalting column.

3.3   Fundus imaging

Intravitreally administered bevacizumab-BDP loaded hydrogels were monitored by fundus imaging and fluorophotometry. Fundus images (Figure 4) showed that after the intravitreal injection bevacizumab-BDP overlays with the hydrogel demonstrating the presence of the protein in the hydrogel matrix. Additionally, shortly after injection, the formed protein depot system in the vitreous was slightly larger for the hydrogels formed with 10 wt% compared with the 20 wt% hydrogels primarily due to the faster gelation kinetics of the 20 wt% gel. At day 2 and later, bevacizumab-BDP progressively distributed gradually over the vitreous and was retained for up to about 41 days within the vitreous (Figure 4, SI-Figure 4-5) with decreasing intensity over time due to gradual elimination of the protein. The eyes that received the 20 wt% formulation retained more protein over the course of the experiment (from day 2 to 41) as compared to the eyes injected with the 10 wt% formulation. This suggests that the 20 wt% formulation has a tighter network structure with smaller mesh size and thus longer retained the protein than the 10 wt% hydrogel. This tighter network is obvious from the higher G' value (see. Section 3.1). Figure 4 shows that parts of the vitreous were hazy after 14 days after intravitreal injection of the hydrogel

formulations, which lead to an unwanted decreased visibility of the vascular markings of the retina and the optic nerve. This haziness can potentially be attributed to both the inflammatory response, as discussed in section 3.5, within the vitreous.
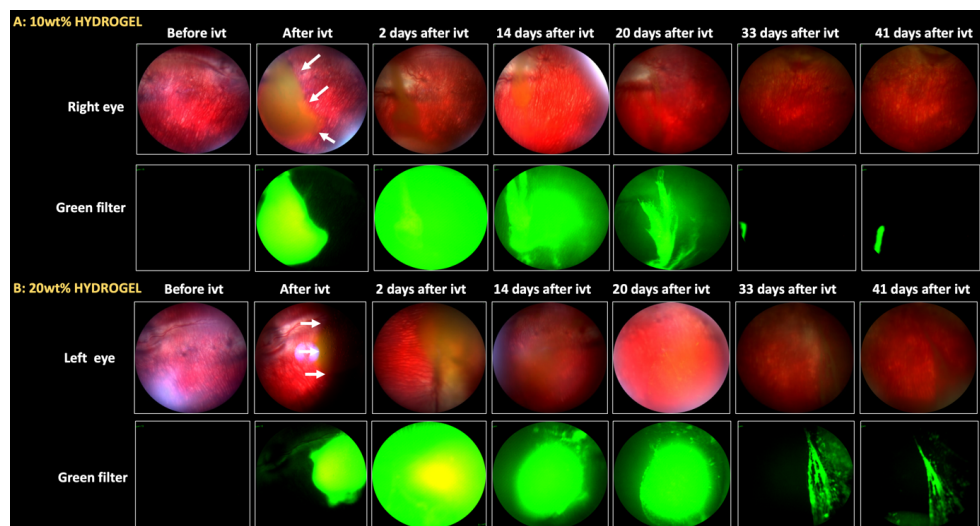
Figure 4 Full color and green fluorescent fundus images of representative rabbit eyes (rabbit-3) before and after day 2, 14, 20, 33 and 41 post intravitreal injection (IVT) of (A) bevacizumab-BDP 10wt% 4APM_HAFU (1:3) hydrogel in the right eye and (B) Bevacizumab-BDP dye 20wt% 4APM_HAFU (1:3) hydrogel in the left eye. Further, SI-Figure 4 and SI-Figure 5 show the images of the eyes of two other rabbits (2 and 4) of this study.

3.4 PK results

The in vivo vitreous and aqueous humor concentrations of bevacizumab-BDP were measured using a fluorophotometer and rate constants were determined with the model as given in section 2.6 (Figure 1A-B). The experimental data, derived from the bolus injection of free bevacizumab as reported by Bakri et al.[54] were fitted to the equations 2-3 to calculate the PK parameters of intravitreally injected bevacizumab in its soluble form in rabbit eyes. The elimination rate constants from the vitreous were 0.13 ± 0.03 day^{-1} and the aqueous humor was 13.2 ± 2.6 day^{-1}. The comparison of predicted and experimental data is shown in SI-Figure 2. The clearance of bevacizumab from anterior chamber was ≈3 µl/min, a value close to the aqueous humor flow rate in rabbits.[60, 61] This is in line with the known elimination of intravitreally administered biotherapeutics by aqueous humor turnover.[19, 62] The elimination rates of bevacizumab from the vitreous and aqueous humor and the compartment volumes were used to estimate the in vivo release rate of bevacizumab-BDP from the hydrogel. Figure 5A-B shows the concentrations of fluorescently labelled bevacizumab-BDP in the vitreous and aqueous humor of five rabbit eyes and corresponding model fits after intravitreal injections of the hydrogels. The results demonstrated that the burst release, arbitrarily defined as the amount of protein released during the first day, was 332 ± 29 µg (53 of the loaded amount) for the 10 wt% 4APM_HAFU (1:3) hydrogel

formulation and 196 ± 24 µg (33 of the loaded amount) for the 20 wt% formulations. These values exceeded the burst release in vitro (< 20 % during the 1st day) previously reported, Ilochonwu et al [48] and can be attributed to the larger mesh size of the gels formed within the vitreous (shown ex vivo) as compared to the gels prepared in vitro (Table 1) likely caused due to vitreous dilution of the formulation. After burst release, the in vivo first order release rates constants of bevacizumab-BDP from the 10 and 20 wt% hydrogel system were 0.26 ± 0.05 and 0.13 ± 0.02 day^{-1}, respectively. Miyake et al. demonstrated that a dose of 6 µg of intravitreal bevacizumab injection is sufficient to inhibit the activity of VEGF in Macaque eyes.[63] After 33 days, the simulated concentrations of bolus-injected bevacizumab in the eyes of rabbits were calculated as 3.1 µg/ml (7.7 µg per 2.5 ml of vitreous) and 0.24 µg/ml in the aqueous humor. Hutton-Smith et al.[62] previously showed that bevacizumab concentrations in the retina are close to its concentrations in the vitreous. Based on the experimental findings (Table 2), the vitreous concentration of bevacizumab released from the 10 wt% hydrogel formulation at day 33 was still 5.2 ± 1.6 µg/ml (equivalent to 12.9 ± 4.0 µg of protein in the vitreous), excluding the protein still entrapped within the gel depot. For the 20 wt% hydrogel formulation, the values were 9.9 ± 1.2 µg/ml (corresponding to 24.7 ± 3.0 µg in the vitreous) at day 33. Compared to a bolus injection of bevacizumab, the vitreous concentrations of free bevacizumab were 1.67 ± 0.52 (10 wt% gel) and 3.21 ± 0.39 (20 wt% gel) times higher, respectively. These findings highlight the significantly superior intravitreal retention of bevacizumab achieved by both the 10 wt% and 20 wt% gel formulations compared to the bolus injection after 33 days. To provide further context, the IC_{50} values of bevacizumab (concentration for half maximal VEGF inhibition) are compared with the observed concentrations of the free drug. The IC_{50} values for bevacizumab against VEGF are 0.126 µg/ml for $VEGF_{A121}$ and 0.219 µg/ml for $VEGF_{A165}$ in vitro[64] Taking into account the concentration of VEGF in diseased human eyes, Yu et al.[31] suggested that a therapeutically effective concentration of free bevacizumab is 0.05 µg/ml. The vitreous concentrations of free bevacizumab due to release from the hydrogels are thus significantly higher than the IC_{50} of this protein. In fact, vitreous concentrations of released bevacizumab were consistently maintained at least 20 times higher levels than the minimum therapeutic concentration (0.05 µg/ml) (Figure 5B). Thus, sustained release of bevacizumab from the hydrogels is expected to inhibit VEGF effectively in the vitreous and retina.

4

Table 2 Pharmacokinetic parameters within the vitreous of 50 μl intravitreally injected bevacizumab-BDP dye (dose 600 μg) released from 4APM_HAFU hydrogel (n=5, eyes) as derived from fluorophotometric measurements. [a] Not applicable.

Formulation	Burst release (%)	First order release rate constant (day^{-1})	Bevacizumab-BDP (μg) in vitreous (day 33)
10 wt% 4APM_HAFU bevacizumab-BDP dye	53	0.26 ± 0.05	12.9 ± 4.0
20 wt% 4APM_HAFU bevacizumab-BDP dye	33	0.13 ± 0.02	24.7 ± 3.0
Simulated bolus- bevacizumab	NA[a]	NA[a]	~7.7
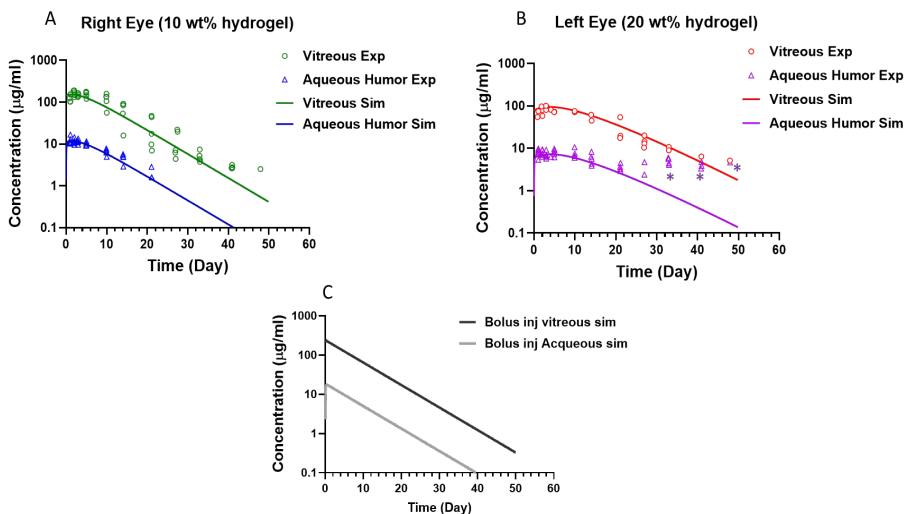
Figure 5 Fluorophotometer results of bevacizumab-BDP released from 4APM_HAFU (1:3) hydrogels. The symbols represent the experimental concentrations (exp) of fluorescently labelled bevacizumab-BDP in the vitreous and aqueous humor of five individual rabbit eyes after injection of 10 wt% 4APM_HAFU (1:3) hydrogel formulation (A) and 20wt% 4APM_HAFU (1:3) hydrogel (B). The lines indicate the simulated (Sim) concentrations using the PK parameters from data fitting (using compartmental model in Figure 1B). *These points were not included in the simulation as the aqueous humor concentration did not exhibit the expected one order of magnitude difference compared to the vitreous concentration, as typically seen in the clearance of biologicals.[19, 65] C) Simulated concentrations of bevacizumab in rabbit eyes after its intravitreal bolus injection (using compartmental model in Figure 1A)

The bevacizumab-BDP concentration in the aqueous humor released from the injected 20 wt% hydrogel plateaued at about 1 μg/ml between 27-55 days, indicating a longer sustained release of bevacizumab from this formulation as compared to 10wt% hydrogel (Figure 6). This is in line with the in vitro release data showing a longer release from hydrogels with a higher polymer content as previously described Ilochonwu at el.[48]
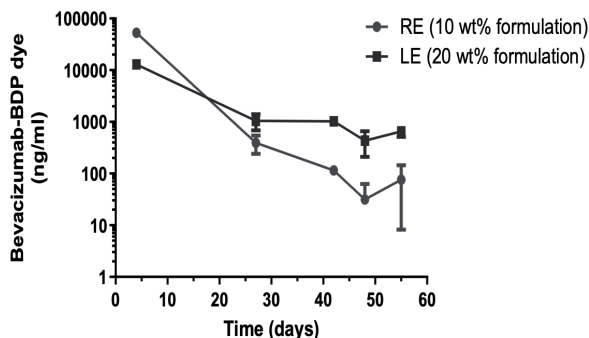
Figure 6 Concentrations of released bevacizumab in aqueous humor of rabbits. NB: The points from day 4 and 42 are from a single animal (n=1), while day 27 (n=5), 48 (n=4) and 55 represent data of three animals.

3.5   Safety observation of bevacizumab-BDP 10 and 20 wt% 4APM_HAFU (1:3) hydrogels

The intraocular pressure (IOP) 30 minutes after injection was 7-11 mmHg (Figure 7.), which falls within the normal range for New Zealand rabbit's eyes being typically in the range of 7-16 mmHg.[66] The normal IOP range and the fact that the measured IOP values are within this range after the injection of the hydrogel formulations, suggests that the hydrogel injections did neither significantly affect nor disrupt the normal intraocular pressure in the rabbit's eyes. This finding is consistent with the clinical practice where similar volumes of intravitreal administered injections do not cause increase in IOP.[67] However, it is important to remark that the present study did not evaluate the long-term effects of the hydrogel formulations on intraocular pressure.
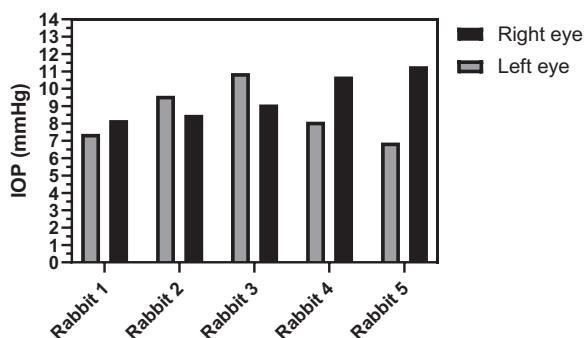
Figure 7 The intraocular pressure (IOP) 30 minutes after injection in the right eye (with 10 wt% 4APM_HAFU (1:3) formulation) and in the left eye (with 20 wt% 4APM_HAFU (1:3) formulation).

On 14- and 49-days post-injection, the ocular health was evaluated with a slit lamp and the results are summarized in table 3. On day 14, two animals had inflammation in the right eye (10 wt% hydrogel injected), and two animals had inflammation in the left eye (injected with 20 wt% hydrogels). One animal had no inflammation in eyes. All animals had some aggregates in the

vitreous. This may be caused by aggregation of the labelled protein in vivo[68], even though the exact identity of the aggregates is unknown. Additionally, it's important to highlight that bevacizumab has a higher propensity for aggregate formation than other monoclonal antibodies due to its distinctive self-association involving non-covalent interactions, as noted by Fei et al.[69-71] On day 42 post-injection, rabbit-5 and rabbit-4, respectively, had to be sacrificed due to severe inflammation in the left eye. Seven weeks post-treatment, uveitis was detected in the three left eyes with additional retinal inflammation in one animal (rabbit-3). In the right eye, rabbit 1 had uveitis. Furthermore, all parameters were normal in 2 animals (rabbit-2 and rabbit-3), this indicates that neither abnormal nor concerning findings were observed. On day 55, the three remaining animals were euthanized. Overall, the left eyes exhibited a more pronounced inflammatory response compared to the right eyes, particularly after 42-49 days post injection of the formulations. This indicates that the 20 wt% hydrogel demonstrated lower biocompatibility compared to the 10 wt% hydrogel. Moreover, during the 42-49 day period, the right eyes displayed reduced inflammation, and in certain cases, no significant issues were observed. Thus, the adverse side effects after administration of the 20 wt % gel might be due to higher polymer concentration as compared to the 10 wt% gels. The exact mechanism through which a higher polymer volume fraction leads to increased inflammation is not understood yet, but several factors can possibly contribute to this phenomenon. One possible explanation is related to the molecular weight of the used hyaluronic acid (HA). HA degrades upon injection due to the actions of hyaluronidases (HYAL1 and HYAL2), potentially leading to an inflammatory response[72, 73] via increased cytokine activity caused by low molecular weight HA fragments.[74] In this study it was found that low molecular weight HA may induce inflammatory responses, while high molecular weight HA exhibits immunosuppressive effects.[74] However, the inflammatory response of chemically crosslinked HA hydrogels upon injection into the eye has not been studied thus far. In this present study, HA with a molecular weight of 24 kDa was crosslinked with 10 kDa PEG using a DA reaction. Significant side effects suggest that degradation of the hydrogel network may release 24 kDa HA that could lead to the inflammation. Our previous study demonstrated that the 4APM_HAFU hydrogels undergo degradation through hydrolysis of the crosslinks via a retro-Diels-Alder (rDA) reaction followed by ring-opening hydrolysis of the resulting maleimide, leading to the formation of unreactive maleamic acid.[48] The presence of maleamic acid and furan moieties might cause detachment of polymer fragments or protein-polymer conjugates (for example bevacizumab-PEG), thus triggering an inflammatory response. It is important also to consider that the in vitro degradation of the 4APM_HAFU (ratio 1:3) hydrogel took approximately 2 months (10wt% hydrogel) and 6 months (20wt% hydrogel) [48]. In vivo degradation is expected to be faster due to the vitreous dilution and enzymatic degradation. Other factors could also contribute to the inflammatory response. When the hydrogel is injected into the eye, it may absorb fluid and swell,[75] potentially causing mechanical irritation (such as vitreous blunt trauma or penetrating trauma) and thereby triggering an inflammatory reaction.[76] Additionally, following the chemical modification of the protein to introduce the BDP dye, the dye-labeled protein can also affect the in vivo stability of the protein, potentially leading to protein aggregation.[68] This is because the labeled protein differs from the original, non-labeled antibody. Finally, the released PEG (polyethylene glycol) from the crosslinked hydrogel network may contribute, since PEG is known

to exert immunogenic properties.[77, 78] However, in the existing literature there is no information regarding potential ocular immunogenic reactions triggered by the release of PEG from biodegradable hydrogels.

It is important to note that all components used in the formulation (polymer, protein, and dye) had endotoxin levels below < 0.2 EU/ml. This translates to endotoxin concentrations of < 0.004 EU/ml per eye (considering 2.5 ml of rabbit vitreous) after a 50 µl intravitreal injection. These concentrations far are below the limit recommended by the FDA for intraocular ophthalmic devices, which is ⩽ 0.2 EU/mL, regardless of whether the intended site of use is the anterior or posterior segment.[79]

Table 3 Ophthalmologists evaluated the rabbit eyes at 14 days and 49 days post-injection of 10 wt% or 20 wt% 4APM_HAFU (1:3) formulation loaded with protein. The right eye (RE) and left eye (LE) were assessed.

14 Days post Injection	RE (10%)	LE (20%)	49 Days post Injection	RE (10%)	LE (20%)
Rabbit 1	Mild* Inflammation	No Inflammation (Suspicion of retinal damage)	Rabbit 1	Uveitis, Retina ok	Uveitis, Retina ok
Rabbit 2	No inflammation,	Mild * Inflammation	Rabbit 2	All parameters normal	Uveitis, Retina ok
Rabbit 3	No inflammation, (Aggregates)	No inflammation (Aggregates)	Rabbit 3	All parameters normal	Uveitis, Retinal inflammation
Rabbit 4	Mild* inflammation (Aggregates)	No inflammation (Aggregates)	Rabbit 4 (sacrificed day 41)	-	-
Rabbit 5	Aggregates (No clear view to the retina)	Severe * Inflammation	Rabbit 5 (sacrificed day 41)	-	-

* Mild to a severe adverse effect as observed by fundus ophthalmic examination. All parameters normal, indicate no abnormal or concerning findings were observed after the fundus ophthalmic examination. Aggregates refers to accumulation of substances (proteins or cell debris) within the vitreous humor.

3.6   Safety observation of placebo 20 wt% 4APM-HAFU (1:5) hydrogels

After observing an inflammatory response in multiple eyes 14 days post-injection of the drug-loaded 4APM-HAFU (1:3) formulation during the PK evaluations. The safety of the 20wt% placebo 4APM-HAFU (1:5) formulation was investigated in three rabbit eyes (n=6). This investigation aimed to determine whether the observed toxicity was at least partially caused by the dye-labelled protein. Due to ethics, the 20wt% placebo 4APM-HAFU (1:5) formula was chosen over (1:3), as the latter hydrogel loaded with bevacizumab-BDP dye showed an inflammatory response (section 3.5). The 4APM-HAFU (1:5) gel showed a higher G', indicating a denser crosslinking and thus smaller mesh size, than the 4APM-HAFU (1:3) (Ilochonwu et al.[48]). This likely leads to

slower degradation and gradual polymer release. Figure 8 shows normal fundus images of rabbit eyes after intravitreal injection of the placebo hydrogel. No abnormalities were identified in the back of the eye in the six injected eyes up to 14 days post-injection. Furthermore, no abnormalities were observed during the posterior segment evaluation using a slit lamp.
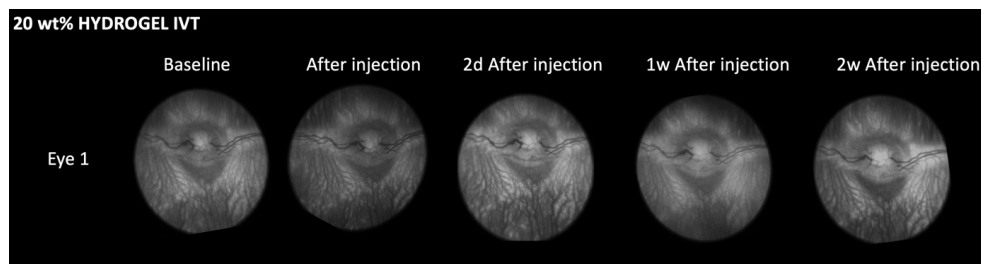
Figure 8 Fundus images of rabbit eyes before and after day 2, one week (1w) and two weeks (2w) post intravitreal injection (IVT) of 20wt% 4APM_HAFU (1:5) hydrogel.

Transient irritation, including discomfort, redness and behavioral responses, was observed in the anterior segment of some eyes. Figure 9 shows a microscopic image of the anterior eye and eyelid. One day post-injection of the placebo formulation, all animals developed moderate to severe redness in the eyelid at least in one eye and neovascularization in the sclera and conjunctiva (indicated by the arrows in Figure 9). The irritation could be controlled by administration of antibiotics/painkillers but flamed up upon handling the eyes during fundus imaging. Anterior neovascularization effects were not observed with the protein-loaded hydrogel formulation. These findings indicate successful release of bioactive bevacizumab from the hydrogel formulation. Bevacizumab is known for its anti-angiogenic properties[64] and inhibits blood vessel formation, resulting in the absence of redness and neovascularization in the anterior chamber.

Seven days post-injection, the eye effects recuperated, neovascularization had ceased, and no irritation was observed in the eyelid. The scleral lenses were normal and comparable to the eye before injection. No additional adverse effects were observed till the experiment ended two weeks post-injection. The biocompatibility of the placebo 20wt% 4APM_HAFU (1:5) hydrogel was found to be better than that of the protein-loaded 10 and 20wt% 4APM_HAFU (1:3) hydrogels. Although the exact reasons are not fully understood, some assumptions can be made based on the in vitro behavior of the formulations from the previous work. One key factor is the slower degradation rate of the 20 wt% 4APM_HAFU (1:5) hydrogel, which takes 300 days for complete degradation, compared to the 20 wt% 4APM_HAFU (1:2) hydrogel, which degrades entirely in 90 days, as previously reported [48]. This trend suggests that the 4APM_HAFU (1:5) hydrogel will degrade faster than the 4APM_HAFU (1:3) ratio. The slower degradation results in reduced loss of polymer precursor from the gel network over time, potentially minimizing the inflammatory response in vivo and enhancing biocompatibility. This indicates that slower degrading hydrogels have the potential to be safer for intravitreal drug delivery applications. Another important factor is that the 20 wt% 4APM_HAFU (1:5) hydrogel may exhibit less swelling over time compared to the protein-loaded hydrogels (10 and 20 wt% 4APM_HAFU (1:3)) in vivo, consistent with the in

vitro trends reported by Ilochonwu et al.[48] At day 30, the swelling ratio of 4APM_HAFU (1:5) was approximately 4, while it was 6.5 for the 4APM_HAFU (1:2) ratio. The decreased swelling capacity of the 4APM_HAFU (1:5) hydrogel formulation might minimize mechanical stress on the surrounding tissue as mentioned above, thereby lowering the likelihood of tissue damage or irritation.[75, 76] Moreover, it is important to note that in vitro cytocompatibility studies demonstrated that neither the hydrogel nor the HA and PEG precursor exhibited cytotoxicity to retinal Muller cells.[48] This observation highlights the necessity of considering the complex in vivo immune response when assessing the overall safety of materials for intravitreal applications. Taken together, these findings suggest that the development of slowly degrading hydrogels and limited swelling properties is essential for the successful development of injectable hydrogel for ocular drug delivery.
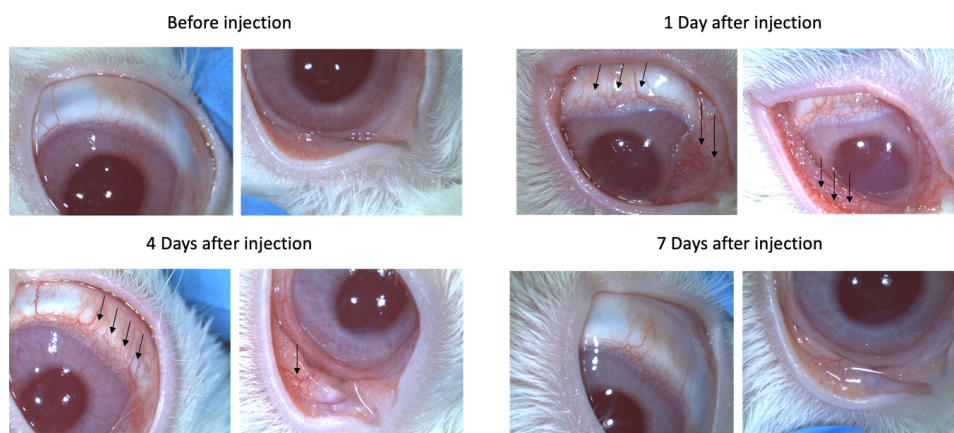
Figure 9 Microscopic images of the anterior segment of New Zealand rabbit eye before and after intravitreal injection of 20wt% 4APM_HAFU (1:5) hydrogel.

4   CONCLUSION

In conclusion, the hyaluronic acid-PEG-based Diels–Alder hydrogel system demonstrates its potential as a depot for sustained release of bevacizumab in the vitreous. Higher polymer concentrations led to improved drug retention and reduced burst release. However, the occurrence of an inflammatory response highlights the potential influence of polymer concentration, swelling properties, and hydrogel stability on toxicity. Moreover, labeling of therapeutic proteins may also affect their stability in vivo, potentially leading to aggregation and an inflammatory response. Furthermore, in depth safety evaluations are required before progressing to translational stages to ensure the suitability of the hydrogel system for clinical use.

5 REFERENCES

[1] W.L. Wong, X. Su, X. Li, C.M. Cheung, R. Klein, C.Y. Cheng, T.Y. Wong, Global prevalence of age-related macular degeneration and disease burden projection for 2020 and 2040: a systematic review and meta-analysis, Lancet Glob Health, 2 (2014) e106-116.

[2] N. Ferrara, A.P. Adamis, Ten years of anti-vascular endothelial growth factor therapy, Nat Rev Drug Discov, 15 (2016) 385-403.

[3] S. Cornel, I.D. Adriana, T.C. Mihaela, S. Speranta, D.S. Algerino, B. Mehdi, H.-R. Jalaladin, Anti-vascular endothelial growth factor indications in ocular disease, Rom J Ophthalmol, 59 (2015) 235-242.

[4] P. Rosenfeld, Brown, D. , Heier, J. , Boyer, D. , Kaiser, P. , Chung, C. & Kim, R. , Ranibizumab for Neovascular Age-Related Macular Degeneration, The New England Journal of Medicine, 355 (14) (2006) 1419-1431.

[5] A.M. Schauwvlieghe, G. Dijkman, J.M. Hooymans, F.D. Verbraak, C.B. Hoyng, M.G. Dijkgraaf, T. Peto, J.R. Vingerling, R.O. Schlingemann, Comparing the Effectiveness of Bevacizumab to Ranibizumab in Patients with Exudative Age-Related Macular Degeneration. The BRAMD Study, PLoS One, 11 (2016) e0153052.

[6] Y. Wang, D. Fei, M. Vanderlaan, A. Song, Biological activity of bevacizumab, a humanized anti-VEGF antibody in vitro, Angiogenesis, 7 (2004) 335-345.

[7] S.A. Vinores, Pegaptanib in the treatment of wet, age-related macular degeneration, International Journal of Nanomedicine 1(2006) 263–268.

[8] Q.D. Nguyen, A. Das, D.V. Do, P.U. Dugel, A. Gomes, F.G. Holz, A. Koh, C.K. Pan, Y.J. Sepah, N. Patel, H. MacLeod, P. Maurer, Brolucizumab: Evolution through Preclinical and Clinical Studies and the Implications for the Management of Neovascular Age-Related Macular Degeneration, Ophthalmology, 127 (2020) 963-976.

[9] F. Semeraro, F. Morescalchi, S. Duse, F. Parmeggiani, E. Gambicorti, C. Costagliola, Aflibercept in wet AMD: specific role and optimal use, Drug Des Devel Ther, 7 (2013) 711-722.

[10] R. Sophie, A. Akhtar, Y.J. Sepah, M. Ibrahim, M. Bittencourt, D.V. Do, Q.D. Nguyen, Aflibercept: a Potent Vascular Endothelial Growth Factor Antagonist for Neovascular Age-Related Macular Degeneration and Other Retinal Vascular Diseases, Biol Ther, 2 (2012) 3.

[11] R.L. Avery, D.J. Pieramici, M.D. Rabena, A.A. Castellarin, M.A. Nasir, M.J. Giust, Intravitreal bevacizumab (Avastin) for neovascular age-related macular degeneration, Ophthalmology, 113 (2006) 363-372 e365.

[12] R. Ehrlich, D. Weinberger, E. Priel, R. Axer-Siegel, Outcome of bevacizumab (Avastin) injection in patients with age-related macular degeneration and low visual acuity, Retina, 28 (2008) 1302-1307.

[13] P.J. Rosenfeld, A.A. Moshfeghi, C.A. Puliafito, Optical Coherence Tomography Findings After an Intravitreal Injection of Bevacizumab (Avastin®) for Neovascular Age-Related Macular Degeneration, Ophthalmic Surgery, Lasers and Imaging Retina, 36 (2005) 331-335.

[14] M. Richard F. Spaide, Ketan Laud, MD, Howard F. Fine, MD, Mhsc, James M. Klancnik Jr, MD, Catherine B. Meyerle, MD, Lawrence A. Yannuzzi, MD, John Sorenson, MD, Jason Slakter, MD, Yale L. Fisher, MD, Michael J. Cooney, MD, Intravitreal bevacizumab treatment of choroidal neovascularization secondary to age related macular degeneration, Retina, 26 (2006) 383–390.

[15] T.C.R. Group, Ranibizumab and bevacizumab for neovascular age-related macular degeneration, New England Journal of Medicine, 364 (2011) 1897-1908.

[16] M. Modarres, M. Naseripour, K.G. Falavarjani, A. Nikeghbali, M. Hashemi, M.M. Parvaresh, Intravitreal injection of 2.5 mg versus 1.25 mg bevacizumab (Avastin) for treatment of CNV associated with AMD, Retina, 29 (2009) 319-324.

[17] W.M. Amoaku, U. Chakravarthy, R. Gale, M. Gavin, F. Ghanchi, J. Gibson, S. Harding, R.L. Johnston, S.P. Kelly, A. Lotery, S. Mahmood, G. Menon, S. Sivaprasad, J. Talks, A. Tufail, Y. Yang, Defining response to anti-VEGF therapies in neovascular AMD, Eye (Lond), 29 (2015) 721-731.

[18] A. Caruso, M. Futh, R. Alvarez-Sanchez, S. Belli, C. Diack, K.F. Maass, D. Schwab, H. Kettenberger, N.A. Mazer, Ocular Half-Life of Intravitreal Biologics in Humans and Other Species: Meta-Analysis and Model-Based Prediction, Mol Pharm, 17 (2020) 695-709.

[19] A.K. Rimpela, I. Kiiski, F. Deng, H. Kidron, A. Urtti, Pharmacokinetic Simulations of Intravitreal Biologicals: Aspects of Drug Delivery to the Posterior and Anterior Segments, Pharmaceutics, 11 (2018).

[20] D.K. Sigford, S. Reddy, C. Mollineaux, S. Schaal, Global reported endophthalmitis risk following intravitreal injections of anti-VEGF: a literature review and analysis, Clin Ophthalmol, 9 (2015) 773-781.

[21] D. Patel, S.N. Patel, V. Chaudhary, SJ. Garg, Complications of intravitreal injections: 2022, Current Opinion in Ophthalmology, 33 (2022) 137-146.

[22] K.M. Sampat, S.J. Garg, Complications of intravitreal injections, Curr Opin Ophthalmol, 21 (2010) 178-183.

[23] R.G. Abell, N.M. Kerr, P. Allen, BJ. Vote, Intravitreal injections: is there benefit for a theatre setting?, British Journal of Ophthalmology, 96 (2012) 1474-1478.

[24] T.Y. Wong, U. Chakravarthy, R. Klein, P. Mitchell, G. Zlateva, R. Buggage, K. Fahrbach, C. Probst, I. Sledge, The natural history and prognosis of neovascular age-related macular degeneration: a systematic review of the literature and meta-analysis, Ophthalmology, 115 (2008) 116-126.

[25] Genentech, Genentech issues voluntary recall of Susvimo (ranibizumab) 100 mg/mL prefilled syringe, in, https://www.gene.com/media/press-releases/15122/2022-10-06/genentech-issues-voluntary-recall-of-susv, 2022.

[26] D.H.L. Charters, Genentech recalling ranibizumab injection ocular implant in US, in, Ophthalmology Times https://www.ophthalmologytimes.com/view/genentech-recalling-ranibizumab-injection-ocular-implant-in-us, 2022.

[27] Genentech, Genentech announces FDA approval of Susvimo, the first and only refillable eye implant to treat neovascular age-related macular degeneration, in, https://www.gene.com/media/press-releases/14907/2021-10-13/genentech-announces-fda-approval-of-su, 2021.

4

[28] A. Sharma, A.M. Khanani, N. Parachuri, N. Kumar, F. Bandello, B.D. Kuppermann, Port delivery system with ranibizumab (Susvimo) recall- What does it mean to the retina specialists, Int J Retina Vitreous, 9 (2023) 6.

[29] B.C. Ilochonwu, A. Urtti, W.E. Hennink, T. Vermonden, Intravitreal hydrogels for sustained release of therapeutic proteins, J. Controlled Release, 326 (2020) 419-441.

[30] G. Fang, X. Yang, Q. Wang, A. Zhang, B. Tang, Hydrogels-based ophthalmic drug delivery systems for treatment of ocular diseases, Mater Sci Eng C Mater Biol Appl, 127 (2021) 112212.

[31] Y. Yu, L.C. Lau, A.C. Lo, Y. Chau, Injectable Chemically Crosslinked Hydrogel for the Controlled Release of Bevacizumab in Vitreous: A 6-Month In Vivo Study, Translational Vision Science & Technology, 4 (2015) 5.

[32] J. Yu, X. Xu, F. Yao, Z. Luo, L. Jin, B. Xie, S. Shi, H. Ma, X. Li, H. Chen, In situ covalently cross-linked PEG hydrogel for ocular drug delivery applications, Int J Pharm, 470 (2014) 151-157.

[33] A. Famili, K. Rajagopal, Bio-Orthogonal Cross-Linking Chemistry Enables In Situ Protein Encapsulation and Provides Sustained Release from Hyaluronic Acid Based Hydrogels, Mol Pharm, 14 (2017) 1961-1968.

[34] W. Liu, M. Griffith, F. Li, Alginate microsphere-collagen composite hydrogel for ocular drug delivery and implantation, J Mater Sci Mater Med, 19 (2008) 3365-3371.

[35] R. Egbu, S. Brocchini, P.T. Khaw, S. Awwad, Antibody loaded collapsible hyaluronic acid hydrogels for intraocular delivery, European Journal of Pharmaceutics and Biopharmaceutics, 124 (2018) 95-103.

[36] A.M. Alhalafi, Applications of polymers in intraocular drug delivery systems, Oman J Ophthalmol, 10 (2017) 3-8.

[37] D. Chang, K. Park, A. Famili, Hydrogels for sustained delivery of biologics to the back of the eye, Drug Discov Today, 24 (2019) 1470-1482.

[38] J.C. Imperiale, G.B. Acosta, A. Sosnik, Polymer-based carriers for ophthalmic drug delivery, J Controlled Release, 285 (2018) 106-141.

[39] M.L. Lovett, X. Wang, T. Yucel, L. York, M. Keirstead, L. Haggerty, D.L. Kaplan, Silk hydrogels for sustained ocular delivery of anti-vascular endothelial growth factor (anti-VEGF) therapeutics, Eur J Pharm Biopharm, 95 (2015) 271-278.

[40] J. Huang, W. Wang, J. Yu, X. Yu, Q. Zheng, F. Peng, Z. He, W. Zhao, Z. Zhang, X. Li, Q. Wang, Combination of dexamethasone and Avastin((R)) by supramolecular hydrogel attenuates the inflammatory corneal neovascularization in rat alkali burn model, Colloids Surf B Biointerfaces, 159 (2017) 241-250.

[41] T.R.F. Britta M. Rauck, Carlos A. Medina Mendez, Daewon Park, Veeral Shah, Richard A. Bilonick and Yadong Wang, Biocompatible Reverse Thermal Gel Sustains the Release of Intravitreal Bevacizumab In Vivo, The Association for Research in Vision and Ophthalmology, 55 (2014) 469–476.

[42] S. Kirchhof, M. Abrami, V. Messmann, N. Hammer, A.M. Goepferich, M. Grassi, F.P. Brandl, Diels-Alder Hydrogels for Controlled Antibody Release: Correlation between Mesh Size and Release Rate, Mol Pharm, 12 (2015) 3358-3368.

[43] E.A. Balazs, Physical properties of hyaluronic acid, Nature, 150 (3811) (1942) 432-433.

[44] R.C. Pruett, C.L. Schepens, D.A. Swann, Hyaluronic acid vitreous substitute: A six-year clinical evaluation, Archives of ophthalmology, 97 (1979) 2325-2330.

[45] H. Barth, S. Crafoord, S. Andreasson, F. Ghosh, A cross-linked hyaluronic acid hydrogel (Healaflow((R))) as a novel vitreous substitute, Graefes Arch Clin Exp Ophthalmol, 254 (2016) 697-703.

[46] W.H. Chang, P.Y. Liu, M.H. Lin, C.J. Lu, H.Y. Chou, C.Y. Nian, Y.T. Jiang, Y.H. Hsu, Applications of Hyaluronic Acid in Ophthalmology and Contact Lenses, Molecules, 26 (2021).

[47] S. Kirchhof, M. Gregoritza, V. Messmann, N. Hammer, A.M. Goepferich, F.P. Brandl, Diels-Alder hydrogels with enhanced stability: First step toward controlled release of bevacizumab, Eur J Pharm Biopharm, 96 (2015) 217-225.

[48] B.C. Ilochonwu, M. Mihajlovic, R.F. Maas-Bakker, C. Rousou, M. Tang, M. Chen, W.E. Hennink, T. Vermonden, Hyaluronic Acid-PEG-Based Diels-Alder In Situ Forming Hydrogels for Sustained Intraocular Delivery of Bevacizumab, Biomacromolecules, 23 (2022) 2914-2929.

[49] N. Hammer, F.P. Brandl, S. Kirchhof, V. Messmann, A.M. Goepferich, Protein compatibility of selected cross-linking reactions for hydrogels, Macromol Biosci, 15 (2015) 405-413.

[50] P.J. Flory, J.R. Jr., Statistical Mechanics of Cross-Linked Polymer Networks I. Rubberlike Elasticity, J. Chem. Phys., 11 (1943) 512-520.

[51] T. Arvinte, C. Palais, E. Poirier, A. Cudd, S. Rajendran, S. Brokx, J. Dowd, Part 1: Physicochemical characterization of bevacizumab in undiluted 25 mg/mL drug product solutions: Comparison of originator with a biosimilar candidate, J Pharm Biomed Anal, 175 (2019) 112742.

[52] A. Sadeghi, M. Ruponen, J. Puranen, S. Cao, R. Ridolfo, S. Tavakoli, E. Toropainen, T. Lajunen, V.P. Ranta, J. van Hest, A. Urtti, Imaging, quantitation and kinetic modelling of intravitreal nanomaterials, Int J Pharm, 621 (2022) 121800.

[53] A. Sadeghi, J. Puranen, M. Ruponen, A. Valtari, A. Subrizi, V.P. Ranta, E. Toropainen, A. Urtti, Pharmacokinetics of intravitreal macromolecules: Scaling between rats and rabbits, Eur J Pharm Sci, 159 (2021) 105720.

[54] S.J. Bakri, M.R. Snyder, J.M. Reid, J.S. Pulido, R.J. Singh, Pharmacokinetics of intravitreal bevacizumab (Avastin), Ophthalmology, 114 (2007) 855-859.

[55] P.J. Missel, Simulating intravitreal injections in anatomically accurate models for rabbit, monkey, and human eyes, Pharm Res, 29 (2012) 3251-3272.

[56] Y. Zhang, M. Huo, J. Zhou, S. Xie, PKSolver: An add-in program for pharmacokinetic and pharmacodynamic data analysis in Microsoft Excel, Computer Methods and Programs in Biomedicine, 99 (2010) 306-314.

4

[57] K. Soetaert, T. Petzoldt, R.W. Setzer, Solving differential equations in R: package deSolve, Journal of statistical software, 33 (2010) 1-25.

[58] K. Soetaert, T. Petzoldt, Inverse modelling, sensitivity and Monte Carlo analysis in R using package FME, Journal of statistical software, 33 (2010) 1-28.

[59] R Core Team (2013) R: A Language and Environment for Statistical Computing. R Foundation for Statistical Computing, Vienna. http://www.R-project.org/

[60] H.A. Reitsamer, J.W. Kiel, Relationship between ciliary blood flow and aqueous production in rabbits, Invest Ophthalmol Vis Sci, 44 (2003) 3967-3971.

[61] H.A. Reitsamer, B. Bogner, B. Tockner, J.W. Kiel, Effects of dorzolamide on choroidal blood flow, ciliary blood flow, and aqueous production in rabbits, Invest Ophthalmol Vis Sci, 50 (2009) 2301-2307.

[62] L.A. Hutton-Smith, E.A. Gaffney, H.M. Byrne, P.K. Maini, D. Schwab, N.A. Mazer, A Mechanistic Model of the Intravitreal Pharmacokinetics of Large Molecules and the Pharmacodynamic Suppression of Ocular Vascular Endothelial Growth Factor Levels by Ranibizumab in Patients with Neovascular Age-Related Macular Degeneration, Mol Pharm, 13 (2016) 2941-2950.

[63] M.K. Taichiro Miyake, Osamu Sawada, Tomoko Sawada, Hajime Kawamura, Masahito Ohji, The Minimum Dose of Intravitreal Injection of Bevacizumab Effective against Vascular Endothelial Growth Factor in Macaque Eyes, Investigative Ophthalmology and Visual Science, 52 (2011) 5635.

[64] N. Papadopoulos, J. Martin, Q. Ruan, A. Rafique, M.P. Rosconi, E. Shi, E.A. Pyles, G.D. Yancopoulos, N. Stahl, S.J. Wiegand, Binding and neutralization of vascular endothelial growth factor (VEGF) and related ligands by VEGF Trap, ranibizumab and bevacizumab, Angiogenesis, 15 (2012) 171-185.

[65] E.M. Del Amo, A.K. Rimpela, E. Heikkinen, O.K. Kari, E. Ramsay, T. Lajunen, M. Schmitt, L. Pelkonen, M. Bhattacharya, D. Richardson, A. Subrizi, T. Turunen, M. Reinisalo, J. Itkonen, E. Toropainen, M. Casteleijn, H. Kidron, M. Antopolsky, K.S. Vellonen, M. Ruponen, A. Urtti, Pharmacokinetic aspects of retinal drug delivery, Prog Retin Eye Res, 57 (2017) 134-185.

[66] X. Wang, J. Dong, Q. Wu, Twenty-four-hour measurement of IOP in rabbits using rebound tonometer, Vet Ophthalmol, 16 (2013) 423-428.

[67] W. Xu, H. Wang, F. Wang, Y. Jiang, X. Zhang, W. Wang, J. Qian, X. Xu, X. Sun, Testing toxicity of multiple intravitreal injections of bevacizumab in rabbit eyes, Can J Ophthalmol, 45 (2010) 386-392.

[68] H.C. Mahler, W. Friess, U. Grauschopf, S. Kiese, Protein aggregation: pathways, induction factors and analysis, J Pharm Sci, 98 (2009) 2909-2934.

[69] M. Fei, Q. Zhang, L. Zhang, X. Zhu, C. Du, Z. Zhang, Development and validation of aggregates analysis method in analytical similarity assessment of HLX04 vs Avastin(R), J Pharm Biomed Anal, 223 (2023) 115121.

[70] N. Chennamsetty, B. Helk, V. Voynov, V. Kayser, B.L. Trout, Aggregation-prone motifs in human immunoglobulin G, J Mol Biol, 391 (2009) 404-413.

[71] M. Veurink, Y. Westermaier, R. Gurny, L. Scapozza, Breaking the aggregation of the monoclonal antibody bevacizumab (avastin(R)) by dexamethasone phosphate: insights from molecular modelling and asymmetrical flow field-flow fractionation, Pharm Res, 30 (2013) 1176-1187.

[72] A.-R. Cho Lee, Size matters: differential property of hyaluronan and its fragments in the skin-relation to pharmacokinetics, immune activity and wound healing, Journal of Pharmaceutical Investigation, (2023).

[73] C. Buckley, E.J. Murphy, T.R. Montgomery, I. Major, Hyaluronic Acid: A Review of the Drug Delivery Capabilities of This Naturally Occurring Polysaccharide, Polymers, 14 (2022) 3442.

[74] B.M. Lee, S.J. Park, I. Noh, C.H. Kim, The effects of the molecular weights of hyaluronic acid on the immune responses, Biomater Res, 25 (2021) 27.

[75] S. Yu, S. Wang, L. Xia, H. Hu, M. Zou, Z. Jiang, J. Chi, Y. Zhang, H. Li, C. Yang, W. Liu, B. Han, Injectable self-crosslinking hydrogels based on hyaluronic acid as vitreous substitutes, Int J Biol Macromol, 208 (2022) 159-171.

[76] R. Razeghinejad, M.M. Lin, D. Lee, L.J. Katz, J.S. Myers, Pathophysiology and management of glaucoma and ocular hypertension related to trauma, Surv Ophthalmol, 65 (2020) 530-547.

[77] D. Shi, D. Beasock, A. Fessler, J. Szebeni, J.Y. Ljubimova, K.A. Afonin, M.A. Dobrovolskaia, To PEGylate or not to PEGylate: Immunological properties of nanomedicine's most popular component, polyethylene glycol and its alternatives, Advanced Drug Delivery Reviews, 180 (2022).

[78] T.T. Hoang Thi, E.H. Pilkington, D.H. Nguyen, J.S. Lee, K.D. Park, N.P. Truong, The Importance of Poly(ethylene glycol) Alternatives for Overcoming PEG Immunogenicity in Drug Delivery and Bioconjugation, Polymers (Basel), 12 (2020).

[79] FDA, Endotoxin Testing Recommendations for Single-Use Intraocular Ophthalmic Devices. Guidance for Industry and Food and Drug Administration Staff, in, https://www.fda.gov/regulatory-information/search-fda-guidance-documents/endotoxin-testing-recommendations-single-use-intraocular-ophthalmic-dev, 2015.

4

6   SUPPORTING INFORMATION
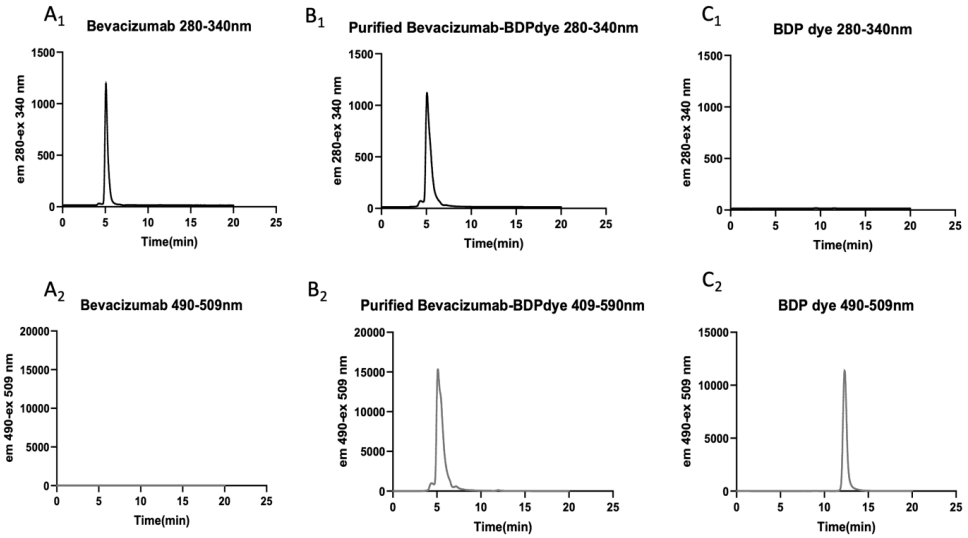
SI-Figure 1 SEC chromatograms of A) bevacizumab at excitation emission wavelengths of 280 and 340 nm, respectively, (A1) and excitation 409 and emission 509 nm (A2); B) Bevacizumab-BDP after purification with a Zeba spin column at excitation 280 and emission 340 nm (B1) and excitation 409 and emission 509 nm (B2); C) free BDP dye excitation 280 and emission 340 nm (C1) and excitation 409 and emission 509 nm (C2).
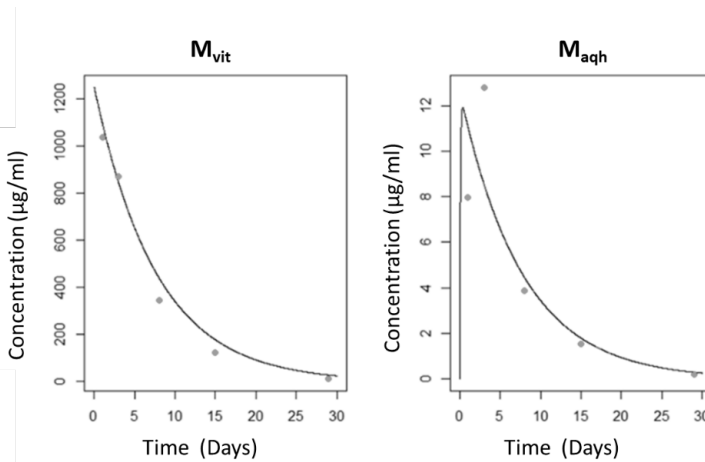
SI-Figure 2 Comparison of experimental data and fitted equations for estimating the PK parameters of free bevacizumab in rabbit eyes following intravitreal injections (dots are experimental data from Bakri et al.[54] and the lines are fitted by least square method (Model in Figure 1 A).
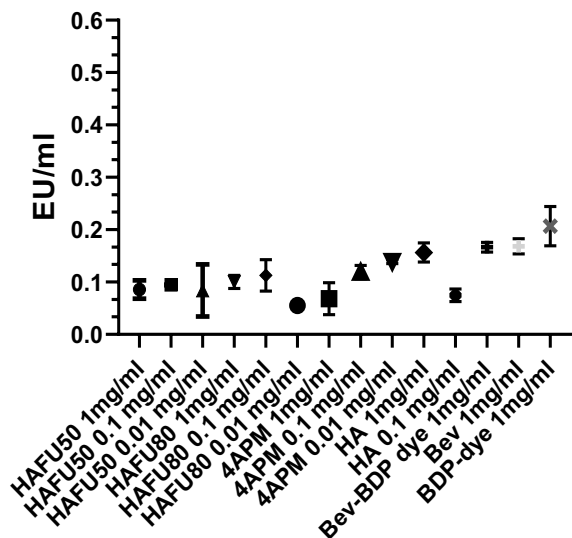
SI-Figure 3 Endotoxin levels of HAFU with degree of modification 50 and 80%, 4APM , bevacizumab-BDP dye (Bev-BDP dye), bevacizumab (Bev) and BDP dye.
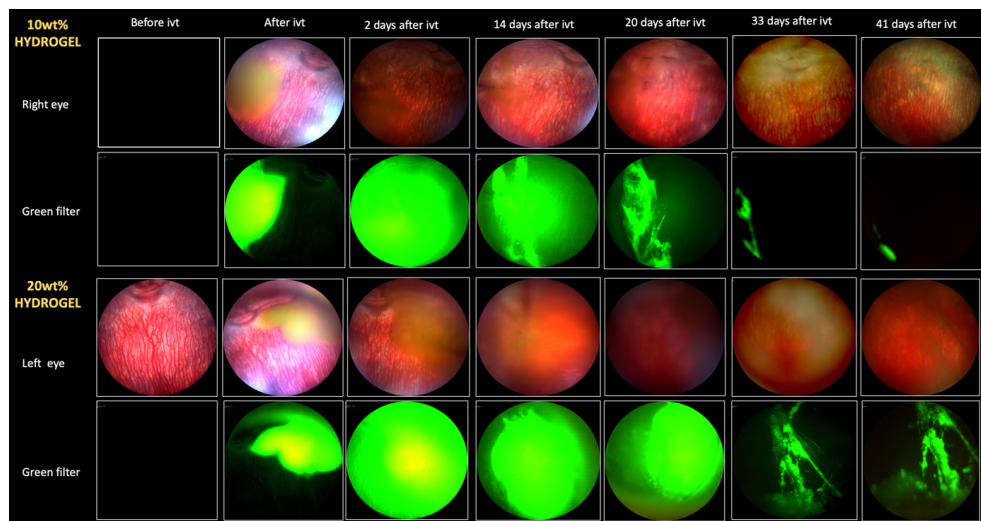
SI-Figure 4 Full color and green fluorescent fundus images of rabbit-2 eyes before and after day 2, 14, 20, 33 and 41 post intravitreal injection (IVT) of bevacizumab-BDP dye 10-20wt% 4APM_HAFU (1:3).

4
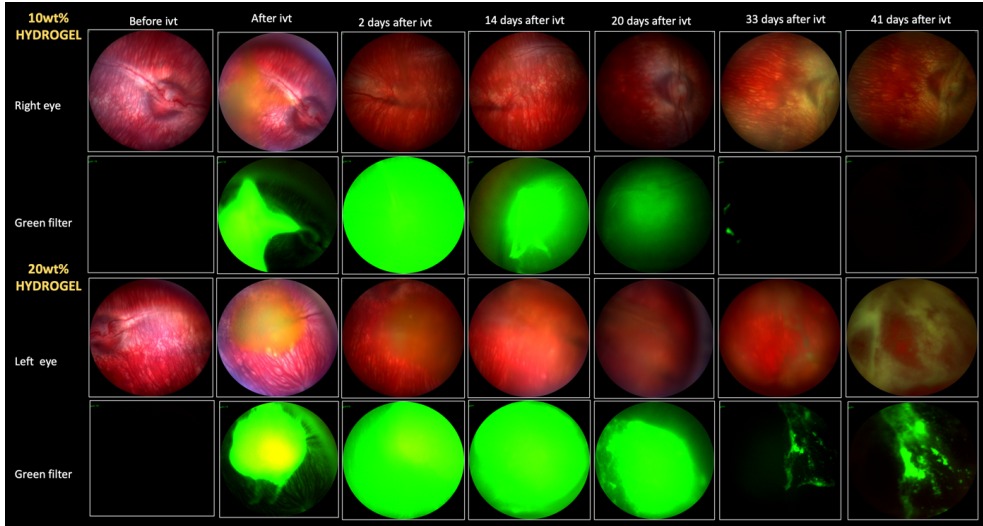
SI-Figure 5 Full color and green fluorescent fundus images of rabbit-4 eyes before and after day 2, 14, 20, 33 and 41 post intravitreal injection (IVT) of bevacizumab-BDP dye 10-20wt% 4APM_HAFU (1:3).

4
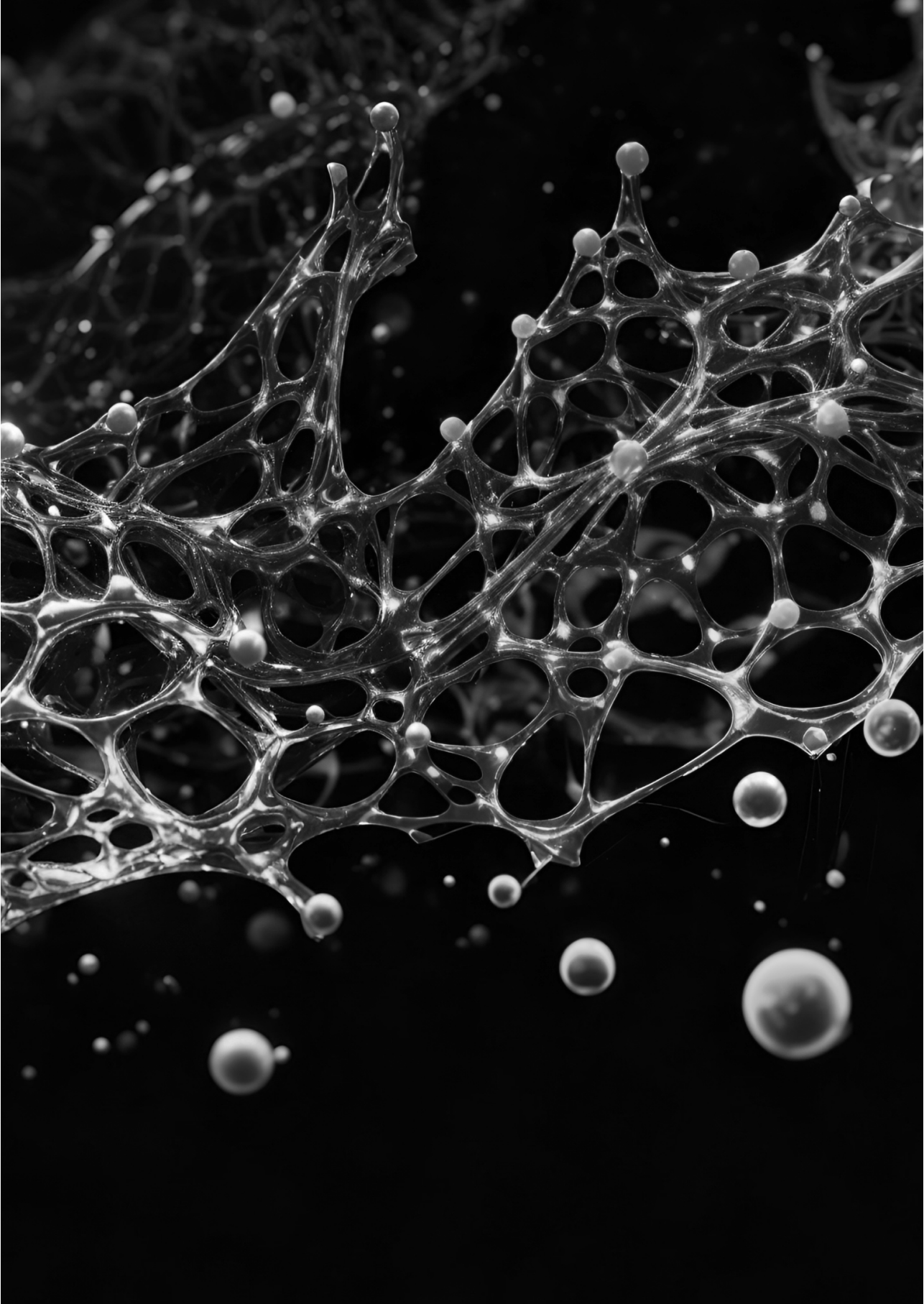
Chapter 5

Thermo-Responsive Diels-Alder Stabilized Hydrogels for Ocular Drug Delivery of a Corticosteroid and an Anti-VEGF FAB Fragment

Blessing C. Ilochonwu[1], Simone A. van der Lugt[1], Ada Annala[1], Greta Di Marco[1], Thibault Sampon[1], Juergen Siepmann[2], Florence Siepmann[2], Wim E. Hennink[1], Tina Vermonden[1]

[1]Department of Pharmaceutics, Utrecht Institute for Pharmaceutical Sciences, Faculty of Science, Utrecht University, PO box 80082, 3508 TB Utrecht, the Netherlands. [2]University of Lille, College of Pharmacy, 3 Rue du Prof. Laguesse, 59006 Lille, France INSERM U 1008, Controlled Drug Delivery Systems and Biomaterials, 3 Rue du Prof. Laguesse, 59006 Lille, France.

ABSTRACT

In the present study, a novel *in situ* forming thermosensitive hydrogel system was investigated as a versatile drug delivery system for ocular therapy. For this purpose, two thermosensitive ABA triblock copolymers bearing either furan or maleimide moieties were synthesized, named respectively poly(NIPAM-co-HEA/Furan)-PEG$_{6K}$-P(NIPAM-co-HEA/Furan) (PNF) and poly(NIPAM-co-HEA/Maleimide)-PEG$_{6K}$-P(NIPAM-co-HEA/-Maleimide) (PNM). Hydrogels were obtained upon mixing aqueous PNF and PNM solutions followed by incubation at 37 °C. The hydrogel undergoes an immediate (less than 1 minute) sol-gel transition at 37°C. *In situ* hydrogel formation at 37 °C was also observed after intravitreal injection of the formulation into an *ex vivo* rabbit eye. The hydrogel network formation was due to physical self-assembly of the PNIPAM blocks and a catalyst-free furan-maleimide Diels–Alder (DA) chemical crosslinking in the hydrophobic domains of the polymer network. Rheological studies demonstrated sol-gel transition at 23 °C, and DA crosslinks were formed in time within 60 minutes by increasing the temperature from 4 to 37 °C. When incubated at 37 °C, these hydrogels were stable for at least one year in phosphate buffer of pH 7.4. However, the gels degraded at basic pH 10 and 11 after 13 and 3 days, respectively, due to hydrolysis of ester bonds in the crosslinks of the hydrogel network. The hydrogel was loaded with an anti-VEGF antibody fragment (FAB; 48.4 kDa) or with corticosteroid dexamethasone (dex) by dissolving (FAB) or dispersing (DEX) in the hydrogel precursor solution. The FAB fragment in unmodified form was quantitatively released over 13 days after an initial burst release of 46, 45 and 28 % of the loading for the 5, 10 and 20 wt% hydrogel, respectively, due to gel dehydration during formation. The low molecular weight drug dexamethasone was almost quantitively released in 35 days. The slower release of dexamethasone compared to the FAB fragment can likely be explained by the solubilization of this hydrophobic drug in the hydrophobic domains of the gel. The thermosensitive gels showed good cytocompatibility when brought in contact with macrophage-like mural cells (RAW 264.7) and human retinal pigment epithelium-derived (ARPE-19) cells. This study demonstrates that PNF-PNM thermogel may be a suitable formulation for sustained release of bioactive agents into the eye for treating posterior segment eye diseases.

Keywords: Hydrogel, FAB, Anti-VEGF, Dexamethasone, Diels-Alder, injectability, in situ crosslinking

Graphical abstract:

Ocular drug delivery
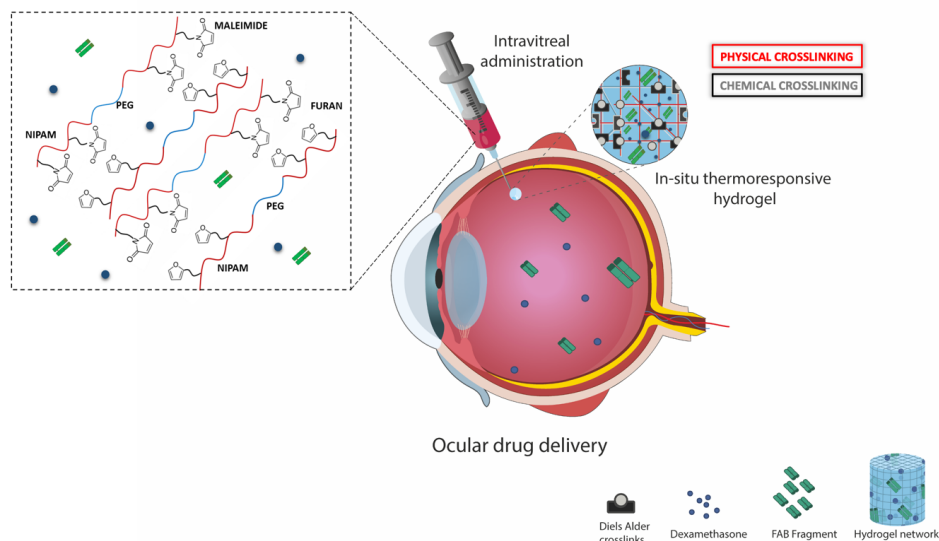
1 INTRODUCTION

Ocular vascular diseases are one of the leading causes of visual impairment worldwide.[1-3] In general, it has been shown that there is an increased number of pro-inflammatory cells and increased levels of vascular endothelial growth factor (VEGF) in the posterior segment of the diseased eye, resulting in neovascularization and vaso-permeability[1, 4]. The current treatment consists of administering anti-VEGF antibodies or an anti-inflammatory drug such as the corticosteroid dexamethasone (DEX), or a combination of these drug[5-9].

Despite being efficacious in controlling ocular neovascularization and inflammation, long-term intraocular drug therapy has certain drawbacks. After IV/oral administration only a fraction of the administered dose reaches the back of the eye due to physiological barriers preventing drugs from reaching the retina.[7, 10] To bypass ocular barriers, clinically used intraocular drug formulations (such as Lucentis®, Eylea®, Kenalog®-40) are administered by intravitreal bolus injection. The advantages of this administration route above others include immediate drug release, increased local therapeutic effects and reduced systemic adverse events[11]. The intravitreal half-life of dexamethasone in vitreous is only 5.5 h [12], while the intravitreal half-life of ranibizumab (an FDA approved anti-VEGF Fab fragment) is around three days. [6, 13] Therefore, repeated injections are required for the treatment of chronic intraocular diseases[14, 15]. Although conventional drug formulations such as eye drops and injectable liquids play an important role in ocular therapies, they are characterized by poor patient compliance and adverse side effects [16]. Hence, to overcome these drawbacks, there is a need for new delivery systems that provide local sustained release of loaded drugs to the retina after intravitreal injection. Several advanced delivery systems have been developed and investigated for this purpose, such as drug loaded surgically sutured implants, nanoparticles, liposomes, polymeric micelles,

dendrimers, microneedles and hydrogels.[16-18] Several implants for the treatment of the posterior segment of the eye are on the market or studied in clinical trials[18] among which the non-biodegradable formulations Vitrasert®, Retisert®[19, 20], Medidur®, Iluvien®[21] and the biodegradable ones Posurdex®, Ozurdex®[22, 23] and Surodex®[24]. However, these implants all contain small molecules such as dexamethasone, ganciclovir or fluocinolone acetonide. However, only a few biotherapeutics-carrying implants are on the market. Genentech's Susvimo, previously called Port Delivery System with ranibizumab[25, 26], is the first and only FDA-approved (in October 2021) protein refillable implant based on a porous titanium release control element used for the treatment of neovascular age-related macular degeneration[27]. Although these implants significantly prolong drug release in the posterior segment of the eye, the majority of these intraocular implants requires invasive administration methods to place the devices at the target site, and subsequent surgical procedures are often needed to remove these non-biodegradable implants.

Hydrogels, hydrophilic crosslinked polymers containing a large amount of water, are widely used for drug delivery, tissue engineering and cell encapsulation.[28-32] Furthermore, by a proper selection of their building blocks, hydrogels can be rendered biodegradable due to chemical and/or enzymatic hydrolysis.[33-35] There are a few hydrogel formulations approved by the FDA for ocular applications, among which Akten, a topical lidocaine hydrochloride ophthalmic gel.[36, 37] Several hydrogel and other delivery technologies systems are currently being investigated for intravitreal protein delivery, as reviewed by Ilochonwu et al. [31] and Chang et al. [32]

In the past years, in situ forming hydrogels based on PEG and/or hyaluronic acid have received interest for ocular drug delivery applications.[38, 39] These hydrogels showed *in vitro* sustained drug release and may play an important role in advancing the currently available ocular therapy as previously discussed by Ilochonwu et al.[38] Although significant progress has been made, several issues still have to be addressed: 1) fast *in situ* gelling of the formed hydrogels is needed as this limits polymer diffusion and dilution within the vitreous body after intravitreal injection and 2) unwanted side reactions between polymer functional groups and loaded drugs must be avoided. Depending on the chemical composition of the polymer building blocks, hydrogels can be designed to respond to various stimuli, such as heat, pH and light.[40-42] An important and attractive class of hydrogels are the thermosensitive in situ forming systems. At ambient temperature, these formulations are low viscous aqueous polymeric solutions, and a temperature change (from room to physiological temperature), affects the hydrophobic and hydrophilic balance of the constituents of the polymer to induce a sol-gel transition of the formulation.[40] Poly(N-isopropylacrylamide) (PNIPAM) is a well-studied thermosensitive polymer which displays lower critical solution temperature (LCST) in aqueous solutions at around 32°C and this polymer has been used as basis for preparation of thermosensitive hydrogels. This way, a liquid formulation can be injected into the vitreous with a minimally invasive method using a small gauge needle, avoiding a surgical intervention.[43, 44] However, the physical crosslinking is reversible and yields gels with low mechanical properties[45]. Therefore, chemical crosslinking has been investigated as a strategy for increasing the hydrogel strength and stabilizing the network structure [46, 47]. For proper injectability, the physical and covalent gelation should only

occur at the site of injection and for sure not in the applied needle which would result in unwanted obstruction. Furthermore, after ocular administration, the crosslinking reactions between the functional moieties should be relatively fast to avoid unwanted reactions and modifications of co-administered pharmaceuticals and drugs. In this study, the Diels-Alder (DA) reaction was used to stabilize the hydrogel network as chemical crosslinking strategy. In general, DA reaction is a [4+2] cycloaddition between a diene and dienophile to form a cyclohexene adduct and was first reported by Alder and Diels in 1929 [48]. In 2009, Wei et al. for the first time employed DA reactions for the preparation of a hydrogel.[49] The reaction between furan and maleimide is the most common DA reaction used for hydrogel crosslinking. However, unfavorable reactions between maleimides and amines or thiols present in e.g. proteins limit the application of this reaction pair for development of protein releasing hydrogels.[50] To overcome this drawback, in the present study, the reactive functional groups were designed to be predominantly located within the hydrophobic domains of the hydrogel polymeric network, to limit protein reactivity with the maleimide moieties as was observed in our previous study.[38]

Therefore, to tackle the current challenges of 1) fast in-situ gelation and 2) prevention of side reactions between therapeutics and crosslinkable groups, we designed a novel injectable hydrogel system. This study investigates the combination of DA crosslinks with thermosensitive gelation. The thermo-responsive DA stabilized hydrogel formulation was characterized and evaluated as a potential drug delivery system for ocular therapy. The aim was to load the engineered hydrogel with dexamethasone and a Fab fragment of an anti-VEGF antibody as drugs and to investigate their gelation kinetics, degradation behavior and release profiles. Compared to previously discussed Diels- Alder hydrogels [35, 38, 39], the anticipated advantages of the present hydrogel system include faster in situ gelation due to thermo-responsive behavior, suitability for simultaneous delivery in one formulation both a biotherapeutic, preventing protein modification, and a small hydrophobic drug. Finally, intravitreal injection of the hydrogel on *ex vivo* rabbit eye explant and retinal cell cytocompatibility were investigated the injection procedure, in situ gel formation and the overall usability of this system for intraocular applications.

2   MATERIAL & METHODS

2.1   Materials

Chemicals were purchased from Sigma-Aldrich (Zwijndrecht, the Netherlands) and used as received unless mentioned otherwise. Dichloromethane (DCM) and tetrahydrofuran (THF) were dried on molecular sieves 24h before use. Phosphate-buffered saline was composed as follows except mentioned otherwise: 0.13 M NaCl, 2.7 mM KCl, 10 mM Na_2HPO_4, and 1.9 mM KH_2PO_4, pH 7.4.

2.2   Synthesis of Polymers

2.2.1   Synthesis of PEG6kDA macroinitiator

PEG was functionalized with α-bromoisobutyrylbromide to yield an ATRP macroinitiator using a procedure described by De Graaf et al.[51] Briefly, dehydrated PEG 6 kDa (10.0 g) was dissolved in 100 mL dry THF at 50 °C under a nitrogen atmosphere. Triethylamine and α-bromoisobutyrylbromide were added (1.5 eq to the hydroxyl groups). The mixture was stirred overnight at room temperature. The formed TEA bromide salt was filtered off and the filtrate was concentrated under vacuum, subsequently dissolved in water (20 mL) and centrifuged (5500 g, 5 min, 25 °C). The supernatant was filtered with a filter paper and the filtrate was dialyzed (3.5 kDa MWCO) against water for two days and then freeze-dried. The product dissolved in CDCl$_3$ was characterized by ^{1}H NMR spectroscopy. ^{1}H-NMR analysis showed the formation of a fully functionalized PEG ATRP macroinitiator. ^{1}H-NMR (CDCl$_3$): δ = 4.3 (t, 4H, OCH$_2$), 3.85 (t, 4H, OCH$_2$), 3.65 (t, 531H, OCH$_2$), 3.35 (t, 4H, OCH$_2$), 1.85 ppm (s, 12H, CCH$_3$). The absence of PEG hydroxyl groups was confirmed by adding two drops of trichloroacetyl isocyanate (TAIC) to the NMR sample to react with possible present unmodified OH groups [52].

2.2.2   Synthesis of P(NIPAM-co-HEA)-PEG-P(NIPAM-co-HEA) (PNH)

PEG 6 kDa macroinitiator (500 mg; 0.083 mmol) was dissolved in 20 mL H$_2$O. Subsequently, NIPAM (2.54 g; 22.5 mmol), CuBr (50 mg; 0.35 mmol) and 2-hydroxyethyl acrylate (HEA) (280 μL; 2.4 mmol) were added and dissolved. The solution was deoxygenated by flushing with nitrogen gas for 15 minutes at room temperature and additionally 15 minutes on ice. The reaction was started by adding tris[2-(dimethylaminoethyl]amine (Me6-TREN) (90 mL; 0.34 mmol) to the reaction mixture, which resulted in a color change from colorless to green/blue. The reaction was carried out for three hours on ice under nitrogen atmosphere. The reaction mixture was subsequently dialyzed against water for 48 h at 4 °C (dialysis tube MWCO 6-8 kDa, Thermo Scientific, Bleiswijk, the Netherlands). The product as white powder was obtained after freeze drying and is further named as PNH. The polymer molecular weight was determined by 1H NMR and GPC. ^{1}H NMR spectrum of PNH in D$_2$O. δ (ppm): 1.13 (6H, CH$_3$CHCH$_3$, NIPAM); 1.30-2.30 (backbone hydrogens); 3.68 (545H, CH$_2$OCH$_2$, PEG); 3.78 (2H, CH$_2$OCO, HEA); 4.20 (2H, CH$_2$OH, HEA); 3.87 (1H, CH$_3$CHCH$_3$, NIPAM); 4.79 (D$_2$O).

2.2.3   Synthesis of P(NIPAM-co-HEA/Maleimide)-PEG-P(NIPAM-co-HEA/Maleimide) (PNM)

PNH (1.00 g; 0.023 mmol, 43.5 kDa) was dissolved in 20 mL dry DCM by stirring for 30 minutes on ice under nitrogen atmosphere. N,N'-dicyclohexylcarbodiimide (DCC) (107 mg; 0.52 mmol), 4-(dimethylamino)pyridine (DMAP) (0.64 mg; 0.0052 mmol) and 6-maleimidohexanoic acid (110 mg; 0.52 mmol) and thus 0.63 eq of HEA in PNH can potentially be modified) were added and the mixture was stirred for 1 h on ice. Next, the reaction mixture was stirred for 16 h at RT, and the formed product was collected by filtration after dropping the reaction mixture in cold diethyl ether. The precipitate was subsequently dissolved in 50 mL H$_2$O, the remaining solid was filtered off using a 0.45 μm syringe filter, and the filtrate was freeze-dried overnight. The obtained product, further named PNM, was collected as a white powder.^{1}H NMR spectrum of PNM in CDCl$_3$:

δ (ppm) 1.13 (6H, CH$_3$CHCH$_3$, NIPAM); 1.30-3.0 (backbone hydrogens); 3.68 (4H, OCH$_2$CH$_2$O, PEG); 4(1H, CH$_3$CCH$_3$, NIPAM); 4.23 (4H, OCH$_2$CH$_2$O) 6.71 (2H, maleimide); 7.26 (CDCl$_3$).

2.2.4 Synthesis of P(NIPAM-co-HEA/Furan)-PEG-P(NIPAM-co-HEA/Furan) (PNF)

PNH (1.00 mg; 0.023 mmol, 43.5 kDa) was dissolved in 25 mL CDCl$_3$ and stirred for 30 minutes while flushed with nitrogen gas. Next, 3-(2-furyl)propionic acid (73 mg; 0.52 mmol; this mean that 0.63 eq HEA in PNH can potentially be modified), DCC (108 mg; 0.52 mmol) and DMAP (0.64 mg; 0.0052 mmol) were added and the mixture was stirred for 16 h at RT. The reaction mixture was dropped in cold diethyl ether and the formed precipitate after filtration was subsequently dissolved in 40 mL H$_2$O. The remaining solid was filtered off using a 0.45 µm syringe filter, the filtrate was freeze-dried overnight, and the product, further named PNF, was collected as a white powder. ^{1}H NMR spectrum of PNF in CDCl$_3$: δ (ppm) 1.13 (6H, CH$_3$CHCH$_3$, NIPAM); 1.30-3.0 (backbone hydrogens); 3.68 (4H, OCH$_2$CH$_2$O, PEG 6 kDa); 4.0 (1H, CH$_3$CHCH$_3$, NIPAM); 4.23 (4H, OCH$_2$CH$_2$O) 6.01 (1H, CCHCH, Furan); 6.26 (1H, CHCHCH, Furan); 7.29 (1H, CHCHO, furan); 7.26 (CDCl$_3$).

2.3 Polymer Characterization

2.3.1 ^{1}H NMR spectroscopy

The synthesized polymers were characterized with ^{1}H NMR spectroscopy using a Bruker 600Hz MR-NMR spectrometer (Bruker BioSpin GmbH). Data analysis was performed using MestReNova Software. The chemical shifts are referred to the residual solvent peak (δ= 7.26 ppm for CDCl$_3$ and δ= 4.80 ppm for D$_2$O).

2.3.2 Cloud point determination

Samples of the thermosensitive polymers were dissolved in PBS at a concentration of 3 mg/ml. The cloud point (CP) was measured using a Jasco FP-8300 spectrophotometer (JASCO, Easton, MD) with a water-cooled Peltier thermostatted 4-position automatic cell changer. The Spectra Manager program was used for measuring scattering at a wavelength of 650 nm while the temperature was raised from 4 to 40 °C at a rate of 1 °C.min^{-1}. The onset point of increased scattering intensity is reported as CP [53].

2.3.3 Rheological characterization

The rheological properties of the formulations were studied using a Discovery HR-2 Rheometer (TA Instruments Inc., Etten-Leur, the Netherland) with a Peltier Plate for temperature control and solvent trap to prevent evaporation of the solvent. Empty and drug loaded PNF-PNM hydrogel formulations with different polymer concentrations (5, 10, 15 wt%) were prepared as described in section 2.4., after mixing the polymer/drug solutions, the resulting solution was placed under the geometry and measured using a plate-plate geometry (aluminum, 20 mm diameter, initial gap was 200 µm). Normal force was controlled during the experiments to enable measurements of samples while volume changes occur. Data were processed using TRIOS Software version 5.0. The storage (G') and loss (G") moduli were measured during a temperature ramp ranging from 4 up to

37 °C at a rate of 0.5 °C.min^{-1} and at a strain 0.5 %. Next, the sample was kept at 37 °C for 30 min and then a frequency sweep ranging between 0.1-100 rad.s^{-1} was performed at strain 0.5 %. The samples were then cooled down from 37 to 4 °C at a rate of 0.5 °C.min^{-1}. From the average G' at 37 °C, the mesh size (ξ in m) of the formed hydrogels was calculated according to the following equation[54], using Avogadro's number (N_{av}) in mol^{-1}, R the molar gas constant in J.K^{-1}.mol^{-1}, and the temperature (T) in K and G' in Pa:

$$\xi = (\frac{G' * N_{av}}{RT})^{-1/3}$$

2.3.4 FTIR analysis

Fourier Transform Infrared (FTIR) spectra were measured for the PNF and PNM polymers and for a dried 10 wt% PNF-PNM hydrogel. The samples were measured as dried solid powers. The spectra, ranging from 600 cm^{-1} to 4000 cm^{-1}, were recorded with a Perkin Elmer Spotlight FT-IR Spectrometer.

2.3.5 Gel permeation chromatography

Polymer samples were dissolved in the eluent, 10 mM LiCl in DMF, at a concentration of 3 mg/mL. The number average molecular weight (M_n) and polydispersity index (PDI) were determined through gel permeation chromatography (GPC), using a Waters 2695 Alliance (Waters Corporation, Milford, MA) with refraction Index detector and with a PLgel 5 μm Mixed-D column. The analysis was performed with the column set at 65 °C and 1 mL/min flow rate. Empower software was used for data analysis. A calibration curve was obtained by measuring PEG standards of narrow molecular weight (Polymer Standard Service GmbH, Mainz, Germany).

2.3.6 DMA characterization

DMA 2980 Dynamic Mechanical Analyzer (TA-Instruments, Etten-Leur, the Netherlands) was used to determine Young's modulus of the hydrogels as previously reported [38] Thermosensitive DA hydrogel samples were prepared as described in section 2.4.1. The gels (diameter 2.6 mm, 5.2 mm height) were placed between the parallel plates, and a force ramp was applied at a rate of 0.5 N/min up to a total force of 8 N at room temperature. The obtained data were analyzed using TA Universal Analysis software and the Young's modulus (E) was calculated from the slope of the linear section of the stress-strain curve. Data are reported as mean ± standard deviation (n=3).

2.4 Preparation of PNF-PNM hydrogels

2.4.1 Non-loaded PNF-PNM hydrogels

PNF and PNM were separately dissolved in PBS (pH 7.4) on ice. The concentrations ranged from 3 to 20 wt% (except when mentioned otherwise). To obtain hydrogels, PNF and PNM solutions

were mixed (weight ratio PNF/PNM 1:1, molar ratio furan/maleimide 1:1) to obtain 80 mg hydrogel formulation (except when mentioned otherwise) at the desired total polymer concentration (3-20 wt%). To form the gels, the polymer solutions were incubated in cylindrically shaped plastic moulds (diameter 4.5 mm, 5 mm height) at 37 °C for 3 h (to allow full chemical DA crosslinking). During the incubation at 37 °C, the gels shrunk and expelled some liquid. After gel formation, the gels were transferred into glass vials for further use, either including expelled liquid (for release experiments) or excluding expelled liquid (for degradation experiments).

2.4.2 Preparation of FAB loaded PNF-PNM hydrogels

FAB antibody (3.1 mg/mL) biosimilar to Lucentis® (Ranibizumab) was received from Boehringer Ingelheim, Germany. This FAB antibody is a FAB fragment of the monoclonal antibody Bevacizumab expressed in E. coli. with a mass of 48.4 kDa. The protein was delivered in a mixture of two buffers, 54 (v/v) % buffer 1 (20 mM (CH_3COONa), 8.5 mM (CH_3COOH), 1.1 N ($NH_4)_2SO_4$, pH 5.0) and 46 v/v % buffer 2 (20 mM (CH_3COONa), 10.5 mM (CH_3COOH), pH 5.0). This buffer solution was exchanged by PBS using a ZebaTM Spin Desalting Column (7K MWCO, Thermo Scientific) and a 2.53 mg/mL PBS FAB antibody solution was obtained (concentration determined by SEC ULPC). FAB loaded hydrogels were prepared according to section 2.4.1 with some modifications. Different gel concentrations (5-20 wt%) were prepared by weighing equal amounts of PNM and PNF, which were separately dissolved (at 4 °C within <2 h) in PBS (volume adjusted based on final polymer concentration) and in PBS containing FAB antibody (48 μL, 2.53 mg/mL), respectively. The obtained PNF-FAB /PNM solutions were mixed to form 80 mg hydrogel formulations (ratio 1:1 furan/ maleimide) and incubated in cylindrically shaped plastic moulds (diameter 4.5 mm, 5 mm height) at 37 °C for 3 h (to allow full chemical DA crosslinking) to obtain a PNF-PMN hydrogels loaded with 121 μg FAB protein.

2.4.3 Preparation of dexamethasone loaded PNF-PNM hydrogels

Dexamethasone-loaded hydrogels of 80 mg were prepared according to section 2.4.1. Briefly, a dex-PBS dispersion was obtained by sonicating 15.98 mg dexamethasone in 960 μL PBS for 10 sec before use. Next, equal amounts of PNF and PNM were separately dissolved in PBS (volume adjusted based on final polymer concentration) and in dex-PBS (24 μL, 16.67 mg/mL) respectively, on ice. The PNF solution was mixed with the PNM-dex suspension to obtain a total polymer concentration of 3, 10, or 20 wt% (molar ratio 1:1 furan/ maleimide) unless indicated otherwise.

The PNM-dex dispersion was heated to 37 °C for 15 minutes prior to mixing with the cold PNF PBS solution. The mixture was transferred into cylindrically shaped plastic moulds (diameter 4.5 mm, 5 mm height) and incubated for 3 h(to allow full chemical DA crosslinking) at 37 °C to obtain a PNF-PMN hydrogel loaded with 400 μg dexamethasone.

2.5   Swelling and degradation characteristics of PNF-PNM hydrogels

2.5.1   Swelling and degradation of PNF-PNM hydrogels in PBS buffer (pH 7.4)

Empty PNF-PNM hydrogels with different concentrations (5, 10, 15 wt%) were prepared as described in section 2.4.1 (n=3). The polymer solutions were transferred into a cylindrically shape plastic mould and the samples were incubated for 3 h (to allow full chemical DA crosslinking) at 37 °C. Only the hydrogels (without the expelled fluid, see below figure 1) were removed from the mould and weighed in a glass vial after which 1 mL PBS (pH 7.4) was added and the gels were incubated at 37 °C. To determine swelling and degradation of the hydrogels, at different time points the supernatant was removed and the gel was weighed at room temperature. Afterwards, 1 mL fresh PBS was added. The swelling ratio of the hydrogel at a certain time point is defined as the weight (W_t) divided by the initial hydrogel weight (W_0).

2.5.2   Swelling and degradation of PNF-PNM hydrogels in BBS and PB buffer (pH 10 and 11)

Empty hydrogels (5 wt%) were prepared (n=3) as described in section 2.4.1. The formed hydrogels were removed from the mould and transferred into glass vials and weighed. Next, 1 mL of either borate buffered saline (BBS) (pH 10; 0.01 M H_3BO_3, 0.04 M KCl, 6 mM NaOH) or phosphate-buffer (PB) (pH 11; 0.138 M Na_2HPO_4, 61.8 mM Na_3PO_4) was added and the samples were incubated at 37 °C. Subsequently, at multiple time points, the buffer was removed, and the gels were weighed, and the swelling ratios were determined as described in (section 2.5.1).

2.6   Drug release from PNF-PNM hydrogels

2.6.1   FAB release from PNF-PNM hydrogels

Fab-loaded hydrogels were prepared as described in section 2.4.2. The crosslinked gels together with the expelled fluid were transferred into glass vials, and subsequently 300 µl PBS with 0.02 % NaN_3 (to prevent bacterial growth) was added, and the vials were incubated at 37 °C. Note that the time point at which 300 µl PBS was added is considered as t = 0 for the release studies as depicted schematically in figure 1. However, FAB had partially been expulsed (approximately, 14, 35, 52 µl for 5, 10, 20 wt% gels, respectively) from the hydrogels during the 3 h incubation in the oven. The liquid which was expelled during this 3 h oven treatment was mixed with the 300 µl PBS release medium. Release samples were taken by replacing 200 µl PBS from the vials with 200 µl of pre-warmed fresh PBS (37 °C) at multiple time points. The release samples were stored at 4°C (company recommended storage conditions) until analysis was performed. To determine the protein concentration, the samples were spun down at 2000 g for 5 minutes and 100 µl of the supernatant was taken for analysis using SE-ULPC on an ARC Acquity UPLC (Waters Corporation, Milford, USA) with an FLR-detector, operated at λ_{ex} and λ_{em} of 280 and 310 nm, respectively. Results were analyzed with Empower Software (Version 3-FR5). A calibration curve was obtained by analyzing solutions of FAB in PBS (from 1.2 to 2600 µg/mL). The standard samples (7.5 µl) and the release samples (7.5 µl) were injected onto Phenomenex BioSep-SEC-S2000 (300 x 7.80 mm) column, and the eluent was 0.3 M sodium sulphate with 100 mM sodium phosphate monobasic

monohydrate buffer (pH 6.7). The system was operated at a flow rate of 0.3 mL/min and the run time per sample was 25 minutes.
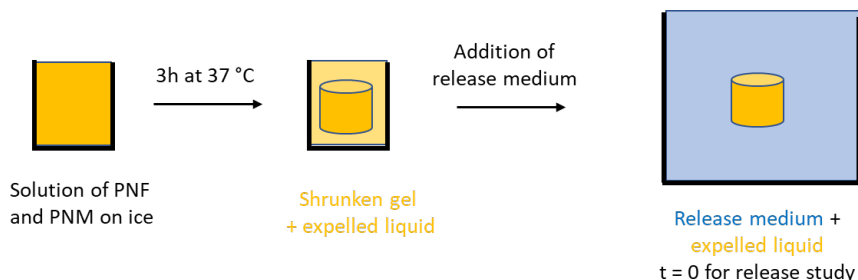
Figure 1 Schematic overview of the experimental setup of the gel formation and subsequent release study, the expelled liquid indicates the water that was expelled from the gels during shrinking.

2.6.2 Dexamethasone release from PNF-PNM hydrogels

After preparation of the different dex-loaded hydrogels (n=3, see section 2.4.3), the gels together with the expelled fluid were transferred into glass vials and   300 µl PBS with 1% tween (to solubilize released dexamethasone) and 0.02 % NaN$_3$ (to prevent bacterial growth) were added to the gels, which were subsequently incubated at 37 °C. Note that, as for FAB, the time point of adding 300 µl PBS is considered as t = 0 for the release studies. The liquid which was expelled during this 3 h oven treatment was mixed with the 300 µl PBS release medium. At different time points samples of 200 µl were taken and replaced with the same volume of fresh PBS/Tween buffer. The dissolution rate of dexamethasone particles in the release medium was also determined. In detail, a dispersion of dexamethasone crystals in PBS (16.6 mg/ml) was sonicated for 10 seconds. Subsequently, 30 µl of this dispersion was mixed with 300 µl PBS with 1% tween and incubated at 37°C. At different time points the dispersion was spun down (at 25,000 g in RT for 15 minutes) and 200 µl of supernatant was taken and replaced by the same volume of PBS with 1% tween with 0.02 % NaN$_3$. To 100 µl of the release samples or dissolution samples, 10 µl DMSO was added to ensure full solubilization of the released dexamethasone. Subsequently, the samples were spun down again at 25,000 g for 15 minutes. Samples of the supernatant (60 µl) were analyzed using Acquity UPLC (Waters Corporation, Milford, MA) equipped with UPLC CSH C18 column (100x2.1mm, 1.7 µm, 130 Å, Waters Corporation). Dexamethasone was detected at 246 nm and quantification was done using a calibration curve of 0.5 to 400 µg/mL dexamethasone in 100% acetonitrile (ACN). Gradient mobile phase was prepared using 5% ACN in water as eluent A and 100% ACN as eluent B, both containing 1% perchloric acid as pH modifier. Samples of 5 µl were injected, the was flow rate 0.75 ml/min and the gradient run from 0-100% B in 10 minutes. Results were analyzed using Empower Software (Version 3-FR5, Waters Corporation, USA).

5

2.7 FAB integrity upon incubation with PNF and PNM in buffer and after release from PNF-PNM hydrogels

2.7.1 FAB integrity upon exposure to PNF and PNM polymers

To investigate whether the integrity of FAB upon exposure to PNF and PNM was affected, SDS-PAGE analysis was used. PNF and PNM were separately dissolved in PBS (2 mg/ml) on ice. Subsequently, 50 µl FAB in PBS (2.52 mg/mL) was added to 50 µl solutions of PNF and PNM, and the obtained samples were incubated at 4 and 37 °C for 3 h and for 13 days. As control, FAB was also incubated with 4arm-PEG10K-Maleimide (PEG-Mal; obtained from JenKem Technology, USA) in PBS at the same concentration and conditions. After incubation, 4 µl samples were withdrawn. Next, 18.5 µl of PBS and 7.5 µL of solution of 250 mM Tris-HCl pH6.5 also containing 8% sodium dodecyl sulphate (SDS) 0.008% (v/v) Bromophenol Blue; and 40% (v/v) glycerol with and without β-mercaptoethanol 5% (100 mM) were added. Hereafter, the samples and controls were heated for 10 minutes at 90 °C to denature FAB. Subsequently, 28 µl of the samples and 5 µl of the PageRulerTM Prestained Protein ladder (Thermo Fischer Scientific) were pipetted into the Bolt 4-12% bis-tris-plus gel (Thermo Fischer Scientific) that was run in a Bolt MOPS SDS running buffer (Thermo Fischer Scientific) at 100- V for 1 h. The proteins in the gel were stained with Coomassie blue (Thermo Fischer Scientific) overnight and washed in demineralized water before imaging the SDS gel.

2.7.2 FAB integrity after release from PNF-PNM hydrogels

FAB loaded hydrogels were prepared as described in section 2.4.2 and the release of the protein was studied as in section 2.6.1. The integrity of the released FAB from the PNF-PNM hydrogels was investigated using SDS-PAGE as in section 2.7.1. SDS (7.5 µl) was added to 22.5 µl of the FAB release samples taken after 1 h, 1 day and 6 days.

2.8 Cytocompatibility of PNF and PNM

2.8.1 RAW 264.7 cell culture

RAW 264.7 macrophage-like mice cells (catalogue number TIB-71, ATTC, Manassas, VA, USA) were cultured in humidified conditions at 37 °C and 5% CO_2 with high glucose Gibco Dulbecco's Modified Eagle Medium (DMEM) (Sigma Aldrich, Zwijndrecht, the Netherlands) with 10% heat-inactivated fetal bovine serum (GibcoTM Thermo Fischer scientific). Cells between passage numbers 15 and 20 were used. The cells were detached from the culture flask using a cell scraper and subsequently counted with a TCTM automated cell counter (Biorad). Next, the cells were seeded in a flat bottom Greiner CellStar 96-well plate (#665090; GreinerBio-One GmbH, GE) at a density of 100,000 cells/cm^2 and allowed to attach overnight prior to experiments.

2.8.2 ARPE-19 cell culture

Human retinal pigment epithelium derived ARPE-19 cells (catalogue number CRL 2302, ATTC) were cultured in humidified conditions at 37 °C and 5% CO_2 with high glucose Gibco Dulbecco's Modified Eagle Medium/Nutrient Mixture F-12 (DMEM/F12) with 10% FBS and 1% L-glutamine.

Cells between passage numbers 13 and 20 were used, detached from the culture flask using a trypsin EDTA solution and counted with a TCTM automated cell counter (Biorad). Next, the cells were seeded in a flat bottom polystyrene 96-wells plate at a density of 32,000 cells/cm^2 and allowed to attach overnight prior to experiments.

2.8.3 Alamar Blue cytotoxicity assay on RAW 264.7 and ARPE-19 cells exposed to the polymers PNF and PNM

After cell culture (see 2.8.1 and 2.8.2), the cell medium was refreshed and the cells were incubated with 100 µl complete cell culture medium containing PNF or PNM (concentration from 0 to 5 mg/mL (n=3)). After 24 h incubation at 37 °C, the medium was refreshed and 10 µl of AlamarBlue reagent (500 µM Resazurin sodium salt (Sigma-Aldrich) in PBS) was added per well. It is noted that the medium was cloudy due to polymer precipitation at 37 °C. As a negative control, the medium of 3 wells was replaced with complete cell culture medium containing 1% Triton X-100 to lyse the cells. After 15 minutes, 10 µl of the AlamarBlue reagent was added. Three empty wells were also filled with 100 µl medium and 10 µl AlamarBlue reagent was added to correct for the background. The 96-wells plates were incubated for 3 h at 37 °C protected from light. The fluorescence was measured using a Fluostar OPTIMA (BMG Labtech GmbH, Ortenberg, Germany) plate reader with a fluorescence excitation wavelength of 550 nm and an emission wavelength of 590 nm. After background correction, the fluorescence intensities were normalized to the intensities of cells cultured in medium without polymers.

2.8.4 Live-dead staining of RAW 264.7 and ARPE-19 cells exposed to the polymers PNF and PNM

Cells seeded in a flat bottom glass 96-wells plate (Greiner CellStar 96-well plate #655090) were cultured as described in section 2.8.1 and 2.8.2. The cells were incubated in medium containing PNF or PNM (0 to 5 mg/ml) (n=2) in humidified conditions at 37 °C and 5% CO$_2$ for 24 h. Because the medium was cloudy due to precipitation of the polymer, it was replaced by 100 µl medium containing 3 µM Calcein AM (Cayman Chemical Company, MI, USA) and 25 µM propidium Iodide (PI) (Invitrogen Thermo Fisher Scientific). As negative control, medium of 3 wells was replaced by medium containing 1% Triton X-100 to lyse the cells. After 15 minutes, the medium was replaced by 100 µl medium containing 3 µM Calcein AM and 25 µM PI. The cells were incubated for at least 5 minutes before imaging. Minimal 3 images were made using a Yokogawa Cell Voyager 7000 Spinning Disconfocal Microscope with a fluorescence emission wavelength of 525 nm to visualize the living cells and 600 nm for the dead cells. The images were further processed with *ImageJ* processing software and the living, and the dead cells were counted using *Columbus* processing software.

2.8.5 Life-dead staining of RPE-19 cells in direct contact with PNF-PNM hydrogels

Human retinal pigment epithelium cells were cultured in a flat bottom glass 12-wells plate (Greiner CellStar glass bottom 24-well plate, #662892) in 500 µl DMEM/F12 (52,000 cells/cm^2) as described in section 2.9.2. Before cell seeding, a 10 wt% PNF-PNM solution (50 µl) was placed in the corner of the well, and the hydrogel was formed upon incubation for 3 h at 37 °C. After

culturing cells with the PNF-PNM hydrogel for 24 h in the wells, a life-dead staining was performed. In short, 100 µl medium was removed and replaced by 50 µl medium containing 30 µM Calcein AM (final concentration 3 µM) and 50 µl medium containing 250 µM PI (final concentration 25 µM). As negative control, 50 µl medium of 3 wells was replaced by 50 µl medium containing 1 % Triton X-100 to lyse cells. After 15 minutes, Calcein AM and PI were added according to the protocol described above. Images were made and processed according to section 2.8.4

2.9 Video: Intravitreal injection of PNF-PNM hydrogel on an ex vivo rabbit eye.

The eyeball from a rabbit cadaver was enucleated within one hour after animal termination. The eye was dissected using a scalpel to make an incision and a towel forceps to ensure control and stability. First, the eyelids of the eye that was enucleated were opened and stabilized by clamping them to the skin. An incision was made on the skin with a scalpel at the nasal and temporal side of the eye by making solid lines. Subsequently, after removing the towel forceps, an incision on the skin and periocular tissues by moving the scalpel parallel to the orbital rim was made. At this point, the eyelids were still attached to the anterior part of the eye. Therefore, the eyeball was slightly pulled out of the orbital cavity with the help of a towel forceps, the optic canal in the sphenoid bone was located by touch, and the optic nerve was dissected as deep as possible. Finally, any other remating periocular tissues surrounding the eye inside the orbital cavity (muscles, connective tissues) were dissected, and the eyeball was entirely pulled out of the orbital cavity. The enucleated eye was stored in PBS buffer (pH 7.4) at 0 °C to arrest the metabolic activity of the tissues. Prior to the intravitreal injection, the eyeballs were incubated at 37 °C for 30 minutes in a water bath. Hydrogel formulations of 10 wt% were chosen to assess if the formulation with the lowest used concentration is able to form a stable gel in an *ex vivo* setting. Therefore, PNF-PNM (10 wt%, 50 µl) samples were prepared as described in section 2.4.1 and injected into the vitreous body of the rabbit eye using a syringe with a 30 G needle. After injection, the eye was incubated at 37 °C for 3 h (to allow full chemical DA crosslinking), after which an incision was made to expose the vitreous body and to visualize the in situ formed hydrogel.

3 RESULTS & DISCUSSION

3.1 Polymer synthesis and characterization

Figure 2 shows the synthesis scheme of the two complementary polymers, PNF and PNM, containing respectively furan and maleimide functional groups. TAIC assay demonstrated that both terminal hydroxyl groups of PEG with a number average molecular weight (M_n) of 6 kDa were quantitively functionalized with bromoisobutyryl bromide groups to yield a PEG macroinitiator. The macroinitiator was subsequently used to copolymerize HEA and NIPAM through ATRP-polymerization to obtain PNH, an ABA triblock copolymer as shown in figure 2A. The B-block consists of PEG for its hydrophilic properties whereas the outer A-blocks consist of two monomers, NIPAM, to render the polymer thermosensitive, and HEA, to enable post-modification of the thermosensitive block via coupling on its hydroxyl group. The PNH triblock copolymer after dialysis and lyophilization was obtained with a yield of 90-95%. Its chemical composition was

confirmed by ^{1}H-NMR analysis (see SI-figure 1A). The molar feed ratio of NIPAM/HEA was 90:10 (Table 1), and a ratio of 88:12 of the copolymers was measured by ^{1}H NMR analysis. Therefore, within the experimental error for NMR analysis, the composition of the thermosensitive A block equals the feed ratio, which is expected since the synthesized polymer was obtained in a high yield. The obtained polymer had an M_n of 43 kDa as determined by ^{1}H NMR analysis and of 33 kDa as determined by GPC with a polydispersity index (PDI) of 1.7. (Table 1). The cloud point (CP) of PNH as determined by light scattering was 32 °C (SI-figure 2), which is in accordance with literature data for block copolymers containing PNIPAM rich blocks[55, 56]. To allow Diels-Alder crosslinking, 67 % (feed ratio) of HEA groups in PNH were functionalized with either 3-(2-furyl)propionic acid or 6-maleimidohexanoic acid via DCC/DMAP coupling to obtain the two complementary thermosensitive triblock polymers PNF and PNM, respectively, as shown in figure 2B, C. The esterification of the HEA moieties was confirmed by ^{1}H-NMR (see SI-Figure 1B, C) which showed a ratio 88:4:8 between NIPAM, residual HEA, and furan or maleimide moieties respectively for PNF or PNM (Table 1). These results show that the esterification was quantitative. The M_n of the synthesized polymers was determined by ^{1}H NMR and GPC analysis. Results showed that PNF had an M_n of 44 kDa (^{1}H-NMR) and 38 kDa (GPC) while PNM had an M_n of 46 kDa both by ^{1}H-NMR and GPC. The PDI of the polymers were between 1.6 -2.2. As expected, the CP of PNF and PNM slightly decreased from 32 to 28 and 29 °C respectively, as PNM and PNF are more hydrophobic than PNH.
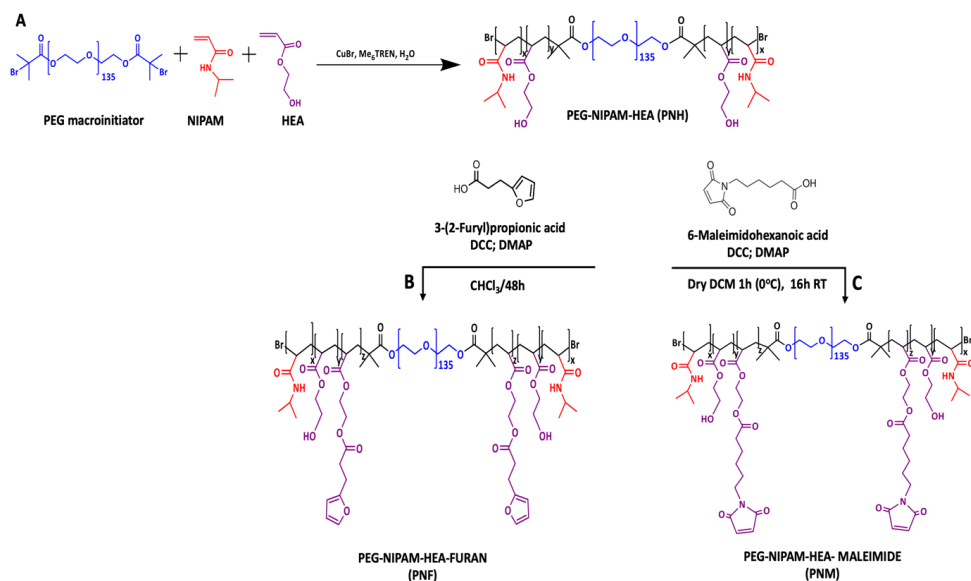
Figure 2 A) Synthesis of PNH by ATRP polymerization and its functionalization with B) 3-(2-furyl)propionic acid resulting in PNF, and C) with 6-maleimidohexanoic acid resulting in PNM.

Table 1 Characteristics of the three ABA triblock copolymers (PNH, PNF and PNM) composed of PEG mid-block of 6 kDa with outer blocks of NIPAM (N) and HEA (H) or furan (F) or maleimide (M).

Polymer	Feed Ratio [N]:[H]:[F]/[M]	Measured Ratio [a] [N]:[H]:[F]/[M]	M_n [a] (kDa)	M_n [b] (kDa)	PDI [b]	Cloud Point [c] (°C)
PNH	90:10:NA	88:12:NA	43	33	1.7	32
PNF	88:4:8	88:4:8	44	38	1.6	28
PNM	88:4:8	88:4:8	46	46	2.2	29

[a] Determined by ^{1}H-NMR; [b] Determined by GPC, [c] Determined by light scattering.

3.2   Hydrogel formation and characteristics

Figure 3A (left column) shows vials containing aqueous solutions of either a mixture of PNF and PNM or the separate polymers directly after dissolution at 4 °C. Subsequently, incubation of the polymer solutions (mixture of PNF/PNM, PNF, PNM) for 2 h at 37 °C (Figure 3A, middle column) resulted in viscous opaque solutions for the individual polymers due to physical self-assembly of the PNIPAM domains. On the other hand, the PNF-PNM mixture under the same conditions formed an opaque gel that lacked flow upon tilting the vial upside down (Figure 3A, middle column). Figure 3A (right column) shows that upon cooling down the samples to 4 °C resulted again in clear liquid solutions for both PNF and PNM. This means that reversible physical interactions are responsible for the change in visual appearance and gel formation of the PNF and PNM systems upon incubation at 37 °C. Importantly, and in contrast, upon cooling to 4 °C, the PNM-PNF mixture remained a gel, which strongly suggests that DA crosslinking indeed had occurred after the physical crosslinking and subsequent incubation at 37 °C.

Furthermore, scanning electron microscopy (SEM) analysis was performed to examine the microstructure of freeze-dried drug-loaded hydrogels and compare it with that of empty hydrogels. SI-Figure 10 shows different pore-type structures at three magnifications. Empty hydrogels exhibited small, interconnected pores, while FAB protein-loaded hydrogels had larger pores with smaller interconnected pores. Dex-loaded hydrogels displayed heterogeneous microstructures with zones of lamellar structures and flat surfaces with smaller pores.

3.2.1   Rheological Characterization

Rheological studies were performed to study the gelation kinetics, the reversibility of both the PNF-PNM formulation and individual polymer solutions upon heating and cooling and the stiffness of the formed PNM-PNF hydrogels.

The temperature at which G′ (storage modulus) crosses G″ (loss modulus) is defined here as the gelation temperature (T_{gel}). The PNF-PNM formulation showed a T_{gel} at 23 °C, while the solutions of the individual PNF and PNM solutions showed a T_{gel} of 24 and 28°C, respectively (Figure 3B). The G′ of the hydrogels (PNM/PNF, PNM and PNF solutions) progressively increased when the temperature increased from T_{gel} up to 37°C most likely due to the thermosensitive nature of the polymers.

After 30 min at 37 °C, the gels were stressed at a fixed strain and increasing frequency. It was shown that the G' of the gels based on PNF or PNM increased (for PNM from 38 to 920 Pa, for PNF from 450 – 3200 Pa) with an increasing frequency (SI-Figure 3A). This is to be expected as only physical crosslinks are present in the gel network. [47, 57] In contrast, after 30 min at 37°C, the PNF-PNM hydrogel showed already a substantial higher G' (2200 Pa) at low frequency compared to the single polymer gels that subsequently increased up 3430 Pa at higher frequency (SI-Figure 3A). This higher G' of the PNF-PNM formulation suggests that additional chemical crosslinks were formed. In addition, Figure 3B shows that a decrease in temperature of the separate polymer systems resulted in a decrease of both G' and G" which can be ascribed to the reversible hydration of the pNIPAM blocks of the polymers. The PNM system showed almost reversible behavior during cooling from 37 to 4 °C with a rapid decrease of G', G" (Figure 3 B1) and complex viscosity (SI-Figure 3D) between ~30 and 25 °C, while substantial hysteresis was observed for the PNF system (Figure 3 B2). This might be due to weak heteroaromatic π-π stacking interaction between the furan moieties[58, 59] formed above the LCST and still present upon cooling of the gel below this temperature.

Figure 3 B3, shows that when the PNF-PNM gel was cooled down from 37 to 4 °C, G' remained higher than G" and G' decreased from 3100 to 650 Pa while cooling from 37 to 23 °C , likely because of the loss of the physical crosslinks below the LCST. Subsequently, G' increased up to 3100 Pa at 4°C, likely because additional DA crosslinks were formed in time.
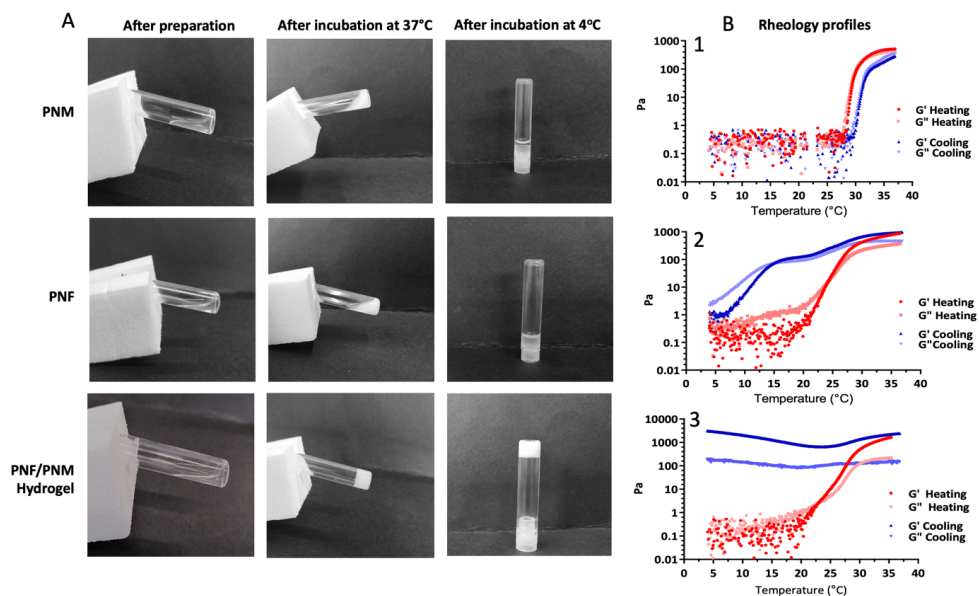
Figure 3 A) Images of PNF, PNM, and PNF-PNM systems at room temperature shortly after dissolution of the polymers, after incubation at 37 °C for 2 h and cooling down to 4 °C. B) Rheogrammes of PNF and/or PNM polymer systems upon heating (4 to 37 °C) and cooling (37 to 4 °C). B1: PNM 10 wt% polymer, B2: PNF 10 wt% polymer, and B3: PNF-PNM mixture 10 wt%, at a 0.5% strain.

Drug-loaded PNF-PNM gels were also rheologically characterized. The plateau modulus as a function of angular frequency at 37°C showed only minor differences between FAB-loaded, dex-loaded, and non-loaded gels (SI-Figure 3 A, B, C). This means that the loaded drugs did not interfere with the polymeric networks. As expected, all gels showed a higher G' with increasing polymer concentration, which points to a higher crosslinking density. The calculated mesh size using the equation mentioned in section 2.3. resulted in a value of 9 nm for 20wt% gel and 21 nm for the 5wt% gel (Table 2) .

3.2.2   FTIR Characterization

FTIR characteristics of the dried hydrogels and polymers were investigated to show DA crosslinking between the furan functionalities of PNF and maleimide functionalities of PNM after incubation in PBS for 3 h at 37 °C. Figure 4 shows that PNF-PNM hydrogels (A), PNM (B) and PNF(C) absorbed IR light of 1455, 1640 and 1535 cm^{-1}, which can be assigned respectively to the CH_3 bending vibration, the amide I band due to the C=O stretching vibration and amide II band (a combination of the N−H bending and C−N stretching vibration) [60, 61] all present in the pNIPAM blocks of the polymers. The absorbance peak at 1737 cm^{-1} is assigned to the C=O stretching vibration of the ester groups present in PNF and PNM and in the hydrogel. Furthermore, the observed broad peaks of the CH_2CH_2 stretching vibrations at 2800-3005 cm^{-1} [62] are ascribed to the PEG blocks of the PNF/PNM polymers and the hydrogel. Additionally, the spectrum of PNM shows peaks at 1707 cm^{-1} and at 695 cm^{-1} which are assigned to the C=O stretch and =C-H-bending vibration of the maleimide group [63, 64], while in the spectrum of PNF a peak at 737 cm^{-1} is present which is ascribed to the =C-H- bend vibration of the furan moiety[65, 66]. The spectrum of the PNF-PNM hydrogel prepared with a molar ratio maleimide/furan 1:1 (figure 4A) clearly showed both the absence of the bending and stretching vibrations at 695 and at 1707 cm^{-1}, characteristic for the maleimide groups, and at 737 cm^{-1}, characteristic for the furan group. The absence of these peaks (indicated by the red arrow in figure 4) shows that maleimide and furan moieties present in the PNM and PNF, respectively, were consumed during network formation, demonstrating that DA chemical crosslinking had occurred. It is noted that the absorbance at 1459 cm^{-1} characteristic for the formed DA-adduct[67] was not detected in the hydrogel due to the strong interference of the PNIPAM amide II band and CH_3 bending vibration at 1535 and 1455 cm^{-1}, respectively.
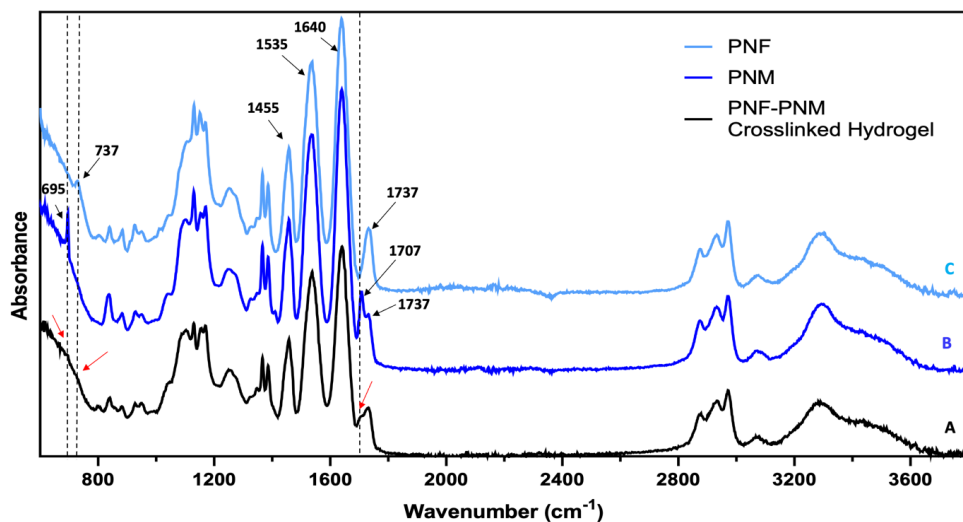
Figure 4 FT-IR spectra of A) PNF-PNM dried hydrogel (molar ratio 1:1 of furan and maleimide), B) PNM, C) PNF. Black arrows indicate the most relevant peaks and the red arrows point to the disappeared peaks after formation of the chemically crosslinked hydrogel due to DA reaction.

3.2.3   Degradation of PNF-PNM hydrogels

During hydrogel formation at 37 °C, a concentration dependent shrinking of the gels occurred, and the 15, 10 and 5 wt% gels lost, respectively, 65, 44 and 17% of their initial volumes. This means that a higher extent of water expulsion and thus shrinking of the gels occurred with increasing polymer concentration. This is likely due to higher PNIPAM content of the gel network with increasing polymer concentration in combination with higher concentrations of the functional groups, resulting in both a higher physical and chemical crosslink densities. SI-figure 5 shows that the hydrogels incubated in PBS at 37 °C remained stable during incubation for more than 460 days, demonstrating that no significant degradation of the gels occurred.

Ilochonwu et al. and Kirchhof et al. [38,39] reported that DA hydrogels degraded in aqueous solution (PBS pH 7.4) at 37 °C by retro Diels Alder (rDA) reactions to generate furan and maleimide. The degradation of DA crosslink-based hydrogels primarily occurs through the irreversible hydrolytic ring opening of the maleimide group. Surprisingly, under the same conditions, PNF-PNM hydrogels did not degrade even after 460 days. This intriguing result may be attributed to the location of the chemical DA crosslinks within the hydrophobic domains of the hydrogel network. These domains limit water accessibility, thereby slowing down the hydrolysis of maleimide groups. It is worth noting that network degradation can also occur through hydrolysis of the ester bonds that connect the P (PEG) to the NF or NM blocks. Neradovic et al.[68] observed a half-life of 34 hours for this ester bond at pH 8.5 and 37 °C in a similar block copolymer. Hence, it can be expected that at pH 7.4 and 37 °C, the half-life would be approximately 340 hours. However, as mentioned before, the degradation time for PNF-PNM hydrogels at pH 7.4 is significantly longer. To gain additional insights into the stability and degradation kinetics, 5wt%

PNF-PNM hydrogels were incubated at 37°C in buffers with pH 10 and 11. This was done to investigate whether hydrolysis can take place under accelerated conditions, either through rDA or ester hydrolysis. SI-figure 5B shows that the swelling ratio of the gel incubated at pH 11 rapidly decreased and complete degradation was observed after 3 days, while the gel incubated at pH 10 showed slight increase in swelling ratio until complete degradation between day 8 and 13. These results demonstrate that PNF-PNM hydrogels are degradable by hydrolysis, but it is likely a very slow process at neutral pH.

Moreover, it is crucial to consider the presence of degradation enzymes in the vitreous humor in an in vivo situation. Esterases, hydrolases, and other enzymes are present in the vitreous humor and possess the ability to catalyze the hydrolysis of ester bonds within the hydrogel.[69] These enzymes have the potential to actively contribute to the degradation process, thereby influencing both the rate and extent of hydrogel degradation within the vitreous humor.

3.3 Drug release from PNF-PNM hydrogels

3.3.1 FAB release from PNF-PNM hydrogel

Figure 5 shows that a substantial burst release was observed for the different hydrogels depending on polymer concentration, most likely due to water, and thus also protein, expulsion caused by dehydration of the pNIPAM domains during hydrogel formation and shrinking (figure 1). It is intuitively expected that this burst is correlated with the extent of water expulsion. However, this was not observed since the burst was 46, 45 and 28% for the 5, 10 and 20 % hydrogels and thus not proportional to the extent of dehydration (17, 44, 65 % for 5, 10, 20 wt% gels, respectively).
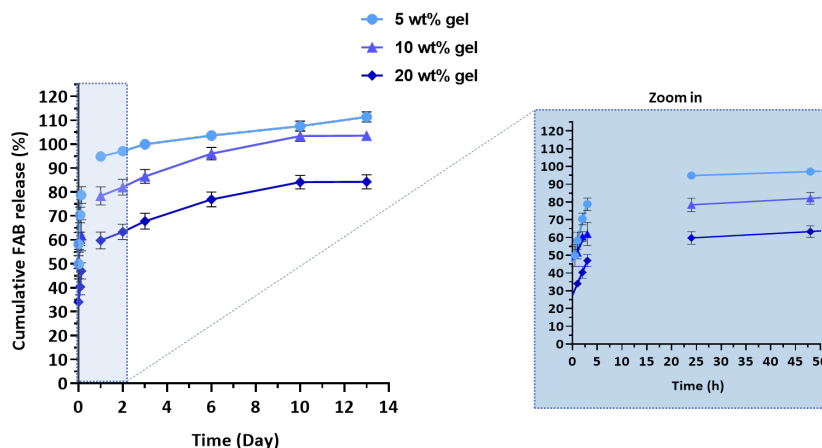
Figure 5 Cumulative FAB release in PBS at 37 °C from cylindrical PNF-PNM hydrogels with initial polymer concentration of 5, 10 and 20 wt% and diameters of 3.4, 2.3, 1.4 mm and heights of 3.8, 2.6, 1.6 mm respectively. The dimensions of the hydrogels were calculated from their weights after preparation (legend

figure 4) assuming isotropic deswelling. The data are presented as mean ± SD of three independent replicates. For clarity, at time 300 ml buffer was added to the hydrogels and expelled fluid (see Figure 1).

It was observed that the storage moduli (see SI-figure 3) and Young's moduli (see SI-Figure 4) increased with polymer weight % of the gels pointing to an increase in crosslinking density with smaller mesh sizes (table 2), which might overall lead to lower burst release of the protein. Figure 5 further shows that during the first day, protein release was rapid, followed by a subsequent slower release phase during the following 12 days. Figure 5 also shows that hydrogels with 5 and 10 wt% polymer content showed quantitative release of the loaded protein in 13 days, while the 20 wt% hydrogel released 83% of the loaded protein during the same time (figure 5). The hydrodynamic radius of the FAB protein is 2.7 nm[70] (protein diameter of 5.4 nm) which is smaller than the estimated average mesh size of the hydrogel network (see table 2). The turbid nature of the PNF-PNM hydrogels indicates that phase separation into polymer- and water-rich areas occurred. As a consequence, protein molecules present in the less densely crosslinked regions of the gel network are mobile and rapidly diffuse out during the first day, whereas in the second phase (day 1-13), protein molecules present in more densely crosslinked zones are released. Similar biphasic release behavior of proteins from phase separated PEG/thermosensitive hydrogels was reported by Censi et al. [71] Likely, in the hydrogel with 20% polymer, protein molecules are entrapped in cages with pores smaller than the hydrodynamic radius of the FAB restricting protein mobility and resulting in incomplete release.

Table 2 G' and mesh size (ξ) of the PNF-PNM hydrogels calculated using equation in section 2.3.3.

Hydrogel	G' of FAB loaded gel (kPa)	Mesh size of FAB loaded gel (nm)	G' of Dex loaded gel (kPa)	Mesh size of Dex loaded gel (nm)
5 wt% PNF-PNM	0.38 ± 0.05	22.5 ± 2.8	0.46 ± 0.07	21.0 ± 3.1
10 wt% PNF-PNM	3.13 ± 0.45	11.1 ± 1.6	0.97 ± 0.15	16.4 ± 2.6
20 wt% PNF-PNM	6.16 ± 1.27	8.9 ± 1.8	5.12 ±1 .00	9.4 ± 1.8

5

To quantitatively evaluate the diffusional mass transport for FAB release, the following analytical solution of Fick's second law was applied. [72, 73]

$$\frac{M_t}{M_\infty} = 1 - \frac{32}{\pi^2} \cdot \sum_{n=1}^{\infty} \frac{1}{q_n^2} \cdot exp\left(-\frac{q_n^2}{R^2} \cdot D \cdot t\right) \cdot \sum_{p=0}^{\infty} \frac{1}{(2 \cdot p + 1)^2} \cdot exp\left(-\frac{(2 \cdot p + 1)^2 \cdot \pi^2}{H^2} \cdot D \cdot t\right)$$

(1)

where M_t and M_∞ are the cumulative amounts of FAB released at time t and infinity, respectively; n and p are dummy variables; q_n are the roots of the Bessel function of the first kind of zero order [J0(qn)=0]; D is the apparent diffusion coefficient of the protein in the hydrogel; R and H denote the radius and height of the cylindrical gels. In this study, the experimentally determined release

plateau values of FAB (figure 5) were considered as amounts released at "infinite" time and thus being the mobile fraction of the loaded protein.

The following boundary conditions apply to the derivation of this equation:

1) Mass transport resistance in the release medium (bulk fluid) is negligible compared to mass transport resistance in the hydrogel.
2) The protein is initially homogeneously and molecularly distributed throughout the gel.
3) FAB transport occurs in radial and axial direction of the cylindrical hydrogel.
4) The diffusion coefficient of the protein is not dependent on time or position.
5) The hydrogel does not dissolve or swell upon exposure to the medium during the release period.
6) Protein release is zero at t = 0. Note that this assumption was not fulfilled in the present study since the obtained gels after their preparation including expelled buffer/proteins were transferred in the release medium. Thus, this expelled liquid was mixed with the release medium at t = 0.

Figure 6 shows an example for the fitting of Equation 1 to experimentally measured FAB release from a hydrogel of 5 % polymer. As it can be seen, the agreement between the fitted curve and actual release data is poor and Equation 1 systematically underestimates protein release at early time points and *over*estimates FAB release at late time points. The same observation was made for all other investigated hydrogels, irrespective of the polymer concentration. This poor fit is not unexpected since some of the boundary conditions mentioned above are not valid. Since as pointed out, the hydrogels are likely phase separated systems with water poor and water rich regions, the release of a protein from such gels cannot be modelled with a single value for the diffusion coefficient of the protein in the heterogeneous hydrogel matrix.
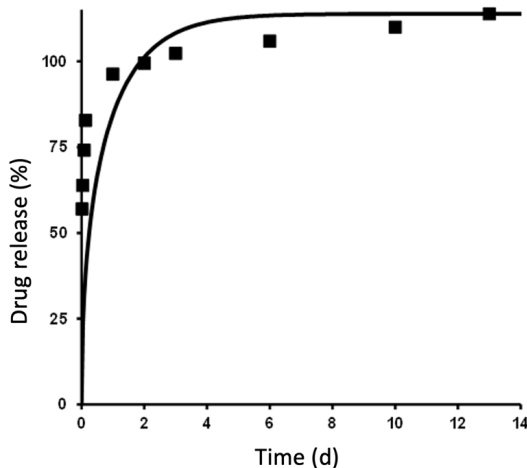
Figure 6 FAB release from a hydrogel based on 5 % polymer. The curve shows the fitting of Equation 1 to the experimental results (symbols). For Equation 1, the experimentally determined plateau value was considered as M_∞.

3.3.2 The structural integrity of the FAB protein during formulation and after release

Figure 7A shows the coomassie blue SDS-PAGE stains (under non-reducing conditions) of FAB incubated with PNF and PNM, at 4 °C (below LCST) and 37 °C (above LCST) for 3 h and 13 days. The hydrophilic non-thermosensitive 4 arm PEG-Mal was used as a positive control because this polymer has been previously shown to form protein-polymer conjugates[74, 75] due to reaction of the maleimide functionality with SH and NH_2 groups of proteins. SDS-page analysis confirmed that PEG-Mal indeed reacted with FAB already after 3 h incubation in PBS at both 4 and 37 °C, and this reaction became more apparent after 13 days (as shown by the arrows in figure 7 A, likely pointing to the formation of PEG adducts with two FAB molecules). Figure 7A also shows that PNF did not react with the FAB protein upon incubation for 3 h and 13 days at both 4 and 37 °C. However, FAB incubated with PNM for 13 days 4 °C showed a smear at higher apparent molecular weight of ~80- 140 kDa pointing to reaction of the maleimide groups of this polymer with the protein. Interestingly, the FAB protein did not react with PNM upon incubation at 37 °C for 13 days, likely because these groups are hidden in the hydrophobic domains of the gel formed above the LCST and were therefore not accessible for reaction with the protein. Importantly, SDS-page and SEC analysis of the released Fab did also not show modification of the protein (Figure 7B, C) likely because the maleimide groups are present in the hydrophobic domains of the gels, and moreover their concentration drops in time due to reaction with the furan groups during hydrogel chemical crosslinking by Diels Alder reaction.
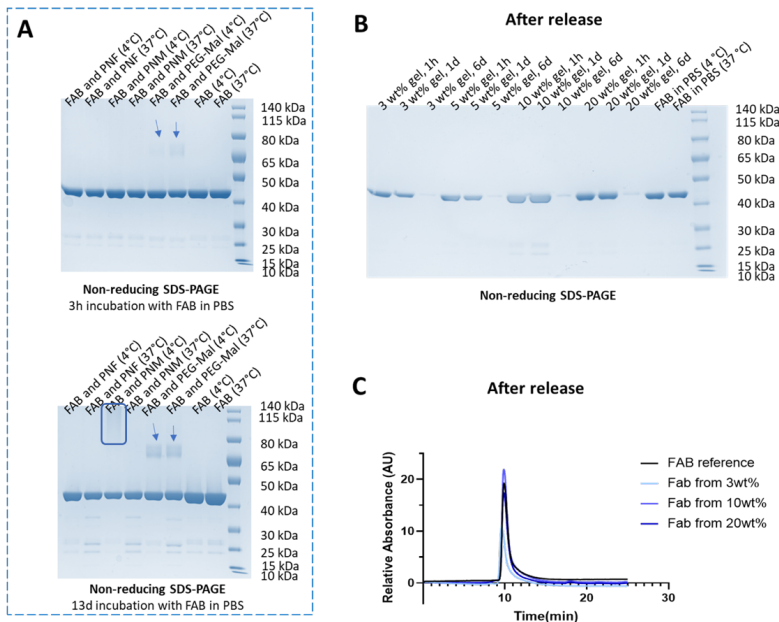
Figure 7 Coomassie blue SDS-PAGE stains under non-reducing conditions of FAB incubated with PNF, PNM, and 4 arm PEG-Mal at 4 and 37 °C for 3 h and 13 days. B) Coomassie blue SDS-PAGE stains under non-reducing conditions of FAB released from 3, 5, 10, and 20 wt% PNF-PNM hydrogels after 1 hour, 1 day, and 6 days. C) SEC-chromatogram of FAB released from 3, 10, and 20 wt% PNF-PNM hydrogels after 2 days.

3.3.3   Release of dexamethasone from PNF-PNM hydrogels

Figure 8 shows the release profiles of dexamethasone from PNM-PNF hydrogels with different initial polymer content and the dissolution profile of dexamethasone crystals in PBS/tween. It is shown that the drug particles quantitatively dissolved within 5 days with ~90% within the first day (figure 8A). On the other hand, the same figure shows that after a small burst (~5 % of the loading) sustained and almost quantitative release (around 95% of the loaded amount) was observed in ~35 days which demonstrate the contribution of the hydrogel in prolonging the release of dexamethasone. Figure 8 also shows that the different gels released their content with the same kinetics. It should be remarked that the gels have different cylindrical dimensions, and this thus points to a different diffusivity of the drug in the gel matrices. Given the low aqueous solubility (0.089 mg/ml) and log P (1.83) of dexamethasone[76], this drug is likely solubilized in the hydrophobic pNIPAM domains of the hydrogel. This design strategy allows for efficient loading and uniform distribution of dexamethasone within the hydrogel matrix. The obtained results suggest that the weight fraction of these domains of the hydrogel with the lowest initial polymer concentration (3wt% gel) is already sufficient to dissolve the loaded dexamethasone dose. Indeed, the weight fraction of the hydrophobic domains is ~3 times higher than that of the drug.
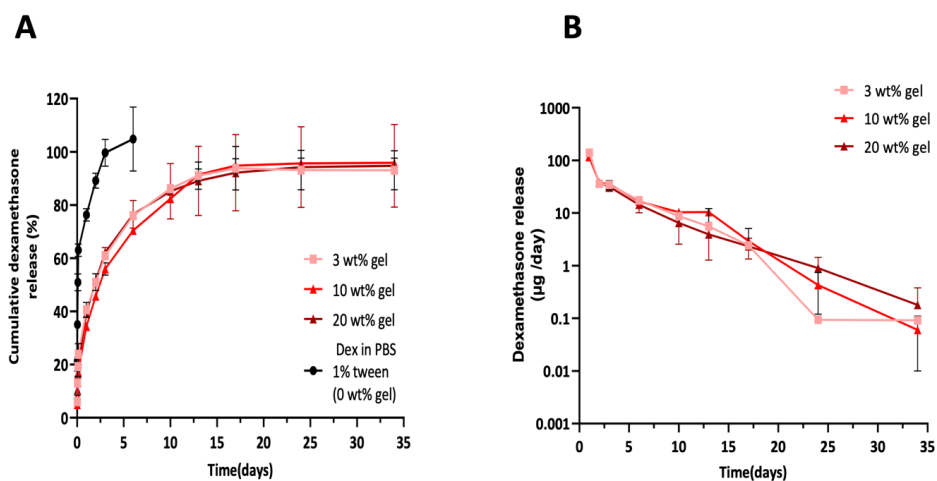
Figure 8 A) Cumulative release profiles of dexamethasone (Dex) loaded PNF-PNM hydrogels in PBS 1% tween at 37°C with initial polymer concentrations of 3, 10 and 20 wt% of cylinders with diameters of 3.9, 2.3, 1.4 mm and of heights 4.3, 2.6, 1.6 mm, respectively, after hydrogel formation and water expulsion. These values are based weight measurement after hydrogel preparation assuming isotropic deswelling. Also shown is the dissolution of dexamethasone crystals dispersed in the release buffer. B) Dexamethasone released (in µg/day) from 3, 10, and 20 wt% PNF-PNM hydrogels.

Equation 1 was fitted to the experimentally obtained release profiles. Figure 9A shows an example for such a fitting. As it can be seen, the experimental data are well fitted with equation 1. This was also true for the other investigated dexamethasone-loaded hydrogels, irrespective of

the polymer concentration (Figure 9B). The following apparent diffusion coefficients of dexamethasone in the investigated hydrogel matrices were calculated: D = (13.0 ± 0.4) x 10^{-9}, (3.1 ± 0.1) x 10^{-9}, and (1.5 ± 0.6) x 10^{-9} cm²/s for hydrogels based on 3, 10 and 20% polymer, respectively (mean values +/- standard deviations, n = 3). These diffusion coefficients are, as expected, substantially smaller than the reported value in water (6800 x 10^{-9} cm²/s [77]). Equation 1 is derived under the assumption that the hydrogel structure is homogeneous, e.g. the existence of more hydrophobic vs. more hydrophilic regions with different drug mobilities is not considered. Thus, apparent diffusion coefficients are calculated, reflecting the overall dexamethasone mobility in the heterogenous hydrogel matrices. The observation that the determined apparent dexamethasone diffusion coefficient in the hydrogel decreases with increasing polymer concentration might be explained by the increasing volume fractions of hydrophobic pNIPAM domains in the hydrogel matrices, with lower drug mobility.
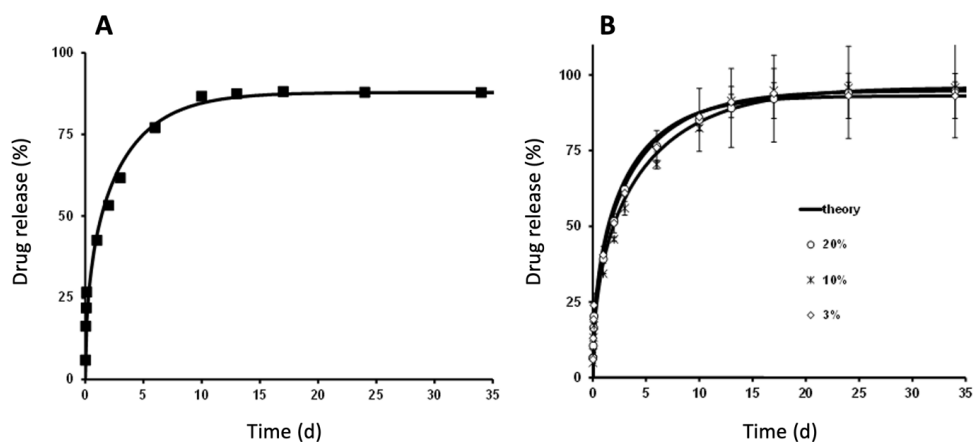
Figure 9 A) Release of dexamethasone from a hydrogel based on 3% polymer. The curve shows the fitting of Equation 1 to the experimental results (symbols). B) the overall dexamethasone release from hydrogels based on 3, 10 or 20% polymer (as indicated in the legend). For the experimental data points, mean values ± standard deviations (n=3) are indicated.

Using the mean values of the determined apparent dexamethasone diffusion coefficients, the drug release kinetics from different hydrogels were calculated and compared to the experimentally measured results. Figure 9B shows the respective fitted and experimental data. The excellent agreement between Equation 1 and the experimentally determined dexamethasone release kinetics suggests that the diffusion of the drug molecules through the hydrogel is much slower than the other phenomena and is thus the releasing-determining factor. For instance, dexamethasone partitioning between the more hydrophobic and more hydrophilic gel regions might is likely more rapid than drug diffusion through these regions.

Figure 8B shows that the average amount of dexamethasone released per day for the gel formulations gradually decreased from ~100 to 0.1 µg/day over 35 days. The vitreous concentration of dexamethasone in patients that received 400 µg bolus injection of the drug was

25 ng/ml 3 days after intravitreal injection, with a half-life of 5.5h[12]. The only currently clinically available sustained release formulation for intraocular dexamethasone delivery is the Ozurdex™ implant. This intravitreal implant results between 90 and 180 days in a concentration of 1.31±1.94 pg/ml which still improves visual acuity[78]. In clinical use, the maximum volume for intravitreal injection in humans is 100 μL[79]. Therefore, the release rate of dexamethasone from the PNF-PNM hydrogel is expected to be sufficient for reaching the therapeutic range both in vitreous and retina for more 35 days after administration. As mentioned, the PNF-PNM hydrogel formulations demonstrated controlled release of dexamethasone over a period of 35 days, with release rates ranging from 100 to 0.1 μg/day. This resulted in vitreous concentrations ranging from 25 to 0.025 μg/mL, considering the approximate vitreous volume of 4 mL. These concentrations are far above the therapeutic effective concentration based on clinical experience with the Ozurdex™ implant. It is worth noting that these concentrations still fall within the safe range observed in clinical practice. Fonseca et al.[80] conducted a clinical study showing that intravitreal administration of a 0.05 mL (200 μg) dexamethasone solution, with a concentration of 4 mg/mL, was safe and effectively reduced macular thickness secondary to diabetic macular edema (DME).

3.4   Cytocompatibility of PNF, PNM and PNF-PNM hydrogels

3.4.1   Cytotoxicity of RAW 264.7 and ARPE-19 cells exposed to PNF and PNM

The Alamar-Blue assay was conducted on RAW 264.7 and ARPE-19 cells, representing inflammatory cells macrophages and human retina cells, respectively, to determine the cell viability through the cells' metabolic activity. As shown in SI-figure 6, unexpectedly, upon exposure of PNF to the cells, both RAW 264.7 and ARPE-19 cells showed metabolic activities over 100 % compared to the control. The highest metabolic activities (153 ± 6 % for RAW 264.7 cells and 169 ± 16 % for ARPE-19 cells) were observed for the cells incubated with solutions of the highest PNF concentration (5 mg/mL). As a control, polymers were incubated in culture medium without cells for 24 h at 37 °C, whereafter the AlamarBlue assay was conducted. It was found that the polymers did not interfere with the assay. Seong et al. [81] reported that cell receptors can interact with hydrophobic portions (hyppos) of molecules. To prevent damage due these hyppos, cells activate repair and remodel pathways causing an increase in metabolic activity. Therefore, the observation of the higher metabolic activity of cells incubated with PNF might be ascribed to the hydrophobic character of the polymer at 37 °C. In contrast, reduced metabolic activities were found for RAW 264.7 and ARPE-19 cells when incubated with solutions of increasing PNM concentrations. Metabolic activities of cells incubated with solutions ⩽ 1 mg/mL PNM were comparable with the positive control (cells incubated with medium only), while incubation of the cells with > 1 mg/mL the solutions resulted in lower metabolic activities suggesting cytotoxicity. This higher toxicity for PNM as compared to PNF, is likely caused by the maleimide groups present, which might interact with membrane proteins resulting in a decrease in metabolic activity of the cells.

The cell cytocompatibility of PNF and PNM was also performed using a live-dead staining on RAW 264.7 and ARPE-19 cells (SI-figure 8 and 9). In line with the results of the AlamarBlue assay, after

24 h of incubation at the studied concentrations (up to 5 mg/mL), PNF showed no toxicity to the RAW macrophages (Figure 8A and B). In contrast, viability was compromised for RAW macrophages incubated with PNM in a concentration-dependent manner (Figure 8A and B). Macrophages incubated with PNM (3-5 mg/ml) stained positive for both calcein and PI, showing that moribund cells still had active esterases present in the cytosol. The cells incubated with PNM at concentrations ⩽1 mg/mL retained their viability which is in line with the results of the Alamar-Blue assay. The results of the life-dead staining on the ARPE-19 cells retinal cells incubated with PNF and PNM at the same concentrations exhibited the same trend as observed for the macrophages (SI Figure 9). ARPE-19 cells and RAW 264.7 cells showed comparable amounts of living cells after 24h incubation with PNF (SI Figure 9 A, B). The retina ARPE-19 cells incubated with solutions ⩾ 2 mg/mL PNM stained majorly red, whereas the viability of cells incubated with PNM at concentration ⩽ 1 mg/mL was not compromised. Overall, it can be concluded form both assays that PNM showed no toxic effects. However, incubation of the cells with PNM caused toxic effects at concentrations > 1 mg/mL. Noteworthy, for the aimed application the two complementary polymers are not administered separately but are applied as an injectable formulation of the two polymers and thus cells are only exposed for a short time to the individual polymers as after injection of the formulation the temperature of the gel will increase to 37 $^\circ$C (thus above the LCST) and physically and chemically crosslinked hydrogels will be formed. To investigate whether the PNF-PNM system can be safely used as intraocular drug delivery system, human retina cells were cultured in direct contact with a PNF-PNM hydrogel for 24 h. Figure 10 shows the ARPE- 19 cells proliferated in close contact with the gel and the cell viability was not affected by the hydrogel, showing the cytocompatibility of the PNF-PNM gel (SI-Figure 7A, B).

5
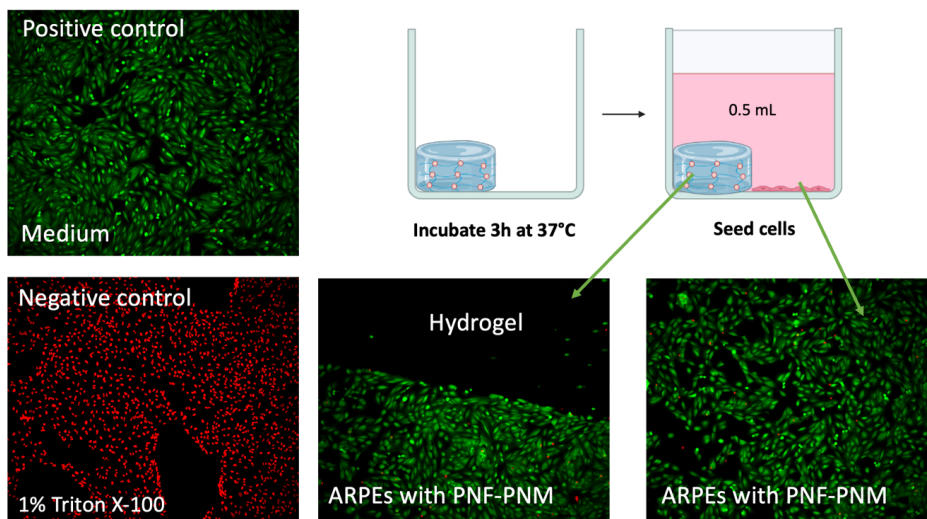
Figure 10 Calcein AM and propidium iodide staining's of ARPE-19 cells cultured in the presence of a 10 wt% PNF-PNM hydrogel. Living cells are imaged green, and dying/dead cells are red.

4 Video: intravitreal injection of PNF-PNM hydrogel through a 30 G needle into the vitreous body of an ex vivo rabbit eye

Injectability and syringeability are crucial for successful intravitreal drug delivery. Injectability ensures easy drug administration via a syringe, while syringeability refers to smooth drug withdrawal into the syringe. Optimizing these aspects enhances translational potential, benefiting treatment. In this study, a 10 wt% PNF-PNM hydrogel formulation was easily withdrawn and injected into the vitreous body of an ex vivo New Zealand rabbit eye. For more information and visual demonstration, the reader is referred to video 1 showing:

- Injection of 50 μL PNF-PNM formulation through a 30 G needle.
- After injection, followed by incubation of the eyeball at 37 °C for 3 h (to allow full chemical DA crosslinking), an incision was made to open the vitreous body.
- The hydrogel was visualized as white mass after the incision with a clear distinction from the transparent vitreous.

The results demonstrate that PNF-PNM formulation can be easily injected through a small 30G needle clinically recommended for intravitreal injections[82]. Furthermore, the PNF-PNM formulation crosslinked *in situ* the vitreous body by physical and subsequent chemical reactions and demonstrated its potential as a local drug delivery system for intraocular therapy. The hydrogel used in this study was intentionally designed to form a localized depot at the injection site. This particular characteristic of the hydrogel prevents it from dispersing throughout the vitreous humor, as it remains confined to a specific position. By localizing the hydrogel depot away from the visual pathway, potential disruptions to vision are minimized, as the hydrogel is not transparent, similar to many intraocular implants.
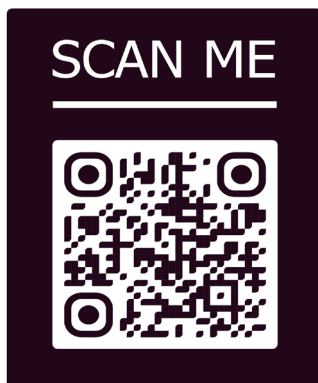
Video 1 Representation of intravitreal injection of 50 μL PNF-PNM 10wt% formulation through a 30G needle into the vitreous body of *ex-vivo* eye of a new Zeeland rabbit.

5   CONCLUSIONS

In this study, thermo-gelation was successfully combined with Diels Alder chemical crosslinking to design stable in situ forming hydrogels. This hydrogel is a versatile drug delivery system able to release two loaded drugs with different physicochemical properties (dexamethasone and FAB antibody fragment). The system can provide sustained release of dexamethasone for 35 days, while the FAB protein was released for 13 days. Interestingly, the maleimide functional group present in the hydrophobic domains of the polymer as well as in the formed hydrogel did not react with the protein at temperatures above LCST, avoiding unwanted protein modification during loading and release. The hydrogel is injectable through a 30 G needle and is well tolerated by retinal cells making the developed system a potential candidate for intravitreal drug therapy. In future directions, further preclinical and clinical investigations are necessary to determine the optimal dosing regimen and fully understand the impact of our hydrogel system on administration frequency. Additionally, exploring the applicability of our hydrogel system beyond ocular therapies, considering its sustained release capabilities, may uncover opportunities for in situ drug delivery in other applications.

6   ACKNOWLEDGEMENTS.

5

7 REFERENCES

[1] R. Lee, T.Y. Wong, C. Sabanayagam, Epidemiology of diabetic retinopathy, diabetic macular edema and related vision loss, Eye Vis (Lond), 2 (2015) 17.

[2] F.C. Gundogan, U. Yolcu, F. Akay, A. Ilhan, G. Ozge, S. Uzun, Diabetic Macular Edema, Pak J Med Sci, 32 (2016) 505-510.

[3] J.M. Colijn, G.H.S. Buitendijk, E. Prokofyeva, D. Alves, M.L. Cachulo, A.P. Khawaja, A. Cougnard-Gregoire, B.M.J. Merle, C. Korb, M.G. Erke, A. Bron, E. Anastasopoulos, M.A. Meester-Smoor, T. Segato, S. Piermarocchi, P. de Jong, J.R. Vingerling, F. Topouzis, C. Creuzot-Garcher, G. Bertelsen, N. Pfeiffer, A.E. Fletcher, P.J. Foster, R. Silva, J.F. Korobelnik, C. Delcourt, C.C.W. Klaver, E.-R. consortium, c. European Eye Epidemiology, Prevalence of Age-Related Macular Degeneration in Europe: The Past and the Future, Ophthalmology, 124 (2017) 1753-1763.

[4] N. Karia, Retinal vein occlusion: pathophysiology and treatment options, Clin Ophthalmol, 4 (2010) 809-816.

[5] R.K. Maturi, A.R. Glassman, D. Liu, R.W. Beck, A.R. Bhavsar, N.M. Bressler, L.M. Jampol, M. Melia, O.S. Punjabi, H. Salehi-Had, J.K. Sun, N. Diabetic Retinopathy Clinical Research, Effect of Adding Dexamethasone to Continued Ranibizumab Treatment in Patients With Persistent Diabetic Macular Edema: A DRCR Network Phase 2 Randomized Clinical Trial, JAMA Ophthalmol, 136 (2018) 29-38.

[6] A.N. Yuti Chernajovsky, Therapeutic Antibodies, Berlin, 2008.

[7] S.A. Gaballa, U.B. Kompella, O. Elgarhy, A.M. Alqahtani, B. Pierscionek, R.G. Alany, H. Abdelkader, Corticosteroids in ophthalmology: drug delivery innovations, pharmacology, clinical applications, and future perspectives, Drug Deliv Transl Res, 11 (2021) 866-893.

[8] E. Donnenfeld, E. Holland, Dexamethasone Intracameral Drug-Delivery Suspension for Inflammation Associated with Cataract Surgery: A Randomized, Placebo-Controlled, Phase III Trial, Ophthalmology, 125 (2018) 799-806.

[9] N.V. Saraiya, D.A. Goldstein, Dexamethasone for ocular inflammation, Expert Opin Pharmacother, 12 (2011) 1127-1131.

[10] A. Farkouh, P. Frigo, M. Czejka, Systemic side effects of eye drops: a pharmacokinetic perspective, Clin Ophthalmol, 10 (2016) 2433-2441.

[11] C.H. Meyer, T.U. Krohne, P. Charbel Issa, Z. Liu, F.G. Holz, Routes for Drug Delivery to the Eye and Retina: Intravitreal Injections, Dev Ophthalmol, 55 (2016) 63-70.

[12] I.M. Gan, L.C. Ugahary, J.T. van Dissel, J.C. van Meurs, Effect of intravitreal dexamethasone on vitreous vancomycin concentrations in patients with suspected postoperative bacterial endophthalmitis, Graefes Arch Clin Exp Ophthalmol, 243 (2005) 1186-1189.

[13] S.J. Bakri, M.R. Snyder, J.M. Reid, J.S. Pulido, M.K. Ezzat, R.J. Singh, Pharmacokinetics of intravitreal ranibizumab (Lucentis), Ophthalmology, 114 (2007) 2179-2182.

[14] K. Radhakrishnan, N. Sonali, M. Moreno, J. Nirmal, A.A. Fernandez, S. Venkatraman, R. Agrawal, Protein delivery to the back of the eye: barriers, carriers and stability of anti-VEGF proteins, Drug Discov Today, 22 (2017) 416-423.

[15] E.M. Del Amo, A.K. Rimpela, E. Heikkinen, O.K. Kari, E. Ramsay, T. Lajunen, M. Schmitt, L. Pelkonen, M. Bhattacharya, D. Richardson, A. Subrizi, T. Turunen, M. Reinisalo, J. Itkonen, E. Toropainen, M. Casteleijn, H. Kidron, M. Antopolsky, K.S. Vellonen, M. Ruponen, A. Urtti, Pharmacokinetic aspects of retinal drug delivery, Prog Retin Eye Res, 57 (2017) 134-185.

[16] A. Patel, K. Cholkar, V. Agrahari, A.K. Mitra, Ocular drug delivery systems: An overview, World J Pharmacol, 2 (2013) 47-64.

[17] A. Mandal, R. Bisht, I.D. Rupenthal, A.K. Mitra, Polymeric micelles for ocular drug delivery: From structural frameworks to recent preclinical studies, J Controlled Release, 248 (2017) 96-116.

[18] P. Bansal, S. Garg, Y. Sharma, P. Venkatesh, Posterior Segment Drug Delivery Devices: Current and Novel Therapies in Development, J Ocul Pharmacol Ther, 32 (2016) 135-144.

[19] L.L. Lim, J.R. Smith, J.T. Rosenbaum, Retisert (Bausch & Lomb/Control Delivery Systems), Curr Opin Investig Drugs, 6 (2005) 1159-1167.

[20] G.J. Jaffe, D. Martin, D. Callanan, P.A. Pearson, B. Levy, T. Comstock, G. Fluocinolone Acetonide Uveitis Study, Fluocinolone acetonide implant (Retisert) for noninfectious posterior uveitis: thirty-four-week results of a multicenter randomized clinical study, Ophthalmology, 113 (2006) 1020-1027.

[21] F.E. Kane, J. Burdan, A. Cutino, K.E. Green, Iluvien: a new sustained delivery technology for posterior eye disease, Expert Opin Drug Deliv, 5 (2008) 1039-1046.

[22] D.S. Boyer, Y.H. Yoon, R. Belfort, Jr., F. Bandello, R.K. Maturi, A.J. Augustin, X.Y. Li, H. Cui, Y. Hashad, S.M. Whitcup, M.S.G. Ozurdex, Three-year, randomized, sham-controlled trial of dexamethasone intravitreal implant in patients with diabetic macular edema, Ophthalmology, 121 (2014) 1904-1914.

[23] A. Chan, L.S. Leung, M.S. Blumenkranz, Critical appraisal of the clinical utility of the dexamethasone intravitreal implant (Ozurdex) for the treatment of macular edema related to branch retinal vein occlusion or central retinal vein occlusion, Clin Ophthalmol, 5 (2011) 1043-1049.

[24] J. Wang, A. Jiang, M. Joshi, J. Christoforidis, Drug delivery implants in the treatment of vitreous inflammation, Mediators Inflamm, 2013 (2013) 780634.

[25] ClinicalTrials.gov, Extension Study for the Port Delivery System With Ranibizumab (Portal) (Portal), in, https://clinicaltrials.gov/ct2/show/NCT03683251 (accessed May 22, 2021), 2018.

[26] ClinicalTrials.gov, Study of the efficacy and safety of the ranibizumab port delivery system (RPDS) for sustained delivery of ranibizumab in participants with subfoveal neovascular age-related macular degeneration (AMD) (LADDER), 2015, accessed May 05, 2021 in, https://clinicaltrials.gov/ct2/show/NCT02510794

[27] ClinicalTrials.gov, A Phase III Study to Evaluate the Port Delivery System With Ranibizumab Compared With Monthly Ranibizumab Injections in Participants With Wet Age-Related Macular Degeneration (Archway), 2021; accessed May 22, 2021 in, https://clinicaltrials.gov/ct2/show/NCT03677934?term=archway&rank=1

5

[28] M.J. Ansari, R.R. Rajendran, S. Mohanto, U. Agarwal, K. Panda, K. Dhotre, R. Manne, A. Deepak, A. Zafar, M. Yasir, S. Pramanik, Poly(N-isopropylacrylamide)-Based Hydrogels for Biomedical Applications: A Review of the State-of-the-Art, Gels, 8 (2022) 454.

[29] T. Vermonden, R. Censi, W.E. Hennink, Hydrogels for protein delivery, Chem Rev, 112 (2012) 2853-2888.

[30] Y. Li, H.Y. Yang, D.S. Lee, Biodegradable and Injectable Hydrogels in Biomedical Applications, Biomacromolecules, 23 (2022) 609-618.

[31] B.C. Ilochonwu, A. Urtti, W.E. Hennink, T. Vermonden, Intravitreal hydrogels for sustained release of therapeutic proteins, J. Controlled Release, 326 (2020) 419-441.

[32] D. Chang, K. Park, A. Famili, Hydrogels for sustained delivery of biologics to the back of the eye, Drug Discov Today, 24 (2019) 1470-1482.

[33] J. Li, DJ. Mooney, Designing hydrogels for controlled drug delivery, Nat Rev Mater, 1 (2016) 1-17.

[34] S.R. Van Tomme, W.E. Hennink, Biodegradable dextran hydrogels for protein delivery applications, Expert Rev Med Devices, 4 (2007) 147-164.

[35] S. Kirchhof, A. Strasser, H.-J. Wittmann, V. Messmann, N. Hammer, A.M. Goepferich, F.P. Brandl, New insights into the cross-linking and degradation mechanism of Diels–Alder hydrogels, J. Mater. Chem. B, 3 (2015) 449-457.

[36] H. Shah, E. Reichel, B. Busbee, A novel lidocaine hydrochloride ophthalmic gel for topical ocular anesthesia, Local and regional anesthesia, 3 (2010) 57-63.

[37] I. Kozak, L. Cheng, W.R. Freeman, Lidocaine gel anesthesia for intravitreal drug administration, Retina, 25 (2005) 994-998.

[38] B.C. Ilochonwu, M. Mihajlovic, R.F. Maas-Bakker, C. Rousou, M. Tang, M. Chen, W.E. Hennink, T. Vermonden, Hyaluronic Acid-PEG-Based Diels-Alder In Situ Forming Hydrogels for Sustained Intraocular Delivery of Bevacizumab, Biomacromolecules, 23 (2022) 2914-2929.

[39] S. Kirchhof, M. Gregoritza, V. Messmann, N. Hammer, A.M. Goepferich, F.P. Brandl, Diels-Alder hydrogels with enhanced stability: First step toward controlled release of bevacizumab, Eur J Pharm Biopharm, 96 (2015) 217-225.

[40] Q. Chai, Y. Jiao, X. Yu, Hydrogels for Biomedical Applications: Their Characteristics and the Mechanisms behind Them, Gels, 3 (2017) 6.

[41] P. Sikdar, M.M. Uddin, T.M. Dip, S. Islam, M.S. Hoque, A.K. Dhar, S. Wu, Recent advances in the synthesis of smart hydrogels, Materials Advances, 2 (2021) 4532-4573.

[42] H.M. El-Husseiny, E.A. Mady, L. Hamabe, A. Abugomaa, K. Shimada, T. Yoshida, T. Tanaka, A. Yokoi, M. Elbadawy, R. Tanaka, Smart/stimuli-responsive hydrogels: Cutting-edge platforms for tissue engineering and other biomedical applications, Mater Today Bio, 13 (2022) 100186.

[43] X. Xu, J. Yu, H. Shi, J. Zhang, X. Li, Prevention of corneal neovascularization by subconjunctival injection of avastin(R) loaded thermosensitive hydrogels in rabbit model, Int J Pharm, 552 (2018) 164-170.

[44] J.J.K. Derwent, W.F. Mieler, Thermoresponsive hydrogels as a new ocular drug delivery platform to the posterior segment of the eye, Trans. Am. Ophthalmol. Soc. , 106 (2008) 206-214.

[45] M.A. Haq, Y. Su, D. Wang, Mechanical properties of PNIPAM based hydrogels: A review, Mater Sci Eng C Mater Biol Appl, 70 (2017) 842-855.

[46] A. Alexander, Ajazuddin, J. Khan, S. Saraf, S. Saraf, Polyethylene glycol (PEG)-Poly(N-isopropylacrylamide) (PNIPAAm) based thermosensitive injectable hydrogels for biomedical applications, Eur J Pharm Biopharm, 88 (2014) 575-585.

[47] V. Cheng, B.H. Lee, C. Pauken, B.L. Vernon, Poly(N-isopropylacrylamide-co-poly(ethylene glycol))-acrylate simultaneously physically and chemically gelling polymer systems, Journal of Applied Polymer Science, 106 (2007) 1201-1207.

[48] O. Diels, K. Alder, Synthesen in der hydro-aromatischen Reihe, II. Mitteilung: Über Cantharidin, Berichte der deutschen chemischen Gesellschaft (A and B Series), 62 (1929) 554-562.

[49] Hong-Liang Wei, Zhe Yang, Li-Mei Zheng, Y.-M. Shen, Thermosensitive hydrogels synthesized by fast Diels–Alder reaction in water, Polymer, 50 (2009) 2836-2840.

[50] C.M. Madl, S.C. Heilshorn, Bioorthogonal Strategies for Engineering Extracellular Matrices, Adv Funct Mater, 28 (2018).

[51] A.J. de Graaf, K.W. Boere, J. Kemmink, R.G. Fokkink, C.F. van Nostrum, D.T. Rijkers, J. van der Gucht, H. Wienk, M. Baldus, E. Mastrobattista, T. Vermonden, W.E. Hennink, Looped structure of flowerlike micelles revealed by ^{1}H NMR relaxometry and light scattering, Langmuir, 27 (2011) 9843-9848.

[52] J. Loccufier, M. Bos, E.H. Schacht, Convenient method for the analysis of primary and secondary hydroxyl end groups in polyethers, Polymer Bulletin, 27 (1991) 201-204.

[53] O. Soga, C.F. van Nostrum, A. Ramzi, T. Visser, F. Soulimani, P.M. Frederik, P.H.H. Bomans, W.E. Hennink, Physicochemical Characterization of Degradable Thermosensitive Polymeric Micelles, Langmuir, 20 (2004) 9388-9395.

[54] P.J. Flory, J.R. Jr., Statistical Mechanics of Cross-Linked Polymer Networks I. Rubberlike Elasticity, J. Chem. Phys., 11 (1943) 512-520.

[55] H.G. Schild, Poly(N-isopropylacrylamide): experiment, theory and application, Progress in Polymer Science, 17 (1992) 163-249.

[56] E.H. Marzieh Najafi, Wim E. Hennink,Tina Vermonden, Poly(Nisopropylacrylamide): Physicochemical Properties and Biomedical Applications, John Wiley Sons, Ltd, 2018.

[57] A. Durand, D. Hourdet, Thermoassociative graft copolymers based on poly(N-isopropylacrylamide): Relation between the chemical structure and the rheological properties, Macromolecular Chemistry and Physics, 201 (2000) 858-868.

[58] R.G. Huber, M.A. Margreiter, J.E. Fuchs, S. von Grafenstein, C.S. Tautermann, K.R. Liedl, T. Fox, Heteroaromatic pi-stacking energy landscapes, J Chem Inf Model, 54 (2014) 1371-1379.

[59] F.R. Cordell, J.E. Boggs, Structure and degree of aromatic character in furan, pyrrole, and thiophene, Journal of Molecular Structure: THEOCHEM, 85 (1981) 163-178.

5

[60] L. Ahmadkhani, M. Abbasian, A. Akbarzadeh, Synthesis of sharply thermo and PH responsive PMA-b-PNIPAM-b-PEG-b-PNIPAM-b-PMA by RAFT radical polymerization and its schizophrenic micellization in aqueous solutions, Des Monomers Polym, 20 (2017) 406-418.

[61] J. Yang, R. van Lith, K. Baler, R.A. Hoshi, G.A. Ameer, A thermoresponsive biodegradable polymer with intrinsic antioxidant properties, Biomacromolecules, 15 (2014) 3942-3952.

[62] R. Li, Y. Wu, Z. Bai, J. Guo, X. Chen, Effect of molecular weight of polyethylene glycol on crystallization behaviors, thermal properties and tensile performance of polylactic acid stereocomplexes, RSC Advances, 10 (2020) 42120-42127.

[63] C.M. Nimmo, S.C. Owen, M.S. Shoichet, Diels-Alder Click cross-linked hyaluronic acid hydrogels for tissue engineering, Biomacromolecules, 12 (2011) 824-830.

[64] O. El Tall, Y. Hou, E. Abou-Hamad, I.U. Raja, M.N. Hedhili, W. Peng, R. Mahfouz, O.M. Bakr, P.M. Beaujuge, Direct Functionalization of Nanodiamonds with Maleimide, Chemistry of Materials, 26 (2014) 2766-2769.

[65] T. Sepperer, J. Neubauer, J. Eckardt, T. Schnabel, A. Petutschnigg, G. Tondi, Pollutant Absorption as a Possible End-Of-Life Solution for Polyphenolic Polymers, Polymers (Basel), 11 (2019).

[66] G. Tondi, M. Link, C.W. Oo, A. Petutschnigg, A Simple Approach to Distinguish Classic and Formaldehyde-Free Tannin Based Rigid Foams by ATR FT-IR, Journal of Spectroscopy, 2015 (2015) 1-8.

[67] A. Oluwasanmi, C. Hoskins, Potential use of the Diels-Alder reaction in biomedical and nanomedicine applications, Int J Pharm, 604 (2021) 120727.

[68] D. Neradovic, M.J. van Steenbergen, L. Vansteelant, Y.J. Meijer, C.F. van Nostrum, W.E. Hennink, Degradation Mechanism and Kinetics of Thermosensitive Polyacrylamides Containing Lactic Acid Side Chains, Macromolecules, 36 (2003) 7491-7498.

[69] S. Aretz, T.U. Krohne, K. Kammerer, U. Warnken, A. Hotz-Wagenblatt, M. Bergmann, B.V. Stanzel, T. Kempf, F.G. Holz, M. Schnölzer, J. Kopitz, In-depth mass spectrometric mapping of the human vitreous proteome, Proteome Science, 11 (2013) 22.

[70] L.M. Hirvonen, G.O. Fruhwirth, N. Srikantha, M.J. Barber, J.E. Neffendorf, K. Suhling, T.L. Jackson, Hydrodynamic Radii of Ranibizumab, Aflibercept and Bevacizumab Measured by Time-Resolved Phosphorescence Anisotropy, Pharm Res, 33 (2016) 2025-2032.

[71] R. Censi, T. Vermonden, H. Deschout, K. Braeckmans, P. di Martino, S.C. De Smedt, C.F. van Nostrum, W.E. Hennink, Photopolymerized Thermosensitive Poly(HPMAlactate)-PEG-Based Hydrogels: Effect of Network Design on Mechanical Properties, Degradation, and Release Behavior, Biomacromolecules, 11 (2010) 2143-2151.

[72] J. Crank, diffuision in a plane sheet, The Mathematics of Diffusion, (1975) 47-48.

[73] J. Siepmann, F. Siepmann, Modeling of diffusion controlled drug delivery, J Control Release, 161 (2012) 351-362.

[74] M.J. Roberts, M.D. Bentley, J.M. Harris, Chemistry for peptide and protein PEGylation, Advanced Drug Delivery Reviews, 54 (2002) 459-476.

[75] N. Hammer, F.P. Brandl, S. Kirchhof, V. Messmann, A.M. Goepferich, Protein compatibility of selected cross-linking reactions for hydrogels, Macromol Biosci, 15 (2015) 405-413.

[76] D. online, Dexamethasone in, https://go.drugbank.com/drugs/DB01234.

[77] R. Schulz, K. Yamamoto, A. Klossek, R. Flesch, S. Honzke, F. Rancan, A. Vogt, U. Blume-Peytavi, S. Hedtrich, M. Schafer-Korting, E. Ruhl, R.R. Netz, Data-based modeling of drug penetration relates human skin barrier function to the interplay of diffusivity and free-energy profiles, Proc Natl Acad Sci U S A, 114 (2017) 3631-3636.

[78] J.E. Chang-Lin, M. Attar, A.A. Acheampong, M.R. Robinson, S.M. Whitcup, B.D. Kuppermann, D. Welty, Pharmacokinetics and pharmacodynamics of a sustained-release dexamethasone intravitreal implant, Invest Ophthalmol Vis Sci, 52 (2011) 80-86.

[79] A. Grzybowski, R. Told, S. Sacu, F. Bandello, E. Moisseiev, A. Loewenstein, U. Schmidt-Erfurth, B. Euretina, 2018 Update on Intravitreal Injections: Euretina Expert Consensus Recommendations, Ophthalmologica, 239 (2018) 181-193.

[80] A.L.A. Fonseca, H. Panetta, M.A. Nascimento, R.P.C. Lira, C.E.L. Arieta, Effect of intravitreal dexamethasone solution on the reduction of macular thickness in pseudophakic diabetic patients in a public hospital in Brazil: a randomized clinical trial, Clin Ophthalmol, 13 (2019) 1523-1531.

[81] S.-Y. Seong, P. Matzinger, Hydrophobicity: an ancient damage-associated molecular pattern that initiates innate immune responses, Nature Reviews Immunology, 4 (2004) 469-478.

[82] R.R. Hartman, U.B. Kompella, Intravitreal, Subretinal, and Suprachoroidal Injections: Evolution of Microneedles for Drug Delivery, J Ocul Pharmacol Ther, 34 (2018) 141-153.

5

8   SUPPORTING INFORMATION
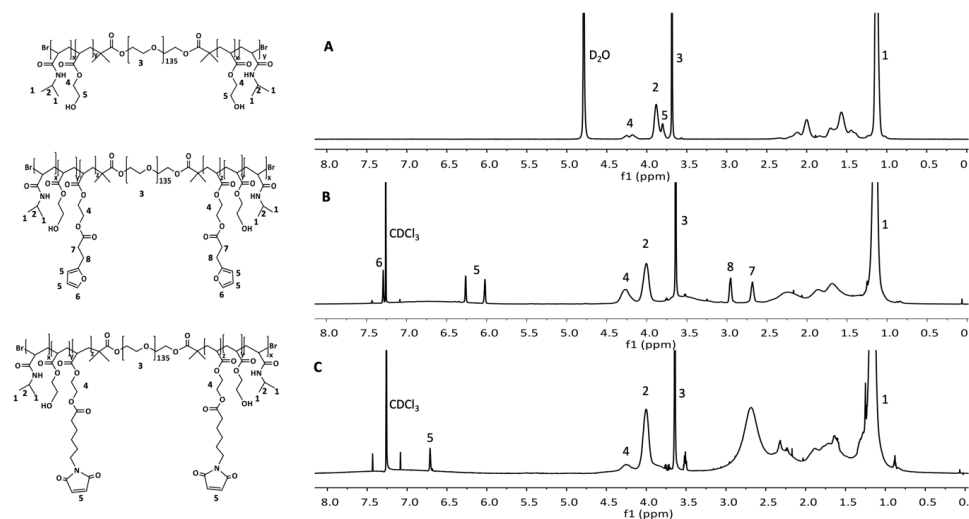
SI-Figure 1 Structures and 1H-NMR spectra of A) PNH B) PNF C) PNM.
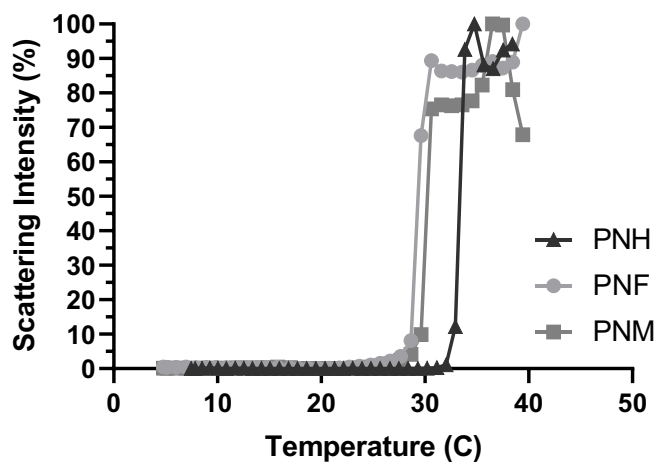
SI-Figure 2 Scattering intensity at a 650 nm as a function of temperature of PNH, PNF, PNM dissolved in PBS at a concentration of 3 mg/ml. The onset point of the increased scattering intensity is reported as the cloud point.
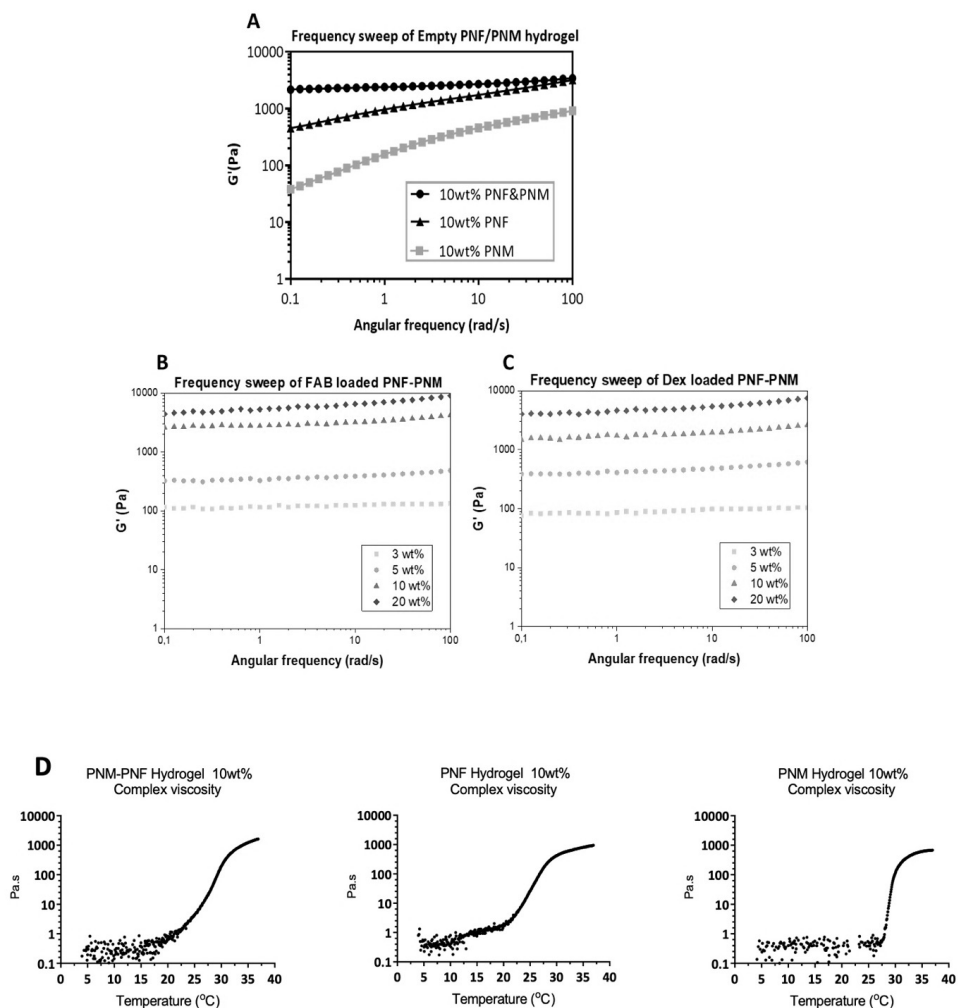
SI-Figure 3 Storage modulus (G') of PNF-PNM hydrogel with/without loaded drug as a function of angular frequency at 37 °C after physical and/or chemical crosslinking during a temperature and time sweep at strain 0.5 % as described in section 2.3.3. A) G' of 10wt% empty PNF-PNM hydrogel, PNF and PNM system with increasing angular frequency. B) G' of 3, 5, 10, 20 wt% FAB-loaded PNF-PNM hydrogel with increasing angular frequency. C) G' of 3, 5, 10, 20 wt% dex-loaded PNF-PNM hydrogel with increasing angular frequency. D) Complex viscosity as a function of temperature for empty 10wt% hydrogels made PNM-PNF, PNF and PNM.
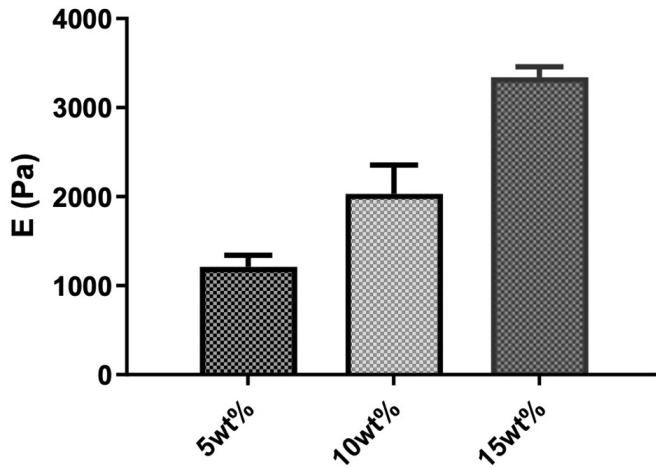
SI-Figure 4 Young's moduli (E) of PNF-PNM DA hydrogels after network formation for 3 h at 37 °C as a function of hydrogel polymer concentration as determined using dynamic mechanical analysis (DMA) at room temperature. The results are reported as mean +/- SD (n=3).
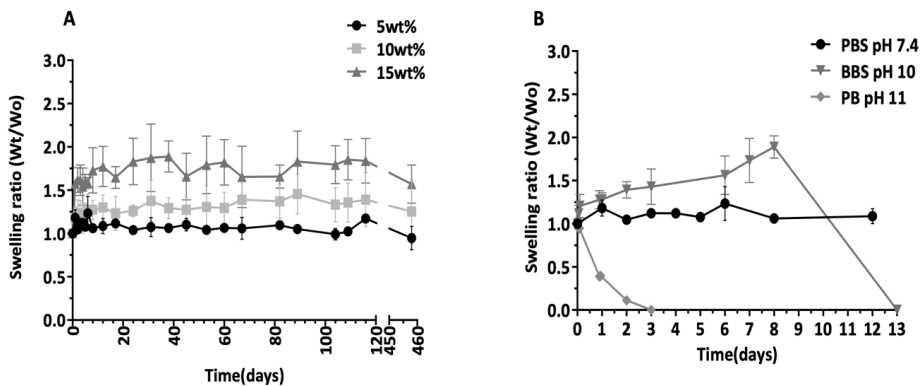
SI-Figure 5 Swelling ratios of PNF-PNM hydrogels as a function of time at different conditions. The swelling ratio is defined as the weight of gels (W_t) at a certain time point divided by the initial hydrogel weight (W_0) after gelation/shrinking. W_0 values at 37 °C were 66±7, 45±8 and 28±6 mg for the 5, 10, 15 wt% gels, respectively. A) Swelling ratio of PNF-PNM hydrogels with initial polymer concentrations of 5, 10, and 15 wt% upon 460 days incubation in PBS pH 7.4 at 37 °C. This figure also shows that the swelling ratio of the PNF-PNM hydrogels increased with increasing initial polymer concentration. The observed swelling likely is an artifact since the weights of the gels were determined at room temperature which is below the LCST of both PNM/PNM, which means that during sample handling the gels reabsorb water. B) Swelling ratio of a 5 wt% PNF-PNM hydrogel incubated at 37 °C in different media: PBS (pH 7.4), BBS (pH 10), PB (pH 11). The data are presented as mean ± SD of three independent replicates.

A   Raw 264.7 cells incubated with PNF or PNM

B   ARPE 19 cells incubated with PNF or PNM
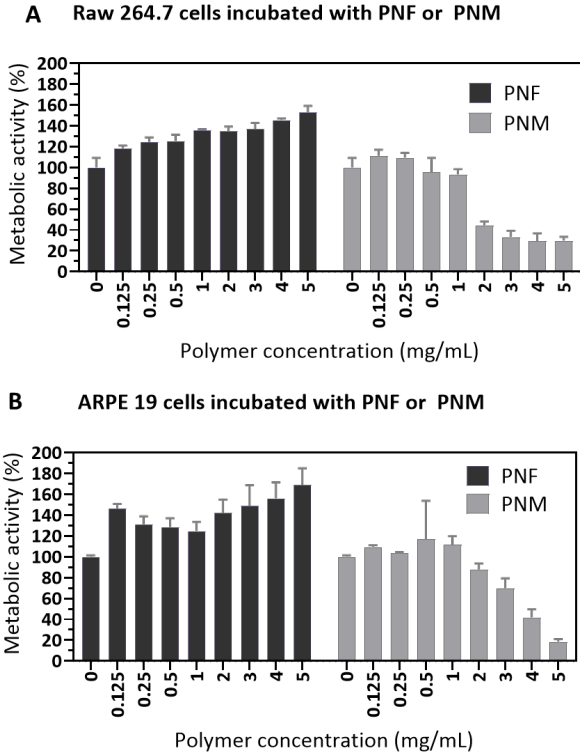
SI-Figure 6 A) Metabolic activity of RAW 264.7 cells incubated in medium containing PNF or PNM for 24h at 37 °C B) Metabolic activity of ARPE-19 cells incubated in medium containing PNF or PNM for 24h at 37 °C.

5
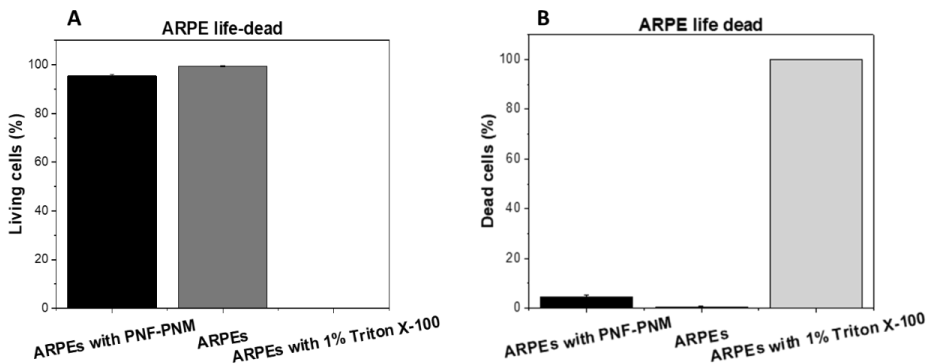
SI-Figure 7 A: Percentages of living cells stained with Calcein AM after incubation with a PNF-PNM hydrogel for 24 hours at 37 °C. B: Percentages of dead cells stained with Calcein AM after incubation with a PNF-PNM hydrogel.
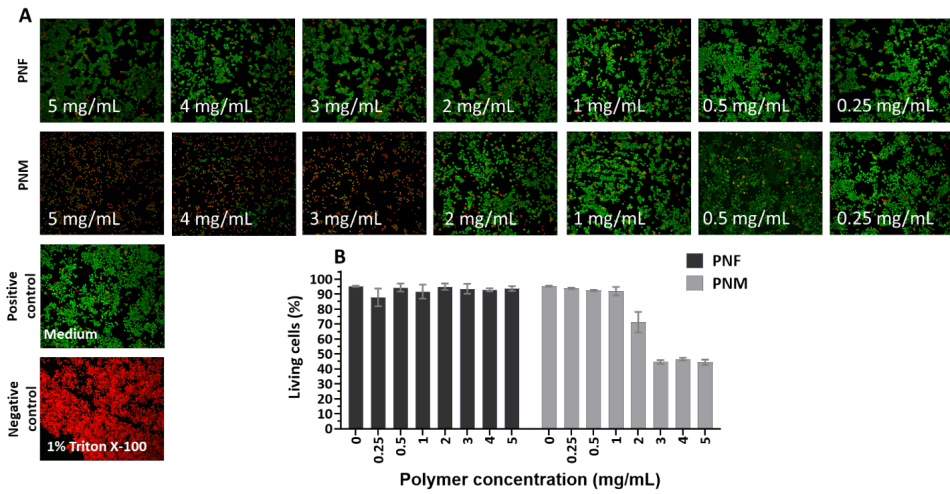
SI Figure 8 Life-dead staining of RAW 264.7 cells after 24 h incubation with PNF and PNM polymers. Living cells were stained green and dead cells were stained red using Calcein AM and propidium Iodide (PI), respectively. A) Calcein AM and propidium iodide staining's of RAW 264.7 cells cultured in medium with PNF or PNM to assess cell viability. B) Percentages of living cells stained with Calcein AM after incubation with PNF and PNM.
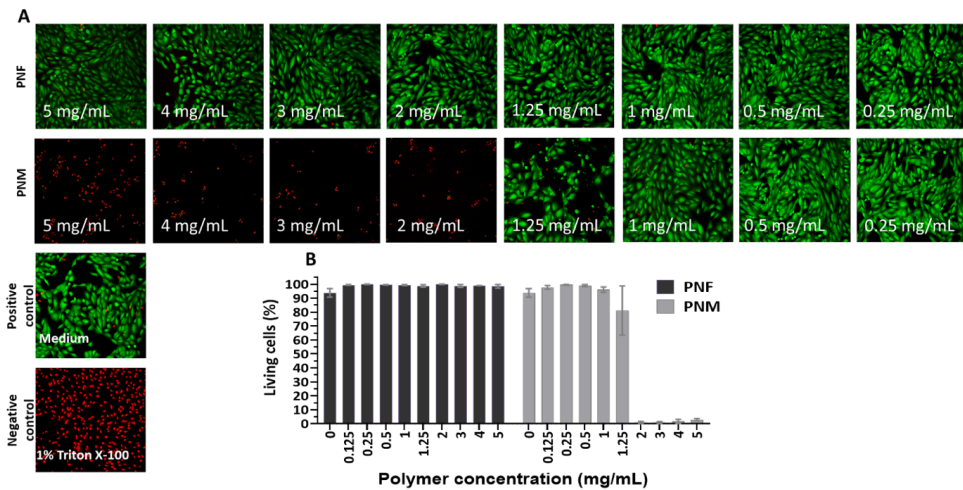
SI-Figure 9 Life/dead staining of ARPE-19 cells after 24 h incubation with polymers (PNF and PNM). Living cells were stained green and dead cells were stained red using Calcein AM and PI, respectively. A) Calcein AM and PI staining of ARPR-19 cells cultured in medium with PNF or PNM. Living cells are imaged green and dead cells in red. B) Percentages of living cells stained with Calcein AM after incubation with PNF and PNM.
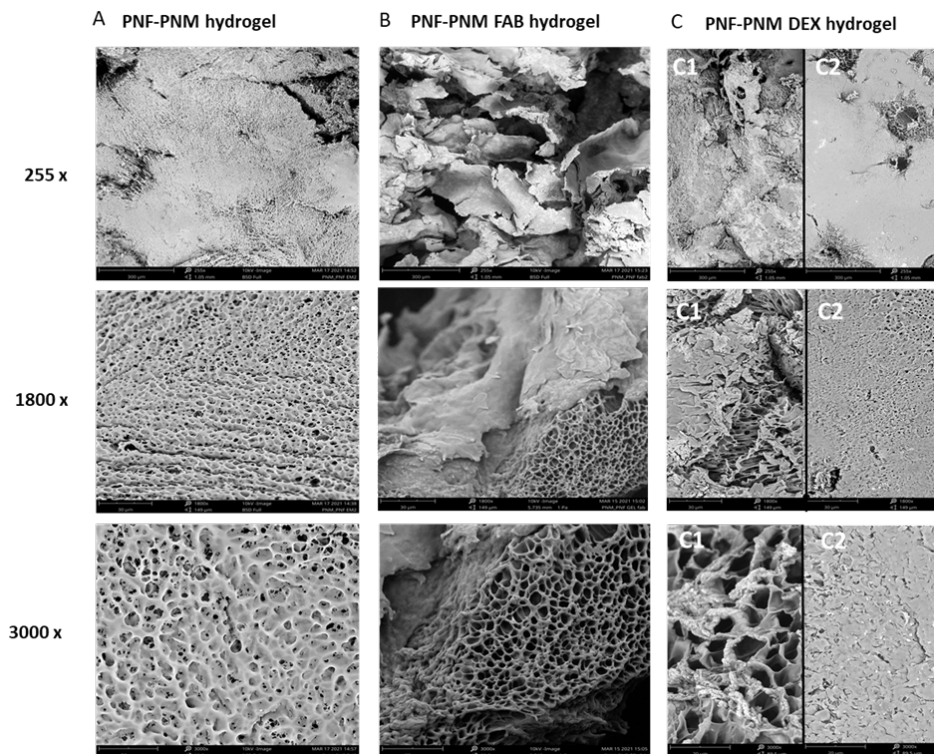
SI-Figure 10 Scanning electron photomicrographs freeze dried hydrogels A) PNF-PNM hydrogel B) FAB-loaded PNF-PNM hydrogel C) dex-loaded PNF-PNM hydrogel at magnifications of 255×, 1800× and 3000×. C1 and C2 represent the dex-loaded hydrogel with the same magnification but different sections of the imaged gel.
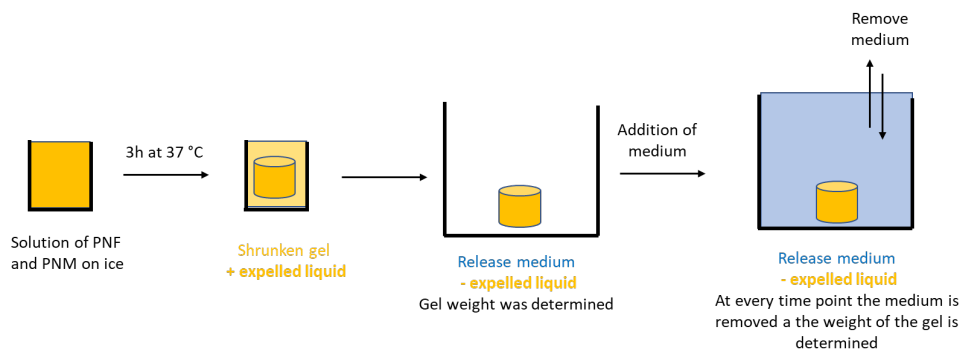
SI-Figure 11 Schematic overview of the experimental setup of the gel formation and subsequent swelling and degradation study. The (+) expelled liquid indicates the water that was expelled from the gels during shrinking during hydrogel formation. The weight of the hydrogel was determined "without (-) expelled liquid" from the hydrogel during shrinking.
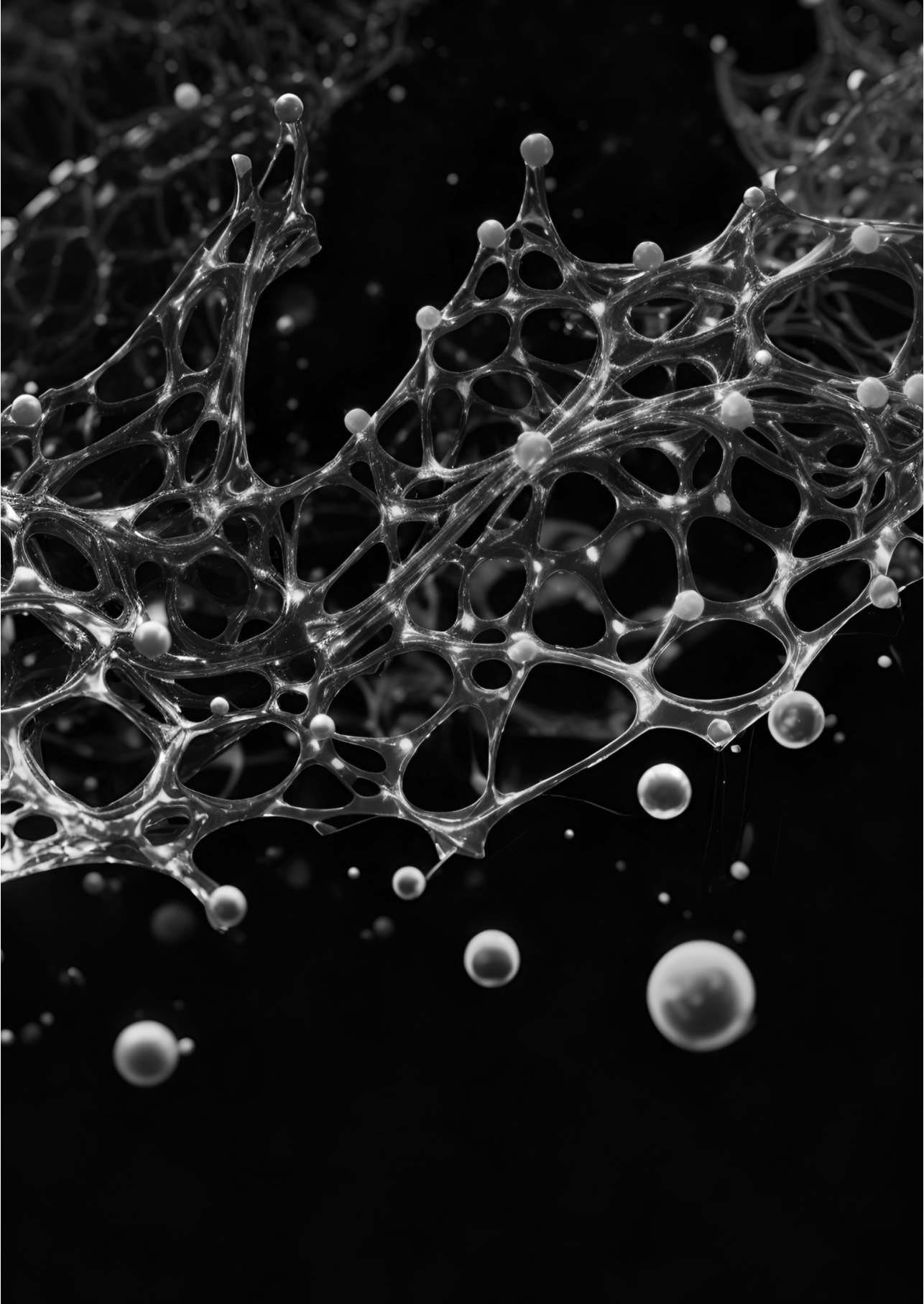
Chapter 6

Diels-Alder Core-Crosslinked Flower-like Micelles for Intraocular Drug Delivery Applications

Blessing C. Ilochonwu[1*], Ada Annala[1,2*], Danny Wilbie[1], Barbara Mesquita[1], Amir Sadeghi[2], J. Puranen[2], Elisa Toropainen[2], Marika Ruponen [2], Arto Urtti [2,3], Wim E. Hennink [1], Tina Vermonden[1]

[1]Department of Pharmaceutics, Utrecht Institute for Pharmaceutical Sciences, Faculty of Science, Utrecht University, PO box 80082, 3508 TB Utrecht, the Netherlands. [2]School of Pharmacy, University of Eastern Finland, Kuopio, Finland. [3]Centre for Drug Research, Division of Pharmaceutical Biosciences, University of Helsinki, Helsinki, Finland. * These authors contributed equally to this work

ABSTRACT

Purpose

This study aims to investigate Diels-Alder (DA) core-crosslinked flower like micelles (FLM) for as a potential drug delivery vehicle for intraocular therapy.

Methods

Two complementary ABA triblock copolymers were synthesized. These copolymers consist of a hydrophilic midblock of polyethylene glycol (PEG), flanked by two types of random blocks, namely thermosensitive N-isopropylacrylamide (NIPAM) and 2-hydroxyethyl acrylate (HEA) modified with either maleimide or furan functionalities, resulting in two distinct polymer variants: P(NIPAM-co-HEA/Maleimide)-PEG-P(NIPAM-co-HEA/Maleimide) (PNM) and P(NIPAM-co-HEA/Furan)-PEG-P(NIPAM-co-HEA/Furan) (PNF), respectively. The block copolymers self-assembled into flower-like micelles in an aqueous solution above the lower critical solution temperature of the thermosensitive block, following exposure to 50°C. Subsequent, core-crosslinking of the resulting FLM structures was achieved through a Diels-Alder reaction between the furan and maleimide groups present in PNF and PNM. In vitro examinations were performed to assess the size and shape of the micelles. The cellular uptake and cytocompatibility of Flower-Like Micelles (FLM) labeled with a fluorescent dye (BDP) were investigated using RAW 264.7 macrophages and ARPE-19 cell lines. In vivo, ocular safety, vitreous and retinal distribution of the fluorescently labelled FLM were investigated after intravitreal injection using a rat model.

Results

Spherically shaped BDP-dye loaded FLM were successfully prepared with hydrodynamic radius of 46.6 ± 3.2 at 37°C. Fluorescently labeled FLM were internalized by RAW 264.7 macrophages and ARPE-19 cells within a 24-hour incubation period and demonstrated good cytocompatibility. Intravitreal injection of fluorescently labelled FLM in the eye of rats showed a rather rapid vitreous clearance of the FLM within two days post injection. Nevertheless, the FLM reached the optic nerve, retinal cells and most importantly, permeate the inner limiting membrane (ILM) at the vitreoretinal barrier. Furthermore, neither adverse effects nor retinal abnormalities were detected by fundus and OCT images.

Conclusions

Diels-Alder core-crosslinked FLM are promising delivery vehicles to target ocular macrophages and the sub-retinal space. However, the retention of the particle in the vitreous after administration should be improved to obtain sustained therapeutic effects upon their loading with e.g. an anti-inflammatory drug like dexamethasone.

Graphical abstract:
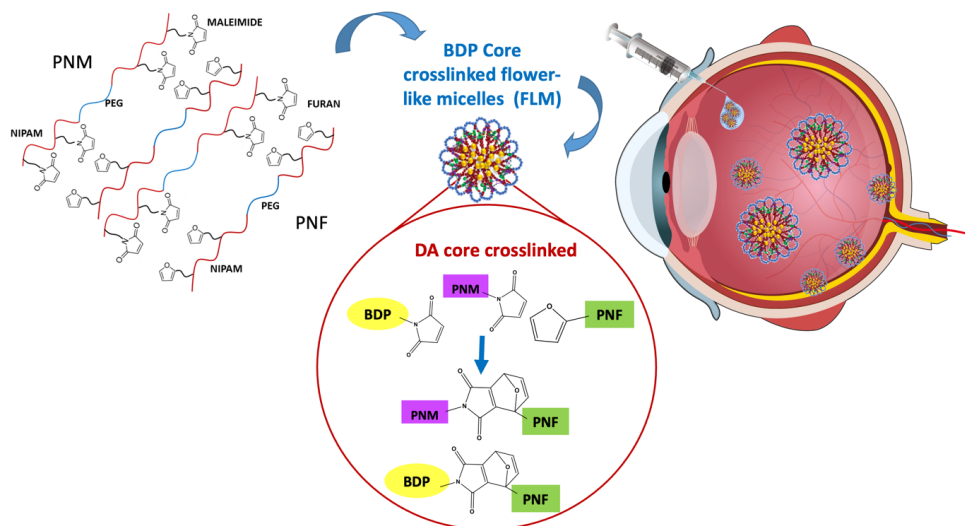
1   INTRODUCTION

In the last decades, a variety of nanoparticles, microparticles, hydrogels and polymer conjugates has been developed and investigated for ocular delivery of therapeutics.[1-7] Recently, researchers have directed their efforts towards utilizing innovative drug delivery systems that target the retinal pigment epithelial cell line (RPE). This strategy targets often ocular inflammations as well as uveitis across anterior and posterior segments of the eye. Bhattacharya et. al.[8] and Kicková et. al.[9] have substantiated this approach, underscoring its potential for innovative ocular disease treatment. Furthermore, macrophages and microglial cells are essential immune cells residing in the eye and retina.[10] These cells play a significant role in releasing pro-inflammatory cytokines such as IL-6 and TNF-alpha, which are associated with inflammatory and hereditary retinal diseases such as age-related macular degeneration, uveitis, glaucoma, and retinitis pigmentosa.[11-13] As a result, targeting ocular macrophages holds promising potential in treating various ocular diseases.[14] However, there is still a need for systems that deliver therapeutics to macrophages, microglia and RPE in order to fully exploit the potential of the approach. Particularly polymeric micelles, core-shell structures based on amphiphilic block copolymers, are promising systems to carry and deliver hydrophobic drugs to targets in the eye. In aqueous media and at concentrations above the critical micelle concentration (CMC), such copolymers self-assemble into nano-sized particles with sizes ranging from 10-100 nm and can be used to solubilize and deliver hydrophobic drugs.[14-17] The shape and size of the micelles can be tailored by polymer molecular weight, composition and architecture. Generally speaking, AB diblock copolymers self-assemble into star-like micelles while ABA triblock copolymers (with a hydrophilic midblock (B)) flanked by two hydrophobic B blocks self-assemble into flower-like micelles (FLM).[18-20] In order to have a clinically interesting nanomedicine formulation for ocular drug therapy, the particles should ensure sufficient stability to prevent premature

disintegration. Core-crosslinking is a frequently applied method to improve the in vivo stability of polymeric micelles. To also enhance drug retention in the particles, core-crosslinked polymeric micelles can be designed in which (pro-)drugs are covalently entrapped.[21] Prior research has demonstrated the significance of nanomedicine size in enhancing therapeutic effectiveness in ocular applications.

This study aims to develop Diels-Alder core-crosslinked FLM for intracellular drug delivery to target vitreoretinal interface barrier. To this end a fluorescent dye with a maleimide group was therefore covalently linked to the core of the FLM for cell uptake and in vivo studies. In the present study, a systematic evaluation of micelles size, shape, and in vitro cellular uptake, was used to assess whether the developed FLM's are suitable for ocular therapy. Moreover, the in vivo ocular safety and retinal distribution of fluorescently labelled FLM were investigated after intravitreal injection in a rat eye model.

2   MATERIALS AND METHODS

Unless indicated otherwise, all commercial chemicals were obtained from Sigma-Aldrich (Zwijndrecht, the Netherlands) and used as received. The used PBS buffer has the following composition: 0.13 M NaCl, 2.7 mM KCl and 11.9 mM phosphates, pH 7.4.

2.1   Synthesis of P(NIPAM-co-HEA/Maleimide)-PEG-P(NIPAM-co-HEA/Maleimide) (PNM)

The PNM polymer was synthesized and charactered according to a previously reported procedure with minor modifications. First, P(NIPAM-co-HEA)-PEG-P(NIPAM-co-HEA) (PNH)) was synthesized as described in a recent paper.[22] Briefly, PNH (with average PEG molecular weight (M_n) of 6.0 kDa was synthesized at feed ratio of NIPAM/HEA 88:12 and the obtained polymer had a total M_n of 42 kDa as determined by ^{1}H NMR analysis. PNH (600 mg; 0.0142 mmol) was subsequently dissolved in 10 ml dry dichloromethane (DCM) at 0 ^{0}C under nitrogen atmosphere. N,N'-Dicyclohexylcarbodiimide (DCC) (112 mg; 0.54 mmol), 4-(dimethylamino)pyridine (DMAP) (0.66 mg; 0.0054 mmol) and 6-maleimidohexanoic acid (114 mg; 0.52 mmol) were added and the mixture was stirred for 1 hour on ice. The reaction was subsequently carried out for 16 h at RT, and the reaction mixture was thereafter dropped into cold diethyl ether to precipitate the formed polymer. Next, the precipitate was dissolved in 25 mL H_2O and residual solids were removed by filtration and the filtrate was freeze-dried overnight. The obtained product was collected as a white powder. ^{1}H NMR spectrum of PNM in CDCl$_3$: δ (ppm) 1.13 (6H, CH$_3$CHCH$_3$, NIPAM); 1.30-3.0 (backbone hydrogens); 3.68 (4H, OCH$_2$CH$_2$O, PEG); 4.00 (1H, CH$_3$CHCH$_3$, NIPAM); 4.23 (4H, OCH$_2$CH$_2$O) 6.71 (2H, maleimide). Spectrum shown in the SI-Figure 1

2.2   Synthesis of P(NIPAM-co-HEA/Furan)-PEG-P(NIPAM-co-HEA/Furan) (PNF)

PNH (600 mg; 0.0142 mmol) was dissolved in 10 mL chloroform and stirred for 30 minutes while flushed with nitrogen. 3-(2-Furyl)propionic acid (253 mg; 1.80 mmol), DCC (373 mg; 1.80 mmol) and DMAP (2.20 mg; 0.0181 mmol) were added and the mixture was stirred for 16 h at RT. The reaction mixture was subsequently dropped into cold diethyl ether and the obtained precipitate was dissolved in 25 mL H_2O. The residual solids were filtered, and the filtrate was freeze-dried

overnight. The formed PNF was collected as a white powder. ^{1}H NMR spectrum of PNF in CDCl$_3$: δ (ppm) 1.13 (6H, CH$_3$CHCH$_3$, NIPAM); 1.30-3.0 (backbone hydrogens); 3.68 (4H, OCH$_2$CH$_2$O, PEG 6 kDa); 4.00 (1H, CH$_3$CHCH$_3$, NIPAM); 4.23 (4H, OCH$_2$CH$_2$O) 6.01 (1H, CCHCH, Furan); 6.26 (1H, CHCHCH, furan); 7.29 (1H, CHCHO, furan). Spectrum shown in the SI-Figure 1

2.3 FLM formation

2.3.1 Preparation of empty loaded FLM

FLM were formed using a fast heating method[18, 23] where PNM with 9% maleimide substitution and PNF with 10% furan substitution were dissolved separately at a concentration of 10 mg/mL in PBS at 4 °C. Subsequently, equal volumes (500 μL) of the two polymer solutions were merged, with the molar ratio of 1:1.2 between maleimide and furan (see calculation in supplementary data). After a brief vortex mixing, the solution was transferred into a 50 °C oil bath and stirred for 3 hours. Next, the obtained FLM were cooled to room temperature, followed by filtration through 0.45 μm filter. For preparing IR samples, the FLM were further purified with a desalting column (Cytiva HiTrap® Desalting column 5 mL, Sigma-Aldrich, Zwijndrecht, the Netherlands) followed by freeze-drying.

2.3.2 Preparation of BDP dye-loaded FLM

BDP dye-loaded FLM (PNM:PNF BDP-Mal FLM) were prepared as described in section 2.3.1 with some modifications. PNM (20 mg/mL) with 9% maleimide substitution and PNF (22 mg/mL) with 10% furan substitution were dissolved separately in PBS at 4 °C. Borondipyrromethene dye with a maleimide tag (BDP-Mal, Lumiprobe GmbH (Europe), Hannover, GE) was dissolved in DMSO at a concentration of 6.0 mg/mL at RT. Equal volumes (450 μL) of two polymer solutions were combined, with maleimide and furan molar ratio of 1:1.3 (see calculation in supplementary data) and the BDP-Mal dye (100 μl) was added at solvent volume ratio 1:10 DMSO:PBS at RT to obtain an overall ratio of 1:1.3:0.3 for maleimide/furan/BDP-Mal, meaning, within experimental error, equal molar amounts of maleimide and furan. The obtained solution was mixed and placed in an oil bath at 50 °C while stirring for 3 hours. Subsequently, the obtained BDP FLM dispersion was allowed to cool to room temperature and purified with a desalting column (Cytiva HiTrap® Desalting column 5 mL, Sigma-Aldrich) to remove unreacted BDP-Mal and DMSO. HPLC (as described below in section 2.4) was used to measure the amount of residual free BDP-Mal dye in the obtained BDP FLM dispersion. The labeled FLM was stored at room temperature until it was used.

2.4 HPLC analysis to determine unconjugated BDP-Mal dye in the BDP FLM dispersion

The concentration of unconjugated BDP-Mal dye in the BDP FLM dispersion (5 mg/ml) after purification was determined by HPLC analysis (Acquity, Waters Corporation, Milford, MA, USA) with a BEH C18 5μm column. The samples were diluted in 50% H$_2$O/acetonitrile. A mobile phase gradient, from 5 % of eluent A (95/50/0.1 % H$_2$O/acetonitrile/trifluoroacetic acid) to 100 of B (100/0.1 % acetonitrile/ trifluoroacetic acid) in 25 minutes runtime was used. The injection

6

volume of the samples was 20 µl, the flow rate was 1.2 ml/min and the detection was done at 500 and 280 nm.

2.5   FTIR analysis

Fourier Transform Infrared (FTIR) spectra were used to characterize PNM, PNF as well as empty FLM. The samples were measured as dry solid powders from 600 to 4000 cm^{-1} and recorded with a Perkin Elmer Spotlight FT-IR Spectrometer.

2.6   Gel permeation chromatography analysis

Polymer samples were dissolved in 10 mM LiCl in DMF at a concentration of 3 mg/mL. The number average molecular weight (M_n) and dispersity (Đ) were determined using a Waters 2695 Alliance (Waters Corporation, Milford, MA) with refraction index detector and with a PLgel 5 µm Mixed-D column. The analysis was performed with the column set at 65 °C and 1 mL/min flow rate. Calibration was done using PEG standards of narrow molecular weights (Polymer Standard Service GmbH, Mainz, Germany).

2.7   Asymmetric flow field flow fractionation analysis

Asymmetric flow field flow fractionation was performed using AF2000 system (Postnova Analytics GmbH, Germany), equipped with an absorbance 2487 and fluorescence 2475 detector (Waters, USA), a PN3150 RI detector (Postnova Analytics GmbH, Germany), a PN3621 MALS detector with 21 detection angles (Postnova Analytics GmbH, Germany) and a Zetasizer Nano S (Malvern Panalytical Ltd, UK). The separation channel included a 500 µm spacer and a regenerated cellulose membrane with a 10 kDa cutoff (Postnova Analytics GmbH, Germany). PBS pH 7.4 filtered with Omipore™ 0.1 v PTFE membrane (Merck Millipore Ltd, Ireland) was used as mobile phase. FLM (30 µL at 2.5 mg/ml) were injected into the channel with an autosampler, focused for 7 minutes at a focus flow rate of 4.3 mL/min and crossflow of 4 mL/min, and separated using the elution profile described in Table 1. NovaFFF AF2000 software was used to process and analyze the raw data. A sphere model was employed for fitting MALS data and calculate the radius of gyration. DLS data were analyzed with Zetasizer Software.

Table 1 Elution profile used for the fractionation of FLM using AF4.

Elution Step	Time (min)	Crossflow (ml/min)	Type	Exponent
1	5	4.00	constant	-
2	30	4.00 to 0.10	Power	0.2
3	30	0.10 to 0.05	Power	0.8
4	20	0.05 to 0.00	constant	-
5	10	0.00	constant	-

2.8 Cellular uptake studies

2.8.1 Cell culture

RAW 264.7 macrophage cells (catalogue number TIB-71) were obtained from ATCC (Manassas, VA, USA) and cultured in high glucose Dulbecco's Modified Eagle Medium (DMEM) growth medium (Sigma Aldrich, Zwijndrecht, the Netherlands), supplemented with 10 % heat inactivated fetal bovine serum (HI-FBS). Retinal pigment epithelium derived ARPE-19 cells were obtained from ATTC and maintained in Dulbecco's Modified Eagle Medium/Nutrient Mixture F-12 (DMEM/F-12) (Gibco™ Thermo Fischer Scientific, Waltham, MA, USA) supplemented with 10 % FBS and 1 % L-glutamine (Sigma Aldrich, Zwijndrecht, the Netherlands). The cells were incubated in fully humidified conditions at 37 °C and 5 % CO_2 unless otherwise indicated. RAW 264.7 cells and ARPE-19 cells were plated at 100,000 cells/cm^2 and 30,000 cells/cm^2, respectively, in a 96-well plate suited for confocal microscopy (Greiner BioOne, Alphen aan de Rijn, the Netherlands, catalog number 655090). Cells were allowed to grow for 24 hours before further experiments.

2.8.2 PNM:PNF BDP-Mal FLM uptake and cytocompatibility studies

The uptake of fluorescently labeled FLM by ARPE-19 and RAW 264.7 cells was investigated. Possible cell death induced by these FLM was simultaneously determined by Hoechst 33342 (Thermo Fisher Scientific,Bleiswijk, the Netherlands) and PI counter-staining at concentrations of 1 µg/mL and 25 µM, respectively.[24] Calcein-AM could not be utilized as the BDP dye attached to the FLM exhibited green fluorescence, which interferes with calcein emission. PNM:PNF BDP-Mal FLM were prepared as described in section 2.3.2. Subsequently, these FLM were diluted with cell culture medium to concentrations of 1-5 mg/ml. Duplicate samples of the diluted FLM were then added to ARPE-19 or RAW 264.7 cells by replacing the existing medium with FLM containing cell culture medium. Cells were incubated for 24 hours at 37 °C and 5 % CO_2. Subsequently, the culture medium was replaced with fresh medium containing Hoechst 33342 and PI to stain all cell nuclei and the nuclei of dead cells, respectively. The wells were imaged using a Yokogawa CV7000 spinning disk confocal microscope (Yokogawa, Tokyo, Japan) with 40x magnification. Image overlays were prepared using ImageJ (version 1.53f51).

2.8.3 Image analysis for live/dead and uptake studies

Images were analyzed using the Columbus software package (Perkin Elmer, version 2.7.1) to quantify cytotoxicity and uptake of PNM:PNF BDP-Mal FLM. Cytotoxicity is defined as the number of PI-stained nuclei divided by the sum of PI- and Hoechst-stained nuclei. Cellular uptake of PNM:PNF BDP-Mal FLM was determined by selecting the region surrounding the nuclei and calculating the mean fluorescence intensity per cell, which was averaged for all cells in the image.

2.9 In vivo animal studies

The in vivo experiments were designed and carried out in accordance with the European and national legislation and ethical guidelines of the University of Eastern Finland under project license (ESAVI -2020-027769). The procedures were designed in accordance with the 3R principle

of replacement, reduction, and refinement. The diffusion in vitreous, retinal permeation and safety of BDP labelled FLM after intravitreal injection was studied in 4 month old male Lister Hooded rats (n=4). Untreated eyes served as naïve control for the histological analysis (n=3). The animals were kept under 12h light/dark cycle and housed post operation individually in IVC cages, with food and water provided ad libitum. The cages were provided with sufficient bedding, nesting material, and enrichment.

For the in vivo experiments, 5 µl intravitreal injections of PNM:PNF BDP-Mal FLM (20 mg/mL in Milli-Q water) were performed to both eyes of the animals using a 32G needle (Hamilton Co, Reno, NV, USA) under anesthesia (subcutaneous injection of medetomidine (dose of 0.4 mg/kg, Domitor vet 1 mg/mL, Orion Pharma, Espoo, Finland) and ketamine (dose of 60 mg/kg, Ketalar/Ketaminol vet 50 mg/mL, Pfizer Oy Animal Health, Espoo, Finland)). The pupils of the rats were dilated 15 minutes prior injections and eye imaging by applying 10 µL of topical tropicamide to each eye (Oftan Tropicamid 5 mg/ml, Santen Pharmaceutical Co., Tampere, Finland). Local ocular surface anesthesia before intravitreal injections was achieved by applying 10 µL of topical oxybuprocaine (Oftan® Obucain, 4 mg/mL; Santen Pharmaceutical Co., Tampere, Finland). Topical ocular carbomer hydrogel was applied after intravitreal injections and during imaging to prevent corneal dryness (Viscotears®, 2 mg/g, Dr. Winzer Pharma, Berlin, Germany). Chloramphenicol eye cream (Oftan® Chlora 10 mg/g, Santen Pharmaceutical Co., Tampere, Finland) was applied topically after intravitreal injections, prior awakening the animals by subcutaneous injection of atipamezole (Antisedan vet 5 mg/mL, Orion, Finland).

Eye imaging was carried out prior injection, immediately after injection and 1 and 2 days after injection using OCT and fundus camera (Phoenix MICRON™ MICRON IV/OCT, CA, USA). For the eye imaging 1- and 2-days post injection, the animals were sustained under isoflurane anesthesia (Attane Vet 1000 mg/mL, Piramal Critical Care B.V., Voorschoten, the Netherlands) with flow rate 250 ml/ml with 2% isoflurane, and the ocular muscles were relaxed by 10 µL topical addition of medetomidine (Domitor vet 1 mg/mL) prior imaging.

The OCT and fundus images were used to confirm the quality of the injections and to visualize the distribution of the FLM in the vitreous compartment. Furthermore, the fundus imaging was used to evaluate the retina for signs of retinal neovascularization, hemorrhages, or any other microvascular abnormalities in the days following the injection. OCT imaging was used to non-invasively evaluate the retinal integrity for signs of retinal detachment, subretinal fluid, holes or any other abnormalities in the retina and signs of neovascularization.

Three days after injection, the animals were sacrificed, the eyes were collected, and incubated overnight in 4% paraformaldehyde solution in PBS, followed by cryoprotection with sucrose gradient treatment (10%, 20% and 30%), and embedding the tissue in cryopreservation matrix (Tissue-Tek® OCT Compound, Sakura® Finetek, Radnor, PA, USA). Sections of 6 µm thickness were prepared, air-dried at 37°C and stored at -20 °C. DAPI (1:10 000 in PBS, Thermo Fischer Scientific) was used to stain cell nuclei and imaging of the retinal sections was carried out using a Zeiss light microscope (Axio Imager M2; Carl Zeiss AG, Oberkochen, Germany) with 20X magnification (EC Plan-NEOFLUAR 20X/0.5 objective, Carl Zeiss AG) using AxioCam MRm (Carl Zeiss AG). The

retina's were analyzed for the outer nuclear layer (ONL) thickness, and evaluated for any signs of morphological abnormalities.

## 3 RESULTS AND DISCUSSION

3.1 Polymer synthesis

Figure 1 shows the chemical structures of the two complementary polymers, PNF and PNM, containing furan and maleimide functional groups, respectively. PNF and PNM were obtained by post modification of P(NIPAM-co-HEA)-PEG-P(NIPAM-co-HEA) (PNH), which in turn was obtained by ATRP polymerization.[25] The mid-block consists of PEG and the outer blocks consist of two monomers randomly polymerized, namely NIPAM to render the polymer thermosensitive and HEA to enable post-modification of the thermosensitive block via coupling of carboxylic acid containing moieties to the hydroxyl groups. The molar ratio of the NIPAM and HEA in of the thermosensitive blocks of PNH was 88:12 and poly(ethylene glycol) had a number-average molecular weight (M_n) of 6 kDa. PNH had a total M_n of 42 kDa as determined by ^{1}H-NMR and a cloud point of 32°C as previously reported Ilochonwu et al.[25] To enable Diels-Alder (DA) core-crosslinking of the FLM, HEA groups in PNH were functionalized with either 3-(2-furyl)propionic acid or 6-maleimidohexanoic acid using DCC/DMAP coupling, resulting in a yield of 90% for PNF and 85% for PNM, respectively. The molecular compositions of the thermosensitive blocks were determined using ^{1}H-NMR analysis (SI-Figure 1 and SI-table 1). For PNF, the molar composition was 88:2:10 NIPAM/HEA/furan, and for PNM, it was 88:3:9 NIPAM/HEA/maleimide. This reveals that the modification degree of the HEA moieties was 83% for PNF and 75% for PNM, using a 1 to 1 molar feed ratio. In terms of molecular weight, PNF had an M_n of 45 kDa (measured using ^{1}H-NMR) and 38 kDa (measured using GPC), while PNM showed an M_n of 46 kDa (^{1}H-NMR) and 49 kDa (GPC). The polymer's dispersity was 1.7 for PNF and 2.6 for PNM (see SI-table 1). The final polymer yields were 85% for PNM and 90% for PNF, respectively. All findings were consistent with prior research.[25]

PEG-NIPAM-HEA-FURAN (PNF)

PEG-NIPAM-HEA-MALEIMIDE (PNM)
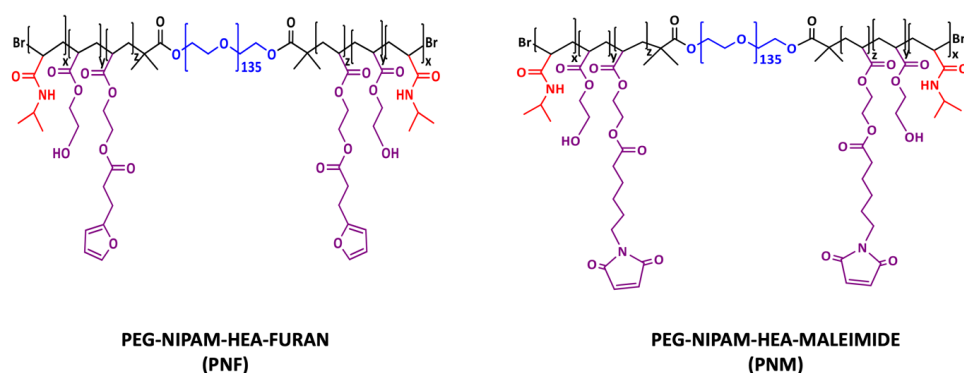
Figure 1 Chemical structures of PNF and PNM.

3.2   Micelle formation and characterization

Both PNF and PNM ABA copolymers exhibit an increase in solution turbidity above 28 °C in an aqueous environment, demonstrating lower critical solution temperature (LCST) behavior, as previously observed for these polymers.[25] When PNF and PNM solutions in PBS of 4 °C were mixed and then rapidly heated above the LCST of the polymers, partial dehydration of the outer NIPAM rich blocks of the polymers occurred, promoting their self-assembly into flower-like micelles (FLM). FLM were formed due to the ABA structure of the polymers, a phenomenon previously demonstrated by e.g. Zhou et al.[20] and de Graaf et al.[20, 26] and also illustrated in Figure 2. This self-assembly results in nanoparticles with a PEG shell and a hydrophobic core composed of the NIPAM rich thermosensitive blocks. In this core, the furan and maleimide groups are present in a relative high concentration and subsequently undergo a so-called DA reaction resulting in the formation core-crosslinked FLM. FTIR analysis (SI-Figure 2) revealed the absence of peaks at 695 cm^{-1} and 737 cm^{-1} in the dried FLM, which are typically assigned to the =C-H-bending vibration of the maleimide group and the =C-H- bend vibration of the furan moiety, respectively.[27, 28] This absence demonstrates that the maleimide and furan moieties, originally present in the PNM and PNF, were consumed during core-crosslinking formation, providing evidence of the occurrence of DA chemical core-crosslinking. Although furan is added in slight excess, the IR measurement is not sensitive enough to detect small amounts of remaining furan moieties within the placebo micelles. Furthermore, it is important to note that the separate solutions of PNF or PNM also displayed formation of FLM at 37 °C, but these structures dissociated upon cooling below the LCST due hydration of the hydrophobic core and the absence of chemical crosslinking between the polymer chains. BDP fluorescently labelled FLM were prepared by addition of Mal-BDP to the solution of PNF and PNM at 4 °C followed by rapid heating. The obtained FLM had Z-average diameters of 85 ± 1 and 107 ± 12 nm at 37°C for empty FLM and BDP FLM, respectively, with PDI values between 0.09 - 0.18 (Table 2). The results were in line with previously reported sizes of FLM based on core-crosslinked ABA thermosensitive copolymers of similar molecular weights.[18] Further, Table 2 shows that the crosslinked FLM incubated at 4°C were slightly larger than the same FLM at 37°C (increase in diameter of 10-20%), which can be explained by hydration and thus swelling of thermosensitive core at a temperature below the LCST of the polymers, as also observed for other core-crosslinked FLM with thermosensitive cores.[18] The extent of this swelling is limited, because of the presence of DA crosslinks in the core of the FLM. It is worth noting that the absence of free/nonconjugated BDP-Mal dye in the BDP FLM formulation was confirmed by HPLC analysis, as shown in the supporting information SI-figure 3.
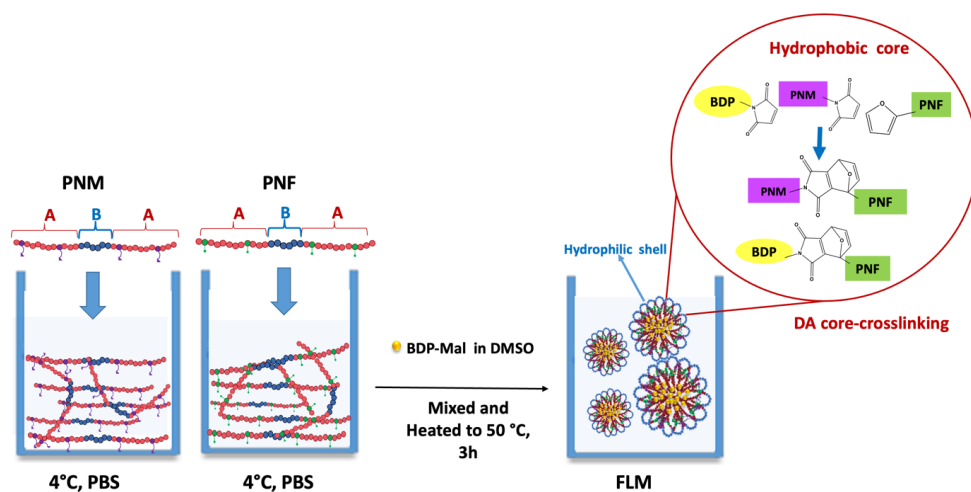
Figure 2 Schematic representation FLM preparation. ABA copolymers PNM and PNF were separately dissolved in PBS at 4 °C and afterwards the polymer solution and the BDP-dye (dissolved in DMSO) were mixed and rapidly heated to 50 °C. FLM were formed with a hydrophilic PEG shell and thermosensitive core. Subsequently, chemical core-crosslinking by DA chemistry in the thermosensitive domain occurs, while also the BDP-dye is clicked by DA reaction into the core of the FLM.

Table 2 Characteristics of PNM:PNF FLM: The data represent the average of two independently prepared micelle batches.

Formulation	T (°C)	Z-Ave diameter (nm)	PDI
Empty PNM:PNF FLM	37	85 ± 1	0.09 ± 0.00
	4	95 ± 2	0.10 ± 0.01
PNM:PNF BDP-Mal FLM	37	107 ± 12	0.18 ± 0.05
	4	120 ± 23	0.17 ± 0.04

6

3.3 Structure of PNF: PNM FLM

To gain insight into the structure of the formed FLM with the different cargos (empty and BDP-functionalized), their radius of gyration (R_g), hydrodynamic radius (R_h) and size distribution (Table 3 and Figure 3) were determined using AF4 coupled with MALLS and DLS. With this method, particle structure and size can be determined. The MALLS and DLS fractograms exhibit comparable peaks for both empty and BDP-functionalized FLM, with average R_g and R_h values of 25.3 ± 0.1 and 45.2 ± 0.7 for the empty micelles, and 25.4 ± 3.8 and 46.6 ± 3.2 for the BDP labeled micelles. These results are illustrated in Figure 3A-B and summarized in Table 3. The shape factor (=R_g/R_h ratio) of particles yields information about their structure.[29] Particles with a homogenous rigid spherical structure have a shape factor of $\sqrt{3}/5$ ~0.775. On the other hand for particles with a dense core and less dense shell (core-shell structure) this factor is lower than ~0.775.[29] Finally, for spherical vesicles (e.g. polymersomes, liposomes), the scattering mass is essentially present on the surface of the sphere resulting in a shape factor close to one.[30] Table 3 shows that the shape factor PNF:PNM FLM was between 0.56 and 0.58 which is < 0.775 pointing to a structure composed of a dehydrated PNIPAM based core and a hydrated PEG hydrophilic shell, as expected for this type of particle.[31]. Furthermore, in Figure 3C, fractograms recorded at 240 and 513 nm are presented. The signals at 240 and 514 nm coincide with the micellar peak detected using MALLS and DLS. The successful functionalization of FLM with the BDP dye is thus confirmed by the overlap of the micellar peak with the peak detected at 513 nm (corresponding to the BDP dye's maximum light absorbance). The area under the curve (AUC) is approximately five times higher than the background signal observed for empty FLM.

Table 3 Characteristics of the different FLM as determined by asymmetric flow field-flow fractionation connected to multi-angle laser light scattering detector and dynamic light scattering in PBS, pH 7.4 at 37 °C. Data represent the average of one FLM batch, and two independent measurements.

Micelles	Hydrodynamic radius (R_h, nm)	Radius of gyration (R_g, nm)	Shape factor =R_g/R_h	AUC[a] Abs 240 nm n=1	AUC[a] Abs 513 nm, n=1
Empty PNM:PNF FLM	45.2 ± 0.7	25.3 ± 0.1	0.56 ± 0.01	5.8	0.48
PNM:PNF BDP FLM	46.6 ± 3.2	25.4 ± 3.8	0.58 ± 0.04	6.5	5.84

[a] AUC = area under the curve.
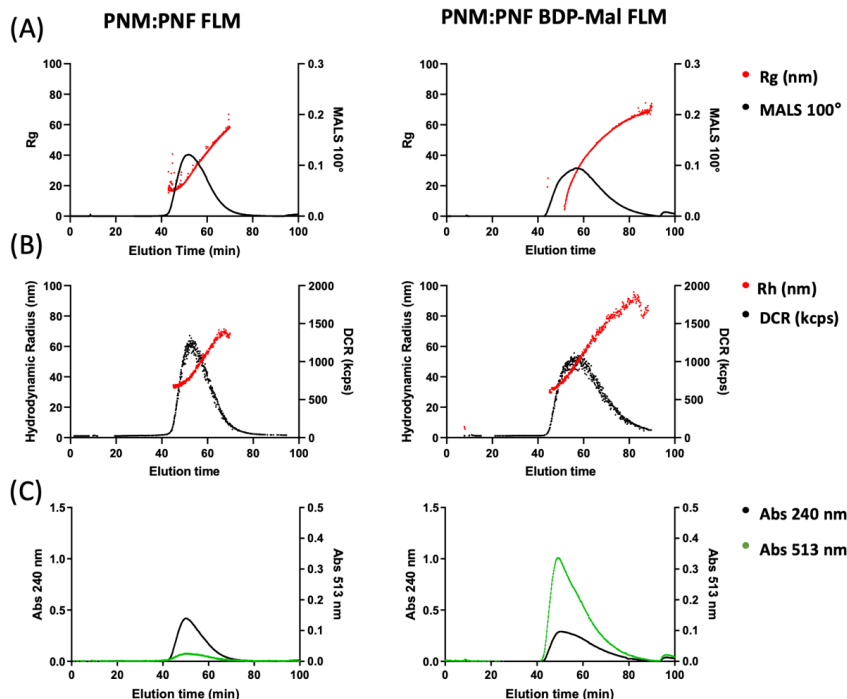
Figure 3 AF4 Fractograms of empty PNM:PNF FLM and PNM:PNF BDP-Mal FLM injected at a concentration of 2.5 mg/ml in PBS at 37°C. A) MALLS fractogram and R_g value radius (nm) calculated by fitting MALLS data with sphere model. B) R_h radius (nm) and derived count rate (DCR) measured by the DLS detector as a function of the elution time. C) Fractograms recorded at 240 nm (left Y-axis) and 513 nm (right Y-axis) as a function of the elution time. Abbreviations: Abs, absorbance; KCPS, kilo counts per second.

3.4   Cell uptake BDP dye loaded FLM

The uptake of FLM labelled with the fluorescent dye (BDP) by ARPE-19 and macrophage cells was studied using confocal microscopy. The RAW264.7 cells showed a 2-5 fold higher mean fluorescence intensity (MFI) for the BDP signal as compared to the ARPE-19 cells (see Figure 4, in green panels E and F). This illustrates a significantly greater uptake of the FLM by the macrophages than by the retinal epithelial cells. This trend aligns with previous observations for fluorescent europium-coated microparticles with a 200 μm diameter.[32] Furthermore, in Figure 4 E and F, a dose-dependent effect on the uptake of the FLM by both ARPE-19 cells and RAW264.7 cells is evident, as indicated by the increasing signal intensity with increasing FLM concentration. Importantly, this dose-response is observed without compromising the cell viability, signifying that the particles are well-tolerated within this dosage range. However, a notable observation is that the uptake of FLM reached a plateau in the case of macrophages (RAW264.7 cells), whereas this plateau was not observed with the retinal epithelial cells (ARPE-19 cells). Polymeric nanoparticles commonly enter cells through endocytic pathways, which include phagocytosis, pinocytosis, and receptor-mediated endocytosis.[33] Unlike macrophages, Irschick et al. [32]

proposed that retinal pigment epithelium (RPE) cells lack classical complement receptors on their surfaces. This suggests potential differences in how these two cell types recognize and ingest particles due to the presence or absence of such surface receptors. Macrophages employ various mechanisms for target recognition, including phagocytosis and receptor-mediated endocytosis.[34] However, studies by Yu et al.[35] and Giacalone et al. [36] put emphasis that the uptake of nanoparticles based on block copolymers of poly(ethylene glycol)-poly(propylene sulfide) or poly(lactic acid)-poly(ethylene glycol) , by macrophages is predominantly influenced by nanoparticle size and, to a lesser extent, charge, while receptor interactions play a minor role. Therefore, further studies are required to gain deeper insights into the cellular uptake mechanisms of the FLM presented in this study.
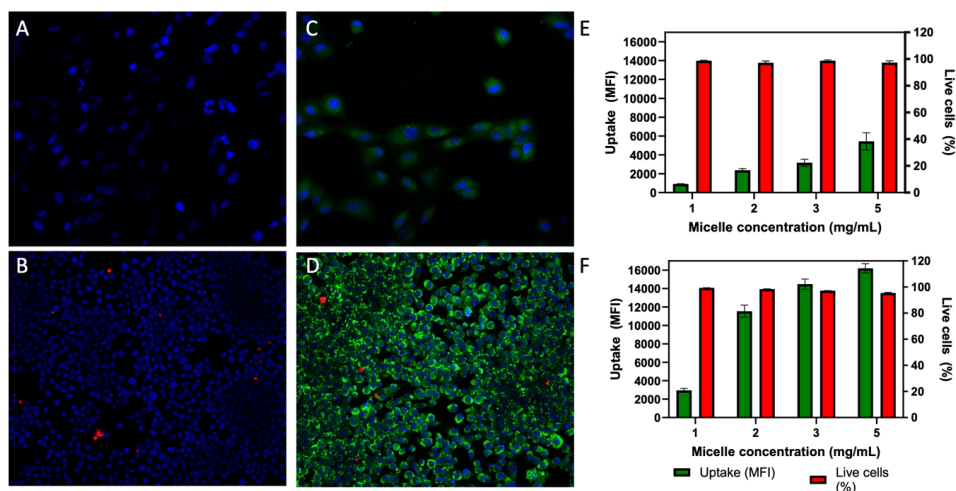
Figure 4 Uptake of BDP-labelled cells by ARPE-19 and RAW264.7 cells, as well as living cell population after incubation for 24 hours at 37 °C. A-D: Blue: cell nucleus (Hoechst33342); Green: FLM (BDP); Red: dead cells (PI); at 40x magnification. A: untreated ARPE-19 cells. B: untreated RAW267.4 cells. C: ARPE-19 cells incubated with FLM 5 mg/ml for 24 hours at 37 °C. D: RAW267.4 cells incubated with FLM 5 mg/ml E: Mean fluorescence intensity (MFI) (left y-axis) and cytotoxicity (right y-axis) of FLM in ARPE-19 cells. F: Mean fluorescence intensity (MFI) (left y-axis) and cytotoxicity (right y-axis) of FLM in RAW264.7 cells. Data represented the average of two n=2 independent measurements.

3.5   Animal studies

3.5.1   Fundus imaging

Representative fundus images of four different rat eyes after 5 µl injection of BDP-Mal FLM (20 mg/mL) are presented in figure 5 (a-d). Images were taken shortly after injection of the FLM, and 1- and 2-days post injection with normal light (left) and green filter (right). The FLM seemed to rapidly distribute within minutes over the vitreous in three out of four eyes. In one eye (Figure 5 d), the FLM did not readily distribute in the vitreous, and green fluorescence was observed only at the site of injection, suggesting that the FLM did not reach the vitreous cavity after intravitreal

injection. In 3 out of 4 eyes the FLM were almost completely cleared from the vitreous within 2 days, as shown by the diminishing fluorescence signal (Figure 5 b-d). This rapid clearance of the FLM was unexpected, as polymeric nanoparticles and liposomes of similar dimensions were detected in the vitreous of rats up to 65 days after injection[37]. Nevertheless, it is essential to recognize that the vitreous humor is not completely stationary and does undergo a certain degree of dynamic flow. Although this flow is not as vigorous as the circulation of blood in the body, there are subtle movements and currents within the vitreous. These subtle dynamics could potentially impact the distribution of drugs and particles, depending on their specific physicochemical properties.[38-40] Accumulation of the green fluorescent signal was observed in the optic nerve of half of the injected eyes (Figure 5 e). This is in line with previous observation of intravitreally administered nanomaterials[37] and indicates that the FLM had reached the retina. One animal (Figure 5 a) showed mild trauma in one eye in the peripheral retina after injection, which was not significant enough to exclude the animal from the studies. Most importantly, no signs of retinal abnormalities were detected in any of the eyes.
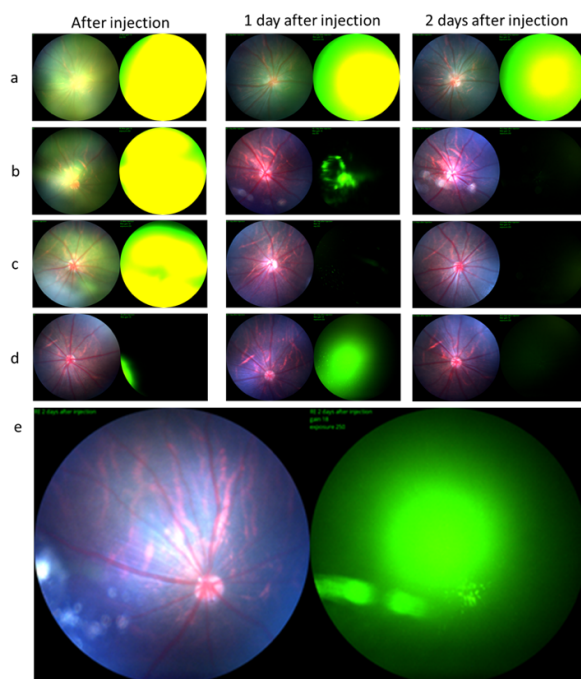
Figure 5 Fundus images of four rat eyes shortly after 5 µl injection of PNM:PNF-BDP FLM and 1 day and 2 days post injection (a-d). Fundus images were taken with bright light (left) to evaluate retinal health, and green filter (right) to visualize the fluorescently labelled FLM. Green fluorescence could be seen at the optic nerve 2 days post injection in 4 of the 8 injected eyes (e) indicating that the FLM had reached the retina.

3.5.2   Optical coherence tomography (OCT) imaging

Representative OCT cross-sections of the retina with corresponding fundus images at baseline (A), shortly after injection (B), 1 day (C) and 2 days (D) after injection are presented in figure 6.

The retinal morphology was non-invasively evaluated for signs of disturbances in the retinal morphology, retinal detachment, or other adverse effects. Importantly, neither adverse effects nor retinal abnormalities were detected based on the OCT images at the studied time-points.
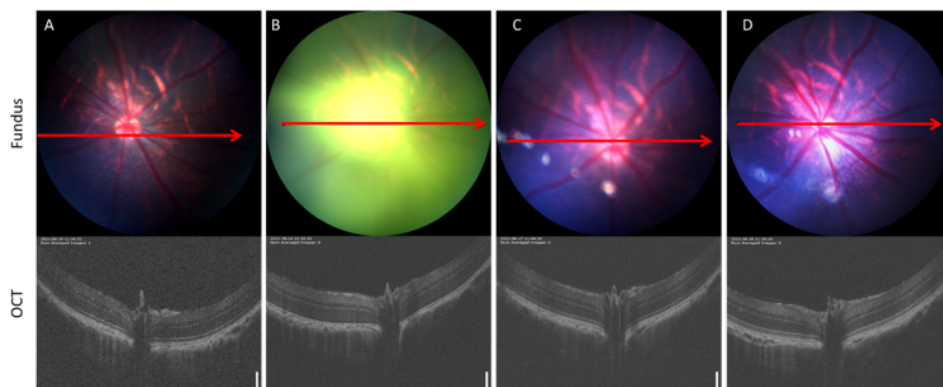
Figure 6 Fundus and corresponding OCT imaging of the retinal cross sections at baseline (A), shortly after injection (B), 1 day after injection (C) and 2 days after injection (D). The red arrows in the fundus images correspond to the plane in which the OCT cross-section has been taken. Vertical and horizontal scale bars in OCT images are 110 and 130 μm, respectively.

3.5.3   Retinal morphology, and tissue permeation of BDP labelled FLM

Three days after injection, the eyes were collected, and cryosections of the retina were prepared to evaluate retinal morphology as well as the distribution of the FLM into the deeper layers or retina and the optic nerve. For histological analysis, 3 untreated eyes served as a control. No changes in the outer nuclear layer (ONL) compared to the control eyes or other abnormalities were detected in the treated eyes (supplementary data table 2). The presence of FLM was observed in the optic nerve in 3 of the 8 injected eyes (Figure 7 A and B), and in 2 eyes accumulation of fluorescently labelled FLM was seen around the inner limiting membrane (C). However, in 1 eye, green fluorescent signal was detected also in the deeper retinal layers (D). The eye in which FLM were detected in the deeper retinal layers, was also the only eye in which fluorescent FLM were observed 2 days post injection (Figure 5 a). It is possible that at the time the animals were sacrificed, the particles were already entirely cleared from the vitreous and the retina, hence accurate assessment of retinal permeation and distribution would require additional studies with shorter sacrifice timepoints to confirm this hypothesis. High accumulation of fluorescently labelled FLM was observed in the trabecular meshwork and the ciliary body (SI-Figure 4) indicating that the FLM were cleared from the vitreous through anterior chamber outflow. Nevertheless, the flower-like micelles (FLM) demonstrated partial permeation of the inner limiting membrane (ILM), a significant barrier for intraocular drug delivery when dealing with polymeric nanomaterials. The FLM characteristics outlined in this study (see sections 3.3) make them an appealing choice for ocular drug delivery. Previous research by Peynshaert et al. [41] and Tavakoli et al. [42] has shown that nanoparticles with diameters below 100 nm can penetrate the vitreoretinal interface. In contrast, Del Amo et al. [43] discussed how particles

exceeding 500 nm face challenges in vitreous distribution. Thus, the studied spherical core-shell FLM are well-suited for vitreous distribution and can potentially target macrophages near the vitreoretinal interface. This targeted approach is crucial, as these macrophages significantly contribute to the inflammatory response in retinal vascular diseases. [44, 45]
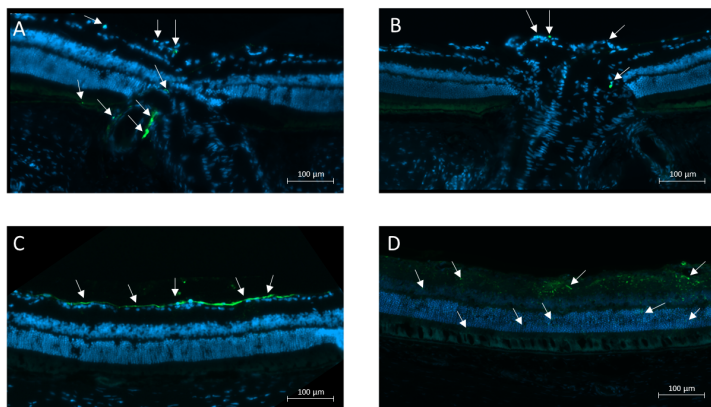
Figure 7 Distribution of fluorescently labelled FLM (indicated by white arrows) in the eyes after intravitreal injection. Some cells that internalized the fluorescent BDP FLM can be seen at the optic nerve (A and B). Accumulation of particles at the was observed in some eyes (C), and penetration of fluorescently labelled particles to the deeper retinal layers was observed in 1 of the eyes studied (D).

4   CONCLUSION AND PROSPECTS

This study highlights the potential of Diels-Alder core-crosslinked FLM for ocular drug therapy. The FLM are cytocompatible and taken up by both ARPE-19 and RAW264.7 cells. In vivo experiments using a rat eye model demonstrated the safe administration of the FLM via intravitreal injection, with neither observed adverse effects nor retinal abnormalities. The FLM reached the sub-retinal space, retinal cells, and the inner limiting membrane (ILM) at the vitreoretinal barrier. However, further efforts are required to optimize ocular pharmacokinetics and prolong vitreous particle retention. Overall, Diels-Alder core- crosslinked FLM show significant promise as a targeted drug delivery system. Specifically targeting the sub-retinal space and retinal pigment epithelium (RPE), they hold great potential in the treatment of ocular inflammatory conditions. Loading of the FLM with e.g. an anti-inflammatory drug such as dexamethasone is a logical next step in their further pharmaceutical development. Loading can be done by either dissolution of the drug in the hydrophobic core of the FLM or by covalent coupling of a drug with a maleimide handle to the excess furan groups present in the core of the FLM. The successful covalent coupling of the maleimide functionalized BDP fluorescent dye to the core of the FLM as shown in this chapter demonstrates that the latter is a viable option. It is stressed that a biodegradable bond has to be present in the linker that connects the drug with the maleimide functionality to ensure sustained and/or triggered release of the native therapeutic.

6

5   REFERENCES

[1] L. Zhang, W. Shen, J. Luan, D. Yang, G. Wei, L. Yu, W. Lu, J. Ding, Sustained intravitreal delivery of dexamethasone using an injectable and biodegradable thermogel, Acta Biomater, 23 (2015) 271-281.

[2] M.A. Kalam, The potential application of hyaluronic acid coated chitosan nanoparticles in ocular delivery of dexamethasone, Int J Biol Macromol, 89 (2016) 559-568.

[3] E. Kickova, A. Sadeghi, J. Puranen, S. Tavakoli, M. Sen, V.P. Ranta, B. Arango-Gonzalez, S. Bolz, M. Ueffing, S. Salmaso, P. Caliceti, E. Toropainen, M. Ruponen, A. Urtti, Pharmacokinetics of Pullulan-Dexamethasone Conjugates in Retinal Drug Delivery, Pharmaceutics, 14 (2021).

[4] M.A. Kalam, Development of chitosan nanoparticles coated with hyaluronic acid for topical ocular delivery of dexamethasone, Int J Biol Macromol, 89 (2016) 127-136.

[5] C. Lu, P. Zahedi, A. Forman, C. Allen, Multi-arm PEG/silica hydrogel for sustained ocular drug delivery, J Pharm Sci, 103 (2014) 216-226.

[6] C. Lu, R.B. Yoganathan, M. Kociolek, C. Allen, Hydrogel containing silica shell cross-linked micelles for ocular drug delivery, J Pharm Sci, 102 (2013) 627-637.

[7] A. Annala, B.C. Ilochonwu, D. Wilbie, A. Sadeghi, W.E. Hennink, T. Vermonden, Self-Healing Thermosensitive Hydrogel for Sustained Release of Dexamethasone for Ocular Therapy, ACS Polym Au, 3 (2023) 118-131.

[8] M. Bhattacharya, A. Sadeghi, S. Sarkhel, M. Hagstrom, S. Bahrpeyma, E. Toropainen, S. Auriola, A. Urtti, Release of functional dexamethasone by intracellular enzymes: A modular peptide-based strategy for ocular drug delivery, J Control Release, 327 (2020) 584-594.

[9] E. Kickova, S. Salmaso, F. Mastrotto, P. Caliceti, A. Urtti, Pullulan Based Bioconjugates for Ocular Dexamethasone Delivery, Pharmaceutics, 13 (2021).

[10] H.R. Chinnery, P.G. McMenamin, S.J. Dando, Macrophage physiology in the eye, Pflügers Archiv-European Journal of Physiology, 469 (2017) 501-515.

[11] Z. Papadopoulos, The role of the cytokine TNF-α in choroidal neovascularization: a systematic review, Eye, (2023).

[12] N. Díaz-Lezama, J. Kajtna, J. Wu, M. Ayten, S.F. Koch, Microglial and macroglial dynamics in a model of retinitis pigmentosa, Vision Research, 210 (2023) 108268.

[13] H. Tawarayama, K. Umeki, M. Inoue-Yanagimachi, N. Takahashi, H. Hasegawa, N. Himori, S. Tsuda, H. Kunikata, T. Akaike, T. Nakazawa, Glutathione trisulfide prevents lipopolysaccharide-induced retinal inflammation via inhibition of proinflammatory cytokine production in glial cells, Sci Rep, 13 (2023) 11513.

[14] H. Cabral, K. Miyata, K. Osada, K. Kataoka, Block Copolymer Micelles in Nanomedicine Applications, Chem Rev, 118 (2018) 6844-6892.

[15] D. Hwang, J.D. Ramsey, A.V. Kabanov, Polymeric micelles for the delivery of poorly soluble drugs: From nanoformulation to clinical approval, Advanced Drug Delivery Reviews, 156 (2020) 80-118.

[16] L. Houdaihed, J.C. Evans, C. Allen, Overcoming the Road Blocks: Advancement of Block Copolymer Micelles for Cancer Therapy in the Clinic, Mol Pharm, 14 (2017) 2503-2517.

[17] A. Varela-Moreira, Y. Shi, M.H.A.M. Fens, T. Lammers, W.E. Hennink, R.M. Schiffelers, Clinical application of polymeric micelles for the treatment of cancer, Materials Chemistry Frontiers, 1 (2017) 1485-1501.

[18] M. Najafi, N. Kordalivand, M.A. Moradi, J. van den Dikkenberg, R. Fokkink, H. Friedrich, N. Sommerdijk, M. Hembury, T. Vermonden, Native Chemical Ligation for Cross-Linking of Flower-Like Micelles, Biomacromolecules, 19 (2018) 3766-3775.

[19] K.T. Oh, Y.T. Oh, N.M. Oh, K. Kim, D.H. Lee, E.S. Lee, A smart flower-like polymeric micelle for pH-triggered anticancer drug release, Int J Pharm, 375 (2009) 163-169.

[20] Z. Zhou, B. Chu, Phase behavior and association properties of poly (oxypropylene)-poly (oxyethylene)-poly (oxypropylene) triblock copolymer in aqueous solution, Macromolecules, 27 (1994) 2025-2033.

[21] M. Talelli, M. Barz, C.J.F. Rijcken, F. Kiessling, W.E. Hennink, T. Lammers, Core-crosslinked polymeric micelles: Principles, preparation, biomedical applications and clinical translation, Nano Today, 10 (2015) 93-117.

[22] B.C. Ilochonwu, S.A. van der Lugt, A. Annala, G. Di Marco, T. Sampon, J. Siepmann, F. Siepmann, W.E. Hennink, T. Vermonden, Thermo-responsive Diels-Alder stabilized hydrogels for ocular drug delivery of a corticosteroid and an anti-VEGF fab fragment, Journal of Controlled Release, 361 (2023) 334-349.

[23] D. Neradovic, O. Soga, C.F. Van Nostrum, W.E. Hennink, The effect of the processing and formulation parameters on the size of nanoparticles based on block copolymers of poly(ethylene glycol) and poly(N-isopropylacrylamide) with and without hydrolytically sensitive groups, Biomaterials, 25 (2004) 2409-2418.

[24] C. Lema, A. Varela-Ramirez, R.J. Aguilera, Differential nuclear staining assay for high-throughput screening to identify cytotoxic compounds, Current cellular biochemistry, 1 (2011) 1-14.

[25] B.C. Ilochonwu, S.A. van der Lugt, A. Annala, G. Di Marco, T. Sampon, J. Siepmann, F. Siepmann, W.E. Hennink, T. Vermonden, Thermo-responsive Diels-Alder stabilized hydrogels for ocular drug delivery of a corticosteroid and an anti-VEGF fab fragment, J Control Release, (2023).

[26] A.J. de Graaf, K.W. Boere, J. Kemmink, R.G. Fokkink, C.F. van Nostrum, D.T. Rijkers, J. van der Gucht, H. Wienk, M. Baldus, E. Mastrobattista, T. Vermonden, W.E. Hennink, Looped structure of flowerlike micelles revealed by 1H NMR relaxometry and light scattering, Langmuir, 27 (2011) 9843-9848.

[27] G. Tondi, M. Link, C.W. Oo, A. Petutschnigg, A Simple Approach to Distinguish Classic and Formaldehyde-Free Tannin Based Rigid Foams by ATR FT-IR, Journal of Spectroscopy, 2015 (2015) 1-8.

[28] T. Sepperer, J. Neubauer, J. Eckardt, T. Schnabel, A. Petutschnigg, G. Tondi, Pollutant Absorption as a Possible End-Of-Life Solution for Polyphenolic Polymers, Polymers (Basel), 11 (2019).

6

[29] D. Kunz, A. Thurn, W. Burchard, Dynamic light scattering from spherical particles, Colloid and Polymer Science, 261 (1983) 635-644.

[30] A.A. Gabizon, O. Pappo, D. Goren, M. Chemla, D. Tzemach, A.T. Horowitz, Preclinical Studies with Doxorubicin Encapsulated in Polyethyleneglycol-Coated Liposomes, Journal of Liposome Research, 3 (1993) 517-528.

[31] C. Ma, P. Pan, G. Shan, Y. Bao, M. Fujita, M. Maeda, Core-shell structure, biodegradation, and drug release behavior of poly(lactic acid)/poly(ethylene glycol) block copolymer micelles tuned by macromolecular stereostructure, Langmuir, 31 (2015) 1527-1536.

[32] E.U. Irschick, R. Sgonc, G. Bock, H. Wolf, D. Fuchs, W. Nussbaumer, W. Gottinger, H.P. Huemer, Retinal pigment epithelial phagocytosis and metabolism differ from those of macrophages, Ophthalmic Res, 36 (2004) 200-210.

[33] L.C. Nelemans, L. Gurevich, Drug Delivery with Polymeric Nanocarriers-Cellular Uptake Mechanisms, Materials (Basel), 13 (2020).

[34] P.R. Taylor, L. Martinez-Pomares, M. Stacey, H.H. Lin, G.D. Brown, S. Gordon, Macrophage receptors and immune recognition, Annu Rev Immunol, 23 (2005) 901-944.

[35] S.S. Yu, C.M. Lau, S.N. Thomas, W.G. Jerome, D.J. Maron, J.H. Dickerson, J.A. Hubbell, T.D. Giorgio, Size- and charge-dependent non-specific uptake of PEGylated nanoparticles by macrophages, Int J Nanomedicine, 7 (2012) 799-813.

[36] G. Giacalone, N. Tsapis, L. Mousnier, H. Chacun, E. Fattal, PLA-PEG Nanoparticles Improve the Anti-Inflammatory Effect of Rosiglitazone on Macrophages by Enhancing Drug Uptake Compared to Free Rosiglitazone, Materials (Basel), 11 (2018).

[37] A. Sadeghi, M. Ruponen, J. Puranen, S. Cao, R. Ridolfo, S. Tavakoli, E. Toropainen, T. Lajunen, V.P. Ranta, J. van Hest, A. Urtti, Imaging, quantitation and kinetic modelling of intravitreal nanomaterials, Int J Pharm, 621 (2022) 121800.

[38] R. Repetto, J.H. Siggers, A. Stocchino, Mathematical model of flow in the vitreous humor induced by saccadic eye rotations: effect of geometry, Biomech Model Mechanobiol, 9 (2010) 65-76.

[39] A. Narasimhan, C. Sundarraj, Convection-Enhanced Intravitreous Drug Delivery in Human Eye, Journal of Heat Transfer, 137 (2015).

[40] D.W. Smith, C.J. Lee, B.S. Gardiner, No flow through the vitreous humor: How strong is the evidence?, Prog Retin Eye Res, (2020) 100845.

[41] K. Peynshaert, J. Devoldere, V. Forster, S. Picaud, C. Vanhove, S.C. De Smedt, K. Remaut, Toward smart design of retinal drug carriers: a novel bovine retinal explant model to study the barrier role of the vitreoretinal interface, Drug Deliv, 24 (2017) 1384-1394.

[42] S. Tavakoli, K. Peynshaert, T. Lajunen, J. Devoldere, E.M. Del Amo, M. Ruponen, S.C. De Smedt, K. Remaut, A. Urtti, Ocular barriers to retinal delivery of intravitreal liposomes: Impact of vitreoretinal interface, J Control Release, 328 (2020) 952-961.

[43] E.M. Del Amo, A.K. Rimpela, E. Heikkinen, O.K. Kari, E. Ramsay, T. Lajunen, M. Schmitt, L. Pelkonen, M. Bhattacharya, D. Richardson, A. Subrizi, T. Turunen, M. Reinisalo, J. Itkonen, E.

Toropainen, M. Casteleijn, H. Kidron, M. Antopolsky, K.S. Vellonen, M. Ruponen, A. Urtti, Pharmacokinetic aspects of retinal drug delivery, Prog Retin Eye Res, 57 (2017) 134-185.

[44] A. Rajesh, S. Droho, J.A. Lavine, Macrophages in close proximity to the vitreoretinal interface are potential biomarkers of inflammation during retinal vascular disease, J Neuroinflammation, 19 (2022) 203.

[45] Z. Wang, A.L. Koenig, K.J. Lavine, R.S. Apte, Macrophage Plasticity and Function in the Eye and Heart, Trends in immunology, 40 (2019) 825-841.

6

6   SUPPORTING INFORMATION

SI-Table 1 Characteristics of PNF and PNM composed of PEG mid-block of 6 kDa with outer blocks of Nipam (N) and HEA (H) or furan (F) or maleimide (M).

Polymer	Feed Ratio [N]:[H]:[F]/[M]	Measured copolymer composition [a] [N]:H:[F]/[M]	M_n [a] (kDa)	M_n [b] (kDa)	PDI [b]
PNF	88:0:12	88:2:10	45	38	1.7
PNM	88:0:12	88:3:9	46	49	2.6

[a] Determined by ^{1}H-NMR; [b] Determined by GPC using PEG calibration.
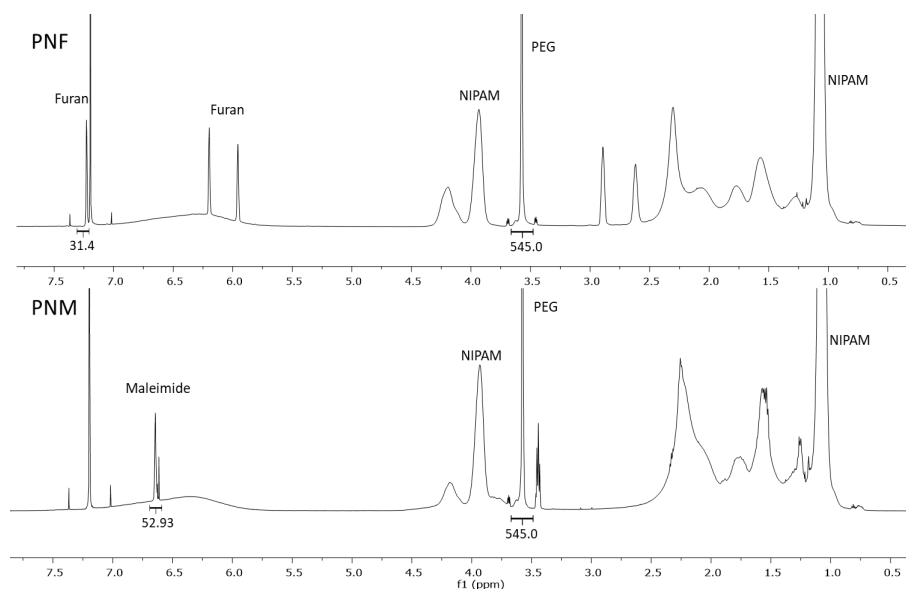
SI-Figure 1 ^{1}H-NMR spectra of PNF and PNM.

Calculation of the total ratio maleimide/furan/or BDP-maleimide in FLM

Placebo FLM:
PNM 500 µl; 10 mg/ml; units of maleimide by ^{1}H-NMR 52.93 H /2= 26.47 units
PNF 500 µl; 10 mg/ml; units of furan by ^{1}H-NMR 31.40 H= 31.40 units
Furan in solution from PNF = (5 mg /45000 Da (molecular weight PNF)) *31.40= 3.5 *10^{-6} mol
Maleimide in solution from PNM = (5 mg /46000 Da (molecular weight PNM)) *26.47= 2.9 *10^{-6} mol
Therefore, final ratio of 1:1.2 for maleimide/furan

BDP-Mal FLM:
PNM 450 µl; 20 mg/ml; units of maleimide by ^{1}H-NMR 52.93 H /2= 26.47 units
PNF 450 µl; 22.2 mg/ml; units of furan by ^{1}H-NMR 31.40 H= 31.40 units

Furan in solution from PNF = (9.99 mg /45000 Da (molecular weight PNF)) *31.40= 7.0 *10^{-6} mol
Maleimide in solution from PNM= (9.00 mg /46000 Da (molecular weight PNM)) *26.47= 5.2 *10^{-6} mol
Maleimide in solution from BDP-maleimide= (0.6 mg / 414.1 Da (molecular weight BDP-maleimide) = 1.4 *10^{-6} mol. Therefore, final ratio of 1:1.3:0.3 for maleimide/furan/BDP-maleimide
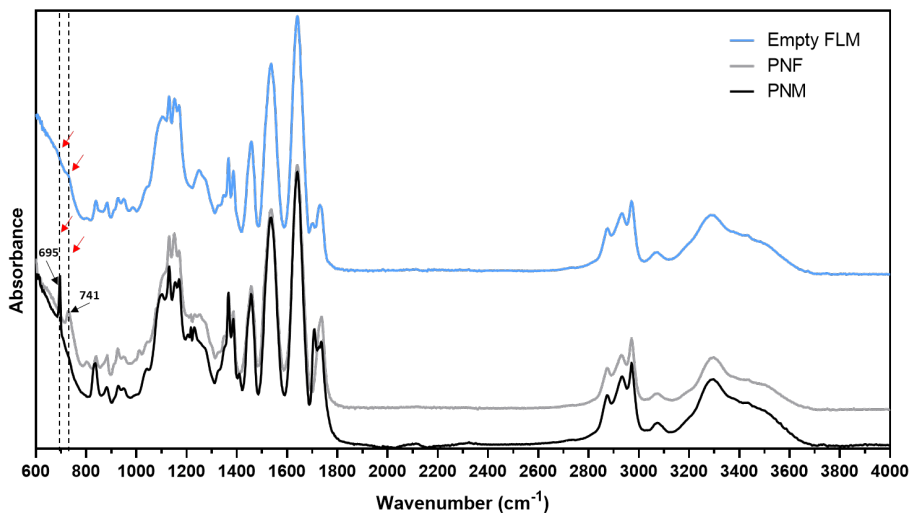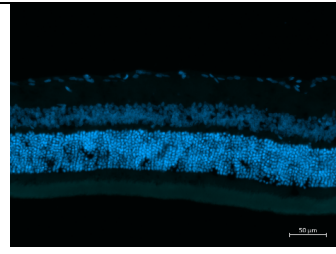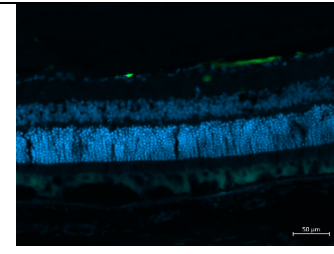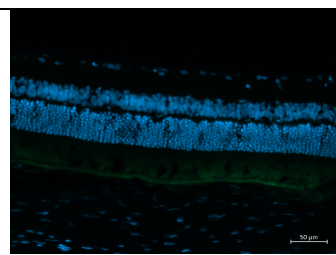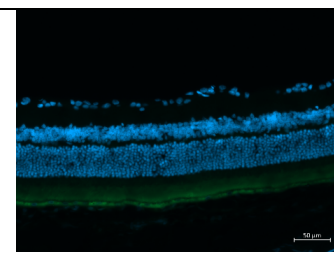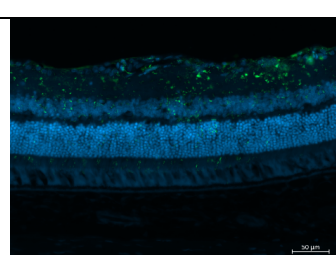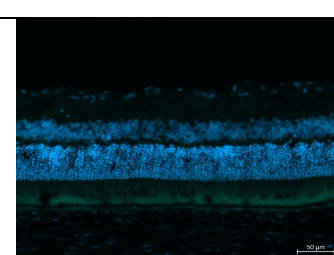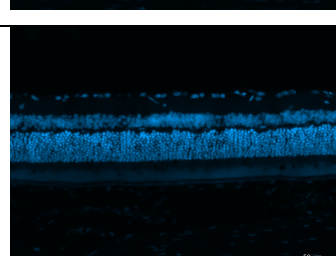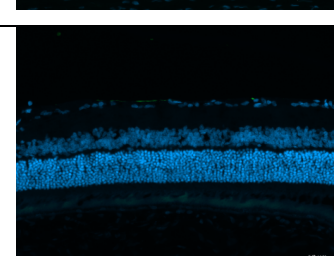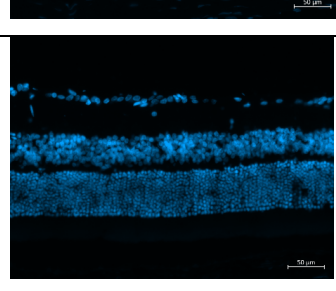

SI-Figure 2 FT-IR spectra of empty PNM-PNF crosslinked FLM (in light–blue), PNF polymer (in grey), PNM polymer (in black). Black arrows indicate the most relevant peaks, and the red arrows point to the disappeared peaks after core crosslinking.
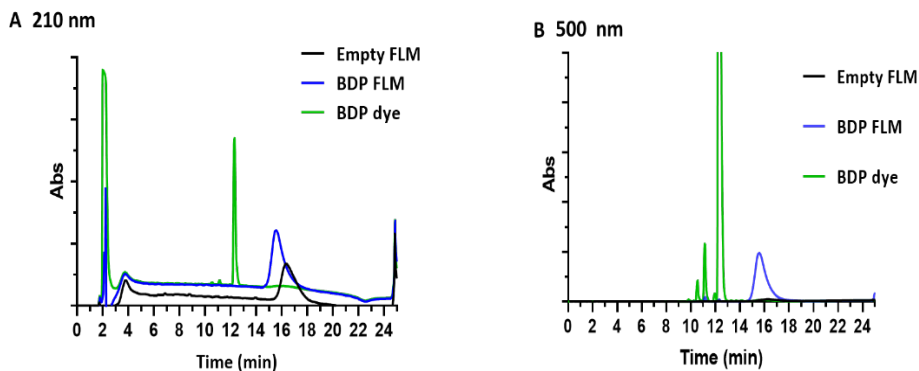
SI-Figure 3 HPLC-Chromatograms of empty FLM, BDP FLM and free BDP in the 210 and 500 nm channel.

SI-Table 2 Retinal cryosection images of animals receiving 5 µl injection of BDP labeled FLM (animals 5-8) and 3 untreated control animals (CTRL 1-3). Images were taken with 20x magnification.

Animal	Left eye	Right eye
5		
6		
7		
8		
CTRL 1		

CTRL 2

CTRL 3
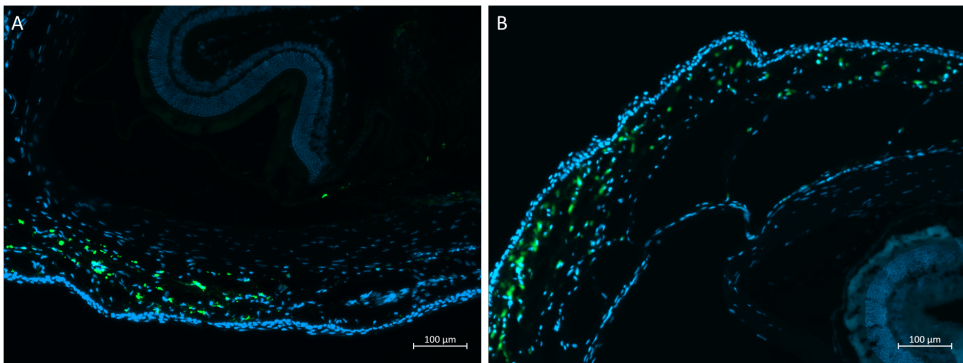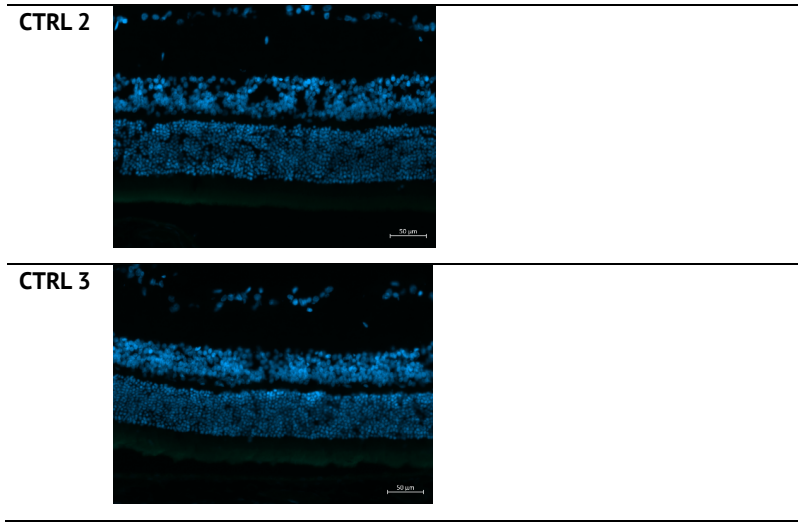
SI-Figure 4 Accumulation of fluorescently labelled particles could be seen at the ciliary body and sclera (A and B)

6

Chapter 7

Eyes on the Future:
Summary, Perspectives, and Industrial Development

Blessing C. Ilochonwu

1 SUMMARY

The work described in this thesis was aimed at designing, developing, and characterizing injectable formulations based on Diels-Alder crosslinked polymers, resulting in hydrogels and core crosslinked polymeric micelles for intravitreal drug delivery.

Chapter 2 provides an overview of the challenges for intraocular drug delivery, emphasizing the limitations of current formulations of therapeutic proteins and the need for sustained drug concentrations in the target tissue. This review highlights the beneficial features of hydrogels that have potential to overcome many of the limitations of the currently used delivery systems, such as injectability, biocompatibility, and biodegradability. Also, the importance of biodegradable sustained release formulations is discussed. Injectable in situ forming hydrogels were identified as promising materials for sustained drug delivery to the back of the eye, offering a potential solution to the unmet needs in intraocular drug therapy.

Chapter 3 focuses on the development and characterization of an intravitreal in situ forming hydrogel. This hydrogel is based on the Diels-Alder crosslinking of hyaluronic acid (HA) and poly(ethylene glycol) (PEG) modified with furan and maleimide groups, respectively, to serve as a sustained delivery system for bevacizumab. This therapeutic monoclonal antibody is able to bind to vascular endothelial growth factor (VEGF) and inhibit its activity. It is clinically used in the treatment of retinal diseases such as age-related macular degeneration (AMD) and diabetic retinopathy. The chapter describes various aspects of the developed hydrogel system, including its gelation kinetics, mechanical properties, injectability, biodegradability, sustained release of bevacizumab, and cytocompatibility with retinal cells. The hydrogels degrade completely under physiological conditions and the degradation rate depends on concentration and ratio of the hydrogel forming building blocks. The hydrogels release bevacizumab for up to a year, suggesting the potential to reduce injection frequency. While the released bevacizumab remains bioactive for at least a month, further research is needed to confirm the release of bioactive protein over a longer period.

Chapter 4 investigates the in vivo pharmacokinetic (PK) profile and ocular safety of the developed hyaluronic acid-PEG-based Diels–Alder hydrogels, as described in **Chapter 3**, for sustained intraocular delivery of bevacizumab in rabbit eyes. Injection of the hydrogel resulted in the in situ formation of a localized depot loaded with this therapeutic protein in the vitreous body. Pharmacokinetic evaluations demonstrated that higher polymer concentrations led to reduced initial bevacizumab release and increased retention of this therapeutic protein in the vitreous and aqueous humour. Unexpectedly, the formulations also induced inflammation in the posterior segment of the eye. The exact cause of this inflammation remains unknown, but the results suggest a relationship between polymer concentration, hydrogel stability, and the observed inflammation. On the other hand, more stable placebo formulations showed no inflammation in the posterior segment and only transient irritation in the anterior segment, indicating that a more stable and slower degrading hydrogel is better tolerated in rabbit eyes. Another potential explanation for the inflammation observed for the drug loaded gel formulations could be related to the released bevacizumab-BDP dye within the vitreous body. It is conceivable that the released

protein-dye may aggregate within the vitreous body, potentially initiating an inflammatory response. Overall, the hydrogel system demonstrates potential for sustained drug release but requires systematic safety evaluations before further translational steps.

Chapter 5 introduces the synthesis route of two novel ABA triblock copolymers. These copolymers consist of a poly(ethylene glycol), hydrophilic midblock (B) and outer blocks (A) primarily composed of thermo-responsive poly(*N*-isopropylacrylamide), along with comonomers containing maleimide or furan functional groups. By combining the thermogelation properties of the polymers and Diels Alder chemical crosslinking, stable hydrogels were formed in situ. *T*hese hydrogels exhibited remarkable versatility as drug delivery systems, facilitating the controlled release of two distinct model drugs: the anti-inflammatory medication dexamethasone and a FAB antibody fragment designed as a biosimilar to Ranibizumab, targeting the inhibition of VEGF. Notably, the hydrogels showed the release of dexamethasone for 35 days and FAB protein for 13 days. Importantly, the maleimide functional groups, based on physicochemical considerations are located in the hydrophobic domains of the polymer matrix do not interact with the protein at temperatures above LCST, preventing undesired protein modification during loading and release. Moreover, the hydrogel can be injected using a 30 G needle and exhibits excellent cytocompatibility with retinal cells, making it a promising candidate for intravitreal drug therapy.

Furthermore, in **Chapter 6**, the ABA thermo-responsive copolymers were employed to create Diels-Alder core crosslinked flower like micelles (FLM) potentially suitable for e.g. dexamethasone delivery in ocular inflammatory therapy. These micelles showed good cytocompatibility and were internalized by both retinal cells and macrophages. In vivo experiments utilizing a rat eye model demonstrated convenient administration of the micelles via intravitreal injection, with no observed adverse effects or retinal abnormalities. The micelles efficiently reached the sub-retinal space, retinal cells, and the inner limiting membrane (ILM) at the vitreoretinal barrier. However, further optimization is required to prolong vitreous particle retention. Overall, Diels-Alder core crosslinked FLM micelles exhibit high potential as delivery system for the future treatment of ocular inflammatory conditions by targeting the sub-retinal space and retinal pigment epithelium (RPE).

2   PERSPECTIVES

2.1   Eyes on the Future: General Outlook

2.1.1   Tailoring Hydrogel and Micelle Characteristics for a Range of Therapeutic Agents

This thesis describes advances in the optimization of hydrogel and micellar characteristics, enabling the sustained release of therapeutic agents with different pharmacological and physicochemical properties. These findings provide the groundwork for establishing an adaptable platform for injectable formulations for ocular treatments. Drugs such as dexamethasone, bevacizumab, and ranibizumab were employed to investigate and validate the release profiles of the designed drug delivery systems. However, numerous additional drugs used in ocular therapy (e.g., pegaptanib, aflibercept, triamcinolone acetonide, brolucizumab, fluocinolone acetonide) could potentially benefit from the sustained, controlled, or targeted delivery facilitated by the

7

hydrogels and FLM micelles developed and described in this thesis. As a result, forthcoming studies should investigate the release kinetics of various therapeutic agents and combinations, offering potential treatments for a spectrum of ocular diseases.

2.1.2   Addressing Ocular Safety Concerns

Notably, significant concerns arose in **Chapter 4** regarding the intravitreal injection of the developed DA hydrogel formulation utilizing hyaluronic acid (HA) with a molecular weight of 25 kDa, suspected to contribute to inflammatory effects upon administration of the hydrogel system. Therefore, systematic preclinical toxicity studies should be conducted to understand potential adverse effects on ocular tissues to develop systems with acceptable biocompatibility. Scientists are progressively delving into the correlation between HA's degradation and its molecular weight concerning inflammatory responses. Meszaros et al.[1] state that: "*the biological functions of HA depend on its molecular size*". Low molecular weight (LMW) HA exhibit higher toxicity compared to higher molecular weight (HMW) HA. This difference is primarily ascribed to the variances in structure and function between LMW and HMW HA, particularly concerning their interactions with hyaluronidase-1.[1-3] Mi Lee et al.[4] revealed that LMW HA (<500 kDa) heightened pro-inflammatory cytokines in macrophages, while HMW HA (>1,250 kDa) reduced cytokine production, suggesting potential immunosuppressive effects. However, the implications of these observations are difficult to understand. HMW HA is in the body enzymatically cleaved into fragments of lower molecular weight. This means that in time cytocompatible HA is converted into HA that causes inflammatory responses.

In future designs of hydrogels based on HA, it is recommended to explore the use of hyaluronic acid (HA) building blocks with molecular weight beyond 1,250 kDa to harness the anticipated anti-inflammatory benefits of higher molecular weight HA. The larger size of HMW-HA restricts its penetration into tissues, thereby reducing its interaction with pro-inflammatory cells. Consequently, this limitation results in a diminished immune response and reduced toxicity. This effect primarily stems from its larger and more complex structure, which makes it less susceptible to the action of hyaluronidase-1. As a result, the degradation into LMW-HA is slowed down.

Furthermore, the impact of crosslinking chemistry, network crosslink density, and stability of hydrogels on ocular safety should be further investigated. For example the application of crosslinkers like 4-arm PEG maleimide (as explored in **Chapter 3 and 4**) and glutaraldehyde (discussed previously by Lai et al. [5]) raises concerns about potential intraocular incompatibility. This concern stems from the fact that when these functional agents are present freely in the vitreous body, they can trigger an inflammatory response due to their heightened reactivity. Consequently, there is a pressing need to identify polymers and crosslinking reactions that have demonstrated safety for intraocular use in both animal and human subjects[6, 7] (as discussed below) . Furthermore, inflammation can also arise as a consequence of dye-labelled drug-loaded gel formulations. It is plausible that the labelling process itself could compromise protein stability within the vitreous, leading to the possibility of protein aggregates being formed within the vitreous body upon release from the gel. This scenario has the potential to trigger an inflammatory response. Therefore, careful selection of the labelling agent and testing drug

stability within the vitreous body after modification is paramount. Additionally, a comprehensive examination of factors, including protein-polymer interactions, hydrogel stability, hydrogel swelling, and injection procedures, encompassing *in vitro-in vivo* comparisons, is crucial for understanding ocular biocompatibility.

2.1.3 Crosslinking Chemistry Challenges and Bio-Orthogonal Crosslinking Chemistry

The stability and controlled drug release from hydrogels and micelles rely on effective crosslinking chemistry. The utilization of furan-maleimide Diels-Alder crosslinking confers valuable advantages, encompassing adjustable crosslinking kinetics, efficient drug encapsulation and tuneable release kinetics, as demonstrated in **Chapter 3** and **5** of this thesis. Its mild reaction conditions render it an appealing choice. However, the reactivity of maleimides with thiols and amines present in biological therapeutics poses challenges. Addressing this limitation may involve employing bio-orthogonal crosslinking chemistry, utilizing functional groups inert to the components present in the cargo drug. In contrast to furan-maleimide crosslinking, a catalyst-free inverse-demand Diels-Alder reaction between tetrazine and norbornene groups[8] and bioorthogonal click chemistry[9] may offer heightened specificity and compatibility with biotherapeutics. While their complexity and costs may pose obstacles, advances in synthetic chemistry can potentially mitigate these challenges. The potential merits of enhanced selectivity and reduced off-target reactions warrant further investigation and optimization.

2.1.4 Network Degradation

The degradation of a hydrogel, a hydrophilic crosslinked network, represents a crucial factor in the development of biomaterials aimed for delivery of protein therapeutics. This thesis demonstrates that complete degradation of the Diels-Alder crosslinking network based on hyaluronic-PEG matrices under physiological conditions occurred, as discussed in **Chapter 3**. In contrast, no degradation was observed in the hydrophobic PNIPAM domain, as detailed in **Chapter 5**, also under physiological conditions. This observation suggests potential strategies to regulate Diels-Alder network degradation rate by adjusting polymer hydrophobic/hydrophilic balance, thereby achieving delivery systems that degrade under physiological conditions at the desired rate.

2.1.5 Advancing Ocular Drug Delivery: Hydrogels and Micelles' Advantages and Considerations

Hydrogels and micelles offer distinct advantages and limitations for ocular drug delivery. Hydrogels provide a local three-dimensional network conducive to drug entrapment and sustained release. Their easily modifiable properties render them versatile for various drug types, particularly biotherapeutics like full sized antibodies as well as antibody fragments commonly employed in retinal therapy. However, in future, continuous efforts should be made to reduce viscosity of the formulations to allow intravitreal injections using a small needle for patient compliance, following the examples shown in this thesis. On the other hand, polymeric micelles with a hydrophilic shell excel at encapsulating hydrophobic drugs in their core,[10] potentially enhancing solubility and stability. Nonetheless, due to the rapid intravitreal clearance of particles, as also observed in the examined PNIPAM-PEG-based FLM (**Chapter 6**), future research

7

endeavours should focus on enhancing ocular pharmacokinetics and vitreous particle retention to potentially prolong drug efficacy. However, the choice between hydrogels and micelles hinges on factors such as drug properties, desired release kinetics, and target tissue characteristics.

In future investigations, it is recommended to explore the development of a next-generation ocular drug delivery system through a synergistic approach that combines hydrogels and micelles to optimize drug delivery and targeting within the eye. Hydrogels can proficiently be loaded with drug loaded micelles or other types of nanoparticles, resulting in controlled/sustained and targeted drug release, as previously demonstrated in polyplex-loaded thermosensitive hydrogels by Fliervoet et al.[11] for localized siRNA delivery. Additionally, micelle cores can accommodate hydrophobic drugs, and both the micelles and hydrophilic drugs like monoclonal antibodies can reside within the hydrogel network, enabling co-delivery of drugs with differing physicochemical and pharmacological properties. This integration has the potential to revolutionize treatments, yielding enhanced therapeutic outcomes and elevating patients' quality of life.

2.2 Industrial development of biomaterials: insights from the pharmaceutical product explored in chapter 3

As extensively discussed in this thesis, injectable polymeric biomaterials have recently gained significant attention in the pharmaceutical field as a promising materials for ocular drug delivery. The use of many polymeric biomaterials has enabled the development of new and effective ocular formulations with improved drug stability and availability at the site of action, and extended-release profiles. However, an overview of the industrial perspective for the development of this type formulations is often missing in early preclinical studies leading to unmet formulation characteristics that hinder clinical translation and ultimately market entry. Within this thesis, a comprehensive analysis of biomaterials for intravitreal drug delivery is provided, focusing specifically on two delivery systems, namely hydrogels (**Chapter 3** and **5**) and micellar-nanoparticles (**Chapter 6**). To facilitate further industrial development, it is essential to address key factors such as scalability, sterilization techniques, storage conditions, product stability, and finally product packaging. By considering these crucial aspects, a seamless transition from laboratory-scale development to large-scale production can be achieved. Furthermore, regulatory compliance and interdisciplinary collaborations are vital in the industrialization of biomaterial-based ocular drug delivery systems. Incorporating of industrial perspectives optimizes formulation design, anticipates obstacles, and drives advancements for improved patient outcomes, bridging the gap between innovation and successful industrial development. To gain valuable insights into industry advancements, particular emphasis is placed on the hydrogel developed in **Chapter 3**.

2.2.1 Scale-up process

Scale-up is a crucial step in the development of any pharmaceutical product, and ocular formulations based on polymeric biomaterials are no exception. Scale-up involves increasing the production capacity of the formulation from laboratory scale to commercial scale. The process

typically involves optimization of the manufacturing process, followed by process validation. Several factors need to be considered during scale-up:

- **Raw material selection:** It is imperative to have access to high-quality raw materials in substantial quantities for successful scale-up. Ensuring a reliable and commercial supply of materials is essential to meet the increased production demands effectively.

- **Selection of appropriate production equipment:** The utilization of scalable equipment plays a pivotal role in the scale-up process. For instance, reactors equipped with specific features like controlled pressure or oxygen-free environments during polymerization steps are commonly employed. Additionally, equipment such as spray dryers are often utilized in biomaterial production to efficiently remove residual solvents on a large scale. Having properly sized equipment available ensures efficient production during scale-up.

- **Streamlined manufacturing process:** During scale-up, it is advantageous to adopt a simplified and straightforward manufacturing process. By minimizing the number of process steps, efficiency is enhanced, and the potential for errors and contamination is reduced. Establishing a well-defined and optimized manufacturing process is critical to ensure consistent batch-to-batch product quality and reproducibility at a larger scale.

In **Chapter 3**, furan-modified hyaluronic acid (HAFU) derivatives were synthesized by functionalizing hyaluronic acid with furfurylamine groups. The raw materials, including HA, furfurylamine, 4-(4,6-dimethoxy-1,3,5-triazin-2-yl)-4-methylmorpholiniumchloride (DMTMM), and MES buffer, which can all be readily obtained from established commercial suppliers. The synthesis process can be carried out in a standard reactor with temperature control but without the need for specialized conditions like controlled pressure or oxygen levels. To purify the product, a two-step manufacturing process involving ethanol precipitation and solvent evaporation was employed, as depicted in Figure 1. To validate the feasibility of scale-up, a pilot small-scale experiment was conducted, scaling up from 0.5 g to 10 g. This proof of concept demonstrated the successful attainment of HAFU derivatives with two different degrees of furan substitution of 50 and 83%. Differences in degree of substitution were established by varying the amount of furfurylamine and coupling agent (DMTMM) in the reaction mixture (Table 1). ^{1}H-NMR analysis confirmed that there were no significant differences in the spectra of the polymers synthesized on 0.5 g and 10 g scales, as shown in Table 1, with yields of 80-90 %. Although from an industrial perspective 10 g is not really a substantial amount, this experiment highlights the further scalability and consistency of the synthesis process in achieving the desired product characteristics for larger polymer batches.

7
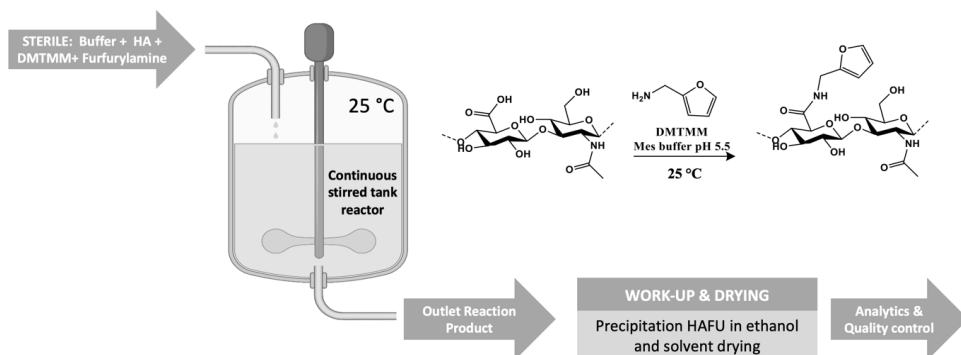
Figure 1 Synthesis and purification process of furan-modified hyaluronic acid (HAFU) derivatives. HAFU derivatives were synthesized by functionalizing hyaluronic acid with furfurylamine using DMTMM as coupling agent. Raw materials are commercially available, and synthesis can be performed in a standard reactor. Purification involves ethanol precipitation and solvent evaporation for product refinement. Created with BioRender.com

Table 1 Degree of substitution (DS) for different ratios of HA, Furfurylamine, and DMTMM in scaling up from synthesis (0.5g) and pilot production (10g). DS determined by comparing N-acetyl glucosamine peak on HA-backbone to aromatic furan peaks using ^{1}H-NMR analysis

Molar Ratio HA: Furfurylamine:DMTMM	Synthesis (0.5g)	Pilot Production (10g)
1:1:2	DS 45%	DS 55%
1:2:6	DS 80%	DS 83%

2.2.2 Sterilization

Clean production and sterilization and are a crucial steps in the manufacturing process of polymeric biomaterial-based formulations.[12, 13] The selection of a sterilization method depends on the type and intended use of the product.[12, 14] High viscosity formulations, including gels, creams, and ointments, are frequently used in ocular applications. Due to their complex composition and susceptibility to microbial contamination, sterilization plays a vital role in their manufacturing process. Various methods can be employed to sterilize objects, products, and packaging surfaces, such as:

- Heat-based sterilization (dry and moist heat)[15-17]
- Filtration-based sterilization[18, 19]
- Radiation-based sterilization (gamma, electron beam, X-ray, and ultraviolet)[20, 21]
- Chemical sterilization (ethylene oxide, ozone, chlorine dioxide, and hydrogen peroxide).[22, 23]

In the context of pharmaceutical products, contaminants can be categorized as intrinsic or extrinsic. Intrinsic contaminants are already present in the untreated or raw product, example, polymer solutions, hydrogel or nanoparticulate dispersions, as well as in or on the packaging materials prior to processing. Extrinsic contaminants, on the other hand, are introduced during handling or the manufacturing process. When it comes to packaging pharmaceutical products, two primary principles are considered: terminal sterilization, and aseptic production and filling as discussed by Jildeh et al.[24] Terminal sterilization (refer to figure 2A) involves subjecting the final product and its packaging containers to a sterilization process compatible with all the materials involved. This method is commonly used for sterilizing contact lenses, implants, and certain pharmaceutical formulations using thermal, physical, and chemical sterilization processes.

However, there are cases where medical products contain sensitive Active Pharmaceutical Ingredients (APIs), proteins and sensitive polymers in their formulation, or they are packaged in materials that are sensitive to heat and radiation. In such situations, aseptic production techniques have to be employed. Aseptic filling machines sterilize the product and packaging materials separately using suitable sterilization techniques (mentioned above). After sterilization, they are combined under sterile conditions within the aseptic zone (refer to Figure 2B). The machine components that come into contact with the products and packaging materials are sterilized using validated processes, such as heat or chemical sterilization.
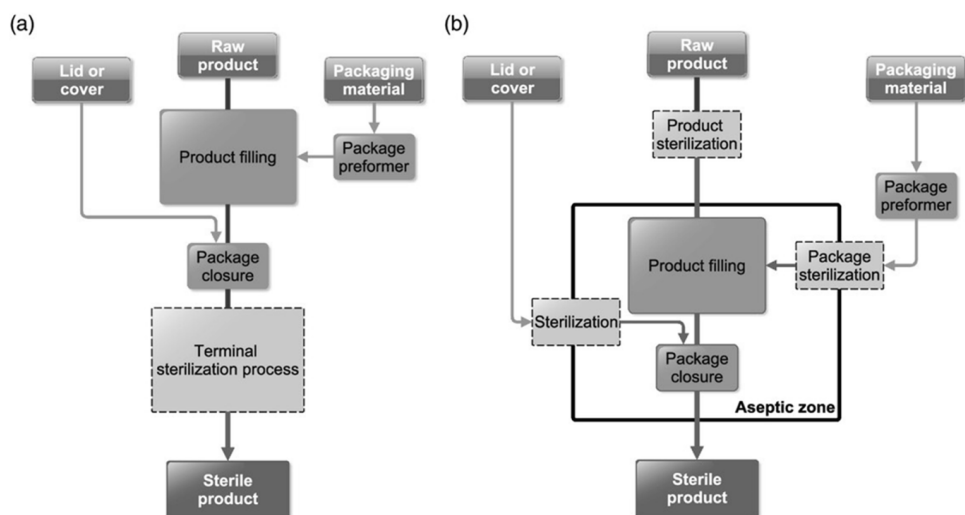
Figure 2 The flowchart visually presents the design of a filling machine in two scenarios: a) employing the terminal sterilization concept, and b) featuring the setup of an aseptic filling machine. Adapted and reprinted with permission from [24] Copyright © Wiley-VCH GmbH.

As discussed in **Chapter 2** of this thesis, the sterilization process presents significant challenges when it involves polymeric biomaterials, particularly those utilized in the preparation of hydrogel

or micellar formulations. These materials often contain sensitive and reactive functional groups that are susceptible to chemical degradation under stressed conditions applied in sterilization protocols. Therefore, it is crucial to carefully select an appropriate sterilization method, considering its potential impact on the properties of the polymers. Various sterilization processes, such as radiation, chemical sterilization, and exposure to high temperatures, can cause undesirable degradation and structural changes in certain polymers. It is important to note that the chosen sterilization method can also have adverse effects on the loaded proteins, further complicating the overall process. Among the available options, the aseptic filling technique emerges as a particularly suitable approach for such materials and their pharmaceutical formulations. This method enables the separate sterilization of the raw and precursor biomaterials using compatible techniques. For example sterile filtration offers attractive alternatives for the pharmaceutical production to achieve sterility without subjecting the polymeric biomaterials to other potentially damaging sterilization processes.

Subsequently, these sterilized components can be combined with the final packaging or, in certain cases, loaded into specialized devices (e.g., syringes or automatic injection devices) within the controlled environment of the aseptic zone. By employing this technique, the risks associated with undesired polymer and protein alterations can be mitigated, ensuring the functionality of the final product.

2.2.3   Final product packaging:

The final packaging of the ocular formulations plays a crucial role in ensuring their stability and sterility. It is essential to design the packaging be compatible with the formulation and protects it from physical damage, light exposure, and moisture uptake while maintaining its sterility. The selection of packaging materials depends on the specific product type and its intended use. For instance, ophthalmic solutions are commonly packaged in single-use vials or prefilled single chamber syringes (figure 3), while ophthalmic suspensions are often packaged in multi-dose bottles.[25, 26] In the case of intravitreal ocular drug solution administration, prefilled syringes are widely preferred due to their convenience and precise dosing capabilities. They offer accurate dosing, reduce the risk of contamination, and are easy to administer. Examples of drugs delivered using prefilled syringes for intravitreal administration include anti-VEGF agents like ranibizumab (brand name: Lucentis) and aflibercept (brand name: Eylea), corticosteroids such as triamcinolone acetonide (brand name: Kenalog), and antibiotics like vancomycin and ceftazidime.[27] Additionally, an intravitreal dexamethasone implant (brand name: Ozurdex) is administered using a specialized syringe called a "preloaded applicator," specifically designed to contain the Ozurdex implant and facilitate its implantation into the eye.[28]

In the context of in situ forming hydrogels, as discussed in **Chapter 3** and **Chapter 5**, the system typically consists of two reactive polymer components. When these components are mixed together, they undergo crosslinking and form a network. However, this network cannot be injected using small needles, typically ranging from 27-34 G, which are recommended for intravitreal applications. To address this issue, dual chamber syringes can be used (see figure 3), allowing for the separation of the formulation components. This approach proves to be highly suitable since

the components are only mixed a few minutes before injection (see syringe 2 in figure 3) or even mixed within the needle during the injection procedure (syringe 1 in figure 3). Specifically, in one type of dual chamber syringe, the plunger pressure facilitates the mixing of the reactive polymer components A and B within the needle, initiating crosslinking and the formation of a hydrogel. Alternatively, a second type of syringe employs the plunger action to induce the movement of liquid component B into component A, and once homogeneous mixing is assured, the formulation can be injected. By employing these dual chamber syringes, the reactive polymer components can be kept separately until the moment of injection, preserving their stability and maintaining their effectiveness. The controlled mixing of the components at the right time and location ensures the successful formation of the in-situ hydrogel, facilitating precise drug delivery and optimizing the therapeutic outcome.
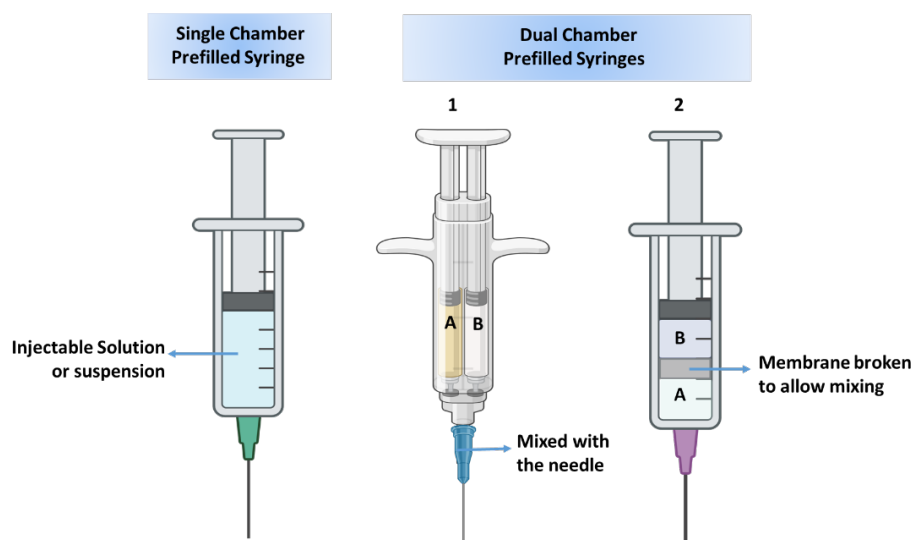
Figure 3 Single and dual chamber syringe designs for intravitreal ophthalmic drug delivery formulations. Created with BioRender.com

In **Chapter 3** and **Chapter 5**, it is noted that the in situ forming hydrogel precursors contain maleimide groups, which are susceptible to hydrolysis in an aqueous medium and have shown reactivity with the protein API. In this context, the type 2 syringe design is recommended. The reason being that the dried polymer powder mixture (in its unreactive form) can be stored in chamber A, while the protein solution can be stored in chamber B. This separation allows for longer stability and shelf life, with the components only being mixed right before injection.

For example, in the case of the in-situ hydrogels discussed in **Chapter 3,** the dried HAFU polymer and dried crosslinker polymer (4-arm PEG maleimide) can be combined as solid powders in chamber A (step 1, see figure 4), while the protein solution, commonly formulated as a solution for intravitreal proteins, is stored in chamber B. By keeping the components separate until the point of injection, their individual stability is preserved, ensuring a longer shelf life for the product. The mixing of the dried polymer powders and the protein solution occurs in the syringe

7

during the injection process, allowing for the formation of the desired hydrogel at the targeted site. In the development of in situ forming hydrogels containing maleimide groups, it is therefore crucial to perform stability testing on the mixed powder formulations. This testing is necessary to evaluate the stability of the dried polymer powders and potential premature crosslinking. Furthermore, it is important to highlight that this manufacturing process might benefit from the aseptic filling technique discussed above. As a result, each formulation component is sterilized individually using the most suitable technique. Subsequently, these components are assembled into the syringe within the aseptic zone, as depicted in Step 2 of figure 4.
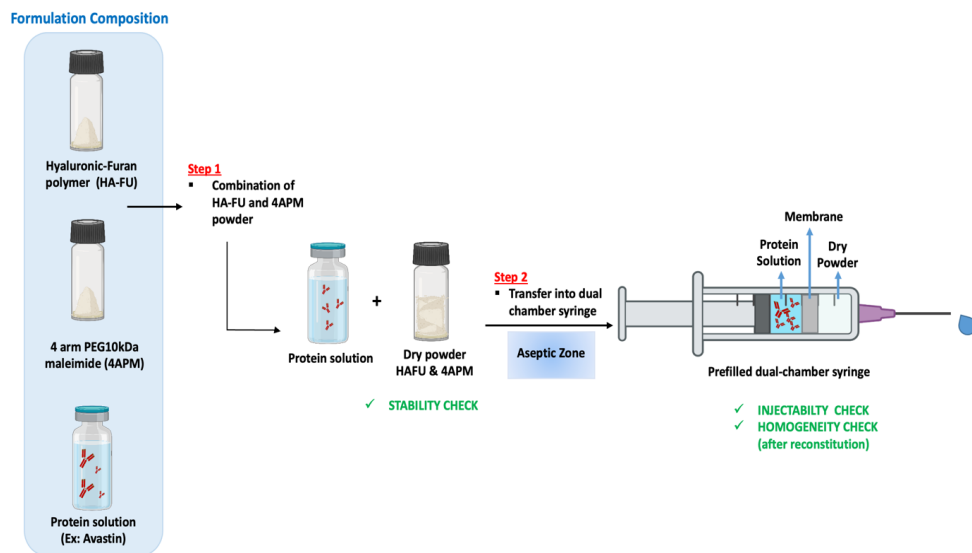
Figure 4 Schematic representation of the manufacturing process of in situ hydrogel based on the Diels-Alder crosslinking of hyaluronic acid (HA) modified with furan groups and poly(ethylene glycol) modified with maleimide groups for sustained delivery of bevacizumab. Created with BioRender.com

In a pilot product development study, a visual assessment of the formulation reconstitution was performed using the Vetter Lyo-ject® dual chamber syringe, as shown in figure 5. Compartment A of the syringe was loaded with HAFU DS 80 %, chosen as a model polymer powder due to its high solution viscosity compared to other polymers examined previously. Water for injection was used to mimic the protein solution. After assembling the syringe, the excipient-only formulation was reconstituted within 1 minute by shaking the syringe. This resulted in a homogeneous polymer solution that was easily injectable. The successful reconstitution and the formation of a uniform polymer solution were visually confirmed, demonstrating the effectiveness of the dual chamber syringe system for solid- liquid formulations.
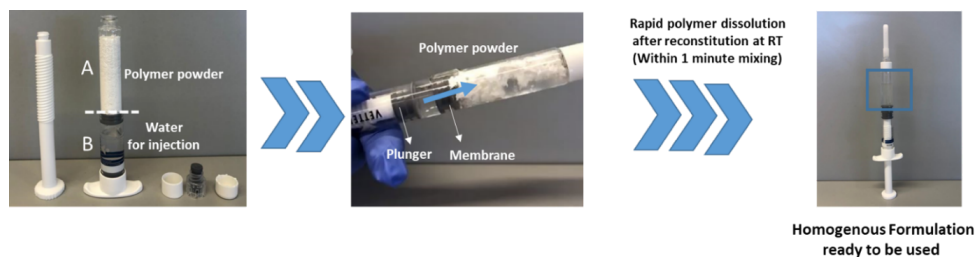
Figure 5 Pilot product development where the successful reconstitution of the formulation was tested using the Vetter Lyo-ject® dual chamber syringe with HAFU DS 80 and water for injection.

2.2.4   Injectability

Injectability and injection force are essential considerations in the context of intravitreal injections (figure 4). Good injectability ensures a smooth flow of the formulation, enabling accurate dosing and reducing trauma to the eye.[29] It allows for precise delivery into the vitreous humour, maximizing treatment efficacy. On the other hand, injection force must be meticulously regulated. Excessive force can cause tissue damage and complications, while insufficient force may result in incomplete administration of the formulation and the loaded drug at the injection site, as some of the formulation may remain within the syringe or needle.[30] Balancing the injection force ensures effective medication delivery and minimizes the risk of adverse events.[31] The injection of viscous formulations using small needles, such as 27 G, 30 G, and 34 G, can present certain challenges.[30] Viscous formulations have higher resistance to flow, making it more difficult to inject them through narrow-gauge needles. The increased viscosity requires an increased injection force needed to administer the medication. The acceptable force during injection depends on various factors, including the specific formulation, preferred needle size, medical professional's comfort and patient tolerance.[30, 32, 33] According to the Congruence Medical Solutions after conducting numerous studies in the ophthalmic space, based on user feedback, the target injection force for manual intraocular injections should ideally be below 20 N, which is comparable to an acceptable injection force in parenteral drug delivery.[34] Congruence's data[34] also indicates three major ways to potentially reduce the injection force to optima force in injection devices :

1.   Select the right injection needle.
2.   Increase injection time.
3.   Use a syringe with a smaller internal diameter (in agreement with The Hagen-Poiseuille law [35]).

In the design of polymer-based delivery systems various strategies can be employed to improve the injectability of formulations some examples include:

▪   Particle size reduction: Techniques like milling, micronization, or high-pressure homogenization can be employed to decrease the particle size of the formulation.

7

- Rheology modifiers: Adding rheology modifiers (such as shear-thinning properties) to alter the flow behaviour and reduce resistance during injection.
- Optimization of formulation parameters: Adjusting polymer concentration and molecular weight, pH of the polymer solution, and temperature to modulate the injectability characteristics of the formulation.

Therefore, it is crucial to assess the injection force of the final formulations during preclinical evaluation. As shown in figure 6, the required injection force of the formulation developed in **Chapter 3** is below 20 N, indicating its suitability for intravitreal application. The injection force is significantly influenced by both polymer concentration and needle size, as discussed earlier.

Strategic advancements in pharmaceutical formulations and injection techniques should focus on optimizing injectability, reducing injection force, and ensuring efficient and comfortable delivery of polymer-based formulations. These advancements are crucial in enhancing safety, efficacy, and patient comfort, ultimately driving the successful clinical adoption of viscous intraocular formulations in the field of ophthalmology.
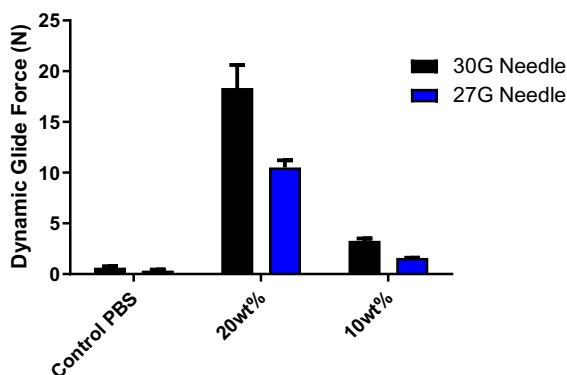
Figure 6 Dynamic glide force (n=3) as a function of polymer concentration and needle size for 4APM-HAFU (ratio 1:3) formulation < 20 min after mixing hydrogel polymer precursors. Dynamic glide force represents the force necessary to achieve smooth and consistent movement of the syringe plunger during the injection process.

2.2.5   Product stability and storage conditions

Storage conditions play a crucial role in maintaining the stability and shelf life of ocular formulations based on polymeric biomaterials, including protein-based ocular formulations like ranibizumab (Lucentis) and bevacizumab (Avastin). Identifying optimal storage conditions involves considering formulation type, final packaging, temperature, humidity, and light exposure.[36] Protein-based medications necessitate specific storage conditions to preserve their integrity and functionality. Typically, these proteins should be refrigerated at temperatures between 2 and 8 °C to prevent denaturation and degradation.[37] Protecting them from light exposure is essential to prevent photodegradation. Additionally, controlling humidity is crucial,

particularly for dried functional polymer precursors, as moisture absorption can lead to degradation or physical/chemical instability of both the excipient and loaded drug of the pharmaceutical product. To assess the suitability of the formulation approach described in figure 4 section 2.2.3, chemical stability of the HAFU and 4APM dried powder mixture was tested in a pilot study. A HAFU and 4APM dried powder mixture was stored in a closed vial in a refrigerator for up to 4 months at 4°C , and its structural integrity was assessed using attenuated total reflection infrared (ATR-IR) spectroscopy to ensure the absence of the formation of chemical crosslinks that will affect injectability. The results demonstrated that functional groups maintained stable for up to 4 months after mixing and storage, as depicted in figure 7. On the other hand, as evident from the absence of absorption peaks assigned to maleimide and furan moieties, when water was introduced to the control sample mixture, complete crosslinking occurred within 24 hours of incubation (figure 7). The obtained control hydrogel maintained its shape and appeared visually identical to the gels prepared from fresh polymers. Furthermore, in addition to the mentioned stability tests, thermal stability analysis using techniques like differential scanning calorimetry (DSC) are recommended for such type of ocular formulations. To explain, DSC measures the heat flow associated with phase transitions or chemical reactions, providing insights into the thermal stability and behaviour of the formulation components.
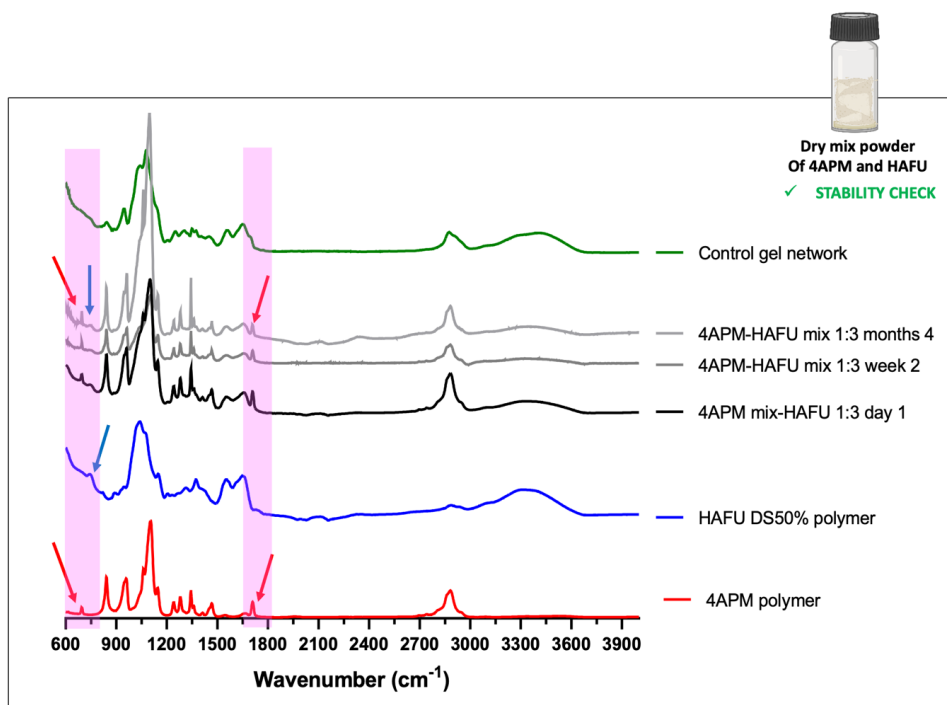
Figure 7 FT-IR spectra of HAFU DS 50%, 4APM, and mixture of HAFU DS 50% and 4APM after storage at 4 °C in a closed vial for 1 day, 2 weeks, and 4 months, compared to the control of 4APM-HAFU crosslinked hydrogel. The red arrows indicate the bending and stretching vibrations at 695 and 1707 cm^{-1}, respectively, which are asigned to the maleimide groups. Furthermore, the blue arrow highlights the peak at 737 cm^{-1},

corresponding to the =C-H bend vibration of the furan moiety in the HAFU polymer.The results illustrate that the functional groups remained intact and thus did not undergo crosslinking during the 4-month storage in closed vials at 4°C. In contrast, the control sample, upon addition of water to the mixture, exhibited complete crosslinking within 24 hours of incubation, as indicated by the absence of peaks asigned to the maleimide and furan moieties.

2.2.6   Regulatory considerations

The development of ocular formulations based on polymeric biomaterials, like any other pharmaceutical product, is subject to stringent regulatory requirements that ensure safety and efficacy. These requirements may vary depending on the country or region where the product is intended to be marketed. For instance, in the United States of America, the Food and Drug Administration (FDA)[38] has the authority to regulate the development and marketing of pharmaceutical products, including ocular formulations.[39] Similarly, in Europe, the European Medicines Agency (EMA) plays a key role in the regulation and approval process. The regulatory requirements for ocular formulations typically encompass preclinical testing, clinical trials, and the submission of a new drug application (NDA) to the respective regulatory authority. Preclinical testing involves assessing the efficacy and safety of the product using animal models. Clinical trials are conducted in controlled settings with human subjects to further evaluate safety and efficacy. The comprehensive data obtained from preclinical testing and clinical trials are compiled into the NDA, which includes vital information such as formulation composition, manufacturing process, device characteristics, stability data, final packaging, labelling. Both the FDA and EMA rigorously review the submitted NDAs to ensure that the ocular formulation send in for evaluation is safe and effective for its intended use. The evaluation process focuses on assessing the product's quality, efficacy, and safety profile. Once the regulatory authority approves the NDA, the ocular formulation can proceed towards commercialization as a medical device or pharmaceutical product, meeting the necessary regulatory requirements. This comprehensive regulatory framework instils confidence in both healthcare professionals and patients, ensuring that these products meet the highest standards of safety and effectiveness before they reach the market.

3   CONCLUSION

This thesis explored innovative avenues for intraocular drug delivery, offering the potential for significant advancements in treating retinal diseases and improving the well-being of patients with ocular conditions. The utilization of polymeric biomaterials investigated in this thesis demonstrates great promise in enabling new drug formulations that boast improved stability, enhanced drug availability at the target site, and extended-release profiles. However, careful consideration of factors like scale-up, sterilization, storage, stability, packaging, and regulatory compliance are vital for successful industrial development and ultimately clinical application. The future of ocular healthcare holds great promise for improved treatment of retinal diseases and ocular conditions.

4 REFERENCE

[1] M. Meszaros, A. Kis, L. Kunos, A.D. Tarnoki, D.L. Tarnoki, Z. Lazar, A. Bikov, The role of hyaluronic acid and hyaluronidase-1 in obstructive sleep apnoea, Sci Rep, 10 (2020) 19484.

[2] A.-R. Cho Lee, Size matters: differential property of hyaluronan and its fragments in the skin-relation to pharmacokinetics, immune activity and wound healing, Journal of Pharmaceutical Investigation, (2023).

[3] C. Buckley, E.J. Murphy, T.R. Montgomery, I. Major, Hyaluronic Acid: A Review of the Drug Delivery Capabilities of This Naturally Occurring Polysaccharide, Polymers, 14 (2022) 3442.

[4] B.M. Lee, S.J. Park, I. Noh, C.H. Kim, The effects of the molecular weights of hyaluronic acid on the immune responses, Biomater Res, 25 (2021) 27.

[5] J.Y. Lai, Biocompatibility of chemically cross-linked gelatin hydrogels for ophthalmic use, J Mater Sci Mater Med, 21 (2010) 1899-1911.

[6] S. Kirchhof, A.M. Goepferich, F.P. Brandl, Hydrogels in ophthalmic applications, Eur J Pharm Biopharm, 95 (2015) 227-238.

[7] C.R. Lynch, P.P.D. Kondiah, Y.E. Choonara, L.C. du Toit, N. Ally, V. Pillay, Hydrogel Biomaterials for Application in Ocular Drug Delivery, Front Bioeng Biotechnol, 8 (2020) 228.

[8] A. Famili, K. Rajagopal, Bio-Orthogonal Cross-Linking Chemistry Enables In Situ Protein Encapsulation and Provides Sustained Release from Hyaluronic Acid Based Hydrogels, Mol Pharm, 14 (2017) 1961-1968.

[9] Y. Jiang, J. Chen, C. Deng, E.J. Suuronen, Z. Zhong, Click hydrogels, microgels and nanogels: emerging platforms for drug delivery and tissue engineering, Biomaterials, 35 (2014) 4969-4985.

[10] B.J. Crielaard, C.J. Rijcken, L. Quan, S. van der Wal, I. Altintas, M. van der Pot, J.A. Kruijtzer, R.M. Liskamp, R.M. Schiffelers, C.F. van Nostrum, W.E. Hennink, D. Wang, T. Lammers, G. Storm, Glucocorticoid-loaded core-cross-linked polymeric micelles with tailorable release kinetics for targeted therapy of rheumatoid arthritis, Angew Chem Int Ed Engl, 51 (2012) 7254-7258.

[11] L.A. Fliervoet, H. Zhang, E. van Groesen, K. Fortuin, N.J. Duin, K. Remaut, R.M. Schiffelers, W.E. Hennink, T. Vermonden, Local release of siRNA using polyplex-loaded thermosensitive hydrogels, Nanoscale, 12 (2020) 10347-10360.

[12] M. Mukhopadhayay, A. Chatterjee, Conventional Processes for Sterilization and Preservation, in: M. Mukhopadhayay, A. Chatterjee (Eds.) Sterilization and Preservation: Applications of Supercritical Carbon Dioxide, Springer International Publishing, Cham, 2023, pp. 61-84.

[13] N. Karipidou, A.-N. Tzavellas, N. Petrou, C. Katrilaka, K. Theodorou, M. Pitou, E. Tsiridis, T. Choli-Papadopoulou, A. Aggeli, Comparative studies of sterilization processes for sensitive medical nano-devices, Materials Today: Proceedings, (2023).

[14] A. Valls-Esteve, P. Lustig-Gainza, N. Adell-Gomez, A. Tejo-Otero, M. Engli-Rueda, E. Julian-Alvarez, O. Navarro-Sureda, F. Fenollosa-Artes, J. Rubio-Palau, L. Krauel, J. Munuera, A state-of-the-art guide about the effects of sterilization processes on 3D-printed materials for surgical planning and medical applications: A comparative study, Int J Bioprint, 9 (2023) 756.

7

[15] W.J. Rogers, 2 - Steam and dry heat sterilization of biomaterials and medical devices, in: S. Lerouge, A. Simmons (Eds.) Sterilisation of Biomaterials and Medical Devices, Woodhead Publishing, 2012, pp. 20-55.

[16] S. Govindaraj, M.S. Muthuraman, Systematic review on sterilization methods of implants and medical devices, Int J ChemTech Res, 8 (2015) 897-911.

[17] H.F. Marei, A. Alshaia, S. Alarifi, N. Almasoud, A. Abdelhady, Effect of Steam Heat Sterilization on the Accuracy of 3D Printed Surgical Guides, Implant Dent, 28 (2019) 372-377.

[18] S.A. Bernal-Chávez, M.L. Del Prado-Audelo, I.H. Caballero-Florán, D.M. Giraldo-Gomez, G. Figueroa-Gonzalez, O.D. Reyes-Hernandez, M. Gonzalez-Del Carmen, M. González-Torres, H. Cortes, G. Leyva-Gomez, Insights into terminal sterilization processes of nanoparticles for biomedical applications, Molecules, 26 (2021) 2068.

[19] H. Shintani, Biocontrol science, 16 (2011) 85-94.

[20] B. McEvoy, A. Maksimovic, D. Howell, P. Reppert, D. Ryan, N. Rowan, H. Michel, Studies on the comparative effectiveness of X-rays, gamma rays and electron beams to inactivate microorganisms at different dose rates in industrial sterilization of medical devices, Radiation Physics and Chemistry, 208 (2023).

[21] B.K. Sharma, M. Singh, S. Lokhandwala, S. Wagh, S.R. Chowdhury, S. Ray, Radiation Processed Emerging Materials for Biomedical Applications, in: S.R. Chowdhury (Ed.) Applications of High Energy Radiations: Synthesis and Processing of Polymeric Materials, Springer Nature Singapore, Singapore, 2023, pp. 185-218.

[22] O. Bozkaya, Chemical Characterization of Ultra High Molecular Weight Polyethylene Based Tibial Inserts After Ethylene Oxide Sterilization, Kocaeli Journal of Science and Engineering, 6 (2023) 51-60.

[23] L.A. de Sousa Iwamoto, M.T. Duailibi, G.Y. Iwamoto, D.C. de Oliveira, S.E. Duailibi, Evaluation of ethylene oxide, gamma radiation, dry heat and autoclave sterilization processes on extracellular matrix of biomaterial dental scaffolds, Scientific Reports, 12 (2022) 4299.

[24] Z.B. Jildeh, P.H. Wagner, M.J. Schöning, Sterilization of Objects, Products, and Packaging Surfaces and Their Characterization in Different Fields of Industry: The Status in 2020, physica status solidi (a), 218 (2021).

[25] G.A. Sacha, W. Saffell-Clemmer, K. Abram, M.J. Akers, Practical fundamentals of glass, rubber, and plastic sterile packaging systems, Pharm Dev Technol, 15 (2010) 6-34.

[26] J.D. Brandt, Human Factors and Ophthalmic Drug Packaging: Time for a Global Standard, Ophthalmology, 122 (2015) 2368-2370.

[27] T.M. Sassalos, Y.M. Paulus, Prefilled syringes for intravitreal drug delivery, Clin Ophthalmol, 13 (2019) 701-706.

[28] T. Sherman, V. Raman, Incomplete scleral penetration of dexamethasone (Ozurdex) intravitreal implant, BMJ Case Rep, 11 (2018).

[29] R.L. Avery, S.J. Bakri, M.S. Blumenkranz, A.J. Brucker, E.T.J. Cunningham, D.J. D'Amico, P.U. Dugel, H.W.J. Flynn, K.B. Freund, J.A. Haller, J.M. Jumper, J.M. Liebmann, C.A. McCannel, W.F. Mieler,

C.N. Ta, G.A. Williams, Intravitreal injection technique and monitoring: Updated Guidelines of an Expert Panel, Retina, 34 (2014) S1-S18.

[30] G.B. Melo, N. Cruz, G.G. Emerson, F.A. Rezende, C.H. Meyer, S. Uchiyama, J. Carpenter, H.F. Shiroma, M.E. Farah, M. Maia, E.B. Rodrigues, Critical analysis of techniques and materials used in devices, syringes, and needles used for intravitreal injections, Prog Retin Eye Res, 80 (2021) 100862.

[31] C.E. Pang, S. Mrejen, Q.V. Hoang, J.A. Sorenson, K.B. Freund, Association between needle size, postinjection reflux, and intraocular pressure spike after intravitreal injection Retina, 35 (2015) 1401-1406.

[32] D.A. Bernards, C.J. Ma, Y. Zhang, T.M. Rodriguez, J. Dickson, B.N. Kharbikar, R.B. Bhisitkul, T.A. Desai, Injectable Devices for Delivery of Liquid or Solid Protein Formulations, ACS Materials Au, 3 (2023) 255-264.

[33] R. Tailor, R. Beasley, Y. Yang, N. Narendran, Evaluation of patients' experiences at different stages of the intravitreal injection procedure – what can be improved?, Clinical Ophthalmology, 5 (2011) 1499-1502.

[34] W.R. Shetty G, Ophthalmic Injection of Viscous Formulations – Why Unique Needs Require a Novel Delivery Approach, ONdrugDelivery, (2022) 54-58.

[35] C. Loudon, K. McCulloh, Application of the Hagen—Poiseuille Equation to Fluid Feeding through Short Tubes, Annals of the Entomological Society of America, 92 (1999) 153-158.

[36] B.R. Matthews, G.M. Wall, Stability Storage and Testing of Ophthalmic Products for Global Registration, Drug Development and Industrial Pharmacy, 26 (2000) 1227-1237.

[37] S.J.S. Bakri, Melissa R. Pulido ,Jose S. Mccannel, Colin A. Weiss, William T. Singh, Ravinder J. , Six-month stability of bevacizumab (Avastin) binding to Vascular endothelial growth factor after withdrawal into a syringe and refrigeration or freezing, Retina, 26 (2006) 519-522.

[38] A.A. Ciociola, L.B. Cohen, P. Kulkarni, C. Kefalas, A. Buchman, C. Burke, T. Cain, J. Connor, E.D. Ehrenpreis, J. Fang, R. Fass, R. Karlstadt, D. Pambianco, J. Phillips, M. Pochapin, P. Pockros, P. Schoenfeld, R. Vuppalanchi, How Drugs are Developed and Approved by the FDA: Current Process and Future Directions, American Journal of Gastroenterology, 109 (2014) 620-623.

[39] K.G. Csaky, E.A. Richman, F.L. Ferris, 3rd, Report from the NEI/FDA Ophthalmic Clinical Trial Design and Endpoints Symposium, Invest Ophthalmol Vis Sci, 49 (2008) 479-489.

7
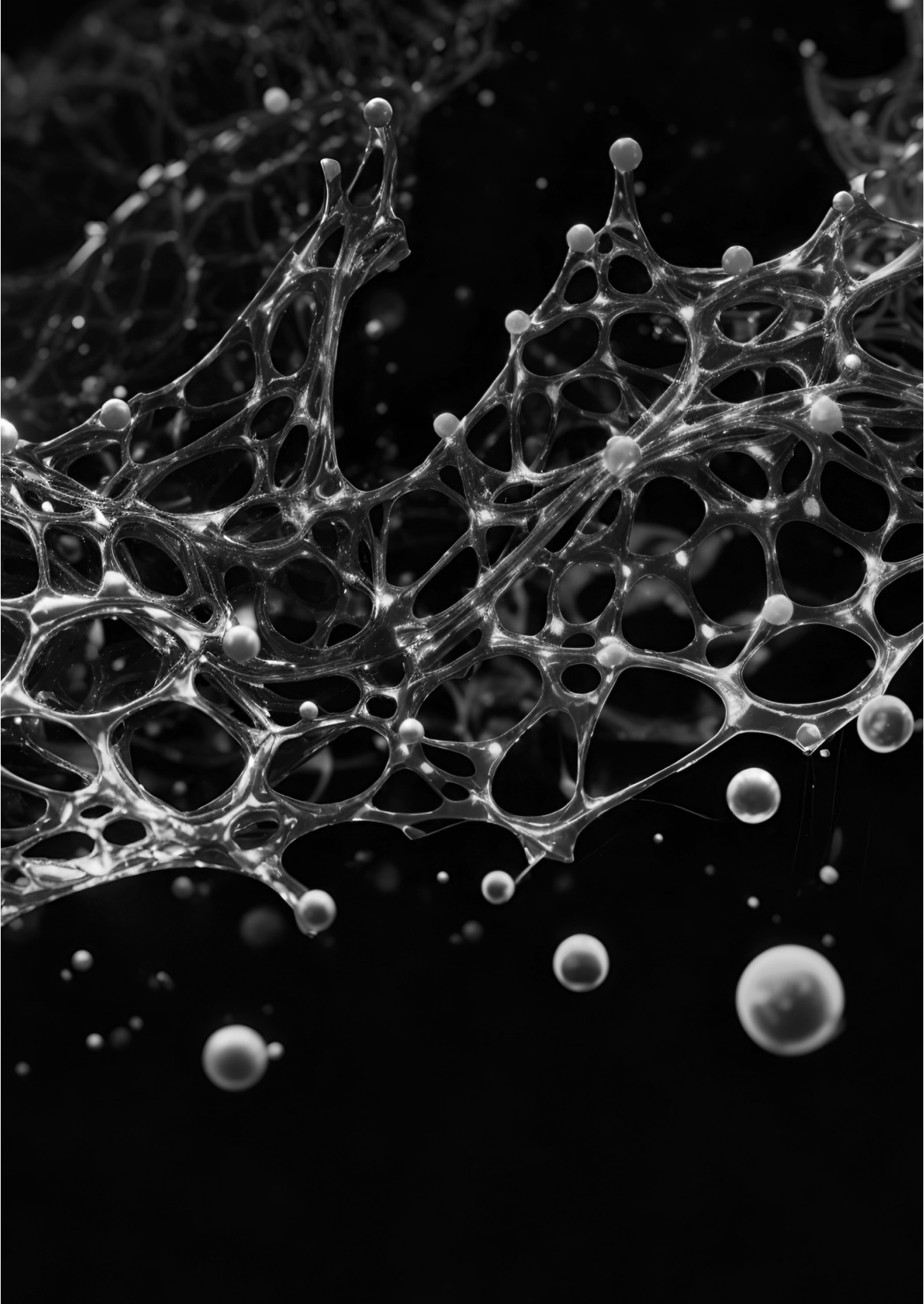
Appendices

NEDERLANDSE SAMENVATTING

Dit proefschrift is het resultaat van onderzoek dat is uitgevoerd binnen het Europese OcuTher Innovatief Training Netwerk (ITN), dat tot doel had een nieuwe generatie jonge onderzoekers op te leiden om de complexiteit van oculaire geneesmiddelenafgifte aan te pakken. De focus van OcuTher lag op de evaluatie van verschillende therapeutica, waaronder zowel bestaande als kandidaat-geneesmiddelen, in combinatie met innovatieve geneesmiddelenafgiftesystemen, allemaal met als doel om de behandeling van netvliesaandoeningen zoals maculadegeneratie, diabetische retinopathie en oculaire ontstekingen te verbeteren. Het OcuTher-consortium heeft academische en industriële experts samengebracht en heeft hun expertise gebundeld om oculaire therapieën vooruit te helpen. Het onderzoek dat in dit proefschrift wordt beschreven, heeft voornamelijk bijgedragen aan de ontwikkeling en beoordeling van nieuwe biomaterialen voor langdurige intraoculaire geneesmiddelenafgifte en heeft daarnaast gekeken naar de biodistributie, werkzaamheid en veiligheid van kandidaat-geneesmiddelen in innovatieve oculaire formuleringen. Dit proefschrift had specifiek tot doel de uitdaging van intravitreale geneesmiddelenafgifte aan te pakken door de ontwikkeling van biomaterialen, zoals hydrogelen en polymere micellen, voor langdurige/gecontroleerde afgifte van geneesmiddelen op basis van Diels-Alder (DA) chemie. De voornaamste doelstelling was het creëren van nieuwe injecteerbare formuleringen voor eenvoudige toediening via dunne naalden, het bieden van langdurige afgifte van geneesmiddelen en het verbeteren van de penetratie van geneesmiddelen in het netvlies.

Hoofdstuk 2 geeft een overzicht van de uitdaging voor intraoculaire geneesmiddelenafgifte, waarbij de beperkingen van huidige formuleringen van therapeutische eiwitten worden benadrukt en de behoefte aan langdurige aanwezigheid van geneesmiddelen in het oog wordt onderstreept. Dit overzicht belicht de gunstige eigenschappen van hydrogelen die veel van de beperkingen van de momenteel gebruikte afgiftesystemen kunnen overwinnen, zoals injecteerbaarheid, biocompatibiliteit en biologische afbreekbaarheid. Ook wordt het belang van biologisch afbreekbare afgifteformuleringen besproken. Injecteerbare in situ-vormende hydrogelen zijn geïdentificeerd als veelbelovende materialen voor langdurige geneesmiddelenafgifte naar het achterste deel van het oog, als mogelijke oplossing voor de huidige problemen in de oculaire geneeskunde.

Hoofdstuk 3 richt zich op de ontwikkeling en karakterisering van een intravitreale in situ-vormende hydrogel. Deze hydrogel is gebaseerd op de Diels-Alder verknoping van hyaluronzuur (HA) en poly(ethyleenglycol) (PEG) gemodificeerd met respectievelijk furan- en maleïmidegroepen, om te dienen als een langdurig afgiftesysteem voor bevacizumab. Dit therapeutische monoklonale antilichaam kan binden aan een vasculaire endotheliale groeifactor (VEGF) en de activiteit ervan remmen. Het wordt klinisch gebruikt bij de behandeling van netvliesaandoeningen zoals leeftijdsgebonden maculadegeneratie (AMD) en diabetische retinopathie. Dit hoofdstuk beschrijft verschillende aspecten van het ontwikkelde hydrogelsysteem, waaronder de kinetiek van gelering, mechanische eigenschappen, injecteerbaarheid, biologische afbreekbaarheid, langdurige afgifte van bevacizumab en cytocompatibiliteit met netvliescellen. De hydrogelen degraderen volledig onder fysiologische

omstandigheden en de degradatiesnelheid hangt af van de concentratie en verhouding van de polymeren in de hydrogel. De hydrogelen geven bevacizumab tot wel een jaar lang af, wat suggereert dat de injectiefrequentie sterk kan worden verminderd. Hoewel het vrijgegeven bevacizumab minstens een maand lang bioactief blijft, is verder onderzoek nodig om de afgifte van bioactief eiwit over een langere periode te bevestigen.

Hoofdstuk 4 onderzoekt het in vivo farmacokinetische (PK) profiel en de oculaire veiligheid van de ontwikkelde hyaluronzuur-PEG-gebaseerde Diels-Alder hydrogelen, zoals beschreven in **hoofdstuk 3,** voor langdurige intraoculaire afgifte van bevacizumab in de ogen van konijnen. Injectie van de hydrogel resulteerde in de in situ-vorming van een gelokaliseerd depot beladen met dit therapeutische eiwit in het glasachtige lichaam. Farmacokinetische evaluaties toonden aan dat hogere polymeerconcentraties leidden tot verminderde initiële afgifte van bevacizumab en verhoogde retentie van dit therapeutische eiwit in het glasvocht en het voorste oogvocht. Onverwacht veroorzaakten de formuleringen ook ontstekingen in het achterste segment van het oog. De exacte oorzaak van deze ontsteking blijft onbekend, maar de resultaten suggereren een relatie tussen polymeerconcentratie, hydrogelstabiliteit en de waargenomen ontsteking. Aan de andere kant vertoonden meer stabiele placeboformuleringen geen ontsteking in het achterste oogsegment en slechts voorbijgaande irritatie in het voorste segment, wat aangeeft dat een meer stabiele en langzamer afbrekende hydrogel beter wordt verdragen in de ogen van konijnen. Een andere mogelijke verklaring voor de ontsteking die werd waargenomen voor de met geneesmiddel beladen gelformuleringen zou kunnen worden gerelateerd aan het vrijgegeven bevacizumab gemodificeerd met een fluorescent label binnen het glasachtige lichaam. Het is mogelijk dat dit vrijgegeven gemodificeerde eiwit kan samenklonteren binnen het glasachtige lichaam en mogelijk een ontstekingsreactie kan initiëren. Over het algemeen is het hydrogelsysteem veelbelovend voor langdurige afgifte van medicatie, maar vereist het systematische veiligheidsevaluaties voordat verdere stappen richting toepassing kunnen worden gezet.

Hoofdstuk 5 introduceert de synthese van twee nieuwe ABA-triblokcopolymeren. Deze copolymeren bestaan uit een poly(ethyleenglycol), een hydrofiel middelste blok (B) en buitenste blokken (A) die hoofdzakelijk bestaan uit temperatuurgevoelig poly(N-isopropylacrylamide), met comonomen die maleïmide- of furangroepen bevatten. Door de thermisch gelerende eigenschappen van de polymeren te combineren met Diels-Alder chemische verknoping, werden stabiele hydrogelen in situ gevormd. Deze hydrogelen vertoonden opmerkelijke veelzijdigheid als geneesmiddelafgiftesysteem waarbij ze de gecontroleerde afgifte van twee verschillende modelgeneesmiddelen faciliteerden: het ontstekingsremmende medicijn dexamethason en een FAB-antilichaamfragment ontworpen als een biosimilar van Ranibizumab, gericht op de remming van VEGF. De hydrogelen maakten de afgifte van dexamethason gedurende 35 dagen en van het FAB-eiwit gedurende 13 dagen mogelijk. Belangrijk om te noemen is dat de maleïmide-functionele groepen zich bevinden in de hydrofobe domeinen van de polymeermatrix en geen interactie aangaan met het eiwit bij temperaturen boven de polymeer specifieke kritische temperatuur, waardoor ongewenste eiwitmodificatie tijdens het beladen en bij vrijgeving wordt voorkomen. Bovendien kan de hydrogel worden geïnjecteerd met een dunne 30 G-naald en de

8

gel vertoont uitstekende cytocompatibiliteit met retinale cellen, waardoor het een veelbelovende kandidaat is voor intravitreale geneesmiddeltherapie.

In **Hoofdstuk 6** zijn de ABA temperatuurgevoelige copolymeren gebruikt om bloemvormige micellen (FLM) te creëren waarbij de kern is gestabiliseerd met Diels-Alder verknopingen. Deze micellen zijn onderzocht omdat ze mogelijk geschikt zijn voor de afgifte van dexamethason bij oculaire ontstekingstherapie. De micellen vertoonden goede cytocompatibiliteit en werden opgenomen door zowel retinale cellen als macrofagen. In vivo-experimenten met een ratmodel toonden aan dat de micellen gemakkelijk konden worden toegediend via intravitreale injectie, zonder waargenomen nadelige effecten of retinale afwijkingen. De micellen bereikten efficiënt de subretinale ruimte, retinale cellen en het binnenste begrenzende membraan (ILM) bij de vitreoretinale barrière. Er is echter verdere optimalisatie nodig om het retentievermogen van de micellen in het glasvocht te verlengen. Samenvattend, Diels-Alder verknoopte FLM-micellen zijn veelbelovend als afgiftesysteem voor de toekomstige behandeling van oculaire ontstekingsaandoeningen door zich te richten op de subretinale ruimte en het retinale pigmentepitheel (RPE).

Tenslotte biedt **Hoofdstuk 7** een samenvattende discussie van de bevindingen beschreven in dit proefschrift, samen met aanbevelingen voor verdere verbeteringen. Bovendien is in **Hoofdstuk 7** de industriële ontwikkeling van het potentiële farmaceutische product dat in **Hoofdstuk 3** werd beschreven, besproken om meer inzicht te krijgen in opschaling van dergelijke biomaterialen.

Conclusie

De studies beschreven in dit proefschrift gaan over innovatieve oplossingen voor intraoculaire geneesmiddelenafgifte, met als doel significante vooruitgang in de behandeling van netvliesaandoeningen en het verbeteren van het welzijn van patiënten met oogaandoeningen. Het gebruik van polymere biomaterialen die in dit proefschrift zijn beschreven, toont veelbelovende mogelijkheden voor nieuwe geneesmiddelformuleringen met verbeterde stabiliteit, verbeterde beschikbaarheid van het geneesmiddel op de gewenste locatie in het lichaam en verlengde afgifteprofielen. Echter, zorgvuldige overweging van factoren die invloed hebben op veiligheid, opschaling, sterilisatie, opslag, stabiliteit, verpakking en regelgeving zijn essentieel voor een succesvolle industriële ontwikkeling en uiteindelijk klinische toepassing. Met alle ontwikkelingen op het gebied van nieuwe formuleringen voor oculaire ziekten ziet de toekomst er veelbelovend uit voor de gezondheidszorg van patiënten met oogaandoeningen

CURRICULUM VITAE

Blessing Chidimma Ilochonwu was born on June 27, 1992, in Nnewi, Nigeria. In 2011, she obtained her high school diploma in scientific disciplines from Galileo Galilei Secondary School in Jesi, Italy.

In the same year, 2011, she commenced her university studies in Pharmaceutical Chemistry, majoring in Pharmacy and Industrial Pharmacy at the University of Camerino, Italy. During her academic pursuit, she underwent professional training at the Hospital Pharmacy, "Ospedale Carlo Urbani Farmacia Interna", Jesi, Italy. In 2016, she received the Erasmus+ scholarship and traveled to Utrecht University, the Netherlands, to conduct her master's thesis project. The project focused on developing innovative crosslinking chemistry based on Proximity-mediated copper-free click chemistry, applied in PNIPAM-based Polymer hydrogels, under the supervision of Dr. Marzieh Najafi and Prof. dr. ir. Tina Vermoden. In April 2017, she successfully graduated from the University of Camerino, Italy.

Subsequently, in June 2017, she returned to Utrecht University, Netherlands, to commence her PhD studies at the division of Pharmaceutics under the co-supervision of Prof. dr. ir. Tina Vermoden and Prof. dr. ir. Wim E. Hennink. Her doctoral research focused on formulating injectable hydrogels and micelles for intravitreal delivery of proteins and corticosteroids to the retina. This research was conducted within the framework of the Ocuther ITN Marie Skłodowska-Curie network, enabling collaboration with various European institutes and companies, enriching her network and knowledge. The findings of her research project are detailed within this thesis.

In 2021, her research gained the interest of a pharmaceutical company, Boehringer Ingelheim, leading to a collaboration focused on developing hydrogels for extended release of anti-VEGF and anti-TNFα proteins to support rat and mouse animal PK and PD studies. In 2022, she joined Boehringer Ingelheim, Germany, as a postdoctoral scientist, where she continues her career in ocular therapy employing innovative biomaterials.

8

PUBLICATIONS IN THESIS

Blessing C. Ilochonwu, Arto Urtti, Wim E. Hennink, Tina Vermonden, Intravitreal hydrogels for sustained release of therapeutic proteins, Journal of Controlled Release, 326, 2020, 419-441.

Blessing C. Ilochonwu, Marko Mihajlovic, Roel F. Maas-Bakker, Charis Rousou, Miao Tang, Mei Chen, Wim E. Hennink, and Tina Vermonden. Hyaluronic Acid-PEG-Based Diels–Alder In Situ Forming Hydrogels for Sustained Intraocular Delivery of Bevacizumab. Biomacromolecules 2022, 23, 7, 2914–2929.

Blessing C. Ilochonwu, Simone A. van der Lugt, Ada Annala, Greta Di Marco, Thibault Sampon, Juergen Siepmann, Florence Siepmann, Wim E. Hennink, Tina Vermonden. Thermo-responsive Diels-Alder stabilized hydrogels for ocular drug delivery of a corticosteroid and an anti-VEGF fab fragment. Journal of Controlled Release, 361, 2023, 334-349.

Blessing C. Ilochonwu, Ada Annala, Amir Sadeghi, Elisa Toropainen, Wim E. Hennink, Jussi Paterno, Marika Ruponen, Arto Urtti, Tina Vermonden. In Situ Diels-Alder Crosslinked Hydrogel for Controlled Release of Bevacizumab in Rabbit Vitreous: Insights from In Vivo Pharmacokinetics and Safety Evaluation. *Manuscript in preparation*

Blessing C. Ilochonwu, Ada Annala, Danny Wilbie, Barbara Mesquita, Amir Sadeghi, J. Puranen, Elisa Toropainen, Marika Ruponen, Arto Urtti, Wim E. Hennink, Tina Vermonden Diels-Alder Core-Crosslinked Flower-like Micelles for Intraocular Drug Delivery Applications. *Manuscript in preparation*

OTHER PUBLICATIONS

Marko Mihajlovic, Margot Rikkers, Milos Mihajlovic, Martina Viola, Gerke Schuiringa, **Blessing C. Ilochonwu**, Rosalinde Masereeuw, Lucienne Vonk, Jos Malda, Keita Ito, and Tina Vermonden. Viscoelastic Chondroitin Sulfate and Hyaluronic Acid Double-Network Hydrogels with Reversible Cross-Links. Biomacromolecules 2022, 23, 3, 1350–1365.

Ada Annala, **Blessing C. Ilochonwu**, Danny Wilbie, Amir Sadeghi, Wim E. Hennink, and Tina Vermonden. Self-Healing Thermosensitive Hydrogel for Sustained Release of Dexamethasone for Ocular Therapy. ACS Polym. Au 2023, 3, 1, 118–131.

Coraline Chartier, Sytze Buwalda, **Blessing C. Ilochonwu**, Hélène Van Den Berghe, Audrey Bethry, Tina Vermonden, Martina Viola, Benjamin Nottelet, and Tatiana Budtova. Release Kinetics of Dexamethasone Phosphate from Porous Chitosan: Comparison of Aerogels and Cryogels. Biomacromolecules 2023, 24, 10, 4494–4501.

WEBINAR

- **Online Webinar Precision Nano-Systems.** Tea-time with Blessing C. Ilochonwu: Delivery of therapeutic proteins to the posterior of the eye link, June 2020 https://www.youtube.com/watch?v=nx5nF7A6Mwk

AWARDS & GRANTS

- **Best Publication Award, 2022**
  Issued by The Utrecht Institute for Pharmaceutical Sciences (UIPS), June 2023

- **1st Prize, CRS Annual Meeting 2020 Youngscivision Contest**
  Issued by Controlled Release Society Young Scientific Committee, July 2020

- **Young Scientist Travel Grant, 2020**
  Issued by CRS BeNelux & France Local Chapter, January 2020

- **Brightlands Rolduc Best Poster Award, 2019**
  Issued by Brightlands Rolduc Polymer Conference, September 2019

- **1st Prize Winner Biomedical Workshop Lecture Award Winner**
  Issued by Dutch Polymer Days Conference Committee, March 2019

- **1st Prize, Advanced Drug Delivery & Drug Targeting Competition**

  Issued by The Utrecht Institute for Pharmaceutical Sciences (UIPS), 2018

8

ACKNOWLEDGEMENTS

I am filled with joy and happiness as I finally write this last section of my thesis. I would like to express my deepest gratitude to all of you who supported me over the years and made this dream a reality.

Dear **Tina,** From the moment I first met you during my master's studies, I was impressed by your kindness and warmth. Over the years, my initial impression of you hasn't changed. Thank you for granting me the opportunity to pursue my PhD within your group. Your scientific guidance, unwavering support, patience, and honesty have been priceless. Your belief in my abilities during challenging moments has meant more to me than words can express. Your encouragement has been a guiding light, and your impressive scientific expertise in material science, along with innovative, out-of-the-box ideas, has been a constant source of inspiration. I could always come to you with any questions, and when I felt overwhelmed, thank you for always keeping the door open. Thank you for promoting my work at any opportunity. When asked about my supervisor during my PhD journey, my response was always: 'I have the best supervisor!'

Dear **Wim,** under your guidance, I feel immensely proud to have completed my thesis and to be among the first recipients of the "Wim Hennink award". Each meeting and manuscript review has been a learning experience, thanks to you. Your commitment to top-notch science, meticulous attention to detail, critical thinking, and unwavering support for your students are genuinely inspiring. I am deeply grateful for the profound impact this will have on my scientific journey. Your responsiveness, even in the late hours, has been a true testament to your dedication. As a night owl, I'll miss those late-night exchanges, as well as your funny stories and lighthearted remarks—like the memorable "lipstick lady" anecdotes. Thank you for tirelessly ensuring the quality of my work!

Dear **Barbara,** thank you for always handling paperwork and meetings with my supervisors and collaborators with a positive vibe and a friendly smile. You're really a sweetheart! I would like to extend my gratitude to our lab technicians, **Mies**, **Roel, Joep, Louis**, **Kim**, and **Esmeralda**. **Mies**, thank you for your support in the synthesis lab, your guidance with equipment, and your readiness to assist whenever I had questions. I truly miss the lively atmosphere you create with your contagious laughter and vibrant voice in the lab. Your amusing acting skills showcased in our PhD videos will always be unforgettable memories. **Roel**, I'm grateful for your assistance with the cell activity assays and for the scientific exchanges we've had. Thank you for always being available to help whenever I approached you, and for the nice conversations we've shared.

Dear **Marcel,** thank you for your assistance with the eye images at the animal facilities, and for guiding me on how to properly store and maintain the eye ex vivo explant models.

I would like to express my gratitude to my collaborators who have been an integral part of this thesis.

8

Marco, **Ada**, **Charis**, thank you for making the consortium meetings and training sessions such a fun and enriching experience. **Charis**, thank you a lot for your support during my small adventure at the hospital in our first Ocuther travel, and also for showing me how to extract the eye from the porcine in the slaughterhouse. I had so much fun with you, especially at the start of our Ph.D.

I would like to express my gratitude to my students, **Desi**, **Christie**, **Annemijn**, and **Simone**. Thank you for your valuable contributions to this thesis. Each of you has taught me more about supervising individuals with different personalities. I wish you all great success in your future endeavors and hope that you carry pleasant memories of your time in the lab.

I would like to thank my colleagues at the Department of Pharmaceutical Science. **Anna**, **Lucia**, **Karina**, **Lies**, **Bo**, **Neda**, **Negar**, **Dandan**, **Yinan**, **Genoveva**, **Sjaak**, **Serena**, **Carl**, **Yanna**, **Thijs**, **Jerry**, **Haili**, **Desiree**, **Aida** and **Marthew**—most of whom I met at the beginning of my Ph.D. or even during my time as a master's student at the department—I want to thank you. You all created a fantastic atmosphere in the lab and at every morning colloquium, and scientific meeting, setting high standards that motivated me to always do my best.

My dear **Marzieh**, your belief in my potential for a PhD was the starting point of an incredible journey. I've learned a lot from you, not only about polymer chemistry but also about life. Your determination, values, and outlook on life are truly inspiring. Thank you for being a great friend and mentor to me!

Piet, Rene, and **Bas**, I want to express my sincere gratitude for your valuable suggestions and unwavering support in navigating polymer synthesis, equations, and modeling. Your guidance proved to be immensely helpful during those moments.

To my Chinese colleagues and friends, **Yanna**, **Menshang**, **Xiangjie**, and **Yan**, I have always been inspired by your work ethics. Thank you for keeping me company during late evening experiments in the lab. I am forever grateful for the wonderful memories I've shared with each of you.

To my very loud and fun Italian friends and colleagues, **Cristina**, **Martina**, **Serena**, **Isabel**, **Greta**, **Marko, Giulia**, **Francesco**, **Martina M**., **Angela**, life at the department felt like home because of all of you. Thank you for the laughter, support, and for every memory. "Mi mancherete tantissimo!" **Cristina,** thanks for lightening the mood after tough meetings. **Martina**, thank you for always being a sweetheart, always willing to help. **Greta**, although you joined the group towards the end of my Ph.D., I connected with you immediately and have wonderful memories. Thanks for the vegan cakes, cookies, and for your support with the shrinking experiments.

Special thanks to my colleagues who worked alongside me throughout my Ph.D. journey. **Danny**, your assistance with cell culture was invaluable. **Erik**, thank you for your support with the HPLC measurements and for the pleasant conversations. **Johanna**, thanks for making the office area so enjoyable, and let's not forget about the Broadway Plan B career! **Stefania**, thank you for hosting wonderful indoor apartment parties. And also, **Matthijs, Vivian**, **Dmitrii**, **Billy**, **Mert**, and **Eleonora**,

thank you all for your delightful company during our coffee and lunch breaks, filled with enjoyable conversations.

Dear **Yan**, **Cristina**, and **Martina**, thanks for sharing the lab area with me. It was truly fun and an honor to be your area manager. The loud music and our lab 'escapees' will always be a memorable part of our time together.

To my Shofar family and small group – **Derk Jan**, **Renee**, **Geofrey**, **Marco**, **Jolande**, **Julia**, **Jade**, **Karlientjie**, **Daphne**, **Esther**, **Lisa**, **Banish**, **Zoyang**, **Derrick**, **Roline**, **Angie**, **Martin**, **Joanne**, **Priscilla**, **Henriette**, **Carolin**, **Danielle**, **Raquel**, **Mareli**, **Maureen**, **Emilinah,** 'My Shofar African Congress' dear friends – **Nsamwa**, **Connie**, **Sandra**, **Geofrey** and our acquired African **Hazely**. I extend my heartfelt thanks to all of you for your prayers and support during my stay in Utrecht. Being the student small group leader was a tremendous honor as it gave me the opportunity to meet many incredible people like you. Our chats, prayers, and singing sessions were the therapy I needed. Thank you for being an integral part of my PhD journey in Utrecht; you will all always hold a special place in my heart.

To my dear Utrecht Auntie and Uncle **Ogechi** and **Peter**, thank you for welcoming me into your home as a little sister; I always felt at home with your family. Thank you for your support and for being there for me throughout this journey. I know I will always have a home in the Netherlands because of you. **Sherlyn**, thank you for the wonderful memories we've created over the years in the Netherlands. I still vividly recall the moment when I was offered the PhD position during the final months of our master internship. I ran to you, and with your reassuring smile, you immediately said, "You got this, girl." **Stephanie**, thanks for all your encouragement and for the fantastic girl trips we've shared. Hoping for many more in the future.

To my managers and colleagues at **Boehringer Ingelheim** — **Achim S.**, thank you for your support in providing the FAB antibody used in this thesis and for facilitating my transition to my new Job. **Achim G.**, **Joachim**, and **Christoph**—thank you for welcoming me into the CMC department. Your support and encouragement during the final stages of writing my thesis were priceless and greatly appreciated! **Alvaro/Alvaritto**, I know I should dedicate a full page to express my gratitude but forgive me for keeping it short. Thank you for all the support, encouragement, brainstorming sessions, and for reminding me to have fun. I am now free as a bird, and it's also thanks to you. **Lena**, thank you for your encouragement and for celebrating every little success with me. I look forward to creating great delivery systems for Ivt with you. And finally, to the **DDS-CMC group**, thank you all for welcoming me into the department and making it feel like a family. Your support and the pleasant atmosphere in the lab helped me stay balanced, even after working weekends on my PhD thesis. I hope to create many more great memories with all of you!

To my Mentor **Cyrille**, I've finally finished, and it's also thanks to you. Even though I met you during the final stage of my thesis, your support, motivation, and prayers helped me through difficult times. I will always be grateful!

8

Yomi, **Amaka**, and **Dike**, thank you for your support and for caring for me.

To my lifelong friend **Maria**, you've always been my greatest supporter and friend from high school. We may not speak every day, but I've always felt your support and love over the years. Thank you for always being there for me.

Dear **Joseph**, you were such an important part of this thesis. Thank you for your support, encouragement, and for keeping me motivated while I wrote. Also, thank you for your assistance in refining my first manuscripts. I will always be grateful for all you've done for me. Thank you for the many beautiful moments we shared in Utrecht!

A special thanks to my paranymphs **Mahsa** and **Barbara**. No one could comfort me in difficult times like you do. **Mahsa**, you are more than a friend; you are like a sister to me. Thank you for the many memories—cooking together, movie nights, trips, etc. Thank you so much for your support and encouragement; I could always rely on you. **Barbara**, thank you for always being a sweet and kind-hearted friend. You are such a good listener, and I really miss your company in the office and our intense discussions about life, careers, hopes, dreams, and working late into the evening. Thank you for all your help and support, even in the lab. **Mahsa**, **Barbara**, I look forward to a lifelong friendship!!

To my family, dear **Mum** and **Dad**, you have always been my rock. I couldn't have asked for better parents. Thank you for all the sacrifices you've made, for the never-ending support and prayers, and for always reminding me to eat and sleep enough. You've always been sure that I could do anything I set my mind to. You left your home country, your families, and even your careers in search of a better future for your kids in Italy. Thank you for never giving up, even when times were very difficult for us. Thanks for dreaming big for us, as it has always been the catalyst for our success. Dear **Samuel** and **Mavelous**, thank you for your support, prayers, encouragement, and for celebrating with me at every little achievement. "*Vi voglio un mondo di bene.*" Dear **Love**, thank you for being my better half! You're my younger sister, yet I've always had to measure up to your determination, resilience, and wisdom. Thank you for all your support and encouragement. As you always say, "Anyone can do something that is easy; it is in the difficult things that you can be exceptional." Our favorite game as kids was to have a fake dinner as successful career women, and we made a promise that one day it would be our reality. "*Amore,*" I think we are making good progress!

And last but not least, thanks to **GOD Almighty**, who made all things possible!

In closing, this thesis journey has been a fantastic ride, with highs and some lows, twists, and turns. Excited for what the future holds, I'm eager to embrace the next chapter of my life.

Blessing

8